ELECTRICAL CHARACTERIZATION OF CERTAIN SEMICONDUCTING THIN FILMS

A. G. VALYOMANA M. Phil.

THESIS SUBMITTED
IN PARTIAL FULFILMENT OF THE REQUIREMENTS
FOR THE DEGREE OF
DOCTOR OF PHILOSOPHY

SOLID STATE PHYSICS LABORATORY
DEPARTMENT OF PHYSICS
COCHIN UNIVERSITY OF SCIENCE AND TECHNOLOGY
KOCHI - 682 022

1992

CERTIFICATE

Certified that the research work presented in this thesis is based on the original work done by Miss. A.G. Valyomana under my guidance in the Department of Physics, Cochin University of Science and Technology, and has not been included in any other thesis submitted previously for the award of any degree.

C. Purushothaman

Dr. C. Purushothaman
Supervising Teacher

Kochi 682022

1 October 1992

DECLARATION

Certified that the work presented in this thesis is based on the original work done by me under the guidance of Dr.C.Purushothaman in the Department of Physics, Cochin University of Science and Technology, and has not been included in any other thesis submitted previously for the award of any degree.

Valyomana

A.G. Valyomana

Kochi 682022

1 October 1992

PREFACE

In recent years there has been considerable interest in the development and characterization of semiconducting materials suitable for device applications. With the impetus provided by these applications, the investigation of these materials in thin film form has undergone revolutionary changes and continues to be recognized as frontier areas of research work. A thorough understanding of their electrical properties is essential for the development of technological applications.

This thesis presents a study of the electrical characterization of cadmium sulphide (CdS), copper sulphide (Cu_xS) and copper indium selenide ($CuInSe_2$) thin films prepared by chemical methods. These include measurements of dark conductivity, photoconductivity, lifetime, ionic thermocurrents (ITC) and thermally stimulated currents (TSC). The study of dark conduction in materials especially in semiconductors has proved themselves to be a valuable tool in the understanding of the formation and migration of charge carriers in them and also it serves to identify the position of impurity levels (trap levels). The investigation of photoconductivity, illuminates the electronic processes in the materials. The information about the nature of defects and the location of trap levels of the carriers can be obtained from lifetime measurements. The purpose of research in the area of TSC method is to determine various parameters such as activation energies,

capture cross section of the traps etc. The results obtained from these studies in CdS, Cu_xS and $CuInSe_2$ thin films are discussed. Special attention has also been paid to understand the structure and chemical analysis of the prepared samples.

The thesis consists of twelve chapters which by and large are self-contained with separate introduction and references. In the first chapter, a general review is given to provide an explanation on the physics of semiconductors. This part covers a clear account on the generation and recombination of charge carriers.

A brief description of the deposition techniques of thin films forms chapter 2. Of the various methods, particular emphasis has been laid upon to describe the importance of chemical methods since only these methods are of direct interest in the present work.

In chapter 3, a theoretical background is outlined to get an understanding of the dark conductivity, photoconductivity, life time, ITC and TSC studies of semiconductors. This section also includes a description on the mechanism of traps and trapping effects in these materials, with attention given to the determination of trapping parameters involved in the electrical transport processes.

Chapter 4 deals with the details of the experimental techniques employed in the present investigations. This part focuses attention on the experimental set up used for the preparation of thin films by

chemical methods. The techniques employed for the identification of structure and chemical analysis of the prepared samples by X-ray diffraction (XRD) and Electron Spectroscopy for Chemical Analysis (ESCA) are presented. A short note is made on the optical microscopic investigations using Union Versamet-2 metallurgical microscope. A general review of differential scanning calorimetry (DSC) is also outlined. This is followed by an account of various experimental systems like annealing chamber, vacuum coating unit, metallic cell and other assemblies in connection with the electrical measurements.

The preparation of CdS films by spray pyrolysis method is given in chapter 5. The spray technique involves spraying aqueous solution containing cadmium chloride ($CdCl_2$) and thiourea [$(NH_2)_2CS$] on precleaned glass substrates maintained at an elevated temperature using compressed air as carrier gas. The films obtained are of good quality, uniform, strong and adherent. The samples are identified from the XRD patterns. The ESCA analysis of CdS films prepared from different concentrations of $CdCl_2$ and $(NH_2)_2CS$ components is done to identify various elements present in the samples. The samples are annealed in the temperature range 373-573 K for the electrical studies. Microscopic examinations of the samples are made to understand the surface features.

Chapter 6 is devoted to the details of the dark conductivity measurements carried out on unannealed and annealed CdS films.

The experiment is performed in different ambient conditions (vacuum and air). The dark conductivity value of the film in air is found to be low compared to that in vacuum. The activation energy of the observed trap levels is estimated from the measurements. The effect of cadmium contents and annealing temperature on the conductivity of the films have been investigated.

In chapter 7, photoconductivity studies of unannealed and annealed CdS films in vacuum and air are reported. The photoconductivity variation with annealing temperature shows a similar trend in vacuum and air upto 473 K. Some interesting results obtained from these investigations are presented here. One of the key parameters involved in photoconductivity is lifetime of charge carriers. So the measurements on lifetime have also been carried out on CdS films annealed at different temperatures.

Chapter 8 includes extensive studies of ITC and TSC measurements of CdS films. In these experiments, the effect of applied field, time of field applied and temperature on current peaks are studied and the trapping parameters have been determined. The results obtained are discussed using the existing theoretical models.

Chapter 9 is intended to give the description of chemical bath deposition method, which is employed for the preparation of Cu_xS thin films. In this method, a chemical bath is constituted from 10 ml of stock solution of 0.5 M copper chloride, 10 ml triethanolamine, 10ml

ammonia and 10 ml of stock solution of 1M thiourea. The deposition of the films is carried out at room temperature without stirring. Good quality thin films of Cu_xS are obtained after a deposition time of 2½ hours. XRD profiles of the samples are analysed to confirm the compound identification of the samples. For the investigations of electrical properties, the samples are prepared from different bath compositions. The samples are viewed under an optical microscope and their surface topographical observations are included in this section.

The experiments on the conductivity of Cu_xS films are explained in chapter 10. The results obtained in the samples deposited from different proportions of copper chloride and thiourea are analysed. The influence of annealing of the samples under vacuum conditions is also studied in detail.

Chapter 11 provides an outlook on the TSC measurements of Cu_xS films. The magnitude of TSC peaks is found to be varying with the applied field. Systematic investigations have been made from liquid nitrogen temperature to high temperature.

The last chapter includes some electrical measurements carried out on $CuInSe_2$ thin films. The results obtained from these studies are discussed at some length.

Part of the investigations contained in this thesis has been published in various journals and presented in national conferences.

LIST OF PUBLICATIONS

1. "Effect of annealing temperatures on the electrical transport properties of spray-pyrolysed CdS films".
   J. Mater. Sci. Lett. 9 (1990) 1025.

2. "Conductivity studies on spray-pyrolysed CdS films in ambient conditions".
   J. Mater. Sci. Lett. 11 (1992) 616.

3. "Influence of annealing on lifetime of minority carriers in n-type CdS films".
   J. Mater. Sci. Lett. (In Press)

4. "Photoconductive and ellipsometric studies of spray pyrolysed CdS thin films".
   Bull. Mater. Sci. (In Press)

5. "Variation of annealing effects on the electrical conductivity of spray pyrolysed CdS thin films".
   Symposium on Current Trends in Pure and Applied Physics, Cochin (October 1988).

6. "Electrical transport in polycrystalline CdS thin films in Vacuum and hydrogen atmosphere".
   Solid State Physics Symposium, Bhopal (20-23 December,1988).

7. "Effects of annealing treatment on the photoconducting properties of CdS films".
   Fourth National Seminar on Crystal Growth, Mysore
   (14-16 August 1989).

8. "Dependence of conductivity of CdS thin film on different cadmium concentrations".
   Second Annual General Meeting of the Materials Research Society of India, New Delhi (9-10 February, 1991).

9. "Variation in the lifetime of holes in CdS films during heat treatment"
   Solid State Physics Symposium, Varanasi (21-24 December, 1991).

10. "The role of excess copper on the electrical conductivity of thin films of $CuInSe_2$"
    Solid State Physics Symposium, Varanasi (21-24 December, 1991).

11. "Influence of annealing on the dark conductivity and thermally stimulated current of $CuInSe_2$ thin films".
    Solid State Physics Symposium, Varanasi (21-24 December, 1991).

12. "Ionic thermocurrent studies in spray pyrolysed CdS films"
    (Communicated)

13. Thermally stimulated currents in CdS thin films.
(Communicated)

14. "Electrical Conduction in Chemically bath deposited Cu_xS films".
(Communicated)

15. "Thermally stimulated currents in Cu_xS thin films prepared by Chemical bath deposition technique".
(Communicated)

16. "Influence of ambient conditions on the electrical conductivity of $CuInSe_2$ thin films".
(Communicated)

17. "Electrical characterization of $CuInSe_2$ thin films".
(Communicated)

CONTENTS

1 PHYSICS OF SEMICONDUCTORS

1.1 INTRODUCTION

Semiconductor physics is one of the comparatively young and rapidly developing branches of science. Semiconductors are of practical importance in a number of connections. Their most direct uses, take advantage of their unique electrical behaviour as in transistors, crystal rectifiers and thermistors. Closely related to these are the applications which combine electrical and optical effects, as in luminescent materials and photoconductors.

The term "Semiconductor" implies that it is a material having an electrical conductivity intermediate between that of metals and insulators. The main feature used to distinguish semiconductors from metals and insulators is their negative temperature coefficient of resistance. The semiconducting properties are brought up by thermal excitation, impurities, lattice defects etc. Metallic conductivity is typically between 10^6 and 10^4 $(\Omega\,\text{cm})^{-1}$, while typical insulators have conductivities of less than 10^{-10} $(\Omega\,\text{cm})^{-1}$. Some solids with conductivities between 10^4 and 10^{-10} $(\Omega\,\text{cm})^{-1}$ are classified as semiconductors.

This chapter introduces some basic ideas on the energy band structure of solids. Some theoretical aspects of the trapping and recombination of charge carriers of semiconductors are also covered.

1.2 ENERGY BAND STRUCTURE

The band theory is based on the periodic nature of the lattice, which causes the wavefunctions to be periodic and hence determines the law of motion of electrons and holes. The same band structures

are found in amorphous semiconductors which lack long range order, the main properties of these substances are determined by nearest neighbour interactions.

The concept that, electronic properties may be described in terms of free electrons was developed long before the invention of wave mechanics. According to Sommerfeld's free electron theory [1], the energy levels which the various electrons can occupy are determined by wave mechanics. It was assumed that, in a metal, the valence electrons are not tied to individual atoms but are free to move through the solid [fig.1.1(a)]

From free electron theory, the energy of the free electron as a function of wave vector is given by $E = \frac{\hbar^2 k}{2m}$ where wave vector $k = \frac{2\pi}{\lambda} = \frac{P}{\hbar}$. Here λ is the wavelength associated with the electron and P is the momentum.

By this theory, the allowed energy levels lie very close together and their values extend from nearly the bottom of the potential trough in which the electrons move to indefinitely high values [fig.1.1(b)]

The fact that, some solids are conductors of electricity while others are not, cannot be explained on the basis of this theory. The next step was to take into account the interaction of valence electrons with atomic cores, assuming these to be placed at the lattice point of the crystal. These electrons are still assumed to move independently but the smoothed out potential used by Sommerfeld is replaced by a

Fig. 1.1 (a): Potential energy of electron in crystalline solid (Sommerfeld model).

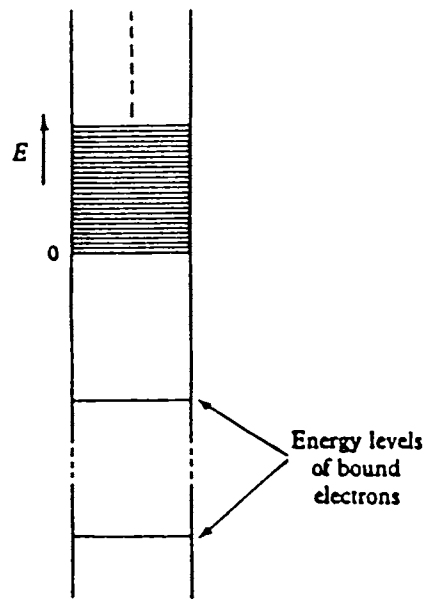

Fig. 1.1 (b): The allowed energy levels of the sommerfeld model of a metal.

periodic potential [fig.1.1(c)]. The particular feature of a potential of this form is that it is periodic having the same periodicity of the lattice. The motion of electrons in such a periodic potential was discussed by Bloch [2].

By considering the motion of electrons in a periodic potential, the energy levels are confined to certain allowed bands of energy seperated by regions in which no energy levels are allowed ie. the number of allowed energy bands are separated by forbidden bands and the energy E is a periodic function of wave vector k. [fig.1.1(d)]. For the inner electrons, these allowed bands are extremely narrow and corresponds to the atomic levels; for the valelnce electrons, the bands are quite broad. There exists a definite number of discrete energy levels just as the inner levels in a heavy atom are all filled with electrons, all the levels in the lower allowed bands are filled and it is only the upper bands which may be wholly or partially unoccupied by electrons.

The electrical properties of solids are determined by the degree of filling of the energy bands. To produce conduction, an electron must receive energy from an electric field. The electrons can contribute to the current only if there are available neighbouring empty levels into which they can go. Such materials which have a partially filled band in their energy spectrum above the completely filled energy bands are called conductors. Fig. 1.1(e) shows the energy bands for conductors, semiconductors and insulators. The division of solids into semiconductors and insulators is determined by the width of the forbidden energy gap

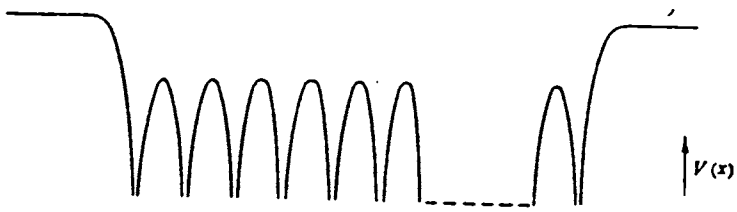

Fig. 1.1 (c): Periodic potential due to atomic cores.

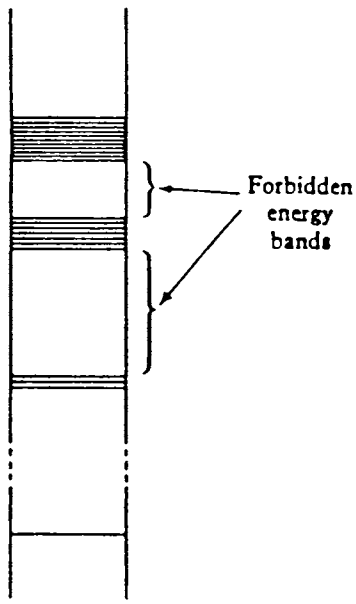

Fig. 1.1 (d): Allowed energy levels for a periodic lattice.

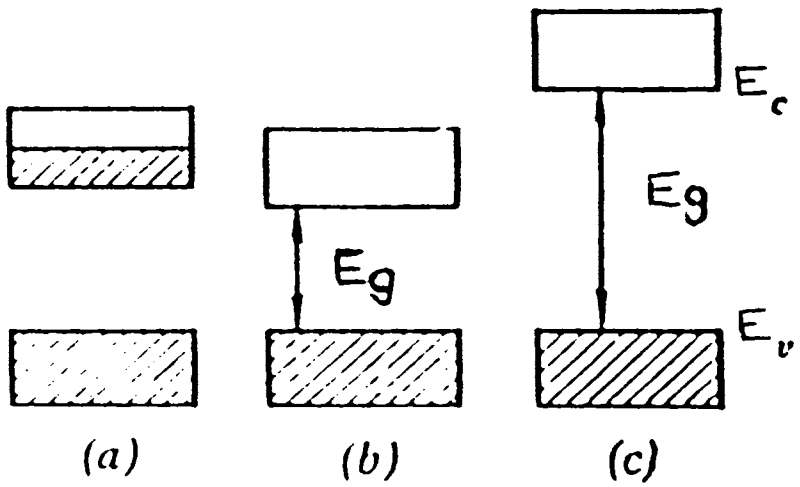

Fig. 1.1 (e): Energy bands for
(a) Metals (b) Semiconductors (c) Insulators.

separating the completely filled band from the empty band. If the forbidden energy gap E_g between the highest filled band and next empty band is large, no electronic conduction can takes place. This type of materials are called insulators. If the value of E_g is small, there is the possibility that electrons may be thermally excited into the band above and these excited electrons can conduct. The number of excited electrons would increase with temperature in a manner governed by a process having an activation energy and cause a rapid increase of conductivity with temperature. Substances behaving in this way were identified by Wilson as Semiconductors [3].

1.2.1 Intrinsic and extrinsic semiconductors

Semiconductors are classified as intrinsic (pure) and extrinsic (impurity). Impurity semiconductors in turn can be divided into n-type semiconductors and p-type semiconductors.

(a) Intrinsic Semiconductors

A highly purified semiconductor exihibits intrinsic conductivity. Semiconductors in which conductivity is controlled by valence electrons are known as intrinsic semiconductors. That is holes and electrons are excited solely by thermal excitation across the energy gap. Holes and electrons which are created in this manner are often referred to as intrinsic charge carriers. [4].

In the band structure of an ideal semiconductor, the energy gap separates the uppermost allowed energy level in the valence band

and the lowest energy state in the conduction band. At absolute zero, the valance band is completely filled and the conduction band is empty. As the temperature is increased, there is a finite probability that an electron in the valence band may gain sufficient energy from the lattice and make a transition into an allowed state in the conduction band. A transfer of electrons to the conduction band is accompanied by the formation of vacancies (holes) in the valence band. From the moment, the energy of thermal lattice vibrations becomes high enough for the electron transfer from the valance band to the conduction band, any further increase in temperature is accompanied by a rapid increase in free charge carrier concentration.

The total number of electrons (n) in the conduction band and holes (p) in the valence band are given by

$$n = N_c \, e^{-(E_c - E_F)/kT} \tag{1.1}$$

$$p = N_v \, e^{-(E_f - E_v)/kT} \tag{1.2}$$

where $N_c = 2\left(\frac{2\pi m_e kT}{h^2}\right)^{3/2}$ and

$N_v = 2\left(\frac{2\pi m_h kT}{h^2}\right)^{3/2}$

The quantities N_c and N_v are the effective density of states in the conduction band and valence band respectively. m_e and m_h are the effective electron and hole masses, E_c and E_v are the corresponding energy levels of the bottom of the conduction band and top of the valence band and E_f is the fermi level [5-7].

For intrinsic semiconductors at finite temperatures there is continous thermal agitation that results in excitation of electrons from the valence band to the conduction band and leaves an equal number of holes in the valence band ie $n=p=n_i$ where n_i is the intrinsic carrier density.

The product of equations (1.1) and (1.2) is

$$np = n_i^2 = N_c N_v \, e^{-(Eg/KT)} \qquad (1.3)$$

where $E_g = E_c - E_v$ is the energy of the forbidden gap.

From equation (1.3) n_i can be expressed as

$$n_i = \sqrt{N_c N_v} \; e^{-(Eg/2KT)} \qquad (1.4)$$

b) Extrinsic Semiconductors

Semiconductors in which conductivity is controlled by impurities and imperfections are called extrinsic semiconductors. The presence of impurities leads to certain changes in the energy spectrum of the semiconductor. Impurities may produce isolated levels in the forbidden energy gap and it turns out that these levels may lie very near to the conduction band or very near to the valence band.

At Absolute Zero of temperature, a semiconductor may contain a certain concentration of occupied electronic levels between the valence and conduction bands. These electrons are localized in the vicinity of

impurities and therefore do not contribute to the conductivity unless they are excited into the conduction band. There are two processes of conduction: (i) Electron or n-type conduction in which electrons only are excited from donor levels near the conduction band (2) Hole or p-type conduction in which holes only are produced by excitation of electrons into acceptor levels near valence band .

As the temperature rises, the conduction electrons in the n-type semiconductor appear much earlier than in the intrinsic semiconductor. As the temperature rises further, the number of impurity electrons arriving to the conduction band increases rapidly while the number of electrons remaining on the donor level decreases and the impurity level is depleted and at a particular temperature Ts, all the electrons from the donor levels are transferred to the conduction band. At $T > Ts$, the number of free electrons remains constant over rather a wide temperature. This can be explained by the fact that, impurity levels are completely depleted and the energy of thermal lattice vibrations is still insufficient to excite the valence electrons. With a further increase in temperature the process of electronic transition from the valence band to the conduction band becomes more intense and at a certain temperature, the number of such transitions becomes so large that the concentration of electrons coming from the valence band becomes comparable with the concentration of impurity electrons. Any further increase in temperature results in such a rapid growth of intrinsic carrier concentration.

1.3 TRAPPING AND RECOMBINATION

Trapping and recombination in semiconductors arise from non-equilibrium distribution of mobile carriers. The change in conductivity

resulting from excitation is terminated by the recombination of the photo-excited electrons and holes. When a carrier is captured by a shallow level from which it can be thermally be emitted into the band before it finally recombines, the process is called trapping. The process by which a free electron and free hole came together to produce their mutual demise is called recombination. Knowledge about the traps in semiconductors is of importance because the traps control the performance, yield and reliability of the device. Generally, the free carrier concentration in a semiconductor rises with temperature. The appearance of free carriers is explained by the transition of electrons from the valence band or from the donor levels to the conduction band. This process is called the generation of free carriers. The generation of carriers is accompanied by the recombination of free carriers. A carrier concetration determined only by the thermal processes is called an equilibrium concentration and the carriers themselves are called equilibrium carriers. Since the generation and recombination of equilibrium carriers are always balanced, the generation and recombination processes are ignored in thermal equilibrium. Also the concentration of equilibrium charge carriers is the same throughout the volume of the semiconductor.

Since most semiconductor devices are operated under non equilibrium conditions, it is essential to know how these free carriers are introduced and transported. The mechanism of generation, recombination and transport of these carriers are of fundamental importance in determining the characteristics of most semiconductor devices. Non-equilibrium describes the condition in which free carrier densities are different from their thermal equilibrium values. The equilibrium condition may be disturbed by the introduction of free carriers exceeding

their thermal equilibrium values. Free carriers can be created in semiconductors by illuminating the material with light and these are excess carriers with respect to the equilibrium carriers and are called non equilibrium carriers.

The free electron or hole motion is interrupted due to impurities. The recombination usually occur through the intermediary of the impurity or defect levels in the gap. In general, these levels correspond to localised electronic states and act as traps for the electrons or holes in the extended band states. The state of occupancy determines whether a level act as a hole trap or electron trap. When the level is unoccupied, it is ready to receive a hole and is therefore a hole trap. However, the carrier can be released and return to the band. If the probability for recombination at the level with a carrier of opposite sign is greater than the probability of release to the band, the level is called a recombination centre. Conversely if the probability for release is greater than recombination, the level is simply called a trap. The electron trapped are localized at an energy level below the conduction band. The localized states at which the holes trapped are lie above the valence band. That is electron trap is in equilibrium with the conduction band and hole trap with the valence band.

The theory of recombination - generation process taking place through the action of energy levels has been worked out by Shockley and Read [8]. This theory has been remarkably successful in explaining a wide variety of phenomena in many semiconductors and semiconductor devices.

The major assumption of the analyss are:

(1) recombination-generation centers also known as traps are located at a single energy level somewhere in the band gap

(2) These centers are uniformily distributed throughout the material.

Fig.1.2 shows the four different processes which are involved in the recombination and generation of carriers. The illustration given in this figure is for the case of a center with a single energy level. The words emission and capture are with reference to the traps. Process (a) is the capture of an electron from the conduction band by the center, process b is the reverse process - the emission of an electron from the centre into the conduction band, process C is the capture of a hole from the valence band by the center and process (d) is the emission of holes.

The recombination centers with density N_t are assumed to be all situated at an energy E_t in the forbidden gaps; each level is capable of capturing one electron when vacant and one hole when occupied by an electron; the capture cross sections for these processes being A_c and A_v respectively. The rates of carrier transitions between the valence and conduction bands and the recombination centres are calculated interms of these capture cross sections the occupancy of the centres and the availability of free carriers to fall into them.

The rates per unit volume at which free holes (p) are captured by occupied centres (n_t) is given by

$$R_{tv} = r_v \, pn_t \qquad (1.5)$$

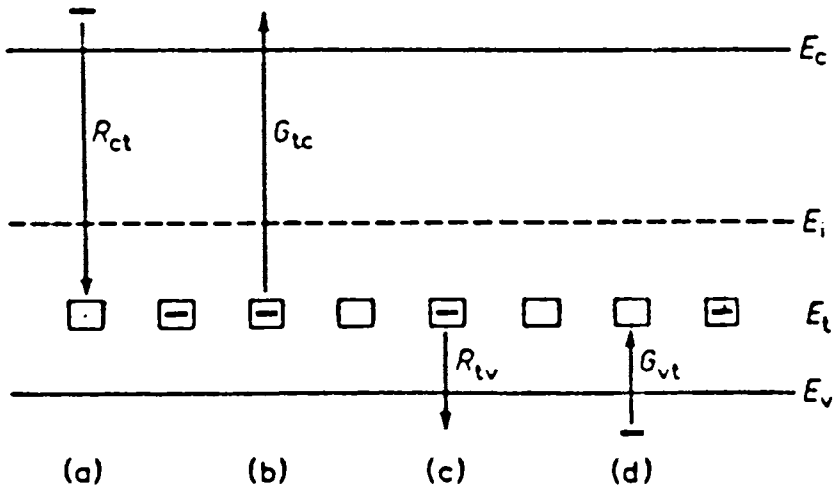

Fig. 1.2: Transitions between the bands and the localized levels. (a) Electron capture (b) Electron emission (c) Hole capture (d) Hole emission.

Similarly the rates of capture of free electrons (n) by vacant centres ($N_t - n_t = P_t$) is given by

$$R_{ct} = r_c \, np_t \qquad (1.6)$$

in which r_v and r_c the capture probabilities are vA_v and vA_c respectively. A is designated as the average capture cross section for recombination. In terms of this cross section, the average probability that in unit time a free carrier makes a transition to a localised level across the gap is given by vA per localized level or per free carrier of the opposite sign where **v** is the thermal velocity. Similarly with the capture of free carriers, bound carriers are continuously re-emitted from the centres back into the bands. The rate of these reverse process for holes (G_{vt}) and for electrons (G_{tc}) are proportional to the densities of vacant (P_t) and occupied (n_t) centres respectively.

The generation rates are

$$G_{vt} = r_v P_1 P_t \qquad (1.7)$$

$$G_{tc} = r_c n_1 n_t \qquad (1.8)$$

where $P_1 = P_o n_{to} / P_{to} = N_v \exp(E_v - E_t)/kT \qquad (1.9)$

$$n_1 = n_o P_{to} / n_{to} = N_c \exp(E_t - E_c)/kT \qquad (1.10)$$

P_o, n_o, p_{to}, n_{to} are the equilibrium values of the free and bound carrier concentrations. N_v and N_c being the effective density of states in the valence and conduction bands respectively. The

magnitudes of p_1 and n_1 are measures of the re-emission rates of bound holes and electrons to their respective bands.

The net rate of transitions from the valence and conduction bands to the recombination centres are given by

$$R_{tv} - G_{vt} = r_v (pn_t - p_1 p_t) \tag{1.11}$$

$$R_{ct} - G_{tc} = r_c (np_t - n_1 n_t) \tag{1.12}$$

A condition which is used to evaluate the fraction of centres occupied by electrons

$$\frac{n_t}{N_t} = \frac{r_c n + r_v p_1}{r_c(n+n_1) + r_v(p+p_1)} \tag{1.13}$$

Substituting this expression for n_t in equation (1.11) or (1.12) the net steady state hole-electron recombination rate is given by

$$U = R_{tv} - G_{vt} = R_{ct} - G_{tc}$$

$$= N_t r_v r_c \frac{Pn - P_o n_o}{r_v(p+p_1)+r_c(n+n_1)} \tag{1.14}$$

The trapping and recombination phenomena was discussed by several authors [9-17]. Schluger et al [18] reported the formation of trapped holes under optical excitation of impurity centres in LiF crystals.

Electron traps induced by boron implanation in gallium arsenide was investigated by Perez et al [19]. Heyns et al [20] studied the role of electron and hole traps in the degradation and breakdown of thermally grown SiO_2 layers. Dalal [21] reported that density of states in amorphous silicon is a fundamental material parameter in determining transport properties. The role of impurities in defect formation in irradiated silicon has been discussed by Awadelkarim et al [22]. Hashizume and Hasegawa [23] studied the variation of deep electron traps created by γ irradiation of GaAs. Rowan and Slifkin [24] have reviewed the dynamics of the formation and migration of the self-trapped hole in silver chloride. Park et al [25] reported the electron trapping properties of silicon nitride. The effects of surface defects on the shallow states of donor impurities at semiconductor surfaces have been described by Sun and Gu [26]. Braunstein et al [27] have investigated the relationship between electrical activation and residual defects in Si implanted GaAs. Recombination properties of epitaxial gallium arsenide structures have been studied by Korotov et al. [28]. Godlewski and Monemar [29] studied deep acceptor like recombination centres in bulk liquid encapsulated Czochralski GaP crystals. The recombination process at deep levels in AlGaAs was investigated by Watanabe et al [30]. Abraham and Halpern [31] reported the effect on recombination in amorphous semiconductors of transitions between localized states.

1.4 REFERENCES

[1] A. Sommerfeld, Z. Phys. 47 (1928) 1.

[2] F. Bloch, Z. Phys. 52 (1928) 555

[3] A.H.Wilson, Proc. Roy. Soc.A, 133 (1931) 458

[4] J.P. Mckelvey, Solid State and Semiconductor Physics (Harper and Row publishers, New York, 1966).

[5] E.S.Yang, Fundamentals of Semiconductor Devices (McGraw Hill, New York, 1978)

[6] S.M. Sze, Physics of Semiconductor Devices (Wiley, New York, 1969).

[7] R.A. Smith, Semiconductors (Cambridge University Press, London, 1959)

[8] W.Shockley and W.T.Read, Jr. Phys. Rev.87 (1952) 835

[9] K.W.Boer, A. Survey of Semiconductor Physics, (Wiley, New York 1990)

[10] R.H.Bube, Photoconductivity of Solids (Robert E. Krieger Pub.Co., New York, 1978).

[11] G.M.Sessler, Topics in Applied Physics, (Springer-Verlag, New York, 1980)

[12] P.T.Landsberg, Solid, Stat. Electron. 30, (1987) 1107

[13] A. Haug, J. Phys. Chem. Sol. 49 (1988) 599

[14] T.S. Moss, 'Hand Book on Semiconductors', Vol.1, (North Holland Publishing Company, Amsterdam, New York, Oxford, 1982)

[15] J.S. Blakemore, 'Semiconductor Statistics', (Pergamon Press, Oxford 1962)

[16] A.S. Grove, Physics and Technology of Semiconductor Devices, (Wiley, New York, 1967)

[17] W.G. Dunlop.Jr, An introduction to semiconductors, (Wiley, New York, 1957)

[18] A. Schluger, S. Mysovsky and A. Nepomnyaschikh, J. Phys. Chem. Solids. 49 (1988) 1043

[19] A. Perez, J. Samitier, J. Esteve-Tinto, A. Romano and J.R.Morante Diffus. Defect. Data, Solid State Data A, Defect Diffus, Forum,62 (1989) 77.

[20] M.M. Heyns and R.F.De Keersmaecker, Symposium on SiO_2 and its Interfaces: USA, 1988.

[21] V.L. Dalal, Proc. SPIE. Int. Soc.Opt.Eng. 706 (1986) 79

[22] O.O. Awadelkarim, A. Henry, B. Monemar and J.L. Lindstrom. Phys. Status Solidi A 120 (1990) 539.

[23] T. Hashizume and H. Hasegawa, J. Appl. Phys. 68 (1990) 4598.

[24] L.Rowan, L.Slifkin, Hopping and Related Phenomena, (Chapel Hill, USA, 1989) P. 393.

[25] Y.C. Park, W.B. Jackson, N.M. Johnson and S.B. Hagstrom. Symposium on Amorphous Silicon Technology, USA, 1989.

[26] H.Sun and S.W. Gu, Phys, Rev. B. Condens. Matter 42 (1990) 7556.

[27] G. Braunstein, L.R. Zheumg, S.Chen, S.Tonglee, D.L. Peterson, K.Y.Ko and G. Rajeswaran
Advances in Materials, Processing and Devices in III-V Compound semiconductors Symposium, USA, 1988.

[28] V.F. Korotov, N. Stanev, V.I. Khitko and A.M. Yanchenko
Sov.Phys - Tech. Phys. 35 (1990) 741.

[29] M. Godlewski and B. Monemar, J.Appl. Phys 64 (1988) 200

[30] M.O. Watanabe, Y. Ahizawa, N. Sugiyama and T. Nakanisi. Proc. of the 13th International Symposium on Gallium arsenide and related compounds, USA, 1986, P. 105.

[31] M. Abraham and V. Halpern, Philos, Mag B. Phys. Condens. Matter Electron Opt. Magn, Prop. 62 (1990) 537.

2 METHODS OF THIN FILM PREPARATION

2.1 INTRODUCTION

A solid material is said to be in thin film form when it is built up, as a thin layer on a solid support, called substrate by controlled condensation of the individual atomic, molecular, or ionic species. With the development of new materials, improved preparation methods and close control of the preparation parameters, thin films can be prepared with desired and reproducible properties and are expected to play an important role in the study of a variety of solid state phenomena of basic and practical interest. Depending on whether the vapour species has been created by a physical process or by a chemical, the methods may be divided into two main groups, namely physical methods and chemical methods. The various methods of film preparation are treated in the literature [1-8].

In this chapter is presented an account of the technological aspects of different preparation methods currently employed . The preparation of thin films from chemical methods is discussed in detail.

2.2 PHYSICAL METHODS

2.2.1 Physical Vapour Deposition (PVD)

The most important physical methods for the preparation of thin films are sputtering and evaporation. The preparation of thin films by physical vapour deposition methods has been described by Reichelt and Jiang [9].

2.2.1.1 Sputtering

When a solid surface is bombarded with energetic particles, the surface atoms are removed due to the collision between surface atoms and the energetic particles. This phenomenon is known as sputtering and the sputtered species can be condensed onto a substrate to form a thin film. The sputtering process is best suited for depositing adherent films of refractory materials. Chambers et al [10] reported the sputter deposition of aluminium and other alloys at cryogenic temperatures. Sputter deposition of Fe films in a high pressure atmosphere has been reported by Ishii [11]. There are various types of sputtering depending upon the method used to reject the atoms or molecules. These are briefly described in the following sections.

(a) Glow-Discharge Sputtering

This versatile, readily controllable process is widely used for the deposition of films, primarily polycrystalline films. In a glow discharge system, the material to be sputtered is used as a cathode and the substrates are placed on the anode. Glow discharge is created by applying a dc voltage of 1-5KV between the cathode and the anode seperated by about 5 cm, with a current density $\sim$ 1-10mA cm^{-2}. The glow discharge between the two electrodes gives the energetic ions that are needed for the ejection of atoms. Chaudhuri et al [12] reported the results obtained from the studies on the indium tin oxide films produced by DC sputtering of In-Sn alloy target in argon + oxygen plasma.

(b) Bias sputtering

In this arrangement, the substrate is biased at a negative potential relative to the anode, so that it is subjected to steady ion-bombardment throughout the growth.

(c) Asymmetric ac sputtering

This method is in essence similar to the preceding one. Altering rather than direct voltage is applied between the cathode and the substrate, so that the electrodes are consecutively bombarded by ions in alternate half cycles. Bombarding the substrate during the half cycle when the cathode is negative removes the adsorbed gases and thus yields a purer film.

(d) Ion plating

In this case, the deposition is actually obtained by vacuum evaporation from a filament. The substrate is kept at the cathode, so that the film is simultaneously sputter-cleaned by ion bombardment to give compact and adherent films. This technique suffers from the disadvantage of trapping of energetic gas ions in the system. A number of experimental results obtained with low voltage reactive ion plating deposition are briefly reviewed [13].

(e) Getter sputtering

In this arrangement, two cathodes of the material to be sputtered are symmetrically located with respect to the anode. A secondary enclosure within the main vacuum system is employed. After sputtering for a few minutes, the sputtered material from the second cathode is allowed to deposit on the substrate.

(f) Triode sputtering

In this configuration, electrons are injected into the discharge by thermionically emitted from a filament. A secondary electron gun is used to increase the concentration of ionizing electron. The sputtering process may further be enhanced by the presence of a magnetic field inclined to the lines of force between the cathode and anode.

(g) R.F. sputtering

Sputtering at low pressures (10^{-3} Torr) is also possible by enhancing gas ionization with the help of an inductively coupled external RF field. It is an indispensable technique for deposition of thin films of semiconductors and insulators. Sarsembinov et al [14] reported the studies on As_2Se_3 films prepared by RF sputtering. Epitaxial growth of ZnTe on GaSb (100) by RF sputtering is also reviewed [15].

(h) Magnetron sputtering

One convenient method of increasing the ionization efficiency of electrons is by increasing their path lengths by applying a transverse magnetic field normal to the electric field. The high deposition rates coupled with the fact that the film is not subjected to plasma and electron bombardment makes magnetron sputtering a very attractive technique for large-area, low temperature deposition. The preparation of thin films by magnetron sputtering technique has been reviewed by several authors [16-21].

(i) Reactive sputtering

This method can be utilized to form compound films, primarily oxides, nitrides and carbides. Reactive sputtering is achieved either by reaction at the cathode, followed by transport of the resulting compound to the substrate or by reaction of the background gas with the growing film.

The preparation and characterization of reactively sputtered SiCxNy film have been reported by Komatsu et al. [22]. Larsson et al [23] pointed out that, reactive sputtering is an attractive method for preparing compound films like nitrides and oxides. Klein et al.[24] presented a review of the reactive DC sputtering of Cu-O films.

(j) Ion beam sputtering

Sputter deposition under controlled high vacuum conditions can be achieved by using an ion beam source. Using this technique metal semiconductor or insulator targets can be sputtered. Varitimos and Tustison [25] reported the deposition of ZnS thin films by Ion beam sputtering.

2.2.1.2. Vacuum evaporation

It is a very promising technique to evaporate a large variety of materials (metals, semiconductors, dielectrics). As the name implies, the technique consists of vaporization of the solid material by heating it to sufficiently high temperature and condensing it onto a cooler substrate to form a film.

According to the Langmuir-Dushman theory of the kinetics of evaporation, the rate of free evaporation of atoms or molecules

from a clean surface of unit area in vacuum is given by

$$Ne = 3.513 \times 10^{22} \, Pe/ (MT)^{\frac{1}{2}} \, [\text{molecules } cm^{-2}S^{-1}] \qquad (2.1)$$

where Pe is the equilibrium vapour pressure (in Torr) of the evaporant under saturated vapour conditions at a temperature T and M is the molecular weight of the vapour species. The vapour atoms thus created are transported through vacuum to get deposited on the substrate surface to form a thin film.

For the ideal case of deposition from a clean and uniformly emitting point source onto a plane substrate, the rate of deposition varies as $\cos \theta/r^2$ (Knudsen Cosines' Law) where θ is the angle between the radial vector and the normal to the substrate plane and r is the radial distance of the receiver from the source. Thin films of GaP were evaporated into glass substrates at various substrate temperatures under vacuum [26].

Thermal evaporation of materials may be achieved by variety of methods.

(a) Reactive evaporation

By allowing a chemical reaction between vapour species of different elements either during their transport from source to substrate or on the substrate surface itself, it is possible to condense films of a great variety of alloys and compounds. Thin films of amorphous germanium-carbon and germanium-nitrogen alloys were prepared by activated reactive evaporation[27].

(b) Resistive heating

The material to be evaporated may be heated directly or indirectly. The simplest method is to support the material in a filament or a boat which is heated electrically. The materials can be heated indirectly by supporting them in crucibles of quartz, graphite, alumina, zirconia and they are heated with the heater windings.

(c) Coevaporation

Thin films of multicomponent materials such as alloys and compounds which are difficult to vaporize either because of very high vaporization temperature or because of problems associated with dissociation/decomposition can be prepared by simultaneous condensation of the vapours of the individual compondents produced from separately controlled sources. This type of PVD process is known as coevaporation. Chromik et al. [28] prepared highly oriented YBa_2 Cu_3O_7 thin films by vacuum co-evaporation.

(d) Flash evaporation

This technique is applicable for evaporation of alloys, metal-dielectric mixtures and compounds. In flash evaporation, small amounts of the material are continuously dropped into the heated source with the help of a mechanical or ultrasonic vibrator and evaporated discretely to completion. Polycrystalline thin films of $CuInTe_2$ were prepared by flash evaporation [29].

(e) Arc evaporation

Materials can be evaporated using very high temperatures by striking an arc between the two electrodes. This technique is widely

used for the evaporation of refractory materials such as Nb and Ta.

(f) Laser evaporation

A material can be evaporated from its surface by keeping the laser source outside the vacuum system and focussing a laser beam onto the surface of the material.

(g) Electron beam evaporation

In electron beam evaporation, the temperature of the evaporant material can be raised by electron bombardment. An electron beam is accelerated through a potential of 5 to 10KV and focussed on the material. The temperature at the focussed spot can become as high as 3000°C. At such a high temperature, most of the refractory metals and compounds can be evaporated.

Basu and Avadhani [30] deposited semiconducting iron silicide films by electron beam evaporation of iron and subsequent furnace reaction at 850°C for two hours.

2.2.1.3 Molecular beam epitaxy (MBE)

As the name implies, MBE involves growth of epitaxial films by condensation of one or more controllably directed atomic or molecular beams each emerging from a point source in ultra high vacuum system. It is particularly important for epitaxial growth studies of multicomponent materials such as II-VI and III-V compound semiconductors.

Studies on molecular beam eptaxial GaAs sample have been reported by Stanley et al [31]. Hoke et al. [32] studied the carbon doping of GaAs film grown by conventional molecular beam epitaxy

Liu et al. [33] reported the behaviour of layer growth in GaAs by molecular beam epitaxy. Electrical properties of InAs epilayers grown by molecular beam epitaxy on Si substrates were also investigated [34]. Feng et al. [35] characterized the shallow native traps in n-type GaAlAs layers grown by molecular beam epitaxy. Baribeau et al [36] studied the epitaxial growth of Ge on (100) Si by molecular beam epitaxy. Selective epitaxial growth of InAs on GaAs by molecular beam epitaxy was reported by Okamoto and Ohata [37]. Komiyama et al [38] carried out the preparation of highly ordered ultra thin films of Copper (II) Phthalocyanine on amorphous substrates by molecular beam deposition.

2.3 CHEMICAL METHODS

The foremost characteristic of chemical methods is that it necessarily involves a chemical reaction for the formation of the thin film without requiring vacuum as an essential condition for deposition. Chemical deposition techniques are the most important methods for the growth of films owing to their versatality for depositing a very large number of elements and compounds at relatively low temperatures. Chemical methods may be broadly classified into two categories: chemical vapour deposition and solution deposition techniques.

2.3.1 Chemical vapour deposition (CVD)

In this case, when a volatile compound of the substance to be deposited is vaporized and the vapour is thermally decomposed or reacted with other gases, vapours or liquids at the substrate to

yield non-volatile reaction products which deposit atomistically on the substrate. CVD techniques have been used for deposition of epitaxial, polycrystalline as well as amorphous films. Kanoh et al [39] have studied on silicon thin films prepared by CVD method. Siefering and Griffin [40] reported the chemical vapour deposition of vanadium oxide thin films.

The various chemical reactions involved in CVD are as follows:

(a) Pyrolysis (Thermal decomposition)

The organometallic compounds, halides and metal hydrides can be pyrolytically decomposed on hot substrates to yield pure elemental deposits. Pyrolysis of Silane (SiH_4) and Germane (GeH_4) is employed to produce epitaxial layers of Si and Ge.

A typical example of a decomposition process is

$$SiH_4 \text{ (gas)} \xrightarrow{800\text{-}1300^\circ C} Si + 2H_2 \text{ (gas)} \qquad (2.2)$$

(b) Hydrogen reduction

Hydrogen reduction is a pyrolysis reaction which is facilitated by the removal of one or more of the gaseous products of decomposition. Hydrogen reduction of silicon tetrachloride is frequently used for depositing silicon films.

The reaction is of the form

$$SiCl_4 \text{ (gas)} + 2H_2 \text{ (gas)} \longrightarrow Si \text{ (solid)} + 4HCl \text{ (gas)} \qquad (2.3)$$

(c) Chemical transport

The chemical transport technique involves the transfer of a relatively nonvolatile material from the source to the substrate with

the help of a highly volatile chemical vapour which convert it to a volatile compound by a chemical reaction. The volatile compound then decomposes on the substrate to yield a film of the source material.

A typical example is the transport of Si in I_2 vapours

$$Si\ (Solid) + 2I_2\ (gas) \xrightarrow{1100°C} SiI_4\ (gas) \qquad (2.4)$$

$$Si\ (Solid) + SiI_4\ (gas) \xrightarrow{1100°C} 2SiI_2\ (gas) \qquad (2.5)$$

$$2SiI_2\ (gas) \xrightarrow{900°C} Si\ (Solid) + SiI_4\ (gas) \qquad (2.6)$$

(d) Polymerization

As the name implies, polymerization involves linking together of monomeric molecules of organic and organic-inorganic composites by the activation processes of electron or ion bombardment, irradiation with light, x-rays or γ-rays or electrical discharge.

(e) Close-spaced vapour transport

In this technique, a temperature gradient is maintained between the closely spaced source and substrate. A gas is used to react with the source to form a volatile compound that is subsequently deposited at the surface of the substrate to form a thin film. Epitaxial films of CdTe and GaAs have been obtained using water vapour as the transporting agent. Murali [41] has grown Zn_3P_2 thin films using this technique.

(f) Plasma deposition

This is essentially a plasma-assisted CVD technique in which glow-discharge plasma is used to break the vapours up into different species that react to deposit as a film. Ozaki and Nishiyama [42]

have prepared carbon films by plasma decomposition of propylene. Complex polymer films can also be prepared by this technique [43].

2.3.2 Solution deposition technique

In these techniques, the unit species of the material to be deposited are dispersed in a liquid medium (generally aqueous). The solution deposition techniques may be classified into electro-chemical deposition (ECD) and chemical solution deposition (CSD) according to the formation of deposit material by electrochemical and/or chemical reactions. Some advantages of solution deposition technique include

1. Experimental set ups are much less sophisticated compared to those in vapour deposition techniques
2. No expensive equipment is required for deposition
3. Deposition can be carried out at much lower temperatures

2.3.2.1 Electrochemical deposition (ECD)

This technique involves electrochemical reactions ie. chemical reactions necessarily involving interaction with an external source of electric current. This may also require electrically conductive substrates. CdTe thin films have been deposited by an electrochemical technique from organic dimethyl Sulfoxide Solvent containing $CdCl_2$ and elemental Te [44].

(a) Electro deposition

Electrodeposition is a process of depositing a substance upon an electrode by electrolysis. Almost all the metals, except for highly electronegative ions can be electrodeposited from aqueous solutions.

Popov et al [45] observed the electrode surface coarsening in Copper electro deposition. Chao-Peng-Chen and Jacob Jorne [46] proposed a simple method for the determination of the fractal dimension during the electro deposition of zinc by current integration.

(b) Anodization

The metal to be anodized is made an anode in an oxygen containing electrolyte so that when an electric current is passed through the electrolyte, the anode surface is converted to one of its compounds. Anodization is used mainly in the formation of films of the oxides of certain metals including Al, Ta, Nb, Ti and Zr.

(c) Electrophoretic deposition

In this technique, electrically charged particles suspended in a liquid medium are deposited on an electrode by the application of an electric field. The technique has been used for deposition of both conductors and non-conductors including metals, alloys, salts, oxides, refractory compounds, polymers and combinations of the various components.

2.3.2.2. Chemical solution deposition (CSD)

These techniques are generally immersion techniques in the sense that they involve simply dipping of the substrate into the reaction mixture for sometime. Advantages of CSD techniques when compared to ECD techniques are, (1) since the question of non uniform current density does not arise in CSD, deposits are formed more uniformly even on complex parts (2) deposits can be laid down on insulators and (3) no power supplies and contacts are needed

(4) Experimental set ups are much less sophisticated compared to other methods. (5) No expensive equipment is required for deposition. (6) deposition can be carried out in much lower temperatures. Preparation and characterization of chemically deposited tin (II) Sulphide thin films has been reported by Pramanik et al [47].

CSD techniques can be classified as follows according to the chemical reaction involved in deposition.

(a) Autocatalytic reduction/Electroless plating

In contrast to electrodeposition, the electroless technique also involves the reduction of metal ions to form the deposits, but no external potential source is required to produce electrons. This technique has been employed to deposit Ni, Co and Pd films. Osaka et al [48] described the behaviour of the electroless composite films plated from a Ni-P bath with metallic dispersion of Zr and Nb powders.

(b) Homogeneous precipitation and solution growth

For depositing thin films of a compound M_mX_n a solution of M^{+n} ions with a complexing agent added to it is prepared. Formation of complex ions is essential to control the reaction and avoid immediately precipitation of the compound in the solution when the precipitating anions are added to it. Complexation of the metal ions also avoids the precipitation of hydroxides in the solutions, thus making film deposition possible. This technique has been used for deposition of II-VI and IV-VI compound semiconductor films.

(c) Conversion coatings

The coating is formed by chemical treatment of a metallic substrate surface which is converted into one of its compounds.

2.3.3 Spray pyrolysis

Spray pyrolysis offers a number of advantages, the main ones being its simplicity and the capability to produce large areas of high sensitive films of uniform thickness. Doping of the semiconductor film is simple, since it is accomplished by mere addition of the dopant to the spray solution. Arya and Hintermann [49] have deposited Y-Ba-Cu-O superconducting thin films by spray pyrolysis method. The preparation of cadmium telluride films using this method has also been reported [50].

The starting materials required to form the desired semiconductor are taken in solution and the composition is sprayed on a heated substrate at an elevated temperature. The sprayed droplets on coming into contact with the hot substrate dissociates and the desired semiconductor film results. The other volatile by-products and the excess solvent escape in the vapour phase. The atomization of the chemical solution into a spray of fine droplets is affected by the spray nozzle with help of compressed air as carrier gas. The carrier gas and the solution are fed into the spray nozzle at a predetermined flow rate. The geometry of the gas and liquid nozzle largely determine the spray pattern, the size distribution of droplets and the spray rate. When both the size and momentum of the spray droplets are uniform optically good quality smooth adherent films are obtained. Amorphous to polycrystalline deposits are obtained depending upon the droplet mobilities and chemical reactivitors of various constituents.

Growth of films by spray pyrolysis is determined by (1) nature of the substrate and (2) chemical nature and concentration of

the spray solution and its additives and (3) spray parameters. Substrate surfaces get affected in the spray process and the choice is limited to glass, quartz, ceramics or oxide, nitride or carbide coated substrates. On thermal decomposition, chemicals in solution form must provide the species complexes that will undergo a thermally activated chemical reaction to yield the desired thin film material and the remainder of the constituents of the chemicals including the carrier liquid, should be volatile at the spray temperature. The composition of the film is expected to depend on the kinetics of the spray process and the thermo-dynamics of the pyrolytic processes. Stoichiometric sulphide and selenide films have been obtained under appropriate conditions. The properties of the film depend upon the substrate temperature, anion-to-cation ratio, spray rate etc. Also if the pyrolytic reactions have not been completed at low temperatures, some by products or intermediate compounds will be trapped as impurities in the film. In the case of chloride salts, residual chlorine is often present in films.

2.4 REFERENCES

[1] K.L. Chopra, Thin Film Phenomena (Mc Graw Hill, New York, 1969).

[2] L.Holland, Vacuum Deposition of Thin Films (Wiley, New York, 1961).

[3] R.W. Berry, P.M. Hall and M.T. Harris, Thin Film Technology (Van Nostrand Reinhold, New York, 1968).

[4] L.I. Maissel and R. Glang, Hand Book of Thin Film Technology, (Mc Graw Hill, New York,1970).

[5] J.C. Anderson, The use of Thin Films in Physical Investigations, (Academic Press, London, 1966).

[6] C.H.S. Dupuy and A. Cachard, Physics of Non metallic Thin Films, (Plenum Press, New York,1976).

[7] K.L. Chopra and L.K. Malhotra, Thin Films Technology and Applications (Tata Mc Graw Hill, New Delhi, 1985).

[8] K.L. Chopra and I.Kaur, Thin Film Device Applications, (Plenum Press, New York, 1983).

[9] K. Reichelt, X. Jiang, Thin Solid Films, 191 (1990) 91.

[10] D.L. Chambers, C.T. Wan, G.T. Susi and K.A. Taylor, J.Vac. Sci. Technol. A, Vac. Surf. Films, 7 (1989) 1305.

[11] K. Ishii, Jpn. J. Appl. Phys. Part 2, 26 (1987) L 932.

[12] S. Chaudhuri, S. Ghosh, A. Sarkar and A.K. Pal, Indian J.Phys. A, 63A (1989) 336.

[13] K.H. Guenther, Proc. SPIE-Int. Soc. Opt. Eng. 1270 (1990) 211.

[14] Sh. Sarsembinov, O.Yu. Prikhodko, M.Zh.Mal'tekbasov, S.A. Dzhakeloy, S.Ya. Maksimova and V.L. Averyanov, Sov. Tech, Phys. Lett. 16 (1990) 462.

[15] Y.Tokumitsu, A. Kawabuchi, H.Kitayama, T. Imura, Y.Osaka and F.Nishiyama, J. Appl. Phys. 66 (1989) 896.

[16] T.Matsuoka, T. Kuwata, M. Nishikawa, Y. Fujita, T. Tohda and A.Abe, Jpn. J.Appl. Phys. I. Regul, Pap. Short Notes 27 (1988) 1088.

[17] R.E.I.Schropp and A. Madan. J.Appl. Phys. 66 (1989). 2027.

[18] S.N.Qiu, C.X. Qiu and I. Shih, Mater. Lett. 5 (1987). 263.

[19] R.Bichsel, J.Phys. D. 19 (1986) 1575.

[20] J.B. Webb, Chemtronics, 2 (1987) 3.

[21] R.Luthier and F.Levy, J.Vac.Sci Technol.A, Vac. Surf. Films 9 (1991) 102.

[22] S.Komatsu, Y. Hirohata, S. Fukuda, T. Hino, T. Yamashina, T. Hata and K. Kusakabe, Thin Solid Films,193 (1990) 917.

[23] T. Larsson, H. O. Blom, C. Nender and S. Berg, J.Vac, Sci. Technol.A, Vac. Surf. Films, 6 (1988) 1832.

[24] W. Klein, H. Schmitt and M. Bottgen, Thin Solid Films, 191 (1990) 247.

[25] T.E.Varitimos and R.W.Tustison, Thin Solid Films, 151 (1987) 27.

[26] K.R. Murali and B.S.V.Gopalam, Surf. & Coatings Technol, 30 (1987) 327.

[27] S.Kumar and H.J. Trodahl, Thin Solid Films,193 (1990) 72.

[28] S. Chromik, V. Strbik, F. Hanic, V.Smatko, R.Adam and S. Benacka, Physica B, 165 (1990) 1493.

[29] W. Horig and H. Neumann, Cryst. Res. Technol. 24 (1989) 823.

[30] S. Basu and V.L.N. Avadhani, Indian J. Phys. A. 63A (1989) 434.

[31] C.R.Stanley, M.C. Holland, A.H.Kean, M.B. Stanaway, R.T. Grimes and J.M. Chamberlan, Appl. Phys. Lett, 58 (1991) 478.

[32] W.E.Hoke, P.J. Lemonias, D.G.Weir, H.T. Hendriks, and G.S. Jackson, J. Appl. Phys. 69 (1991) 511.

[33] D.G. Liu, C.P. Lee, K.H. Chang, J.S. Wu and D.C. Liou, Appl. Phys. Lett. 57 (1990) 1392.

[34] S. Kalem, J. Chyi, C.W. Litton and H.Morkoc, Appl. Phys. Lett, 53 (1988) 562.

[35] S.L. Feng, M. Zazoui and J.C. Bourgoin, Appl. Phys. Lett, 55 (1989) 68.

[36] J.M. Baribeau , D.C. Houghton, T.E. Jackman and J.P.Mc Caffrey, J. Electrochem. Soc. 136 (1989) 1158.

[37] A. Okamoto and K. Ohata, Jpn, J. Appl. Phys. Part 2, 26 (1987) L 1174.

[38] M. Komiyama, Y. Sakakibara and H. Hirai, Thin Solid Films , 151 (1987) L 109.

[39] H. Kanoh, O. Sugiura, P.A. Breddels and M. Matsumura, Jpn. J.Appl. Phys. I, Regul. Pap. Short Notes, 29 (1990) 2358.

[40] K.L. Siefering and G.L. Griffin, J. Electrochem Soc. 136 (1989) 897.

[41] K.R. Murali, Mater. Sci & Eng., 92 (1987) 193.

[42] J. Ozaki and Y. Nizhiyama, J. Appl. Phys. 69 (1991) 324.

[43] H.K. Lintz, S.R. Murrell, R.L. Crawley and J.C. Daukas, J.Vac. Sci. Technol. A, Vac. Surf. Films, 6 (1988) 1869.

[44] A.C. Rastogi and K.S.Balakrishnan, J. Electrochem. Soc. 136 (1989) 1502.

[45] K.J. Popov, M.G. Pavlovic, L.J. Pavlovic, M.I.Cekerevac and G.Z. Removic, Surf. Coat. Technol. 34 (1988) 355.

[46] Chao-Peng Chen and Jacob Jorne, J. Electrochem Soc. 137 (1990) 2047.

[47] P.Pramanik, P.K. Basu and S. Biswas, Thin Solid Films, 150 (1987) 269.

[48] T.Osaka, I. Koiwa, M.Usuda, K. Arai and I. Saito, J. Electrochem. Soc. 136 (1989) 1124.

[49] S.P.S.Arya and H.E. Hintermann, Thin Solid Films ,193 (1990) 841.

[50] A. Banerjee, H. Saha and R. Guha, Indian J. Phys. A 63A (1989) 326.

3 ELECTRICAL PROPERTIES OF SEMICONDUCTORS

3.1 INTRODUCTION

The impurity states play an important role in the kinetics of the capture and release of free carriers from trap levels and the recombination of these carriers in Semiconductors. The investigation of the electrical properties gives valuable information of the above phenomena in semiconducting materials. The aim of this chapter is to provide a brief summary on the mechanism of electrical conduction, photoconductivity, lifetime and thermally stimulated processes.

3.2 MECHANISM OF ELECTRICAL CONDUCTION

Lattice defects profoundly affect the electrical behaviour under certain conditions of defect concentration and temperature. Acceptor and donor impurity atoms also account for the extrinsic semiconducting properties. The Mechanism of electrical conductivity was discussed by several authors [1-4]. When an electron is thermally excited from the valence band to the conduction band the vacant sites left behind in the valence band are called 'holes'. The electrical conduction in an ideal semiconductor consists of motion of electrons in the conduction band under the influence of an electric field and holes in the valence band. Thus the basic idea of electrical conduction in a semiconducter is that electrons occupying donor levels (or holes occupying acceptor levels) may contribute to the electrical conductivity in a manner other than the usual process of thermal excitation followed by band conduction.

The transport of carriers under the influence of an applied electric field produces a current I.

The resistivity ρ is given by

$$E = \rho J \tag{3.1}$$

Where E is the electric field intensity and J is the current density. The conductivity σ is the reciprocal of resistivity.

$$J = \sigma E \tag{3.2}$$

The current density can be expressed as

$$J = enV_d \tag{3.3}$$

where n is the carrier density, e is the carrier charge and V_d is the drift velocity.

Substituting $V_d = \mu E$ into equation (3.3), equating (3.3) and (3.2) and solving for conductivity leads to

$$\sigma = e \mu n \tag{3.4}$$

From the expression for conductivity,

$$\text{electron conductivity } \sigma_n = e_n \mu_n n \tag{3.5}$$

$$\text{and hole conductivity } \sigma_p = e_p \mu_p p \tag{3.6}$$

The total conductivity of the semiconductor must be expressed by

$$\sigma_s = \sigma_n + \sigma_p . \tag{3.7}$$

Often either n or p dominates, and one of the terms on the right hand side of equation (3.7) may be neglected.

The conduction mechanism can be determined by measuring the variation of current in a semiconductor with temperature. The conductivity of a semiconductor depends on two factors: (1) the number of current carriers per unit volume and (ii) the mobility of the carriers through the substance under an applied electric field. As the temperature is increased from absolute zero, the electrons in the defect level get excited to the conduction band or to the valence band in the case of holes and contributes to the conduction. This process continues until all the defect levels are enhausted. The conductivity may decrease with further increase of temperature due to the decrease in mobility of the charge carriers. At still high temperatures, the excitation of electrons from the valence band to the conduction band takes place and yields to intrinsic conduction.

The exponential variation of conductivity for intrinsic semiconductors with temperature is given by

$$\sigma = \sigma_0 \exp\left(\frac{-\epsilon}{2kT}\right) \tag{3.8}$$

for extrinsic semiconductors,

$$\sigma = \sigma_0 \exp\left(\frac{-\epsilon}{kT}\right) \tag{3.9}$$

where σ_0 is a constant, k is the Boltzmann's constant, T the

absolute temperature and ϵ is the activation energy of charge carriers. The exponential increase in conductivity with temperature is connected with the activation energy required for the thermal motion of charge carriers. The value of the activation energy for the donor level can be evaluated from the slope of the conductivity versus temperature curve. The slope of the intrinsic region of this curve represents the activation energy required for an electron to go from the valence band to the conduction band which gives the band gap of the material.

Considerable interest has been stimulated in the study of electrical properties of several materials [5-13]. Sadaoka et al [14] described the effect of heat treatment on the electrical conductance of lead phthalocyanine films. The electrical properties of polycrystalline $ZnIn_2Te_4$ thin films such as electrical resistivity and activation energy have been investigated by Patel and Ali [15]. Weclewicz and Zdanowicz [16] reported the electrical properties of amorphous cadmium arsenide films prepared by thermal vacuum deposition. Dudas et al [17] studied the temperature dependence of the electrical resistance of thulium thin films in the temperature range from 4.2 K to 300 K. Electrical conductivity of polypyrrole films has been investigated by Kuwabata et al [18, 19].

The measurement of electrical conductivity of thin films during heat treatment can give important information regarding the defect structure and density of defects present in as grown films and can

also throw light on the changes that takes place during the annealing processes in the films.

The influence of annealing on the electrical properties and uniformity of LEC undoped semiinsulating Ga As wafers has been investigated by Haizhou et al [20]. Saxena and Mathur [21] reported the effect of annealing on the conduction mechanism of n-type silicon. Saito et al [22] studied the effect of annealing on the resistivity of phosphorous doped polycrystalline silicon films.

The conductvity technique provides an important tool for the determination of activation energies and hence this study can yield the information regarding the defect levels as well as the band gap in solids.

3.3 PHOTOCONDUCTIVITY

It has been observed that the surface can influence the current induced in a semiconducting material by a beam of light. The surface composition and structure are changed and such effects are best observed with a photoconductive method which is very sensitive. Photo current variations associated with surface modifications may be due to the changes in the number of free carriers excited from surface states and changes in the 'roughness' of the surface.

An excellent account of the theoretical and experimental aspects on photoconductivity has been reviewed by Rube [23], Smith [24], Kireev [25], Boer [26] and Moss [27].

Semiconductors that show strong photo conductivity are called photoconductors. Photoconductive materials are classified into two types. (i) iodiochromatic materials (intrinsic photo conductors) are those which show photoconductivity when in a pure condition which being associated with the intrinsic properties of the material (ii) allochromatic materials (impurity or imperfection photoconductors) are those in which the photo conductivity is associated with impurities or crystal imperfections such as vacancies. With excitation from the valence to the conduction bands, the photoconductivity is termed intrinsic photoconductivity ie, it involves only electrons and holes in the conduction and valence bands. With excitation involving levels in the band gap, it is called extrinsic photoconductivity. The conductivity σ_d due to equilibrium carriers is termed dark current conductivity.

The incoming radiant energy causes the appearances of nonequilibrium carriers. Using equation (3.7) the photoconductivity can be expressed as

$$\sigma_{pc} = en\mu_n \delta n + e_p \mu_p \delta p \qquad (3.10)$$

The total conductivity may be represented in the form of a sum of dark and light conductivities.

$$\sigma = \sigma_d + \sigma_{pc} \qquad (3.11)$$

$$\sigma = en\ \mu_n\ (n+\ \delta n)\ + e_p\ \mu_p\ (\ p+\ \delta p\ ) \qquad (3.12)$$

Schildkraut [28] described about electro-optic polymer films that exhibit photoconductivity. Absorption of light by the sensitizer resulted

in a photocurrent and charge trapping. The temperature dependance of the transient photoconductive response in trans-polyacetylene films have been studied by Walser et al [29]. Maan et al [30] investigated the temperature dependence of steady state photocurrent and dark current in thin films of a-$In_{20}Se_{80}$ and reported that both dark and photoconductivity are found to be activated processes. Photo excitations and photoconduction in highly oriented poly acetylene has been reported by Tubino et al [31]. Werner et al [32] studied the transient photoconductivity in GaAs films grown by molecular beam epitaxy. The room temperature photoconductivity in ZnP_2 single crystals was observed by Misiewicz [33]. Photoconductivity spectra of Ga_2Se_3 : Co^{2+} single crystals grown by the Bridgemann technique were investigated over the temperature range 19-300K by Jeong et al [34]. Mirianashvili et al [35] investigated the photo conductivity of P-type InSb samples. Kirilyuk et al [36] observed photoconductivity in YBaCuO films near the semiconductor-superconductor transition.

Several parameters involved in photoconduction mechanisms are photosensitivity, specifice sensitivity or photoresponse, photoconductivity gain, lifetime, capture cross section, etc.

(i) Photosensitivity: it is the photoconductivity per unit excitation intensity.

(ii) Specific sensitivity: It is obtained by multiplying the photoconductance by the square of the electrode spacing and dividing by the absorbed radiation power.

(iii) Photoconductivity gain: For a semiconductor in which one carrier conductivity dominates, the gain may be expressed as

$$\text{Gain} = \frac{\tau}{\tau_r} \tag{3.13}$$

Where τ is the lifetime of a free carrier and τ_r is the transit time of this carrier.

(iv) Life time: The lifetime of photoexcited carriers is the key parameter for an understanding of photoconductivity.

If light falling on a photoconductor creates f electron hole pairs per second per unit volume of the photoconductivity then

$$f\,\tau_n = \delta n \text{ and } f\,\tau_p = \delta p \tag{3.14}$$

Where τ_n is the free lifetime of an electron, τ_p is the free lifetime of a hole and δn and δp are respectively the additional free electron and hole densities present as a result of the absorption of light.

(v) Capture cross section: If there are N recombination centers per unit volume which can capture a free carrier, the life time may be expressed as

$$\tau = (vSN)^{-1} \tag{3.15}$$

where v is the thermal velocity of the carrier and S is the capture cross section of the recombination center for that type of charge carrier.

The spectral response curves of photoconductivity shows a fairly sharp maximum at a wavelength slightly longer than that corresponds to the absorption edge.

If E_I is the ionization energy in electron volts, the relationship between E_I and the threshold wavelength λ^* in microns may be expressed as

$$E_I = (h\nu^*)_I = \frac{hc}{\lambda^*} = \frac{1.239}{\lambda^*} \qquad (3.16)$$

The modern investigation of photoconductivity has benefited greatly from the recent rapid growth of interest in all phases of solid state physics and chemistry. Many of the characteristics of a semiconductor material which determine its sensitivity to radiation are associated with imperfection in the material. Therefore the field of photoconductivity has been considerably enriched by the studies on kinetics of trap levels. Photoconductivity provides an important means of detecting light or measuring light transmitted signals. It illuminates the internal electronic processes in semiconductor materials and in their device forms: transistors and phosphors. The use of photoconductivity as a powerful tool in the understanding of solids is perhaps better known than that its growing importance on devices.

3.4 LIFETIME

In recent years, an appreciable part of the work in the semiconductor field has been devoted to the investigation of the lifetime

of excess holes and electrons. Many methods of measuring lifetime were devised to test and control the semiconductor material in the various stages of processing. There has also been interest and consequent growth in the understanding of the physical processes determining recombination of holes and electrons.

In nonequilibrium situations, produced by external excitations, the concentration of holes and electrons are generally changed both in the valence and conduction bands and in localized defect levels in the forbidden gap. Preservation of neutrality requires that the total of free and bound hole and electron excess concentrations be equal. To consider the processes that tend to establish equilibrium, suppose that a flash of excitation initially establish an equal excess of free holes and electrons. Subsequently these free carriers may disappear in pairs by transition across the gap, or they may fall into the localized levels. If the net rates of fall-in are equal for both type of carriers, then the occupation of the levels remains unchanged on the average. In both of the above cases, the excess concentration of free holes and electron, remain equal. The net fall-in rates are not equal, a situation which results in a change of occupation of the levels and inequality in free excess carriers concentration. In this case, some of the carriers of one type have been trapped.

Lifetime is defined by

$$U = \frac{\Delta p}{\tau} \qquad (3.17)$$

where U is the net rate of recombination per unit volume and $\Delta p = p - p_o = n - n_o$ is the excess concentration of holes or electrons.

Lifetime can be controlled by controlling the density of deep level traps in the semiconductor material or on its surface. The major difficulty lies in the fact that there is a great variety of imperfections and impurities which are capable of providing trapping centres. The imperfection in a semiconductor is expected to decrease the free carrier lifetime and hence the photoconductivity. Samaj [37] studied the lifetime of minority carriers in polycrystalline semiconductors. Spirito et al [38] reported the lifetime studies in thin Si epitaxial layers. The control of minority carrier life time in n-type silicon by means of low dose, high-energy proton irradiation at room temperature has been investigated by Huppi [39]. Fastow [40] have measured the transient and steady state excess carrier lifetime in p-type HgCdTe as a function of temperature . Lin et al [41] determined the minority carrier life time in annealed silicon. The effect of annealing temperature and cooling rate on the lifetime of minority charge carriers in silicon crystals has been investigated by Baranskii [42]. Haegel et al [43] measured the free carrier lifetime in as grown and a series of annealed samples of semi insulating gallium arsenide.

3.4.1 Methods of measuring lifetime

Inorder to determine the carrier lifetime in a semiconductor, excess minority carriers must be created and detected. They can be created by irradiation by light or X-rays. To detect the excess minority carriers, photoconductivity and photomagnetoelectric effect can be used. Ryvkin[44] suggested that lifetime of carriers can be determined from the photoconductivity measurements. The monochromatized beam of light illuminates the sample and the light beam was modulated by a mechanical chopper. The frequency of the square pulses of the modulated beam was varied and the corresponding photocurrent was measured till the saturation region

of the photocurrent sets in. If t_o is the period of illuminated pulse, the life time τ for minority charge carriers was calculated using the equation

$$\sigma_{AC} = \sigma_{St} \tan h\left(\frac{to}{2\tau}\right) \qquad (3.18)$$

where σ_{Ac} is the AC photoconductivity and σ_{St} is the steady state photoconductivity.

Lifetime is also measured by using photoinduced open circuit voltage decay technique [45]. This technique was used to determine the minority carrier lifetime in several single crystal silicon solar cells. Suzuki and Hayashi [46] reported the measurements of the minority carrier lifetime in a semiconductor wafer by a two mercury probe method and its application to surface recombination velocity. A simple evaluation technique of life time τ and diffussion coefficient of minority carriers in a semiconductor wafer by using the two mercury probe method and a graphical analysis was also described by Suzuki and Hayashi [47].

In the photoconductivity decay method, the sample is usually in the form of a rod, with current carrying electrodes at both ends. A short pulse of light illuminates the sample and hole-electron pairs are generated. When the light pulse is turned off, the carriers recombine towards their equilibrium concentrations. The corresponding voltage change is amplified and presented on the Oscilloscope. Any departure of the recombination from a simple experimental decay curve can readily be observed in this method of measuring lifetime. Fastow and Nemirovsky[48]

measured the excess carrier lifetime in p-type HgCdTe using the technique of photoconductive decay. Minority carrier lifetime measurement using a microwave photoconductivity decay method was examined by Nammori[49].

The principle of the photomagneto electric effect is that hole electron pairs are created at the upper surface of the material by non penetrating light. They diffiuse towards the opposite face while in an external magnetic field. The field seperates electrons and holes and creates a potential. This voltage is a sensitive measure of the surface recombination velocity which determines the concentration gradients and hence diffusion length in the material. Lifetime τ can be determined from this known value of diffusion length. The lifetime of free electrons and holes in solids are of great importance in the broad field of luminescence, photoconductivity and semiconductor devices. Lifetime has been found useful for determining the presence of special types of crystal imperfections which are usually present in such small concentrations that they cannot be detected by the conductivity measurements and are indeed quite difficult to determine by other means. Also a measure of lifetime permits the determination of ionization energy of imperfection centres.

3.5 THERMALLY STIMULATED PROCESSES

In a thermally stimulated process, the sample is heated in a controlled manner and a certain physical property is continuously measured. If the varying parameter is measured and recorded as a function of the sample temperature, the resulting curve may provide informatio concerning the process which takes place in the sample during heating.

Thus thermally stimulated process is used as standard methods of research and analysis in various branches of physics and chemistry. The thermally stumulated methods are thermally stimulated currents (TSC) and ionic thermo currents (ITC). The other methods are thermo-luminoscence (TL), thermally stimulated electron emission (TSEE), thermogravimety (TG) etc.

3.5.1 Ionic thermocurrent (ITC) Measurements

ITC method consists of the measurement of thermally activated release of polarization [50]. It is used for the investigation of the electrical properties of high resitivity solids via the study of thermal relaxation effects. This technique was first introduced and studied in great detail by Bucci and Fieschi [51]. It relies upon utilizing the response to an electric field of the dipole moment formed between a point defect and an impurity ion. Here the impurity ions and vacacies can be presented as individual defects independent of one another or they may be present as impurity vacancy (I-V) dipoles. A significant concentration of the paired impurity - vacancy defects can be oriented away from random orientations within a lattice by the application of a steady electric field. The resulting non-random orientation can be immobilised by freezing the sample to a low temperature with the electric field still applied. Upon removing the electric field and warming the specimen at a constant heating rate, the aligned defects relax and oriented back to random positions. In doing so, they produce burst of displacement current which can be monitored as a peak in a detected displacement current.

Bucci et al [51,52] studied ITC in ionic crystals due to dipole orientation. Denoted as ionic thermocurrent or ionic thermoconductivity method by Bucci and Fieschi, it also received a number of names due to the fact that it was reinitiated and developed by several investigators: Electret thermal analysis [53], thermally stimulated discharge (TSD) [54], thermal current spectra (TCS) [55], thermally stimulated depolarisation (TSD) [56,57] and thermally activated depolarisation (TAD) [58]. The ITC techniques have been applied to the study of many ionic and divalent compounds, semiconductors, polymers and dielectrics [59-78].

(a) The Bucci - Fieschi theory of ITC

In ionic solids dipoles may be formed when host ions are substituted by impurity ions of different charge. Charge compensation is usually achieved by lattice vacancies, interstitial host ions or impurity ions of other types. If the compensating charge is near the impurity ion, a dipolar complex is formed. In polymers ITC peaks appear at low temperatures as a result of the disorientation of polar group. When the polymer is heated to its softening temperature, the dipoles are disoriented by the motion of the main chain segments [79].

The time and temperature dependence of the dipolar polarization is determined by the competition between the orienting action of the field and randomizing action of thermal motions. The build up of polarization P in a unit volume of the material during the time τ after the

application of electric field E_p at a temperature T_p is described by an exponential function of time

$$P(t) = P_o [1-\exp (\frac{-t}{\tau})] \qquad (3.19)$$

The term τ is the time taken to polarize the I-V dipoles at temperature T_p. In equation (3.19), P_o is the maximum amount of polarization possible at temperature T_p and this for all but the lowest temperatures and very high fields has been shown to be

$$P_o = \frac{N_D \mu^2 E_p}{3 kT_p} \qquad (3.20)$$

where N_D is the concentration of dipoles present, k is the Boltzmann's constant, μ is the dipole moment, E_p is the polarizing field. Equation (3.19) describes the build up of polarization from $p(o) = o$ to $P (\infty) = P_o$. If the field is removed at $t = \infty$ then the polarization will decay according to

$$P (t) = P_o \exp (-t/\tau_R) \qquad (3.21)$$

where τ_R is the relaxation time for the dipoles at temperature T. In a crystalline solid, association of an impurity ion with a vacancy can form such a dipole which undergo re-orientation. Here , use the assumption that the time taken for these dipoles to depolarize at the same temperature.

The temperature variation of τ is given by the Arrhenius equation

$$\tau (T) = \tau_o \exp (\frac{E}{kT}) \qquad (3.22)$$

where τ_o^{-1} is the characteristic frequency factor for a vacancy jump from one lattice site to another for orientation of the I-V dipole and is independent of temperature and E is the activation energy for the rotation of a dipole. T is the absolute temperature and k is the Boltzmann's factor.

Equation (3.21) can be re-written as

$$p(t) = P_o \left[\exp\left(-\int_0^t dt/\tau\right)\right] \tag{3.23}$$

$$= P_o \left[\exp\left(-\frac{\int_o^t \exp\left(\frac{-E}{KT}\right) dt}{\tau_o}\right)\right] \tag{3.24}$$

The current density arising from this depolarization is

$$J_D(T) = \frac{\partial P(t)}{\partial t} \tag{3.25}$$

To perform this differentiation, it is necessary to make use of the fact that, in the experiment, the temperature is to be raised to a constant heating rate β, according to the equation

$T = T_o + \beta t$ giving

$$\beta = \frac{dT}{dt} \tag{3.26}$$

The thermally stimulated depolarization current density $J_D(T)$ is

$$J_D(T) = \frac{-Po}{\tau_o} \exp -\left\{\frac{E}{KT} + \frac{1}{\beta \tau_o}\int_{T_o}^{T} \exp -\left(\frac{E}{kT'}\right) d\tau'\right\} \qquad (3.27)$$

Using Garlick and Gibson's[80] approximation which is based on the assumption that the integral term in equation (3.27) is negligible over the initial part of the curve, the equation (3.27) can be written in the form,

$$J_D(T) = \text{constant} \quad \exp\left(\frac{-E}{kT}\right) \qquad (3.28)$$

A straight line is obtained by plotting $\ln J_D(T)$ against 1/T. The slope of the plot gives -E/K , from which the activation energy can be determined with very good accuracy.

ITC is a fastest method, since by means of a single measurement, a complete picture of the relaxation processes in the sample is achieved. ITC is thus extensively used for the study of electrets which have found many technological applications. Provided that large electric field is employed for the polarization, very low concentration of dipolar impurities can be defected. It provides a key role in the determination of electrical properties of solids. It is a method for studying all the fundamental mechanism for charge storage and release in non metallic solids. This method has found widespread popularity in view of its

high sensitivity and can be analysed inorder to get information on the characteristic parameter of the dipoles.

3.5.2 Thermally stimulated currents (TSC)

TSC methods have been shown to be a powerful tool in the evaluation of various properties of carrier transport and carrier trapping in semiconductor and insulating materials. The main aim in this study has been to gather information on the energy levels related to impurities and defects in insulators and semiconductors and the processes of electronic transitions between such energy levels. The location of a TSC peak on the temperature scale encoded information on the value of activation energy and capture cross section of the traps. The involvement of different types of traps change with temperature. The temperature range in which a specific trap dominates must therefore be identified. This is conveniently achieved with the aid of monitoring of TSC.

Haering and Adams [81] were the first to propose models for TSC. A detailed theory of TSC was presented by Dussel and Bube [82]. Extensive studies have also been reported on TSC curves. [83-86].

In TSC measurement, two electrodes are attached to the sample which is excited at a low temperature T_o. The sample is then heated

linearly in the dark with a constant voltage applied between the electrodes and the current through the sample is measured using a sensitive electrometer. The graph of current versus temperature is called the TSC curve. The traps are filled by irradiation at T_0 and upon heating, electrons (or holes) trapped at the localized state gain enough energy to jump into the conduction (valence) band. The carriers thus thermally released from traps to the band, give rise to transient increase in the conductivity of the sample. This increase in conductivity appears as a peak in the TSC curve, which is characteristic of the trapping sites in the material. A curve of thermally stimulated current for a single trap depth has the form of a somewhat a symmetric curve with a sharp maximum at a temperature which is determined by the trap depth, the capture cross section of the trap and the heating rate. If more than one type of trap is present, curves obtained by thermal stimulation may be expected to show several maxima. If carriers are trapped at a single energy level, TSC will show one peak. Normally, a TSC spectrum consists of more than one peak which may be attributed to species of traps. The thermally stimulated current I is given by

$$I = I_0 \exp - \left\{ \frac{E}{KT} + \frac{1}{\tau_0 \beta} \int_{T_0}^{T} \exp - \left(\frac{E}{KT'} \right) dT' \right\} \qquad (3.29)$$

In equation (3.29), T_0 is the initial temperature, $\nu = \frac{1}{\tau_0}$, the attempt to escape frequency and β is the heating rate.

Due to the presence of donors and acceptors (electron and hole traps), some of the charge carriers get attached to these defect or impurity levels. Ionization of traps or in other words, thermal release

of trapped electrons or holes is required to bring about the redistribution of these carriers back to the equilibrium distribution. An activation energy $E = E_C - E_D$ or $E = E_A - E_V$ has to be provided to ionize electron traps and hole traps respectively.

The discrete trap level can be calculated from the equation.

$$E = \frac{2kTm^2}{T_2 - T_1} \qquad (3.30)$$

where $T_2 - T_1$ is the width of the peak at the points where the current has half of its maximum value and Tm is the temperature of the peak maximum.

The TSC spectra may also be useful in obtaining the cross section 'a' of the traps [87]

$$a = \nu a_o \qquad (3.31)$$

where

$$\nu = (\beta / Tm)\ (\alpha \exp \alpha),$$

$$\alpha = E/kTm \text{ and } a_o = 10^{-26}\ Cm^2 S$$

3.6 REFERENCES

[1] L.H. Lenert, Semiconductor Physics, Devices and Circuits (C.E. Merrill Pub. Co., Ohio, 1968)

[2] O'Dwyer, The Theory of Electrical conduction and Breakdown in Solid Dielectrics, (Clarendon Press, Oxford, 1973).

[3] K. Seeger, Semiconductor Physics, An Introduction, Vol.40, (Springer, Heidelberg, 1988)

[4] R.E. Hummel, Electronic Properties of Materials, An Introduction for Engineers (Springer, Heidelberg, 1985)

[5] L.I. Isaenko, I.F. Kanaev, V.K. Malinovskii and V.I. Tyurikov, Sov. Phys. Solid State 30 (1988) 199.

[6] I. Kashif, S.A. El-Sahhar, A.M. Sanad and S.A. El-Henawii, J. Mater. Sci. Lett. 5 (1986) 827.

[7] J.H. Lee, S.J Park and K. Hirota ,J.Am. Ceram. Soc. 73 (1970) 2771.

[8] Yu. A. Vidadi, B.A. Mamedov, F. Sh. Mamedov and A.V. Ragimov Sov. J. Chem. Phys. 6 (1990) 2734.

[9] K.R. Paramasivam, M. Radhakrishnan and C. Balasubramanian, J. Mater. Sci. 16 (1981) 1183.

[10] G. Adachi, N. Imanaka, S. Matsubayashi and J. Shiokawa, J. Mater. Sci. Lett. 4 (1985) 192.

[11] Z.T. Al-Dhhan and C.A. Hogarth, J. Mater. Sci. 22 (1987) 3698.

[12] R. Ramanujam, M. Radhakrishnan and C. Balasubramanian, J. Mater. Sci. 19 (1984) 2401.

[13] D. Ravinder and T.S. Rao, Cryst. Res. Technol. 25 (1990) 1475.

[14] Y. Sadaoka, T.A. Jones and W. Gopel, J. Mater, Sci. Lett, 8 (1989) 1095.

[15] S.M. Patel, M.H. Ali, J. Mater. Sci. 24 (1989) 3176.

[16] Cz. Weclewicz and L. Zdanowicz, Thin Solid Films 151 (1987) 87

[17] J. Dudas, D. Knezo, A. Feher and H. Ratajczak, Physica B, 165 (1990) 217

[18] S. Kuwabata, J. Nakamura, H. Yoneyama, J. Electrochem. Soc. 137 (1990) 1788

[19] S. Kuwabata, J. Nakamura, H. Yoneyama, J. Electrochem. Soc. 137 (1990) 2417

[20] G. Haizhou, Z. Shuncai, Z. He and W. Yingwei, Res. Prog. SSE 8 (1988) 256

[21] R. Saxena and P.C. Mathur, J. Mater. Sci. Lett. 5 (1986) 869.

[22] Y.Saito, C. Kawamoto and H. Kuwano, Trans. Inst. Electron & Commun. Eng. Jpn. Sect E, E69 (1986) 235.

[23] R.H.Bube, Photoconductivity of Solids, (R.E.Krieger Pub.Co., New York, 1978)

[24] R.A. Smith, Semiconductors, (Cambridge University Press, London, 1959)

[25] P.S. Kireev, Semiconductor Physics (MIR Publishers Moscow, 1974)

[26] K.W.Boer, A Survey of Semiconductor Physics (Wiley, New York, 1990)

[27] T.S. Moss, Handbook on Semiconductors, Vol.1 (North Holland Pub. New York, 1982)

[28] J.S. Schildkraut, Appl. Phys. Lett. 58 (1991) 340

[29] A.D. Walser, R. Dorsinville and R.R. Alfano, J. Appl. Phys.69 (1991) 1116

[30] A.S. Maan, D.R. Goyal and A. Kumar, J. Non. Cryst. Solids 110 (1989) 53

[31] R. Tubino, R. Dorsinville, J.L. Birman and R.R. Alfano,Proc. of the 4th International School on Condensed matter Physics: Molecular electronics, Bulgaria, 1986, P: 308

[32] A. Werner, T.D. Moustakas and M. Kunst., III-V Hetero Structures for Electronic/Photonic Devices Symposium, USA, 1989 P.461

[33] J. Misiewicz, Infrared. Phys. 28 (1988) 215

[34] H.M. Jeong, C.D. Kim, J.J. Lee, Y.G.Kim,K.H.Park,H.G.Kim and W.T. Kim, New Phys. (Korean Phys soc.) 29 (1989) 379

[35] S.M.Mirianashili, E.P. Tumanishvili, N.N. Chikovani and L.G. Khavtasi, Sov. Phys-Semicond.24 (1990) 363

[36] A.I.Kirilyuk, N.M.Kreines and V.I. Kudinov. JETP Lett. 52 (1990) 49.

[37] L.Samaj, Phys. Status. Solidi (a), 101 (1987) 137

[38] P. Spirito, S. Bellone, C.M. Ransom, G. Busatto and G. Cocorullo, Proc. of the 1989 International Conference on Micro electronic Test Structures, U.K. 1989, P.175.

[39] M.W.Huppi, J. Appl. Phys. 68 (1990) 2702

[40] R.Fastow, Appl. Phys. Lett. 55 (1989) 1882

[41] X.Lin, Z. You and H. Guo, Phys. Status Solidi A. 120 (1990) K 177

[42] P.I. Baranskii, Sov. Phys. Coll, 26 (1986) 64

[43] N.M. Haegel, A. Winnacker, K. Leo, W.W. Ruhle and S.Gisdakis, J. Appl. Phys. I 62 (1987) 2946

[44] S.M. Ryvkin, Photoelectric effects in Semiconductors, (Consultance Bureau, New York, 1964).

[45] M.R.I. Ramadan, Sol. Wind. Technology 6 (1989) 615

[46] E.Suzuki and Y. Hayashi, Japan J. Appl. Phys. Lett. 29 (1990) L 162

[47] E. Suzuki and Y. Hayashi, J. Appl. Phys. 66 (1989) 5398

[48] R. Fastow and Y. Nemirovsky, J.Appl. Phys. 66 (1989) 1705

[49] T. Nammori, Jpn. J. Appl. Phys. Lett. 29 (1990) 166.

[50] P. Braunlich, Thermally stimulated Relaxation in Solids, (Springer - Verlag, Heidelberg, 1979).

[51] C.Bucci and R. Fieschi, Phys. Rev. Lett. 12 (1964) 16

[52] C. Bucci R. Fieschi and G. Guidi, Phys. Rev. Lett, 148 (1966) 816

[53] T. Takamatsu and E.Fukada, Polym. J.1, (1970) 101

[54] J. Van Turnhout, Polym. J.2 (1971) 173.

[55] R.A. Creswell and M.M. Perlman, J.Appl. Phys. 41 (1970) 2365.

[56] T.Nedetzka, M.Reichle, A.Mayer and H.Vogel, J.Phys. Chem. 74 (1970) 2652.

[57] B.T. Kolomietz, V.M. Lyubin and V.L. Averyanov, Mat. Res.Bull.5 (1970) 655.

[58] P.R.Moran and D.E. Fields, J.Appl. Phys. 45 (1974) 3266

[59] N.Beltrami, R. Capelletti and R. Fieschi, Phys. Lett. 10 (1964) 279.

[60] R.Muccillo and J.Rolfe, Phys. Stat. Sol (b) 61, (1974) 579.

[61] G.P. Jr.Williams and D.Mullis, Phys. Stat. Sol. (a) 28 (1975) 539.

[62] R.Capelletti and A. Gainotti, J. De Physique, 37 (1976) C7-316

[63] A.M.Hor and P.W.M.Jacobs, J.Electrochem. Soc., 125 (1978) 430

[64] D.Figuerpa, E. Laredo and M. Puma, Solid State Comm. 25 (1978) 509

[65] R.D. Shelley and G.R.Miller, J. Solid State Chem. 1 (1970) 218

[66] J.Wagner and S.Mascarenhas, Phys. Rev.B. 6 (1972) 4867

[67] E.L.Jr.Kitts, M.Ikeya and J.H.Jr.Crawford, Phys. Rev.B,8 (1973) 5840

[68] N.Kristianpoller and Y.Kirsh, Phys. Stat. Sol.(a) 21 (1974) 87.

[69] B.P.M. Lenting, J.A.J.Numan, E.J.Bijvank and H.W.den Hartog, Phys. Rev. B, 14 (1976) 1811

[70] G.E. Matthews and J.H.Jr.Crawford, Phys. Rev. B. 15 (1977) 55

[71] I. Kunze, N.Starbov and A. Buroff, Phys. Stat. Sol (a) 16 (1973) K59

[72] I. Kunze and P. Muller, Phys. Stat. Sol. (a) 13 (1972) 197

[73] A. Kessler, J.Physique 34 (1973) C9-79

[74] B.G.Pfister and M.A. Abkowitz, J. Appl. Phys., 45 (1974) 10001

[75] F.I. Mopsik and M.G. Broadhurst, J. Appl. Phys. 46 (1975) 4204.

[76] P. Fischer and P. Rohl, J.Polym. Sci., 14 (1976) 543

[77] J.Van Turnhout, Thermally Stimulated Discharge of Polymer Electrets (Elsevier, Amsterdam, 1975)

[78] T.Tanaka, S. Hiralayashi and K. Shilayama, J.Appl. Phys. 49 (1978) 784.

[79] J.Van Turnhout, Thermally stimulated Discharge of Electrets, in Electrets, ed. G.M. Sessler (Springer - Verlag, Heidelberg, 1978)

[80) G.F.J.Garlick and A.F.Gibson, Proc. Phys. Soc.60 (1948) 574

[81] R.R. Haering and E.N.Adams, Phys. Rev., 117 (1960) 451

[82] G.A. Dussel and R.H. Bube, Phys. Rev. 155 (1967) 764

[83] J.P. Fillard and J. Van Turnhout, Thermally Stimulated Process in Solids, (Elsevier, Amsterdam, 1977)

[84] M.M. Perlmann, Electrets, Charge Storage and Transport in dielectrics (The Electrochemical Society, N.J., 1973)

[85] M.M. Perlmann and L.M. Baxt, Electrets and Related Electrostatic Charge Storage Phenomena, (The Electrochemical Society, N.J.1968)

[86] R.H. Bube, Photoconductivity of Solids (Wiley, New York, 1960)

[87] T. Datta, R. Noufi and S.K. Deb J. Appl. Phys. 59 (1986) 1548.

4 EXPERIMENTAL TECHNIQUES

4.1 INTRODUCTION

A brief account of the various techniques employed in the investigations presented in the thesis are described in this chapter. The experimental set up used for the preparation of thin film samples and the details of the annealing chamber are outlined. The techniques employed for the identification of the prepared samples by X-ray diffraction (XRD) and Electron Spectroscopy for Chemical Analysis (ESCA) are given. The details of the techniques employed for the determination of the band gap , phase transition and observation of surface features are presented. In this chapter, a short note on the vacuum system used for the deposition of electrodes is included. The last part of the chapter also gives a brief account of the metallic cell and the various set-ups employed for the electrical measurement of the films.

4.2 PREPARATION AND ANNEALING OF FILMS

The preparation of CdS films was carried out by spray pyrolysis method. For this, a specially designed sprayer was used and the set up is shown schematically in Fig. 4.1. A unique feature of the sprayer is that the nozzle permitted a spray rate of 12 cc/min. It consists of a glass vessel of about 250 cc capacity with an atomizer. A specially made glass tube is introduced into this vessel through the atomizer. Another glass tube with a spray nozzle is fused to one side of the atomizer. The above arrangement allowed the atomization of chemical solution into a spray of fine droplets by admitting carrier gas (air) into the spray solution. The spray deposition with this linearly moving spray nozzle ensures uniformity of film thickness.

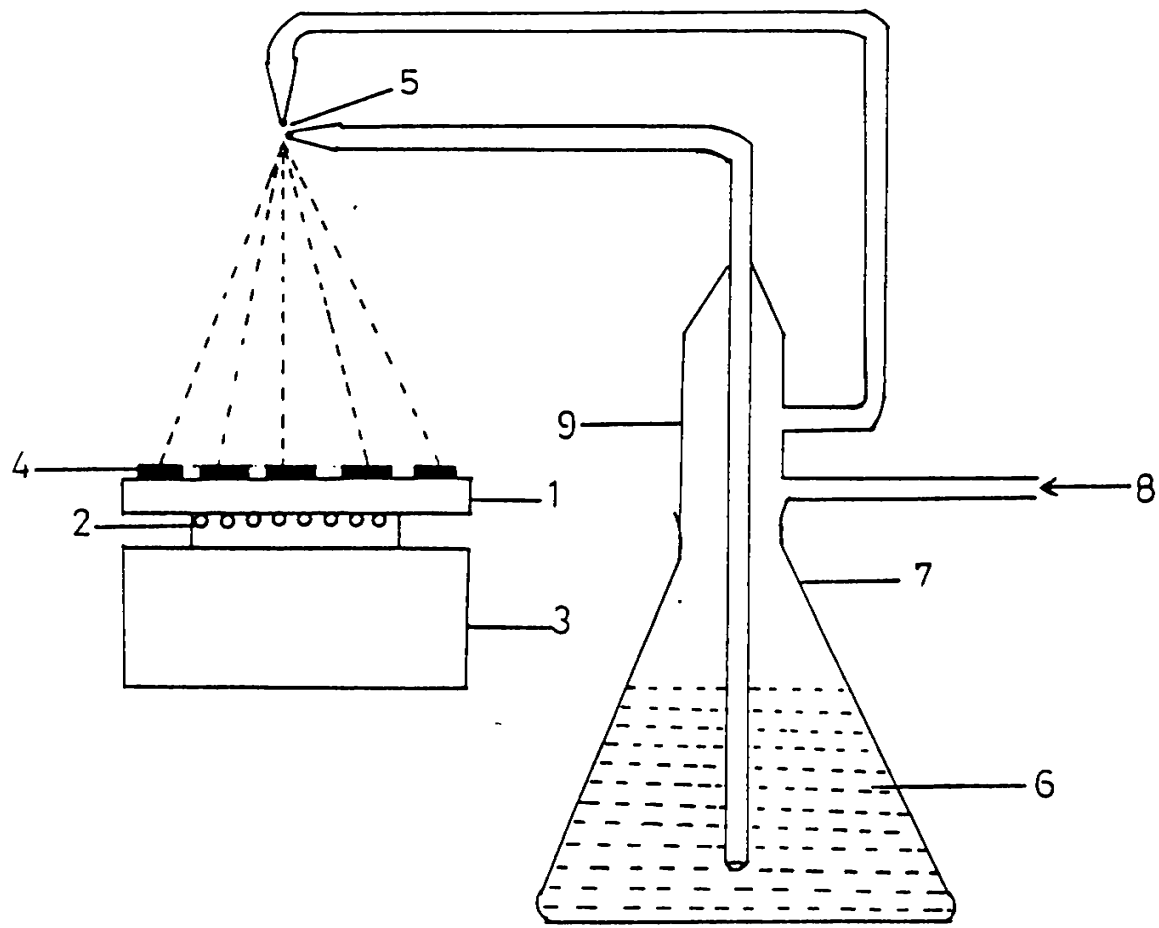

1. M.S. Plate
2. Heater
3. Support for the heater
4. Substrate
5. Nozzle
6. Solution
7. Glass vessel
8. Compressed air
9. Atomizer

Fig. 4.1: Schematic diagram of the spray pyrolysis set up for the preparation of CdS films.

A hot circular MS plate was used to keep the glass slides at an elevated temperature. The temperature of the substrate was measured using a chromel alumel thermocouple. This good quality films of consistent thickness were obtained with the help of the sprayer.

For the preparation of copper sulphide thin films, chemical bath deposition technique was employed, the details of which are discussed in Chapter.9.

A composite layer of copper and indium was deposited by using a high vacuum system (Fig 4.2) for the preparation of $CuInSe_2$ films. The evaporation chamber has provision for two independent resistively heated sources and substrate heating. Molybdenum boats were used for supporting the materials. The temperature of the substrate was measured by a chromel alumel thermocouple and were controlled to an accuracy of $\pm 1^{\circ}C$. After the deposition of the composite layer the slides were dipped into the solution containing selenium dioxide and dil. H_2SO_4 and finally dried. The films were found to be p-type and are suitable for the electrical measurements.

The annealing of the films were carried out in vacuum and air. For vacuum annealing, a high vacuum coating unit was employed. A substrate holder provided with a heater is mounted inside this unit using which the temperature of the films during annealing could be varied. The films were placed in the substrate holder and the chamber was pumped down to 10^{-5} Torr. The films were annealed at different temperatures for 30 min and were subjected to electrical

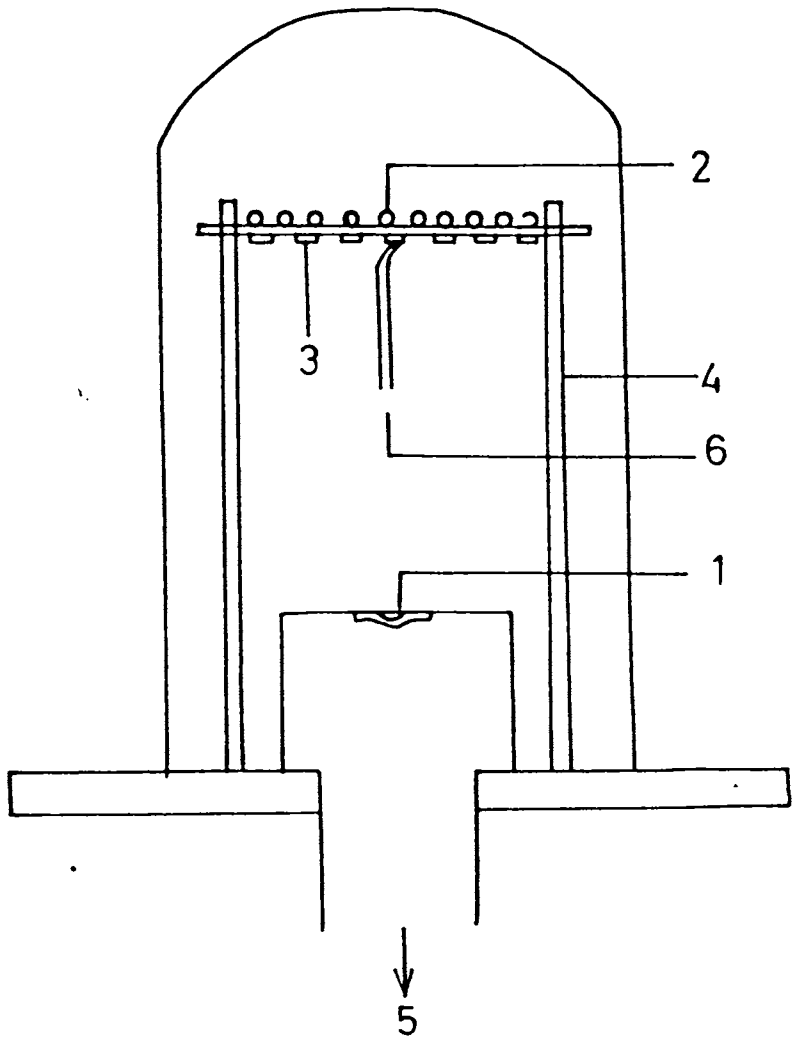

1. Molybdenum boat
2. Heater windings
3. Substrate
4. Support for heater and the substrate.
5. Diffusion pump
6. Thermocouple

Fig. 4.2: Schematic diagram of the vacuum system for the deposition of composite layer of copper and indium.

measurements.

A glass chamber with heater assemblies was used for the annealing of films in air. The system was insulated using mica sheet windings. It has provision for inserting the chromel alumel thermocouple. The schematic diagram of the annealing chamber is shown in fig 4.3.

4.3 X-RAY DIFFRACTION (XRD) STUDIES

The basic principle used in X-ray diffraction is Bragg's law which is

$$2d \sin\theta = n\lambda \qquad (4.1)$$

where d is the lattice spacing, θ the incident angle of X-ray beam, n is an integer and λ the wavelength of the incident radiation.

In X-ray diffractometers, the X-ray source, the specimen and the detector are so arranged to obey the Bragg's law [1]. Filtered Cukα radiation was used as the X-ray source. The intensity of the diffracted radiation against 2 θ was recorded by a recorder running in synchronization with goniometer. If proper care is taken, X-ray diffraction can yield good results and any particular compound can be identified without difficulty.

4.4 ELECTRON SPECTROSCOPY FOR CHEMICAL ANALYSIS (ESCA)

Recent years have seen a spectacular development in experimental techniques and one of the fastest growing areas is electron spectroscopy. When any material is bombarded by X-rays, the incident

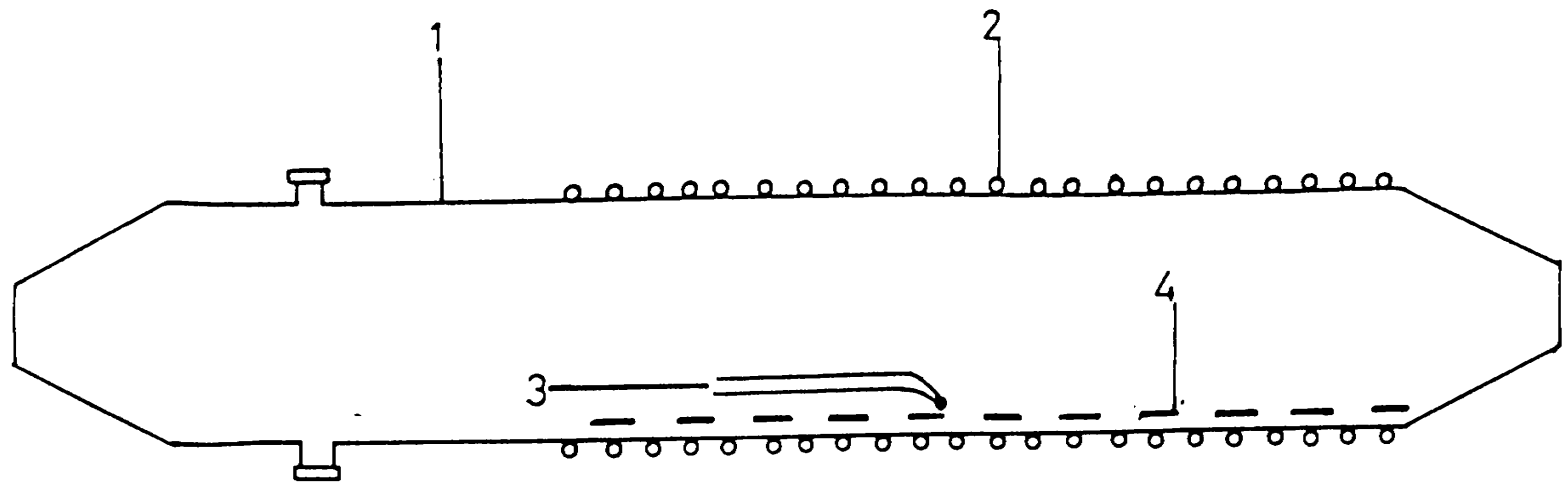

1. Glass Chamber
2. Heater windings
3. Thermocouple
4. Sample

Fig. 4.3: Schematic diagram of the annealing chamber.

photons will be absorbed by the atom and an atomic electron is ejected as a photoelectron. Thus ESCA measures the kinetic energy distribution of photoelectrons produced by the ionising radiation of a fixed frequency [2].

The kinetic energy of the photoelectron is given by

$$E_p = h\nu - E_b \qquad (4.2)$$

where E_p is the kinetic energy of the photoelectron, $h\nu$ is the energy of the incident photon and E_b is the binding energy of the electron.

Since the electrons ejected in ESCA technique are necessarily of low energies, the smaller energy differences can be easily measured, the electrons can not escape from any significant depth in the sample. The phenomenon is therefore confined to atoms on the surface of the sample and provides a method of surface analysis. The photoelectron energies are characteristic of the atomic levels of a given element and can be used as the basis for elemental identification.

The ESCALAB MK II spectrometer (VG Scientific Ltd. UK) with Mgkα ($h\nu$ = 1253.6 eV) radiation as the source was used for the analysis.

4.5 SPECTRO PHOTOMETRY

Absorption measurements were carried out for the determination of the band gap of films. The spectra in the UV and visible regions were recorded by employing a U-3410 Hitachi Spectrophotometer, A photograph of this instrument is shown in Fig. 4.4. For the transmission measurements, a Beckmann Infrared Spectrophotometer was used.

Fig. 4.4: Photograph of the U-3410 Hitachi Spectrophotometer.

4.6 DIFFERENTIAL SCANNING CALORIMETRY

Differential scanning calorimetry (DSC) is one of the advanced techniques in the field of thermal analysis. Several phenomena such as the equilibrium between the different phases in complexes, the thermodynamic properties, crystallization energies, microstructural evolution in alloys, phase transitions, effect of temperature rise on structural change, heat capacity, enthalpy etc can be studied with the help of thermal analysis using DSC. Basically the DSC technique allows the determination of the time derivative of the heat content per unit mass of the sample, $\dot{H}(t) = dH/dt$ as a function of time t for a given heating rate, $\dot{T} = dT/dt$ and a given temperature, T (t). A perkin Elmer Delta series Differential Scanning Calorimeter (model DSC-7) was used for recording the DSC spectrum of the films. The photograph of the instrument is shown in Fig. 4.5. The spectrum was recorded with a scanning rate of $5\,^{\circ}C$/min. The distinct variation in the heat flow of the films was studied and the phase transition temperature has been determined.

4.7 OPTICAL MICROSCOPY

The inverted metallurgical type Union Versamet - 2 microscope (Fig 4.6) was employed for the optical studies of the film surfaces. This microscope carries a binocular vision system. The illuminating system can be shifted from reflecting to transmitting modes. For change over between reflected light illumination (24V, 150W, halogen) and transmitted light illumination (12V, 50W, halogen), a light source change over switch was used. The unit carries one pair of 10 x eye pieces.

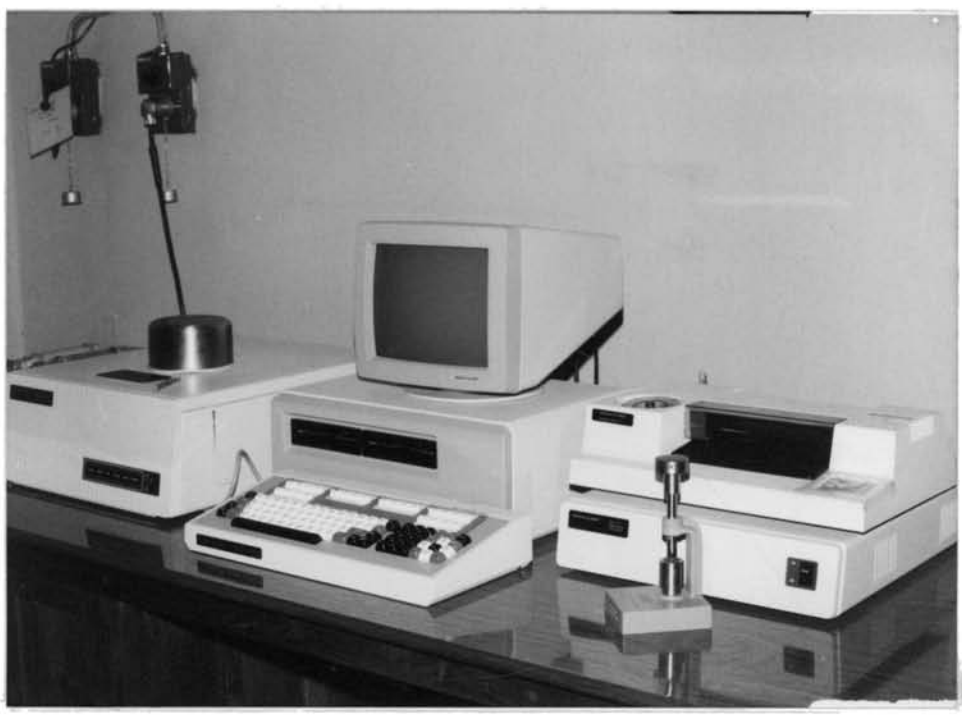

Fig. 4.5: Photograph of the Perkin Elmer Delta Series Differential Scanning Calorimeter.

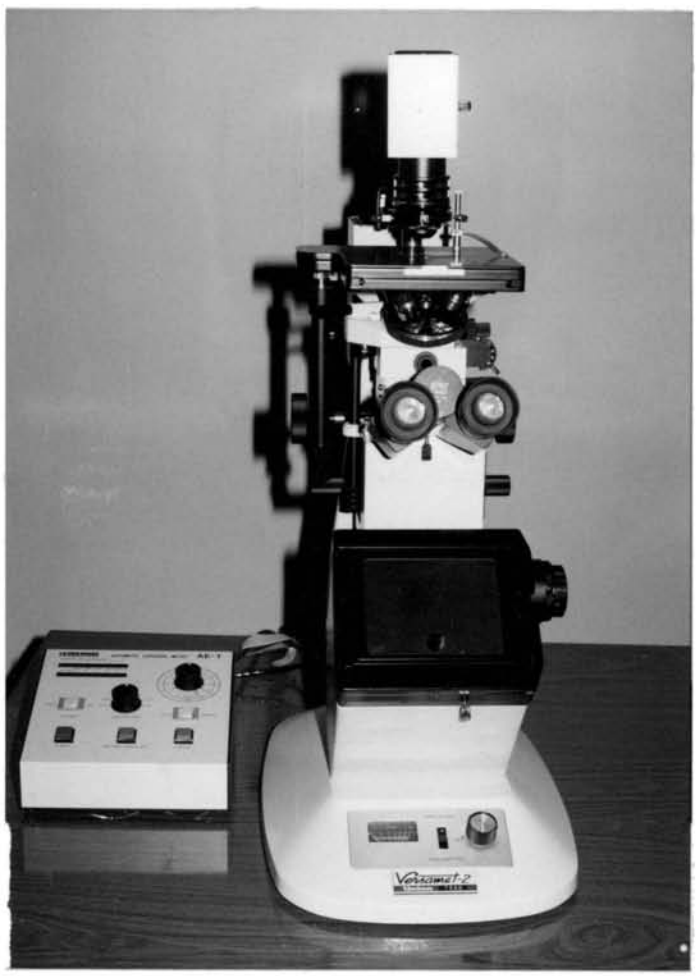

Fig. 4.6: Photograph of the Union Versamet - 2 Microscope.

The magnification of the lenses can be seen through a display window. The microphotographs of the film surfaces were taken with the help of a photographic attachment of the microscope.

4.8 VACUUM SYSTEM FOR THE DEPOSITION OF ELECTRODES

A conventional vacuum coating unit (Fig 4.7) capable of attaining pressures around 10^{-5} Torr was employed for the deposition of metal electrodes. The chamber was evacuated by a diffusion pump backed by a rotary pump. A transformer was used for the resistive heating of the vapour source for depositing films. The normal pumping down time to get ultimate vacuum was around 45 min. Inorder to support the materials for deposition, a filament source was used. In the present study, a tungsten helix was mounted tightly on the filament holders.

The substrates containing film are mounted at a distance of about 15-20 cm above the filament. The films were placed over mica masks to achieve the necessary configuration. The materials to be evaporated were taken in the filament and are evaporated at a pressure of 10^{-5} Torr. Thus electrodes can be deposited on the surface of the films in the planar structure with a gap (0.1 - 0.5cm) between them.

4.9 METALLIC CELL FOR ELECTRICAL MEASUREMENTS

The fabrication of the cell aims at measuring the electrical properties of thin films over a wide range of temperature in different ambient conditions (Vacuum and air). The cell can be used

Fig. 4.7: Photograph of the Vacuum System for the deposition of electrodes.

in the temperature range 80 to 450 K without disturbing the vacuum conditions. It can be used for the measurements at very low pressures. The liquid nitrogen consumption is found to be extremely small for a single cycle of operation. The measurements of dark conductivity, photoconductivity, lifetime, ionic thermocurrent (ITC) and thermally stimulated currents (TSC) can be carried out using the same cell.

The chamber consisted of a cylinder (Fig. 4.8 a) whose ends were permanently fixed with MS flanges. The top and bottom covers of the cell can be sealed vacuum tight by using neoprine O-rings. Four window ports were provided to the chamber at 90°C to each other. One of the ports was used as a pumping port which could be connected to a vacuum pump for evacuating the chamber. Others were used accordingly to perform optical excitation for photoconductivity, lifetime, and TSC measurements and to see whether the films undergo any change with temperature. The schematic representations of the sample holders used for the electrical measurements are shown in Figs. 4.8 (b) and 4.8 (c). A cold finger (SS tube) was inserted through top plate and was fixed onto this plate using O-ring and allen screws. A sample holder was fitted onto the bottom of the cold finger by welding. The holder was provided with heater windings inorder to vary the temperature of the samples for measurement purposes. The electrical insulation was made using mica sheets and teflon. The length of the cold finger and the sample holder is adjusted such that the centre of the sample is in a line with the axis of the window. For the photoconductivity, lifetime and TSC measurements, a rectangular copper bar was

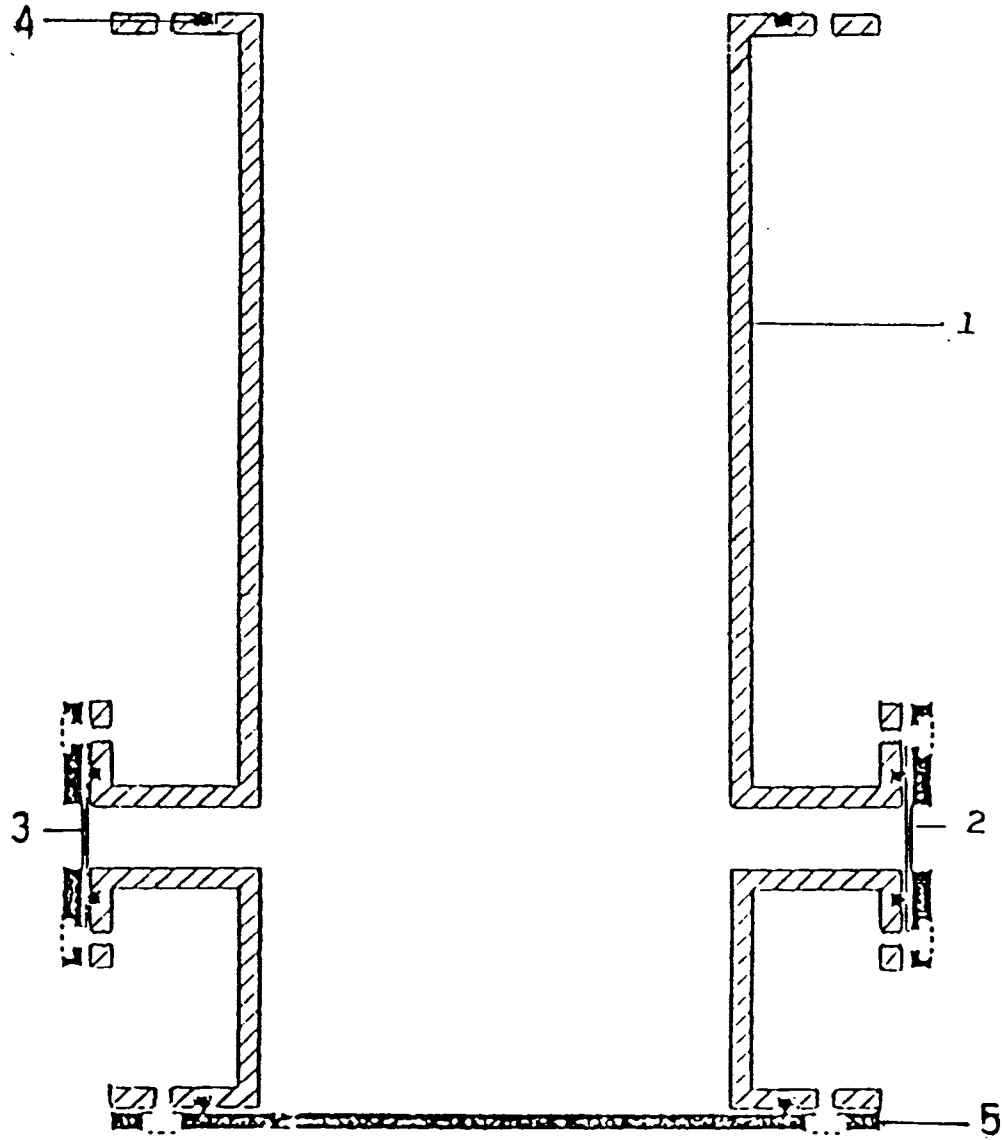

1. M.S. Chamber
2. Glass window
3. Vacuum pump
4. Neoprine O-ring
5. M.S. Flange

Fig. 4.8 (a): Schematic diagram of the metallic cell for the electrical measurements.

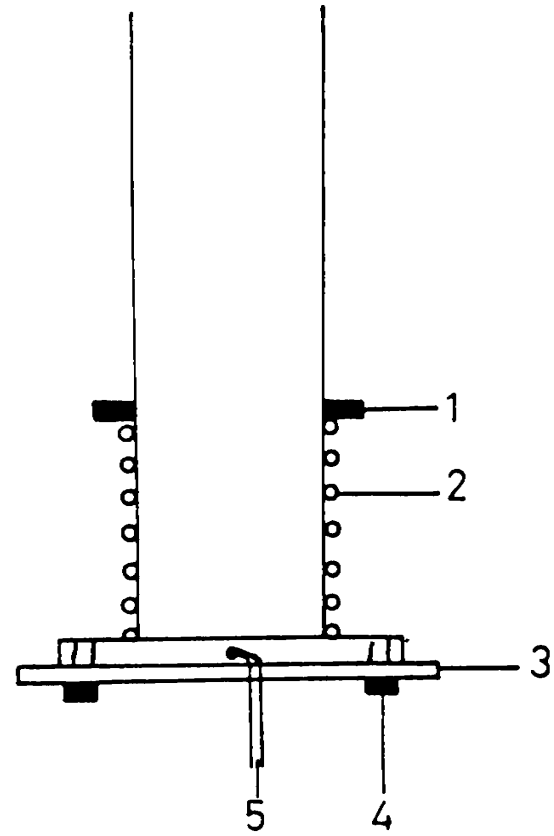

1. Sample holder
2. Heater windings
3. Substrate with film
4. Substrate holder (Teflon) strips.
5. Thermocouple.

Fig. 4.8 (b): Schematic diagram of the sample holder for the dark conductivity and ITC measurements.

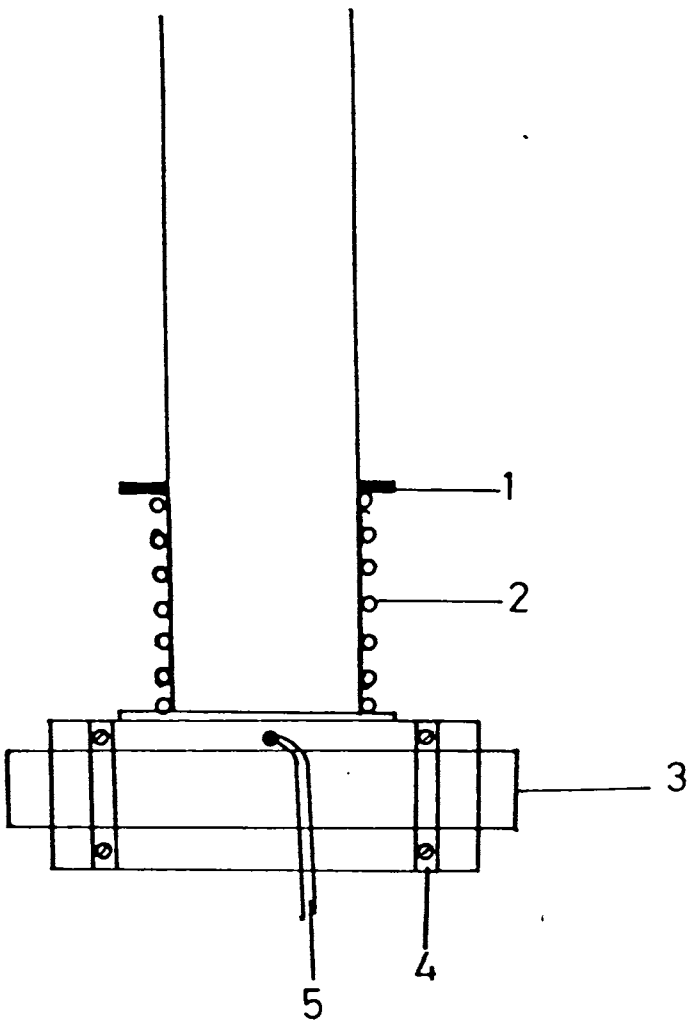

1. Sample holder
2. Heater windings
3. Substrate with film
4. Substrate holder (teflon) strips.
5. Thermocouple

Fig. 4.8.(c): Schematic diagram of the sample holder for the photo conductivity, lifetime and TSC measurements.

attached and the film was kept on this bar by pressing it with the help of two teflon strips which can be seen from Fig 4.8 (c). A chromel-alumel thermocouple was kept in contact with the substrate for temperature measurement. The electrical connections for thermocouple and heater were made through teflon insulations. Two BNC connectors were provided for connections to the sample.

4.10 MEASUREMENT OF ELECTRICAL PROPERTIES

4.10.1 Dark conductivity Measurements

The dark conductivity measurements in vacuum and air were carried in the metallic cell described previously. The electrometer was connected in series with the power supply and the film and the electrical circuit for the measurement is shown in Fig. 4.9. Electrical contacts to the films were made by depositing electrodes in the planar structure. The sample was then inserted in the sample holder and a steady voltage of $\sim$ 9V was applied across it by a battery. The current through the sample was measured using an electrometer. The power to the heater was provided from a stabilized voltage source. The samples were heated from 100 to 425 K at the rate of 0.06K/Sec and the current was recorded at different temperatures. Sample temperature was measured using a chromel-alumel thermocouple kept in contact with the sample surface. The conductivity can be evaluated with the known values of the magnitude of the current, area of the film, the applied voltage and the distance between the two electrodes. A photograph of the experimental set up used for the measurement of dark conductivity is shown in Fig. 4.10

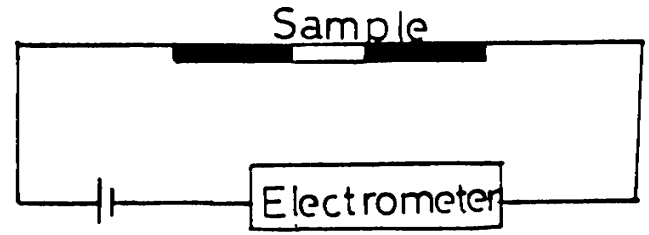

Fig. 4.9: Schematic diagram of the experimental set up used for the dark conductivity measurements.

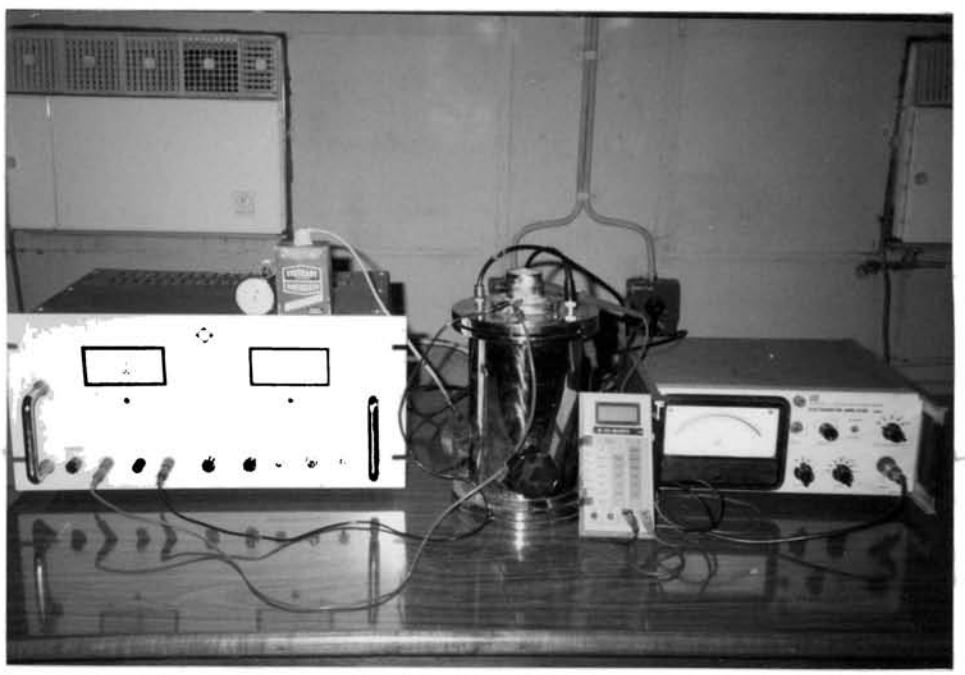

Fig. 4.10: Photograph of the experimental set up used for the dark conductivity measurements.

4.10.2 Photoconductivity measurements

A schematic diagram of the measurement of photoconductivity is shown in Fig. 4.11. The set up used for this measurement consisted of a quartz tungsten halogen lamp (Oriel No. 7340), a monochromator (Oriel No. 7240) and a metallic cell. The monochromatized output of the tungsten halogen lamp was illuminated the sample through the optical system. Special care was taken to avoid spurious light falling on the sample kept in the measurement chamber. The area of illumination on the surface was always 0.6 cm^2. The necessary electrical connections were made which was similar to that of dark conductivity measurements. After setting the sample in the evacuated cell, a voltage of $\sim$ 9V was applied across it and the photo current through the film was measured using an electrometer. Readings were noted at wave-length interval of 40 nm. Then the photoconductivity can be evaluated with the known values of magnitude of photo current, applied voltage, distance between the two electrodes and area of the film. The experiment was performed in the temperature range from 100 to 425 K. The temperature of the sample during measurement was controlled to an accuracy of ± 0.1°C by controlling the current through the heater. The photoconductivity measurements were also done in air atmosphere in the temperature range from 303 to 425 K. The ratio between the measured conductivity and the power of the light source at each wavelength was calculated and is plotted against wavelength. A photograph of the experimental set up used for the measurement of photoconductivity is shown in Fig. 4.12.

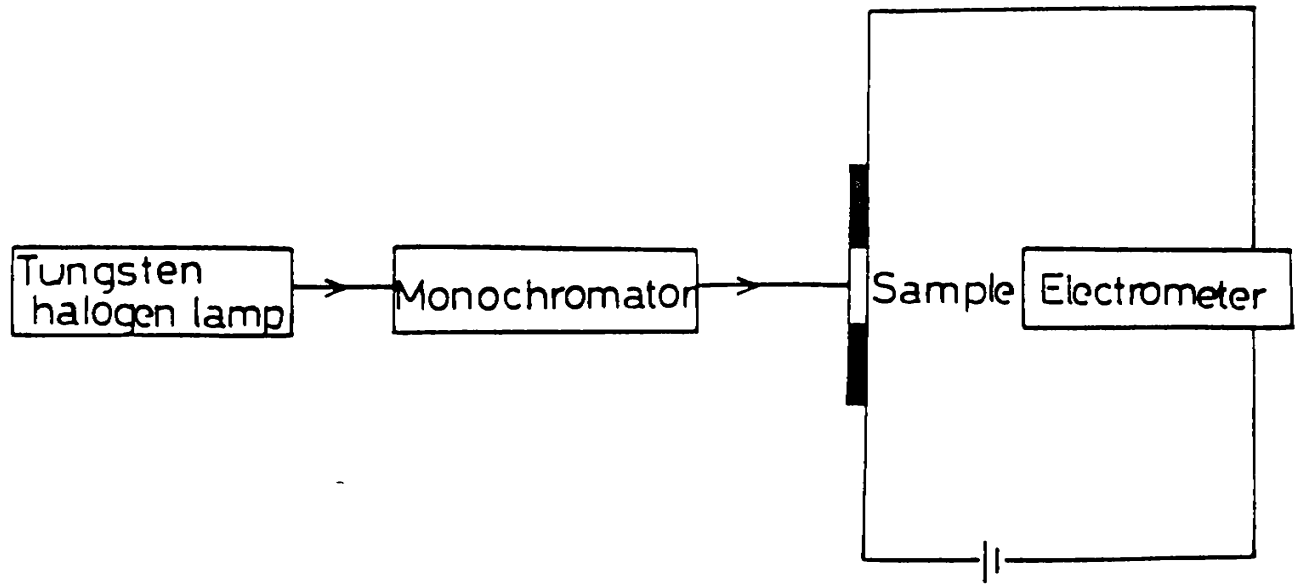

Fig. 4.11: Schematic diagram of the experimental set up for the photo conductivity measurements.

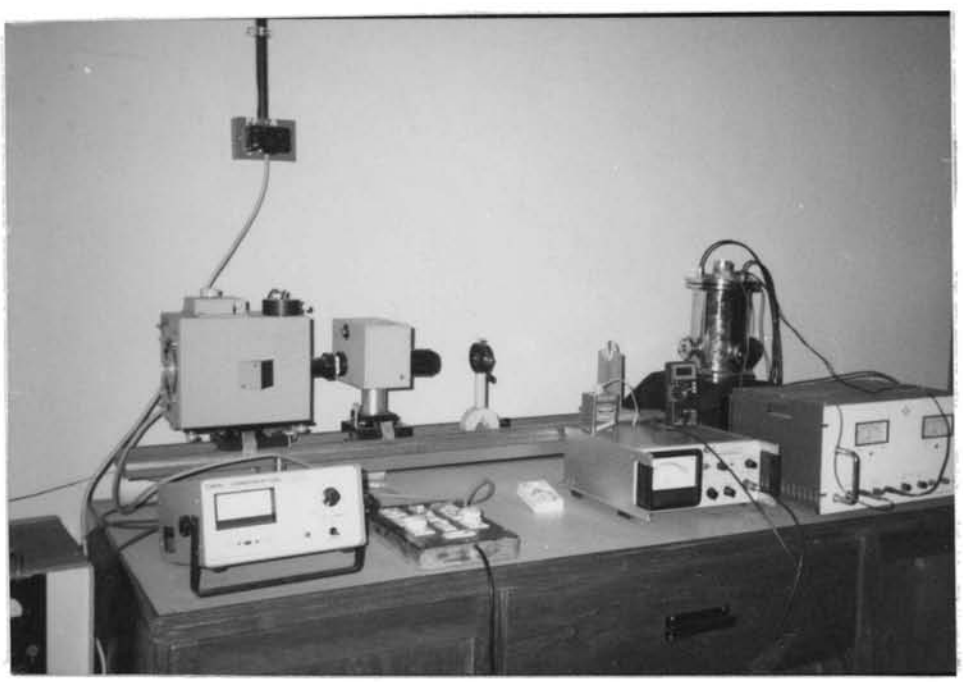

Fig. 4.12: Photograph of the experimental set up used for the photo conductivity measurements.

4.10.3 Lifetime measurements

The schematic diagram of the experimental set up used for the lifetime studies is shown in 4.13. The set up consisted of a metallic cell, a light source (Quartz tungsten halogen lamp, Oriel No.7340), a monochromator (Oriel No. 7240), a mechanical chopper (HMS light beam chopper model 230) and a microvoltmeter (model HIL 2645). Monochromatized light from a tungsten halogen lamp is focussed on a mechanical chopper and to the sample. Special care was taken to avoid spurious light falling on the sample. The area of illumination on the film surface was 0.6 cm^2. The cell was evacuated and the necessary electrical connections were made for the measurements. A voltage of $\sim$ 9V was applied across the film through a series resistance. The chopped light was allowed to fall on the film. The frequency of the chopped beam was varied and the photocurrent was determined. The measured photocurrent was varied with the frequency of the pulses till the saturation region of photocurrent sets in at a particular frequency. The lifetime of minority carriers τ can be calculated by using the equation derived by Ryvkin [3]. The lifetime at 400, 520 and 640 nm was determined in the temperature range 100-425 K. A photograph of the experimental set up is shown in Fig 4.14.

4.10.4 ITC Measurements

The experimental set up (Fig. 4.15) consisted of a metallic cell, electrometer and a stabilized dc power supply. For the measurement of ITC [4,5], the sample was polarized by applying an electric field at a suitable temperature for a required time. The

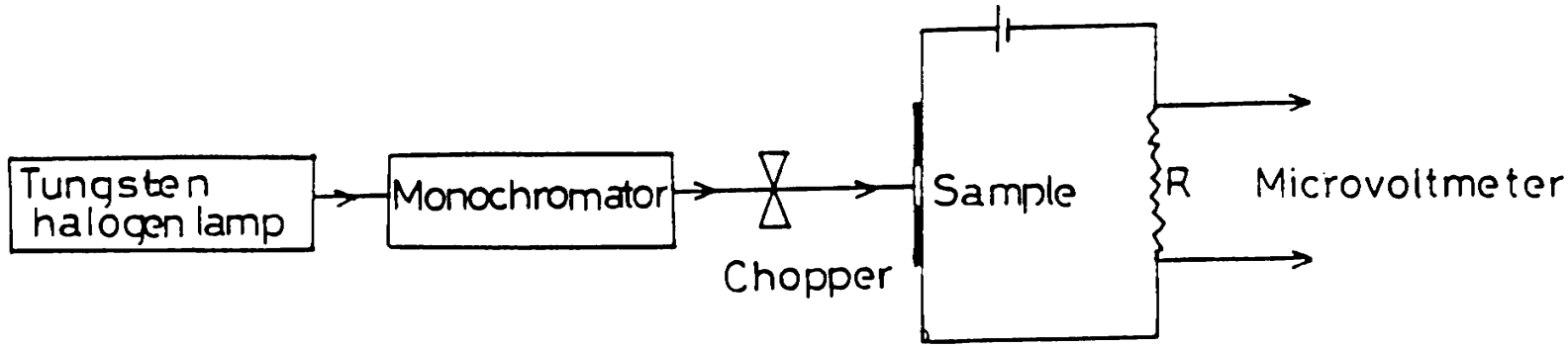

Fig. 4.13: Schematic diagram of the experimental set up used for the lifetime measurements.

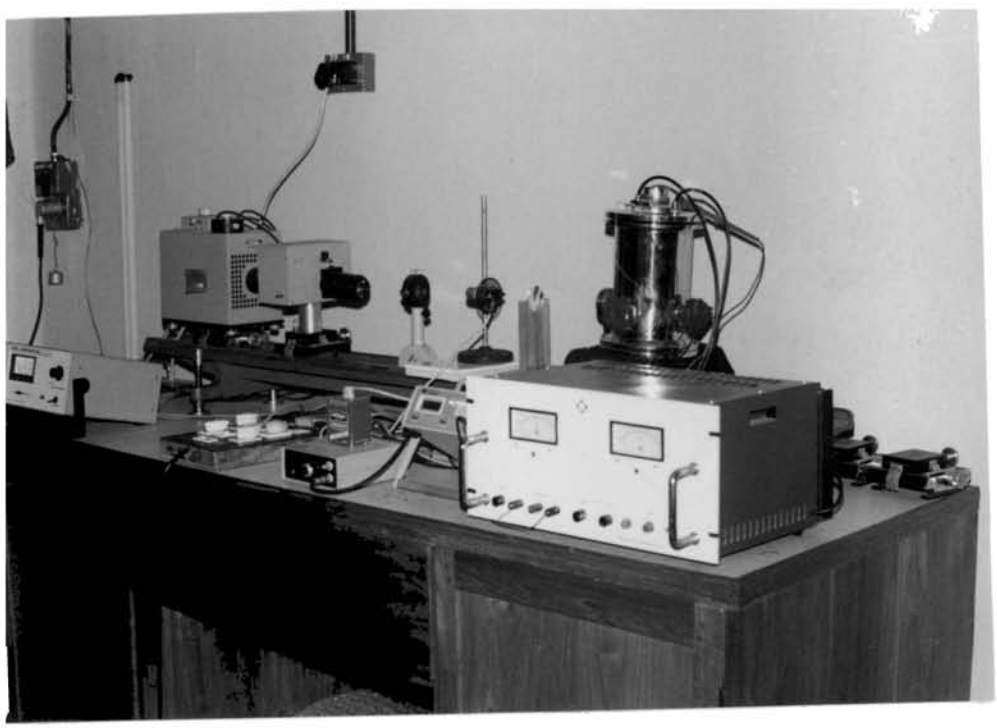

g. 4.14: Photograph of the experimental set up used for the lifetime measurements.

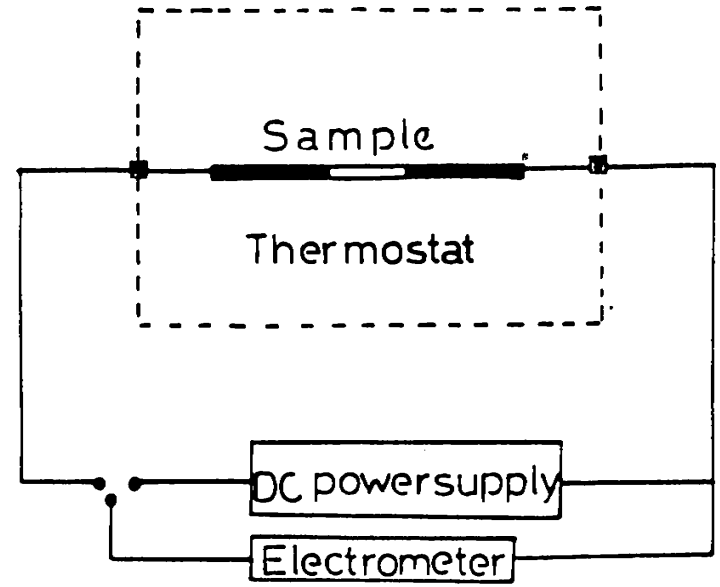

Fig. 4.15: Schematic diagram of the experimental set up used for the ITC measurements.

film was cooled down to a low temperature. At this temperature, the electric field was turned off and the current through the film was measured as a function of temperature by heating it at a rate of 0.06K/sec. A photograph of the experimental set up is shown in Fig. 4.16.

4.10.5 TSC Measurements

For the TSC measurements, the experimental set up consists of a metallic cell, tungsten halogen source, electrometer and a stabilized dc power supply [Fig. 4.17]. The sample was initially cooled from room temperature to a low temperature and then subjected to photo - excitation using a tungsten halogen lamp. After a sufficiently long exposure, the excitation was turned off. The dc bias was then applied to the sample and its temperature was increased at a heating rate of 0.06K/sec. The current through the film as a function of temperature was monitored using an electrometer. A photograph of the experimental set up used for the measurement of TSC is shown in Fig. 4.18.

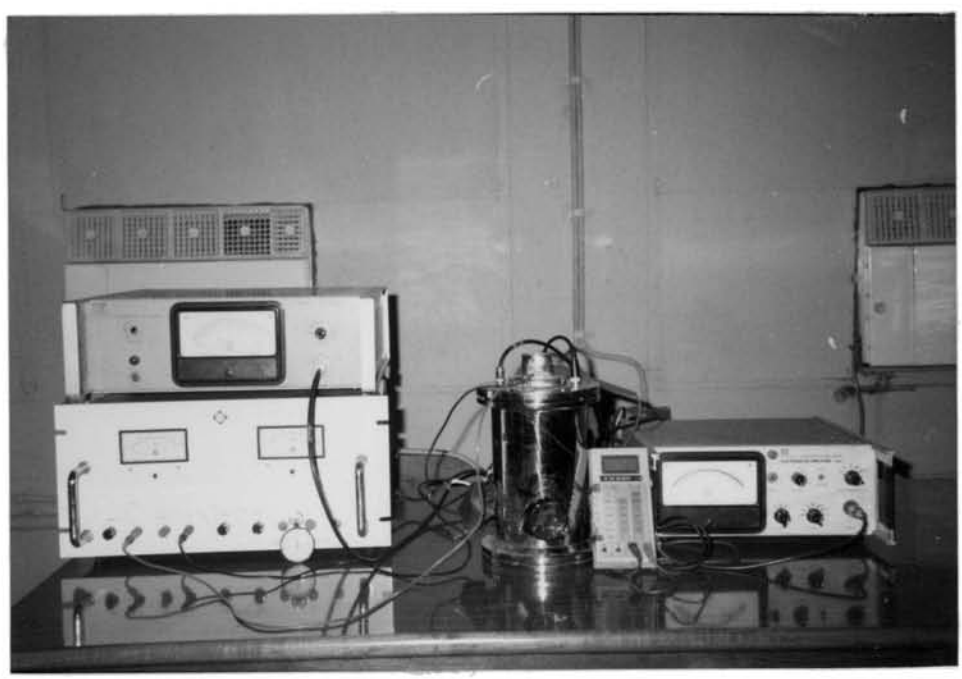

Fig. 4.16: Photograph of the experimental set up used for the ITC measurements.

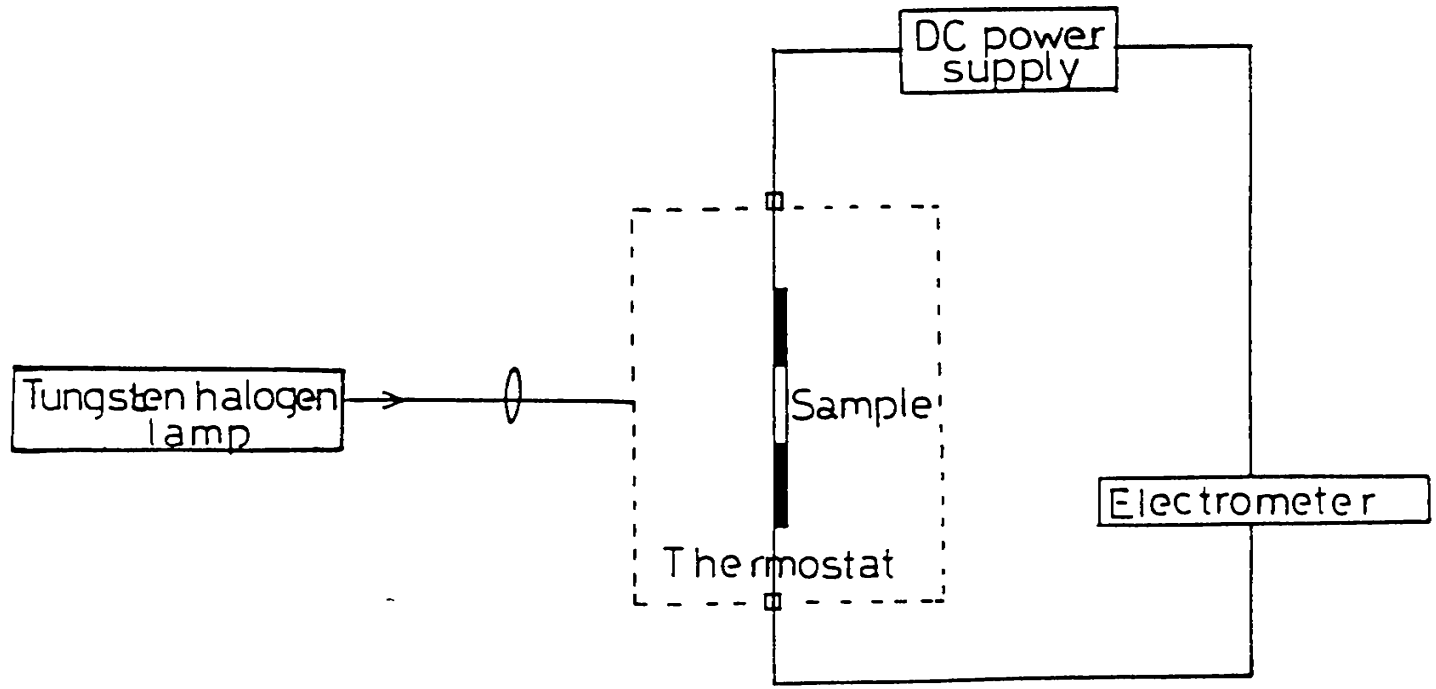

Fig. 4.17: Schematic diagram of the experimental set up used for the TSC measurements.

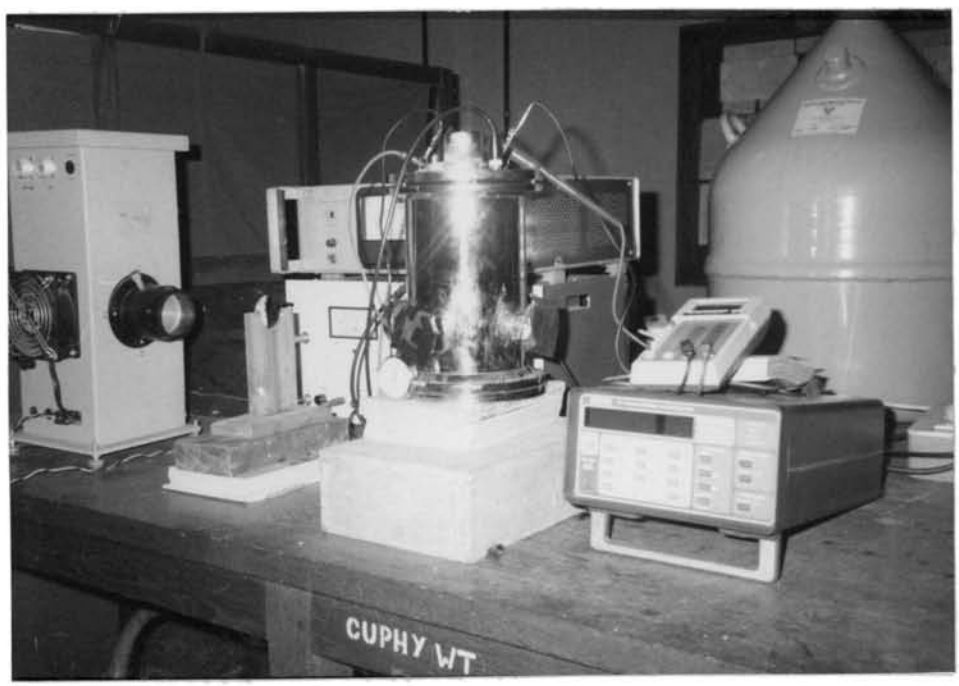

Fig. 4.18: Photograph of the experimental set up used for the TSC measurements.

4.11 REFERENCES

[1] B.D. Cullity, Elements of X-ray Diffraction (Addison - Wesley Pub. Co., USA, 1959)

[2] W.E. Swartz, Jr., in: Instrumentation in Analytical chemistry, Vol.2. ed. S.A. Borman (American Chemical Society, USA, 1982)

[3] S.M. Ryvkin, Photoelectric effects in semiconductors, (Consultants Bureau,New York, 1964)

[4] G. Pfister and A. Abkawitz, J. Appl. Phys. 45 (1974) 1001.

[5] C. Bucci and R. Fieschi, Phys. Rev. Lett. 12 (1964) 16.

5 PREPARATION OF CdS THIN FILMS

5.1 INTRODUCTION

Cadmium sulphide is a II-VI group semiconductor. It has received considerable attention because of its potential use in the fabrication of solar cells [1-5]. Several authors have deposited CdS thin films by evaporation and sputtering methods [6-23]. Cameron et al. [24] have prepared these films by molecular beam epitaxy and studied the structural and electron transport properties. The growth of CdS films by open tube chemical vapour deposition has been studied by Blasi et al. [25]. Also partain et al [26] have deposited these films by chemical vapour deposition method. The growth of CdS films by close spaced vapour transport technique has been carried out by Dawar et al [27].

The preparation of CdS films by solution deposition methods have been carried out by many researchers [28-32]. Uda et al [29] have prepared CdS films by chemical solution deposition method and studied the structural and electrical properties. Lokhande et al [30] have carried out the elecrodeposition of CdS films and reported a band gap of 2.4 eV. The structure and growth kinetics of electrodeposited CdS thin films have been investigated by Balakrishnan and Rastogi [31]. Karajai and Das Gupta [32] have prepared CdS films by the dip technique. Chamberlin and Skarman [33] developed a method of producing large-area thin films of CdS by the solution spraying technique. A few works were also later reported on the films prepared by this technique [34-38]. Berg and Nasby [38] have studied the structure of chemically sprayed CdS films. They prepared the films by spraying 0.1 M aqueous solutions of $CdCl_3$ and NH_2CSNH_2 on to SnO_2-

coated glass substrates heated to 380°C. This chapter contains the investigations carried out on spray pyrolysed CdS films prepared from different concentrations of cadmium chloride, keeping the concentration of thiourea as constant. The films are identified from the X-ray diffraction profiles and the surface features are observed. The results obtained from the surface analysis of the films using the ESCA technique are presented. Absorption and transmission spectra of the films are also recorded.

5.2 EXPERIMENTAL

Thin films of CdS were prepared by spray pyrolysis. The spray solution was made from a 0.20 M solution of cadmium chloride [$CdCl_2$] and 0.20 M solution of thiourea [$(NH_2)_2CS$]. Optically flat glass slides of dimension 2.5 x 7.5 cm were used as the substrates (supplied by Blue Star Co.). They were cleaned thoroughly by washing first with detergent soap solution, then washed and cleaned ultrasonically with doubly distilled water. After these steps, the slides were dried. The substrates were heated and the solution was sprayed by employing compressed air as carrier gas. $CdCl_2$ and $(NH_2)_2CS$ form a soluble complex [$CdCl_2(NH_2)_2CS$] in the solution and do not precipitate. On coming into contact with hot substrate, the complex in the fine spray dissociates and the desired yellow semiconductor film results with thickness $\sim$ 3000Å. The films obtained were stable and adherent. Films with different cadmium contents were also prepared by increasing the concentration of cadmium chloride from 0.20 to 0.28 M, keeping the concentration of thiourea as constant for studying the electrical characterization. For the sake of convenience, the film prepared by

taking 0.20M cadmium chloride and 0.20 M thiourea is defined as A_1. The designation of other films were made similar to the above, for example, A_2 represents the film prepared from 0.22 M cadmium chloride and 0.20 M thiourea. The details are presented in Table 5.1. The films were found to be n-type as was confirmed by the hot probe method.

Annealing of the films in air were carried out in a glass chamber with provision for temperature measurement and heating. The schematic diagram of the annealing chamber and its details are given in Chapter 4. The as prepared films were placed inside the chamber and were heated gradually by controlling the current through the heater windings. The annealing temperature of the film was controlled for 30 min after attaining the particular temperature. The samples were then cooled slowly. A chromel-alumel thermocouple was used to measure the temperature of the samples inside the chamber.

Photographs of the surfaces of films were taken with a Union Versamet-2 metallographic microscope to analyse the microstructure of these films. X-ray diffraction measurements were done with CuKα radiation. XPS analysis was carried out using an ESCALAB MK II spectrometer (VG Scientific Ltd., UK). The experiment was performed using a MgKα ($h\nu$ = 1253.6 eV) source. The optical absorption measurements of the films were performed with a U-3410 Hitachi spectrophotometer in the spectral range 400 to 640 nm. The transmission spectra of the films were also recorded using a Beckmann Infrared Spectrophotometer.

Table 5.1 Designation of CdS films

Sample	Reactants used for the Film preparation.
A_1	0.20M Cadmium Chloride, 0.20M thiourea
A_2	0.22M Cadmium chloride, 0.20M thiourea.
A_3	0.24M Cadmium chloride, 0.20M thiourea
A_4	0.26M Cadmium chloride, 0.20M thiourea
A_5	0.28M Cadmium chloride, 0.20M thiourea.

5.3 RESULTS AND DISCUSSION

The films were annealed in the temperature range 373-573K for investigating their electrical properties. On annealing, the surfaces of the films were appeared as shown in Fig. 5.1. In some cases imperfections were also observed on the films (Fig.5.2). X-ray diffraction patterns of the films were obtained (Fig.5.3) and it was found that the diffraction lines compared well with the literature data [39]. The surface analysis of the films was carried out using ESCA. The XPS survey scan of a typical film is depicted in Fig. 5.4. Both cadmium and sulphur peaks are clearly visible. As shown in this figure, the Cd $3d_{5/2}$ and Cd $3d_{3/2}$ levels are sharp. The various other elements present in the sample are also seen in the figure. Figs. 5.4 (a) to 5.4 (f) indicate the high resolution spectra of Cd 3d, S 2p, S 2s, Cl 2s, Cl 2p and 01s levels.

Fig 5.5 shows the absorption spectrum of CdS film obtained for the wavelength in the range 400-640 nm. The dip in the curve at a wavelength of 512.5 nm corresponds to the energy gap of 2.41 eV, which is in agreement with the values obtained in the crystals [40]. The transmission spectra of the films annealed at 373 and 573K are given in Figs. 5.6. Fig. 5.7 depicts the spectrum obtained for the films annealed at 473 K. The figure shows a broad absorption in the region 5000 to 8220 nm which indicates the existence of a trap level in this sample.

5.4 CONCLUSION

The films of CdS have been prepared by the spray pyrolysis method and the surface features are observed. The films are identified

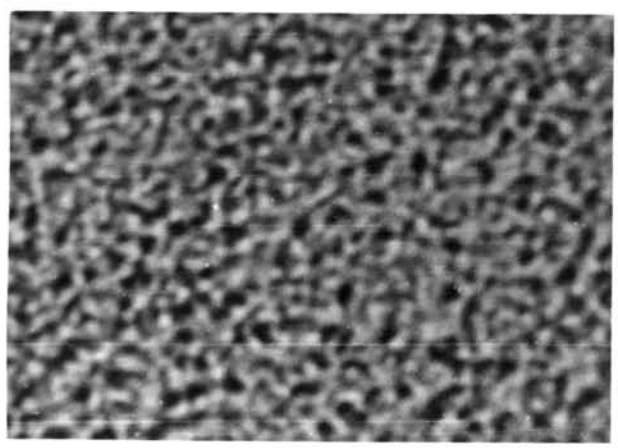

Fig. 5.1: Photograph showing the surface of the film without imperfections. (x 250)

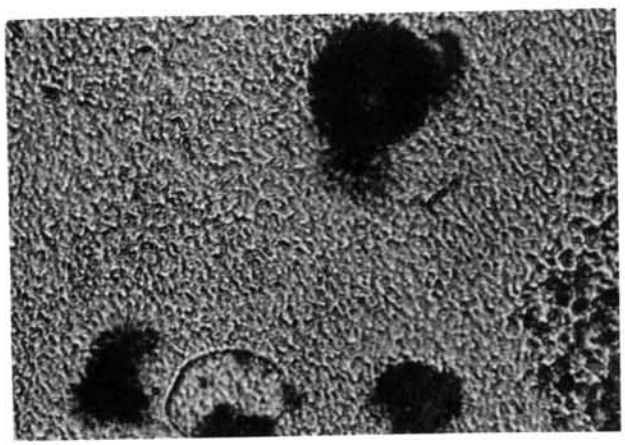

Fig.5.2: Photograph showing the surface of the film with imperfections. (X100)

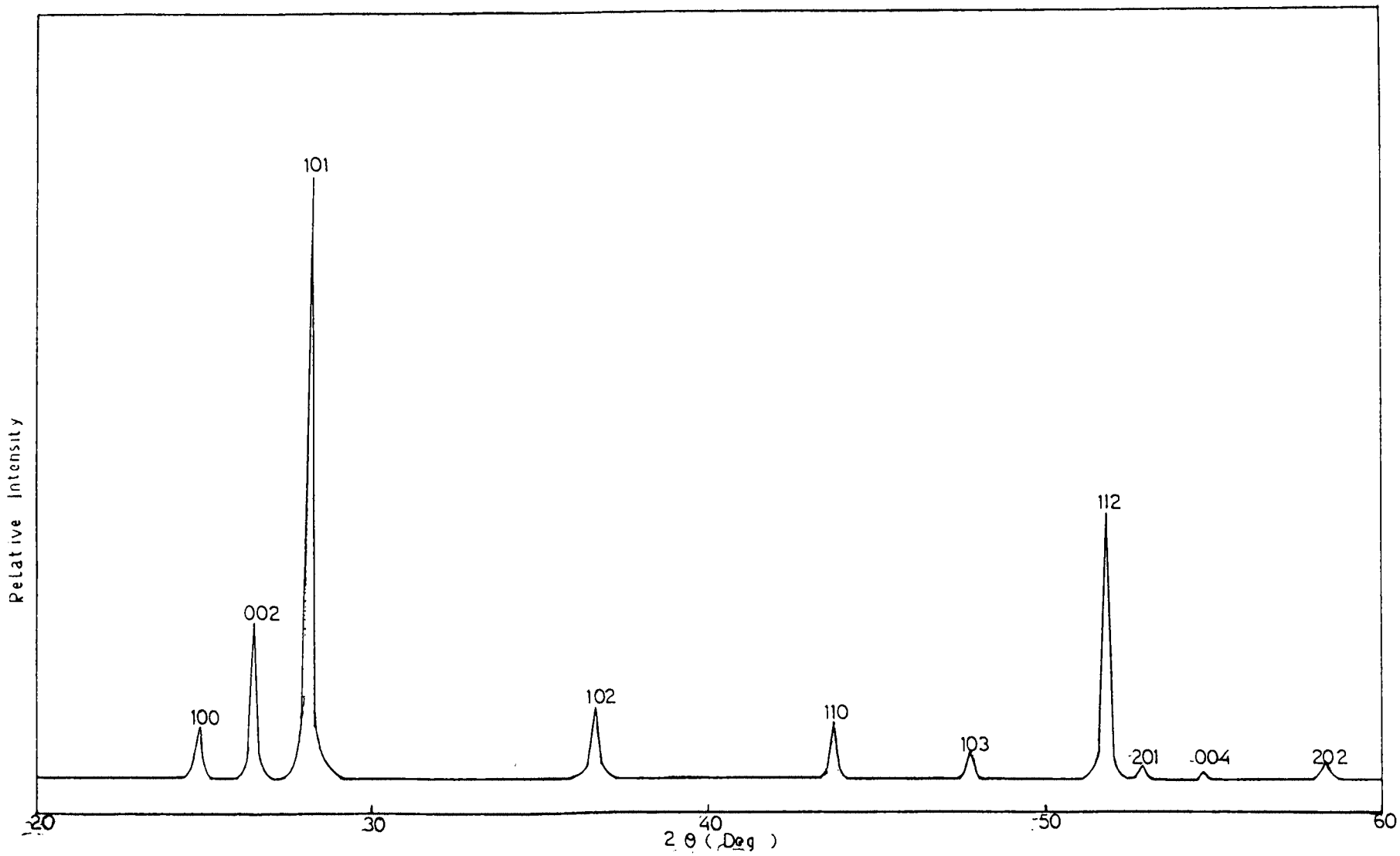

Fig. 5.3: X-ray diffraction pattern of the film.

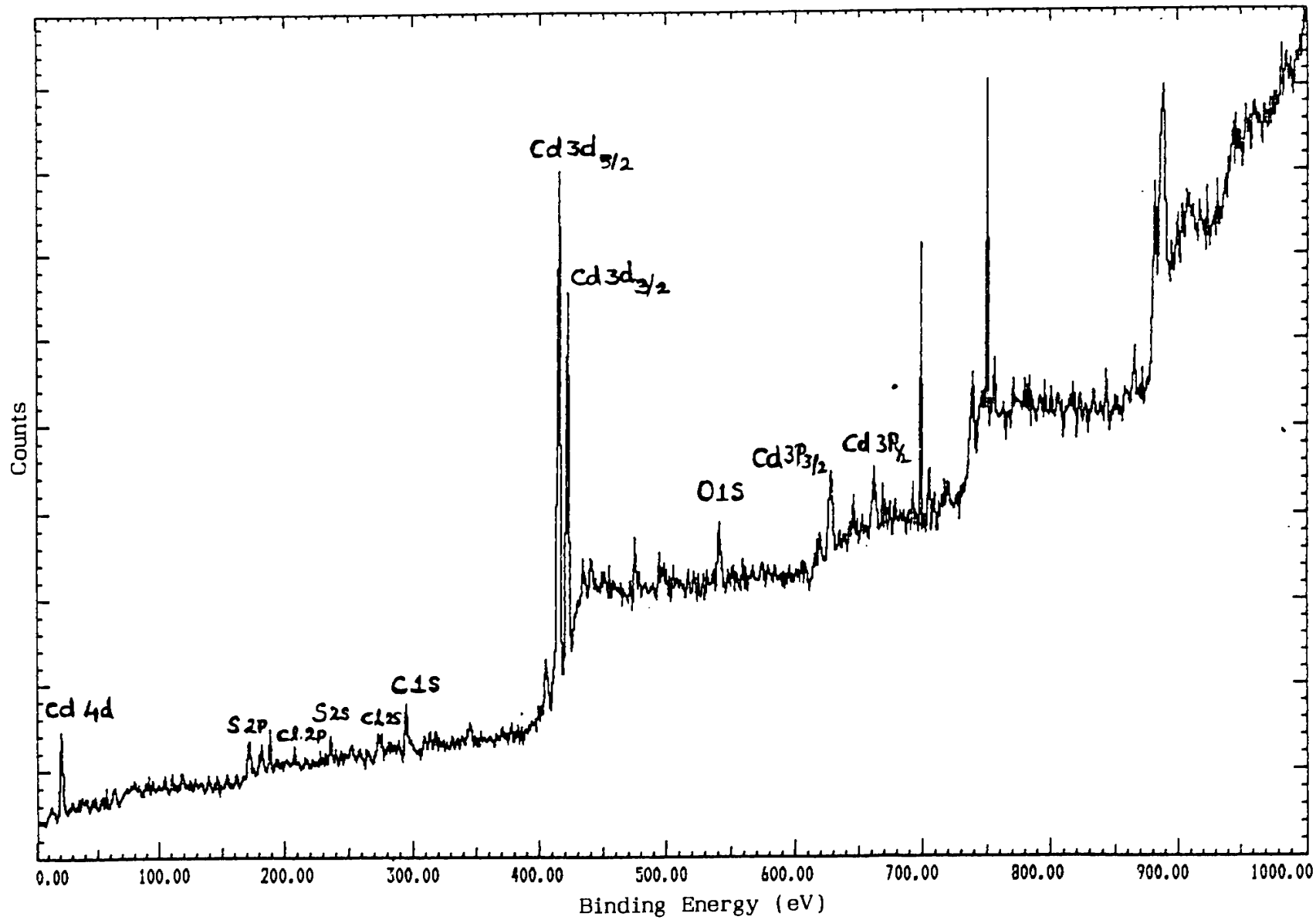

Fig. 5.4: X-ray photoelectron spectrum of the film indicating various elements present.

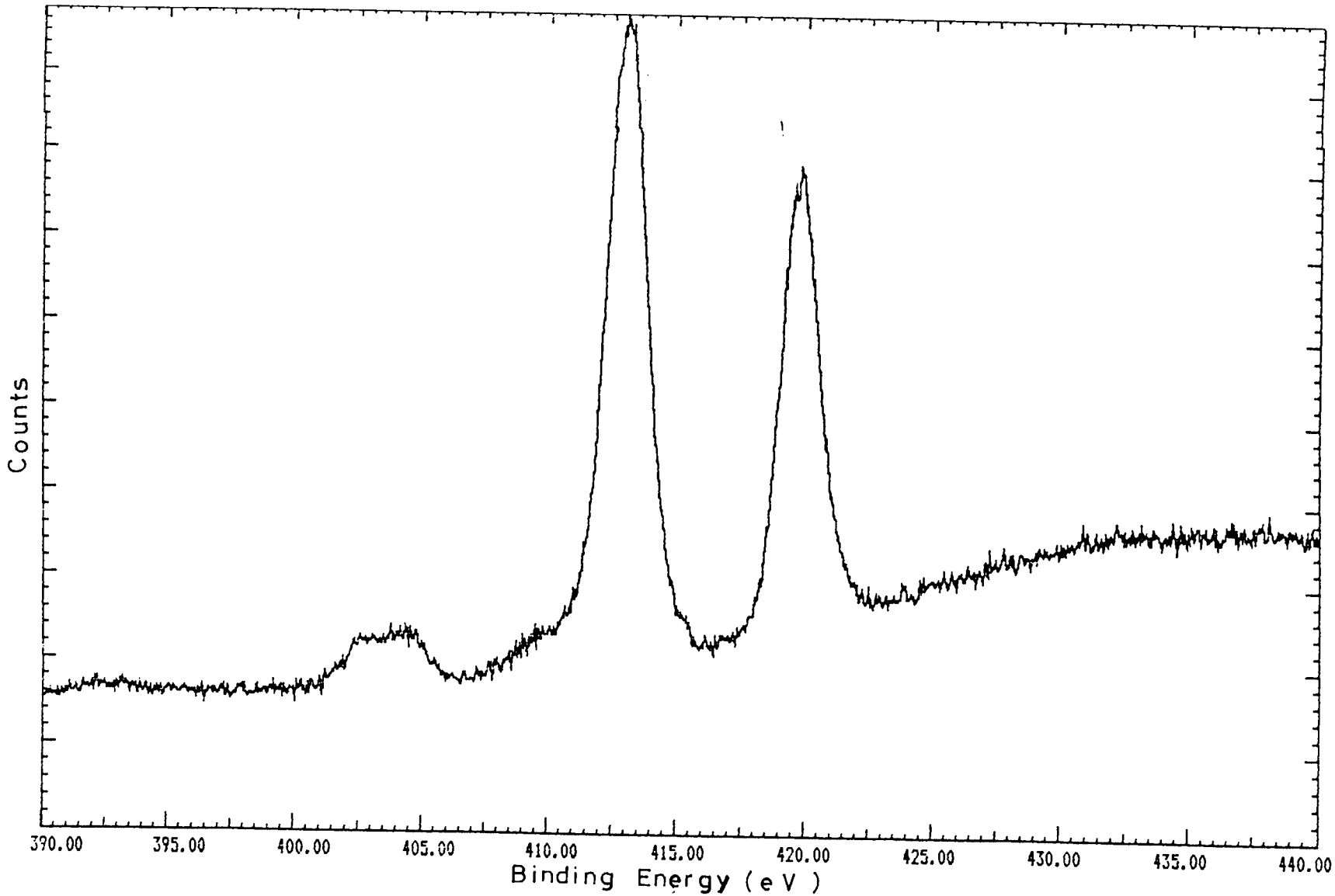

Fig. 5.4 (a): High resolution spectrum of Cd 3d level.

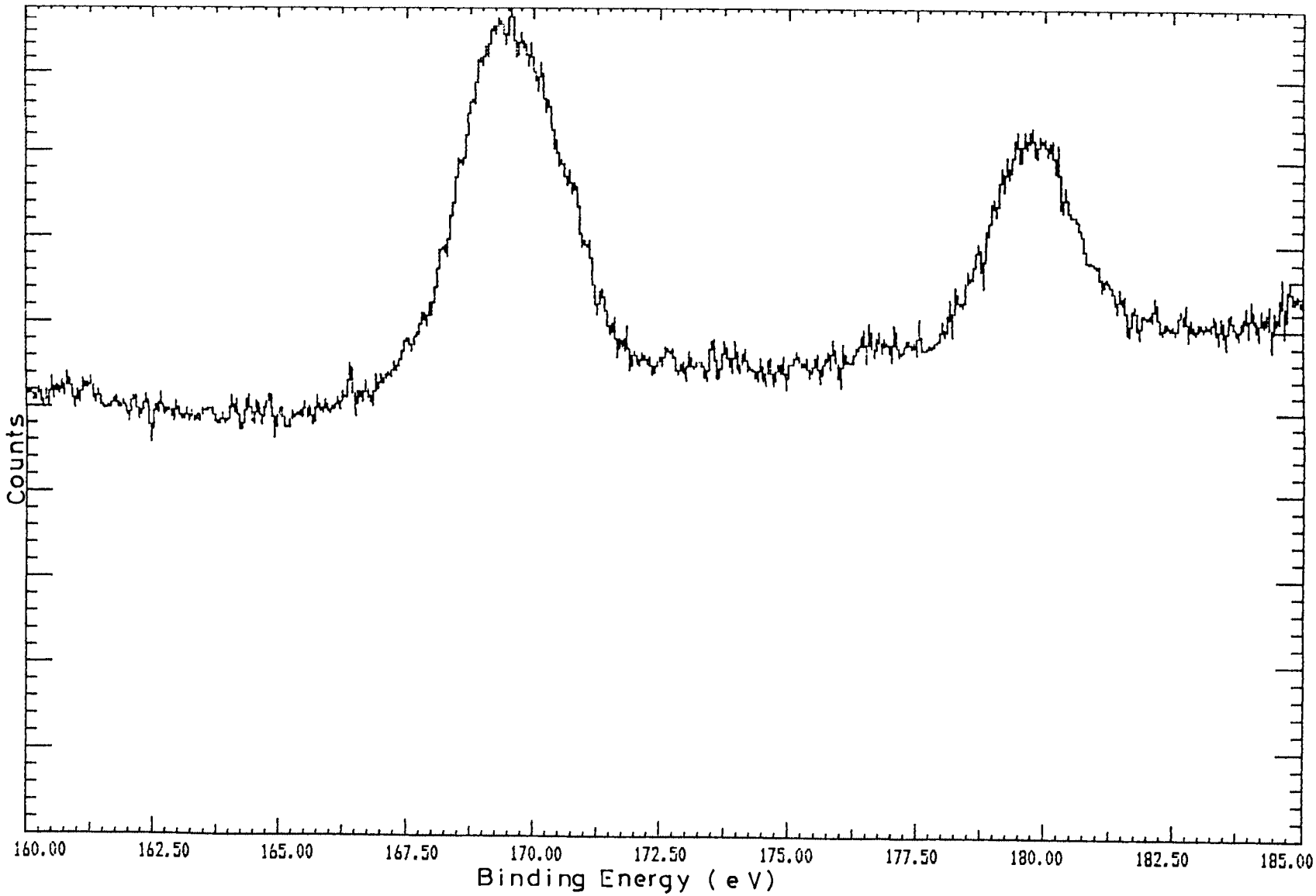

Fig. 5.4 (b): High resolution spectrum of S 2p level.

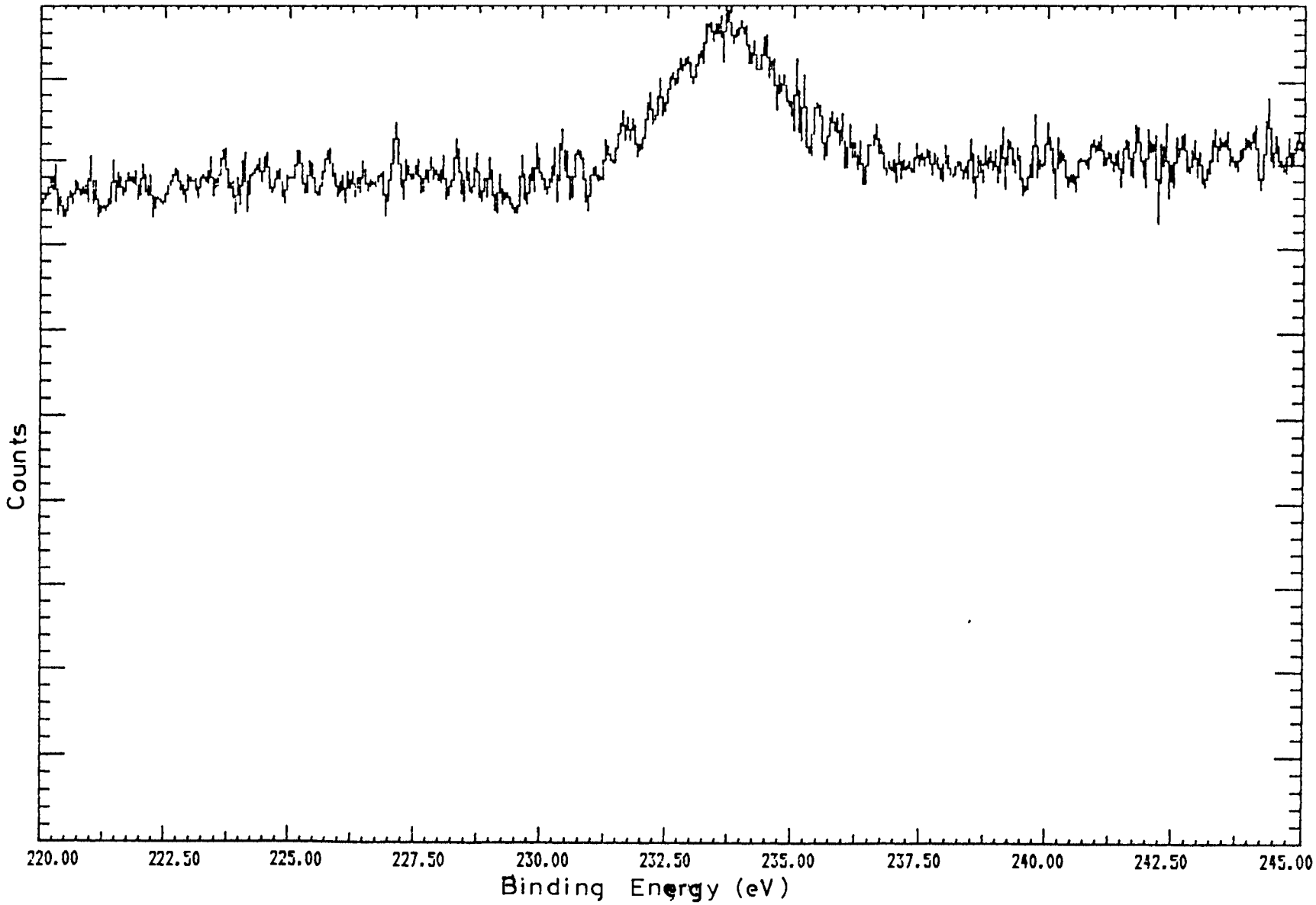

Fig. 5.4 (c): High resolution spectrum S 2s level.

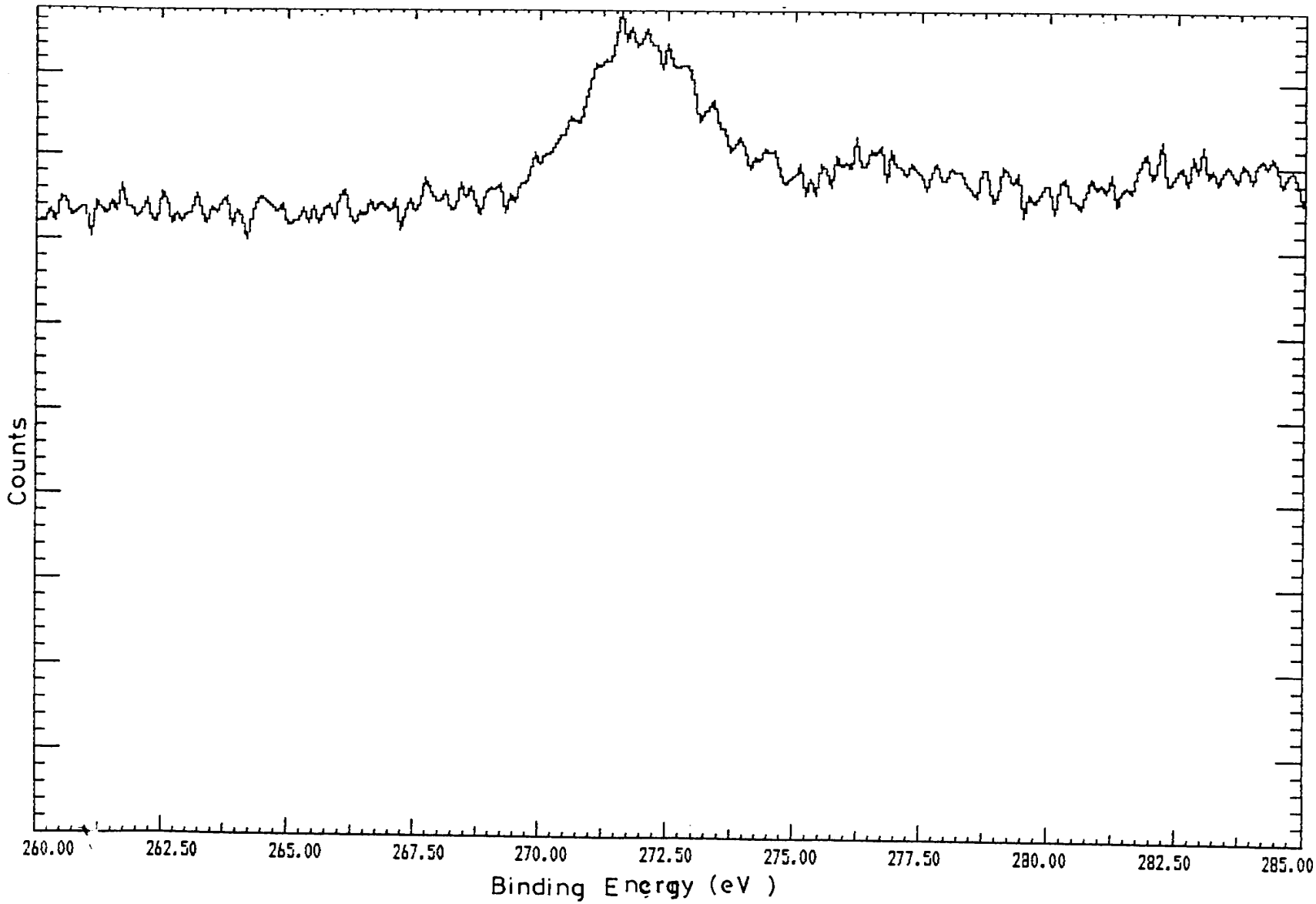

Fig. 5.4 (d): High resolution spectrum of Cl 2s level.

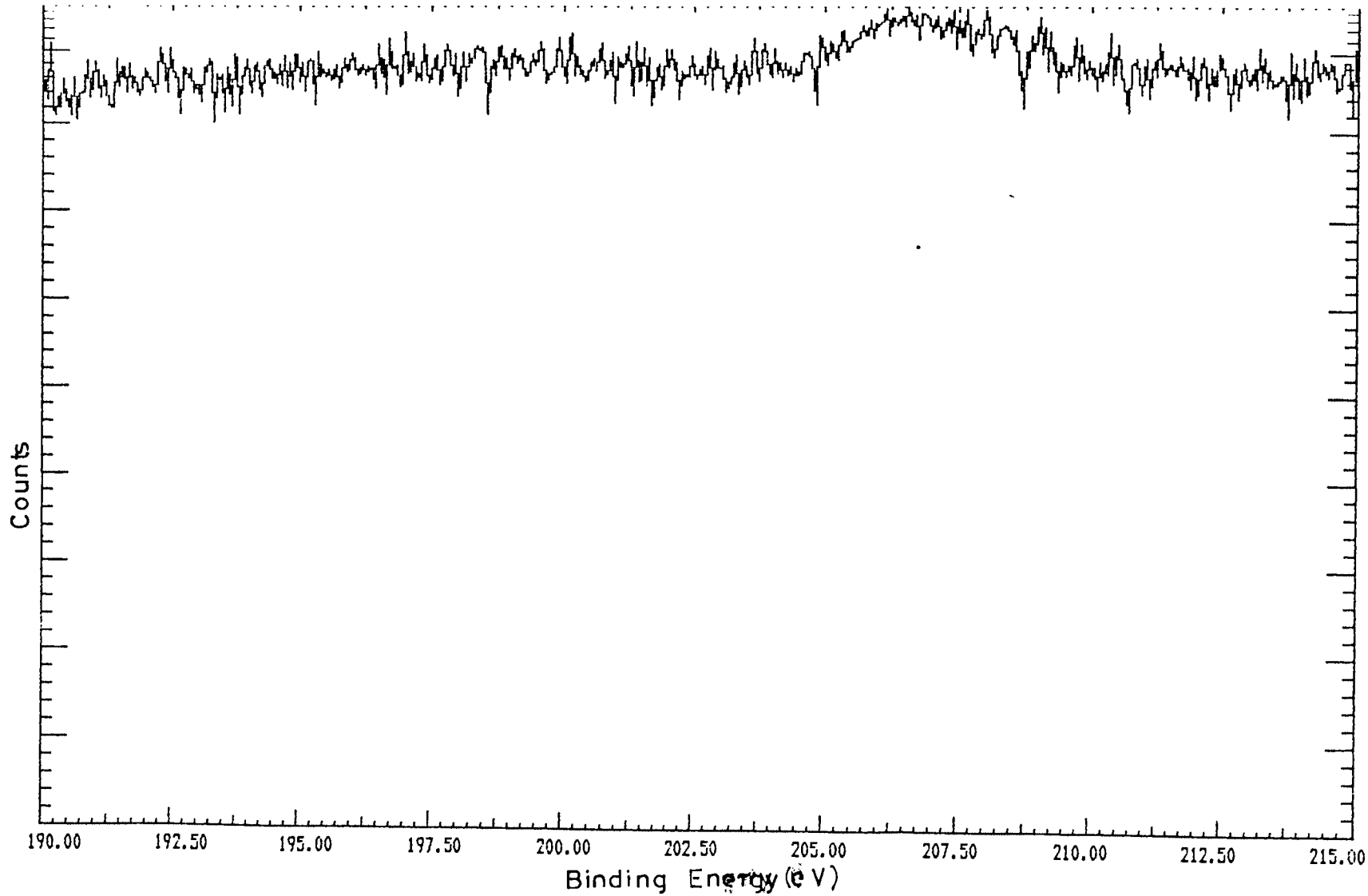

Fig. 5.4 (e): High resolution spectrum of Cl 2p level.

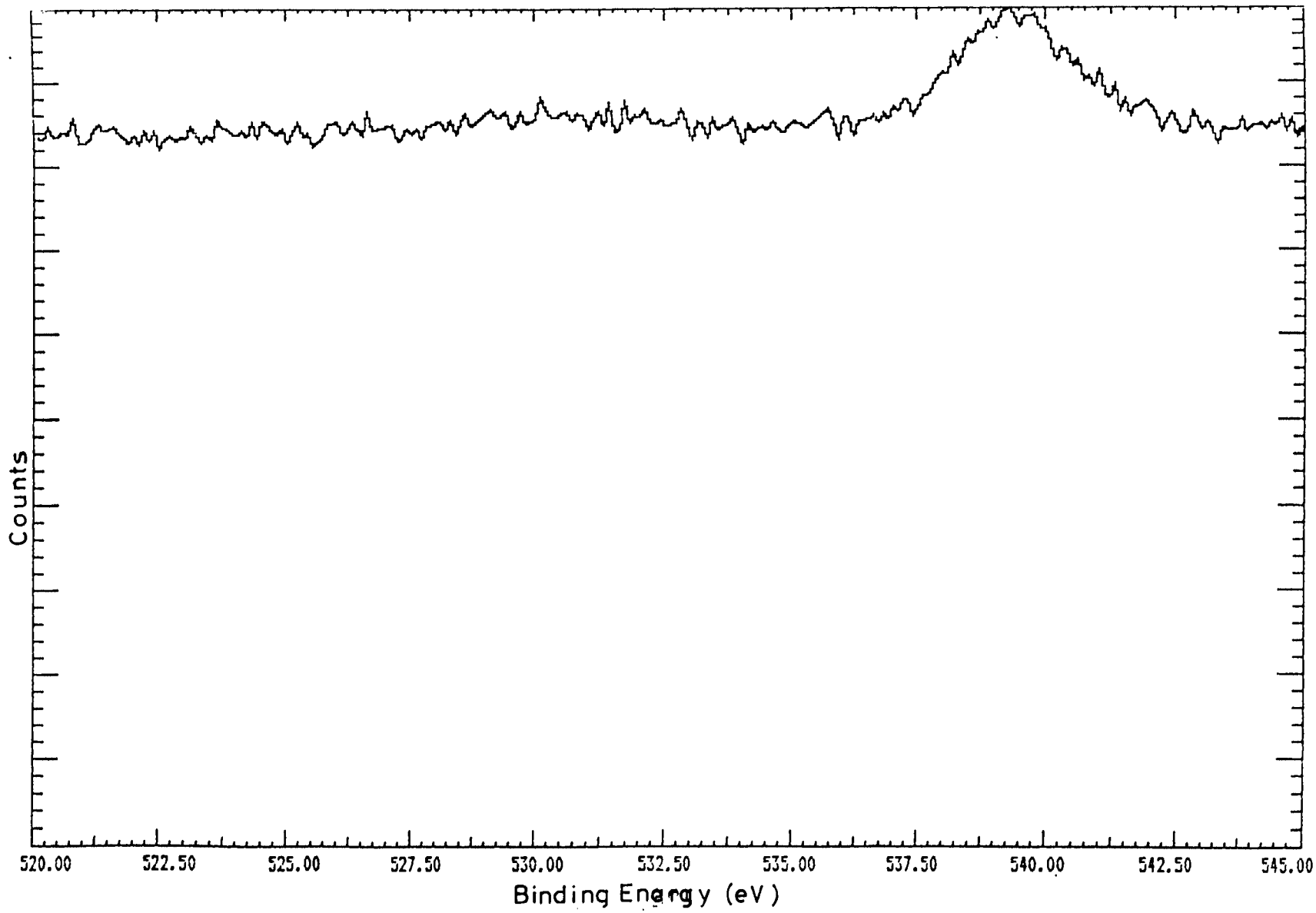

Fig. 5.4 (f): High resolution spectrum of O 1s level.

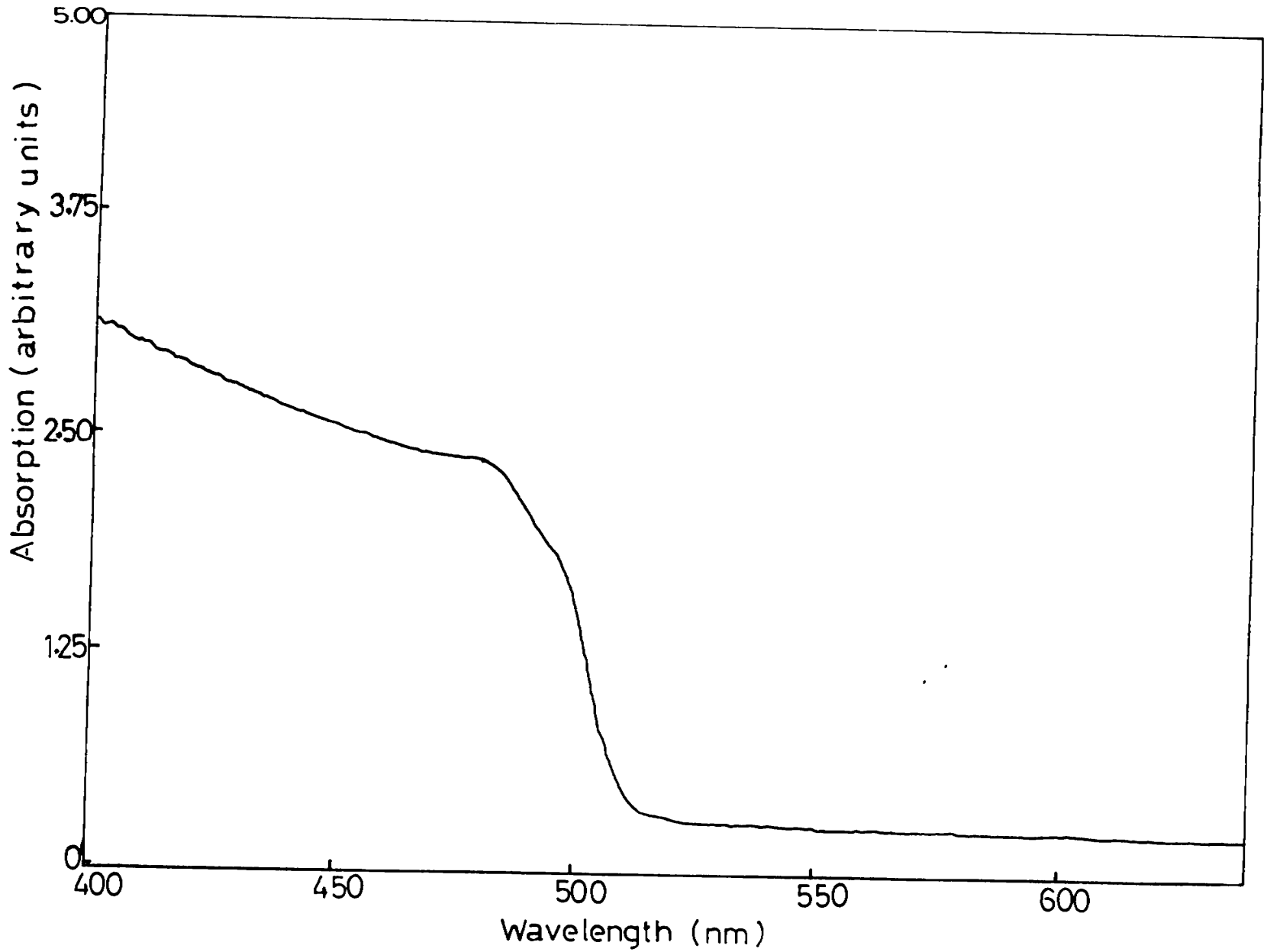

Fig. 5.5: Absorption spectrum of the film

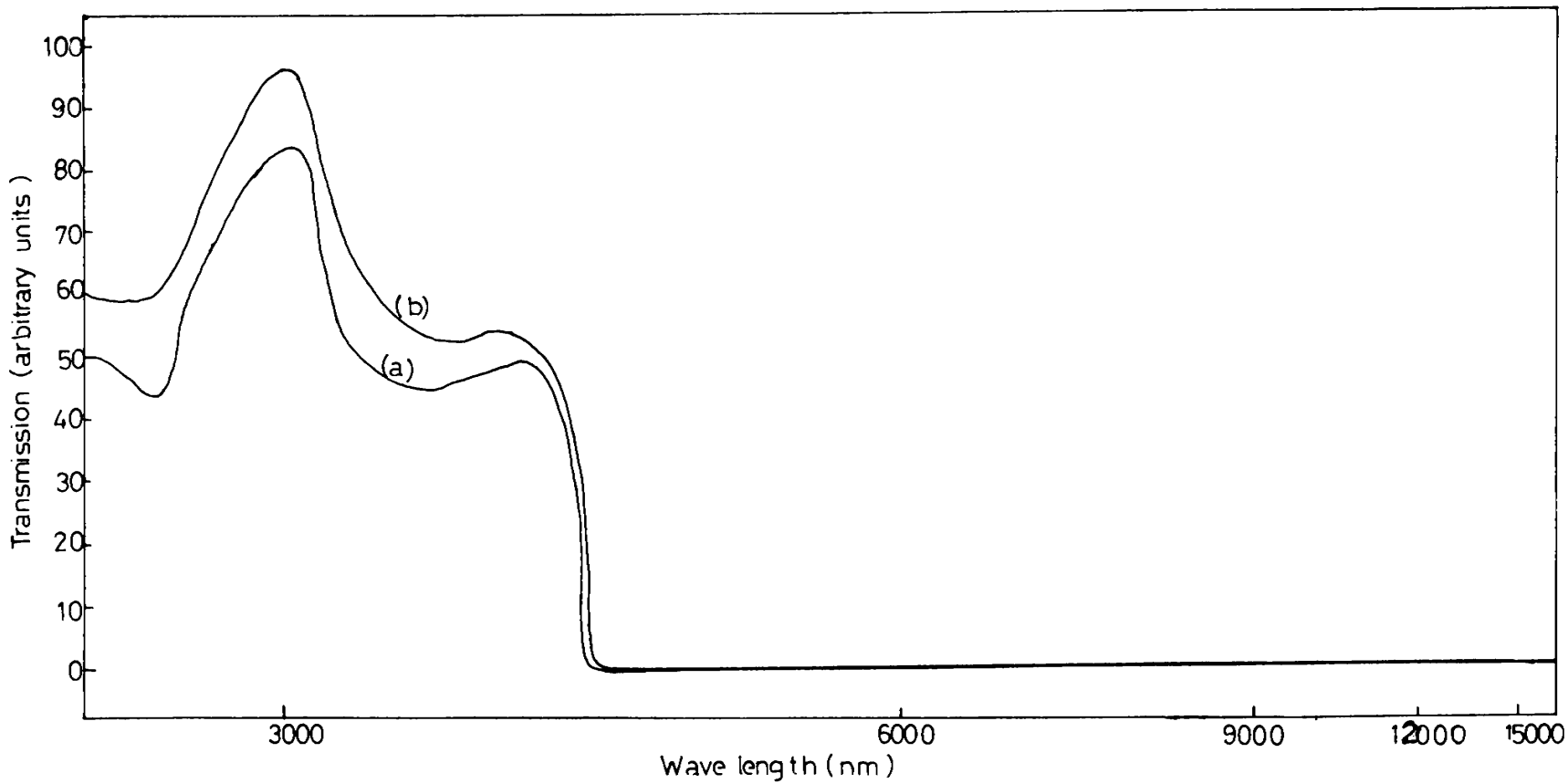

Fig. 5.6: Transmission spectra of the films annealed at different temperatures: (a) 373 K and (b) 573 K.

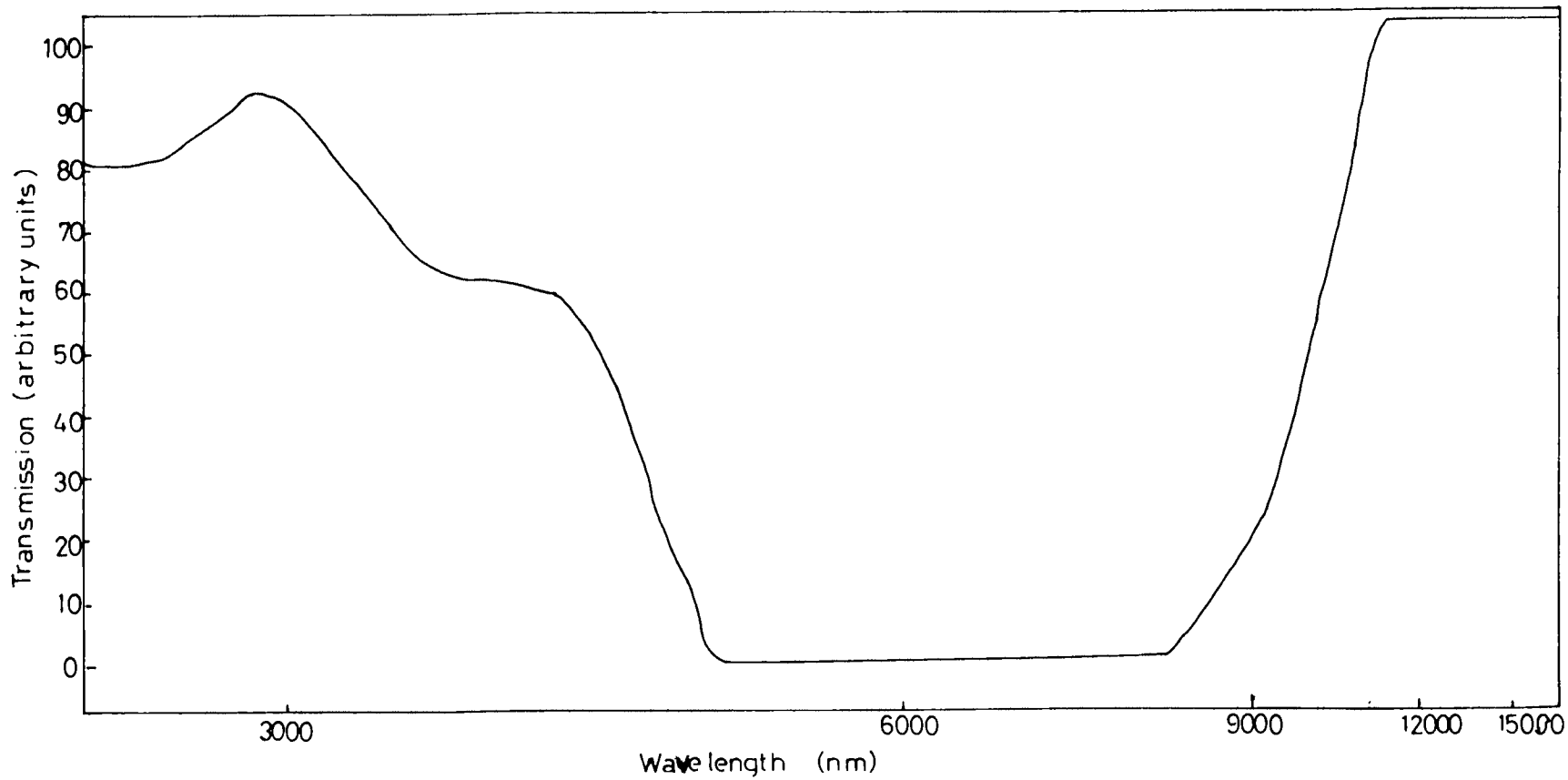

Fig. 5.7: Transmission spectrum of the film annealed at 473 K.

by the X-ray analysis. The various elements present in the films are analysed from the ESCA spectra. The band gap calculated from the absorption spectrum is found to be 2.41 eV. The transmission spectra of the films annealed at 473 K indicates the existence of a trap level in the sample.

5.5 REFERENCES

[1] N. Nakayama, H. Matsumoto, A. Nakano and S. Ikegami, H. Uda and T. Yamashita, Jpn. J. Appl. Phys. 19 (1980) 703.

[2] J.S. Lee and H.B. Im, J. Mater. Sci. 21 (1986) 980.

[3] J.S. Lee, H. B. Im, A. L. Fahrenbruch and R.H. Bube, J. Electrochem. Soc. 134 (1987) 1790.

[4] Y.Y. Ma, A. L. Fahrenbruch and R.H. Bube, Appl. Phys. Lett. 30 (1977) 423.

[5] H.J. Hovel, in: Semiconductors and semimetals, eds. R.K. Willardson and A.C. Beer, Vol.II (Academic Press, New York, 1975).

[6] R. Hill and I.A.S. Edwards, Vacuum 27 (1977) 277.

[7] I. Dresner and I.V. Shallcross, Solid-state Electron.5 (1962) 205.

[8] W. Kahle and H. Berger, Phys. Stat. Solidi A.2 (1970) 717.

[9] R.W. Buckley and J. Woods, J. Phys. D. Appl. Phys. 6 (1973) 1084.

[10] K.H. Norian and J.W. Edington, Thin Solid Films 75 (1981) 53.

[11] S. Ray, R. Banerjee and A.K. Barva, Jpn. J. Appl. Phys. 19 (1980) 1889.

[12] A.J. Behringer and L. Corrsin, J. Electrochem. Soc. 110 (1963) 1083.

[13] P.H. Wendland, J. Opt. Soc. Amer. 52 (1962) 581.

[14] L. Magafas, A.N. Anagnostopoulos and J.G. Antonopoulos, Phys. Stat. Solidi A. 111 (1989) K 175.

[15] P.S. Aggarwal and A. Goswami, Indian J. Pure Appl. Phys.1 (1963) 366.

[16] H. Berger, E. Gutsche and W. Kahle, Phys. Stat. Solidi 7 (1964) 679.

[17] W.C. Boesman and G.G. Avis, Transactions of the Tenth National Vacuum Symposium of the American Vacuum Society, New York, 1963.

[18] A. Bennouna, E.L. Aneziane, A. Haouini, N. Ghermani, M. Azizan and M. Brunel, Sol. Energy. Mater. 20 (1990) 405.

[19] F. E I Akkad and M.A. Naby, Sol. Energy. Mater. 18 (1989) 151.

[20] R.W. Berry, P.M. Hall and M.T. Harris, Thin Film Technology, (Van Nostrand - Reinhold, New York, 1968) P. 191

[21] D.B. Fraser and H. Melchior, J. Appl. Phys. 43 (1972) 3120.

[22] I. Martil de la Plaza, G. Gonzalez - Diaz, F. Sanchez - Quesada and M. Rodriguez - Vidal, Thin Solid Films 90 (1982) 253.

[23] J.R. Clarke and J.E. Greene, J. Vac. Sci. Technol. 18 (1981) 382.

[24] D.C. Cameron, W. Duncon and W.M. Tsang, Thin Solid Films 58(1979) 61.

[25] C. De Blasi, A.M. Mancini, D. Manno and L. Vasanelli, J. Cryst. Growth 101 (1990) 185.

[26] L.D. Partain, G.J. Sullivan and C.E. Birchenall, J. Appl. Phys. 50 (1979) 551.

[27] A.L. Dawar, P.K. Shishodia, G. Chauhan, A. Kumar and P.C. Mathur, J. Mater. Sci. Lett. 9 (1990) 547.

[28] N. Croitoru and S. Jakobson, Thin Solid Films, 56 (1979) L5.

[29] H.Uda, S. Ikegami and H. Sonomura, Jpn. J. Appl. Phys. I. Regul. Pap. Short Notes 29 (1990) 30.

[30] C.D. Lokhande, V.S. Yermune and S.H. Pawar, Mater. Chem. Phys. 20 (1988) 285.

[31] K.S. Balakrishnan and A.C. Rastogi, Sol. Energy, Mater. 20 (1990) 417.

[32] M.K. Karajai and D. Das Gupta, Thin solid films 155 (1987) 309.

[33] R.R. Chamberlin and I.S. Skarman, J. Electrochem. Soc. 113 (1966) 86.

[34] T.P. Walker and B.J. Fedman, Solid State Commun. 38 (1981) 353.

[35] A. Ern, M. Krunks and M. Mellikov, Proceedings of the Ninth E.C. Photovoltaic Solar Energy Conference, West Germany, 1989, P. 525.

[36] S. Martinuzzi, J. Qualid, F. Cabane - Brouty, A. Mostavan and J. Gervais, Revue Phys. Appl. 14 (1979) 237.

[37] W. Dulak, Acta. Phys. Pol.A. A 69 (1986) 945.

[38] R.S. Berg and R.D. Nasby, J. Vac. Sci. Technol. 15 (1978) 359.

[39] JCPDS: International Centre for Diffraction Data, USA, 1978 .

[40] A.L. Fahrenbruch and R.H. Bube, Fundamentals of Solar Cells (Academic Press, New York)

6 DARK CONDUCTIVITY STUDIES OF CdS THIN FILMS

6.1 INTRODUCTION

The electrical conductivity studies of CdS films prepared by vacuum evaporation, sputtering, molecular beam epitaxy and close spaced techniques have been done by various authors [1-9]. Panov et al. [10] studied the temperature dependence of the dark conductivity of CdS films prepared by the deposition of ions from aqueous solution with the aid of thiourea. But not much data has been seen reported on the conductivity studies of spray pyrolysed CdS films. Bougnot et al [11] studied the effect of annealing of sprayed CdS films with excess sulphur in H_2 atmosphere on the resistivity. They reported that annealing in H_2 can significantly decrease the value of resistivity. Ma and Bube [12] have investigated the dependence of electrical conductivity on the deposition temperature. Gupta et al. [13] reported the dark conducting properties of films prepared by changing the concentration of sulphur ions in the thiourea solution. However sufficient information on the electron trapping in sprayed CdS films has not been found. Also, not much studies have been carried out on the films containing different contents to examine the annealing kinetics or to get a vivid picture of the variation of the conductivity of the film heat treated under different ambients. As such, it was thought useful to make an analysis of dark conduction to study the different trap levels in spray pyrolysed CdS thin films. The effect of cadmium contents, annealing temperatures and ambient conditions on the dark conducting properties of these films have been investigated and are presented here.

6.2 EXPERIMENTAL

CdS films A_1 to A_5 were prepared on optically flat and thoroughly cleaned glass slides by the spray pyrolysis method. The details of the designation of these films are given in Table 5.1, Chapter 5. These films were annealed in air for 30 min. For the conductivity measurements, the thickness of the films was accurately determined and aluminium electrodes were then deposited by vacuum evaporation. The films were then mounted inside the metallic cell and the measurements were carried out by applying a steady voltage of about 9V across the film. The resulting current was measured by using an electrometer. The experiment was also performed in air. During the measurements, temperature of the film was controlled by the current applied to the heater from a stabilized voltage Source. Details of the sample holder and metallic cell have been already described in Chapter 4. The activation energy (E) of charge carriers was also determined.

6.3 RESULTS AND DISCUSSION

The dark conductivity studies were performed in different ambient conditions (vacuum and air) on a number of films for different cadmium contents. The electrical properties which are related to the conditions used for the preparation and annealing of the films, determine the native defects such as sulphur vacancies and cadmium interstitials. These defects act as donors or electron traps. The experimental conditions are able to favour or suppress certain types of

traps. So during the present investigations, special attention has been made to understand these characteristics while measuring the dark conductivity.

The dependence of temperature on the dark conductivity of unannealed and annealed films A_1 to A_5 containing different cadmium contents are found to show similar trends. The typical conduction characertistics obtained for the film A_1 prepared. from 0.20 M cadmium chloride and 0.20 M thiourea is shown in Fig. 6.1. The conductivity is found to be lower at very low temperature (100K). It increases slowly with temperature in the low temperature region, while at high temperatures, the increase in conductivity with temperature is comparatively sharper upto 423 K. This indicates that, conduction is persumed to be taking place by an activated process. Carriers available for conduction (donors) in n- type CdS is due to the native defects or due to the presence of impurities such as Cl in the CdS lattice. At low temperatures, the conductivity is low because most of the carriers are frozen out on the donor centres. As the temperature rises, an increasing fraction of the centres is ionized and consequently the number of electrons from the donor levels is proportionately increased. This explains why the films have higher conductivity at 423K.

From Fig 6.1, it is seen that there are three trap levels that are effective for different temperature ranges. In Table 6.1, the values of activation energy estimated from the slope of log ($10^8 \sigma$) versus 10^3 / T plot for all the films are listed. The energy depths

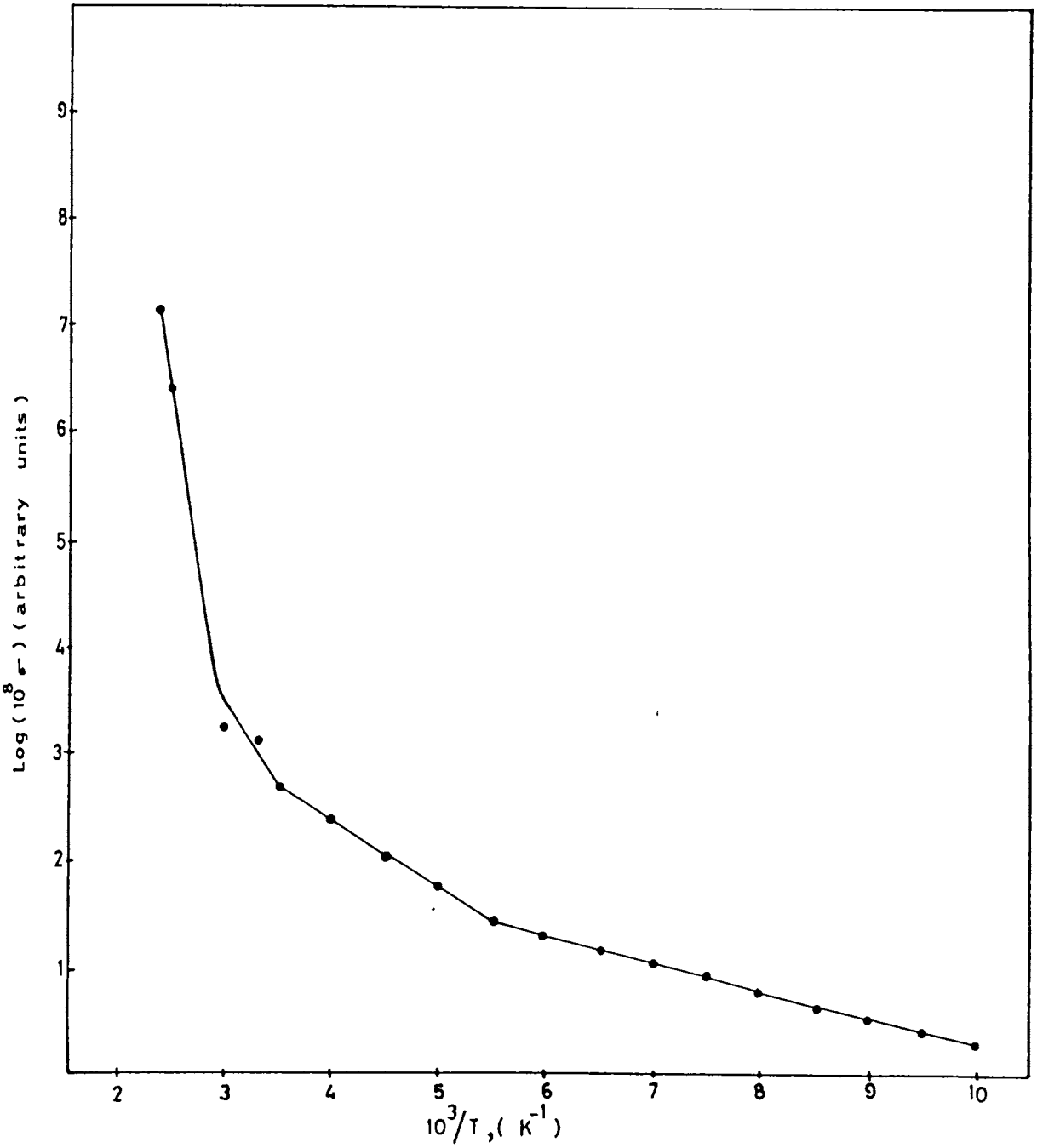

Fig 6.1 : Plot of log ($10^8 \sigma$) against $10^3/T$ for the unnannealed film A_1 in vacuum.

Table 6.1 The values of activation energy obtained from the conductivity measurements of the films in vacuum.

Sample	Activation energy in the temperature range at 100-166K (eV)	182-286K (eV)	333-423K (eV)
A_1			
Unannealed	0.049	0.100	1.280
Annealed(373K)	0.032	0.257	0.810
Annealed(423K)	0.048	0.248	0.790
Annealed(473K)	0.049	0.249	0.797
Annealed (523K)	0.050	0.251	1.100
Annealed (573K)	0.051	0.250	1.150
A_2			
Unannealed	0.030	0.248	0.513
Annealed (373K)	0.029	0.250	0.790
Annealed (423K)	0.051	0.253	0.810
Annealed (473K)	0.052	0.249	0.811
Annealed (523K)	0.048	0.150	0.794
Annealed (573K)	0.049	0.147	0.820

Contd...

Contd... Table 6.1

A_3			
Unannealed	0.032	0.258	0.520
Annealed (373K)	0.029	0.253	0.828
Annealed (423K)	0.049	0.252	0.830
Annealed (473K)	0.052	0.251	0.810
Annealed (523K)	0.051	0.249	0.790
Annealed (573K)	0.049	0.248	0.795
A_4			
Unannealed	0.030	0.253	0.510
Annealed (373K)	0.031	0.252	0.410
Annealed (423K)	0.057	0.248	0.430
Annealed (473K)	0.054	0.251	0.794
Annealed (523K)	0.052	0.253	0.790
Annealed (573K)	0.053	0.250	0.828
A_5			
Unannealed	0.032	0.250	0.530
Annealed (373K)	0.030	0.258	0.411
Annealed (423K)	0.049	0.249	0.410
Annealed (473K)	0.054	0.248	0.840
Annealed (523K)	0.053	0.253	0.810
Annealed (573K)	0.052	0.251	0.828

of discrete trap levels observed in the films are found to be ~ 0.03, ~0.05, ~0.05, ~ 0.10, ~ 0.14, ~0.25, ~0.40, ~ 0.50, ~ 0.80 and ~1.2 eV. It is clear from this table that the activation energy has an influence on the concentration of cadmium chloride and the annealing temperature. Since the sprayed films were prepared from the solutions of cadmium chloride and thiourea, they contain impurities such as chlorine. So the 0.03 eV shallow trap in the films (Table 6.1) is regarded as the ionization energy of chlorine donor level. There is a fairly good agreement between this value and that reported for single crystals of CdS [14].

Nishimura [15] reported an activation energy of 0 • 138 eV which is necessary to create a sulphur vacancy in CdS crystals. The sulphur vacancy can move a few lattice distances so that complexes of these vacancies are possible and hence the observed trap centre ~0.25 eV is constituted by a complex of sulphur vacancies. The level ~0.25eV associated with these native defects is observed in all films irrespective of the annealing temperature. The electron traps 0.05, 0.14 and 0.25 eV are usually observed in Cd-rich crystals [16]. As the cadmium content increases the excess cadmium replaces sulphur and sulphur vacancy is formed. Hence isolated and complex sulphur vacancies are present so that ~ 0.05, ~ 0.14 and ~0.25 eV traps are detected. The donor centres are originated from the trapping of electrons in an anion vacancy which is the dominant electrical defect in II-VI compounds such as CdS.

The unannealed film A_1 is found to display a trap level $\sim$ 0.10 eV [17], which is characteristic of the motion of sulphur interstitials. The sulphur vacancy might undergo trapping at impurities or other defects in the temperature range 182 - 286 K. Sharman [18] and Susa et al. [19] have observed a 0.50 eV level in CdS single crystals containing an excess of cadmium. Shaw and Whelan [20] attributed these levels to interstitial cadmium. It therefore appears that in unannealed films containing higher cadmium contents an excess cadmium is always present, particularly in interstitial sites and hence the observed 0.50 eV level is identified as interstitial cadmium.

The values of activation energy $\sim$ 0.41 and $\sim$0.83 eV deduced from the high temperature dependence of dark current corresponds to the activation energy of the charge carriers released from the complex of cadmium and sulphur vacancies localised in nearest neighbour sites. These traps are reported to be present in CdS crystals [16]. Associated cadmium vacancies which comprise a sulphur complex form the above trap levels. Van Gool and Diemer [21] reported that association of single point defects of opposite charge is known to take place in II-VI compounds. So in these vacancy complexes, the number of constituent vacancies of each type are unequal. For the unannealed and annealeld (523-573K) film A_1, an activation energy of $\sim$ 1.2 eV is observed, which corresponds to the mobility of sulphur vacancies [17].

The dark conductivity of the films is found to be strongly dependent on the cadmium contents and the annealing temperature.

[Figs. 6.2 (a) to 6.2 (c)] . The variation is much smaller at 100K [Fig 6.2 (a)]. It is seen that, the magnitude of the conductivity of films A_2 to A_5 is higher than that of the film A_1. Vacant anion lattice sites are more in the films containing higher cadmium contents. There is a strong tendency for the trapping of extra electrons in the anion vacancy. During the heat treatment, the trapped electrons are released and thus increases the conductivity for the films A_2 to A_5.

It is observed that the conductivity of the films annealed at 373K is higher than that of the films annealed at higher temperatures. Air annealing of the films at 373K causes excess sulphur vacancies and hence the conductivity is increased. This is also due to the presence of chlorine impurities. The decrease in the conductivity observed in the films annealed above 373K is probably due to the decrease in the number of carrier generation. It is seen from Figs. 6.2 (a) to 6.2(c) that the unannealed film A_1 has a low value of conductivity than that of unannealed films A_2 to A_5. The sulphur interstitial corresponding to the trap level 0.10 eV is observed only in the unannealed film A_1. These sulphur interstitials are responsible for the reduction in the concentration of the effective donors which gives rise to a drop in conductivity. It is thus established from the electrical characteristics of films that the conduction is dominated by the donor concentration from the native defects and impurities.

The chemisorption of oxygen strongly influences the conductivity of the films heat-treated in air from 303 to 423K. Fig 6.3 shows the variation of conductivity as a function of inverse temperature for the

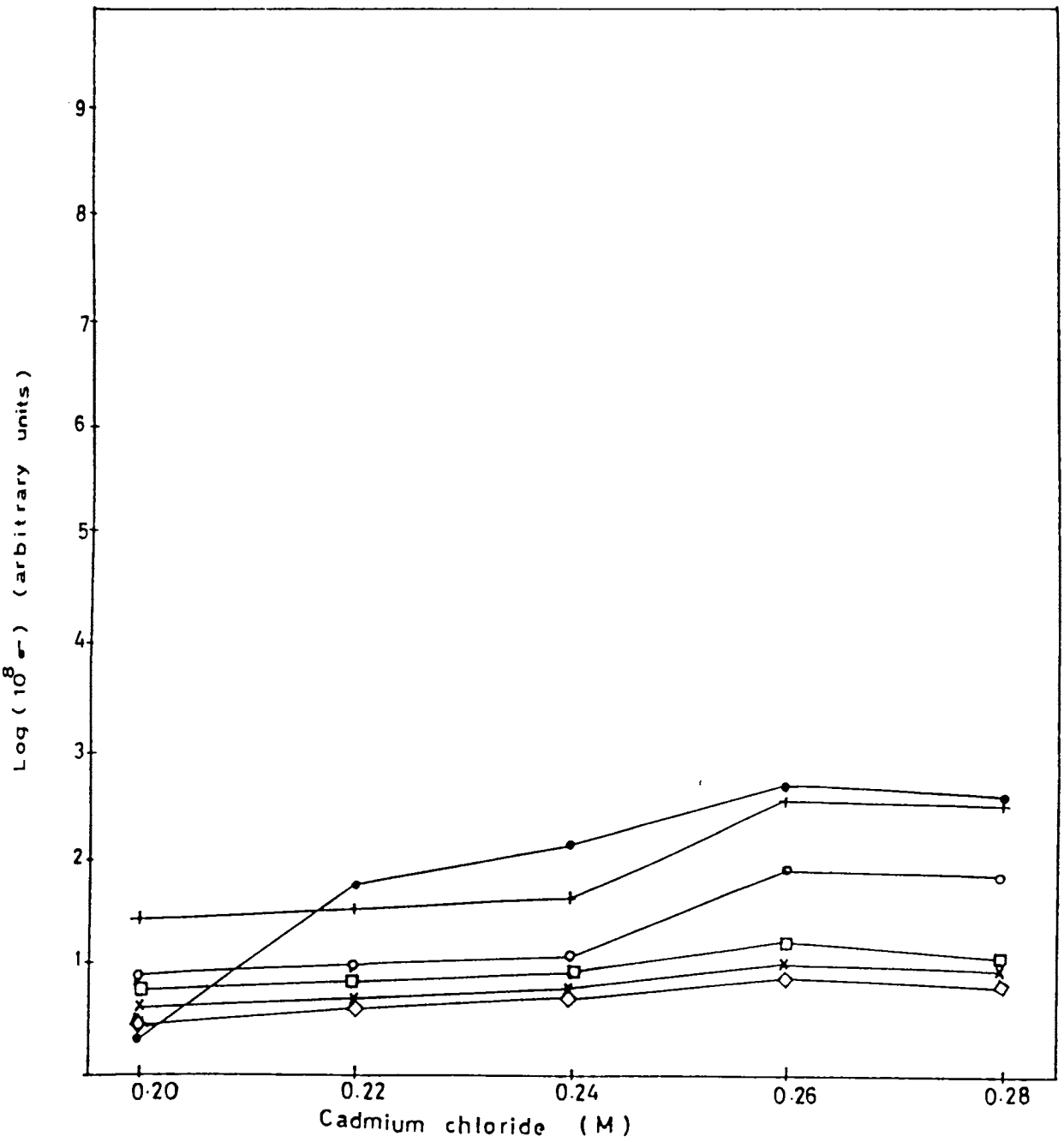

Fig 6.2 (a) : Variation of conductivity as a function of concentration of Cadmium Chloride for the films in vacuum at 100K : (•) unannealed and annealed at (+) 373K, (o) 423K, (□) 473K, (X) 523K and (◇) 573K.

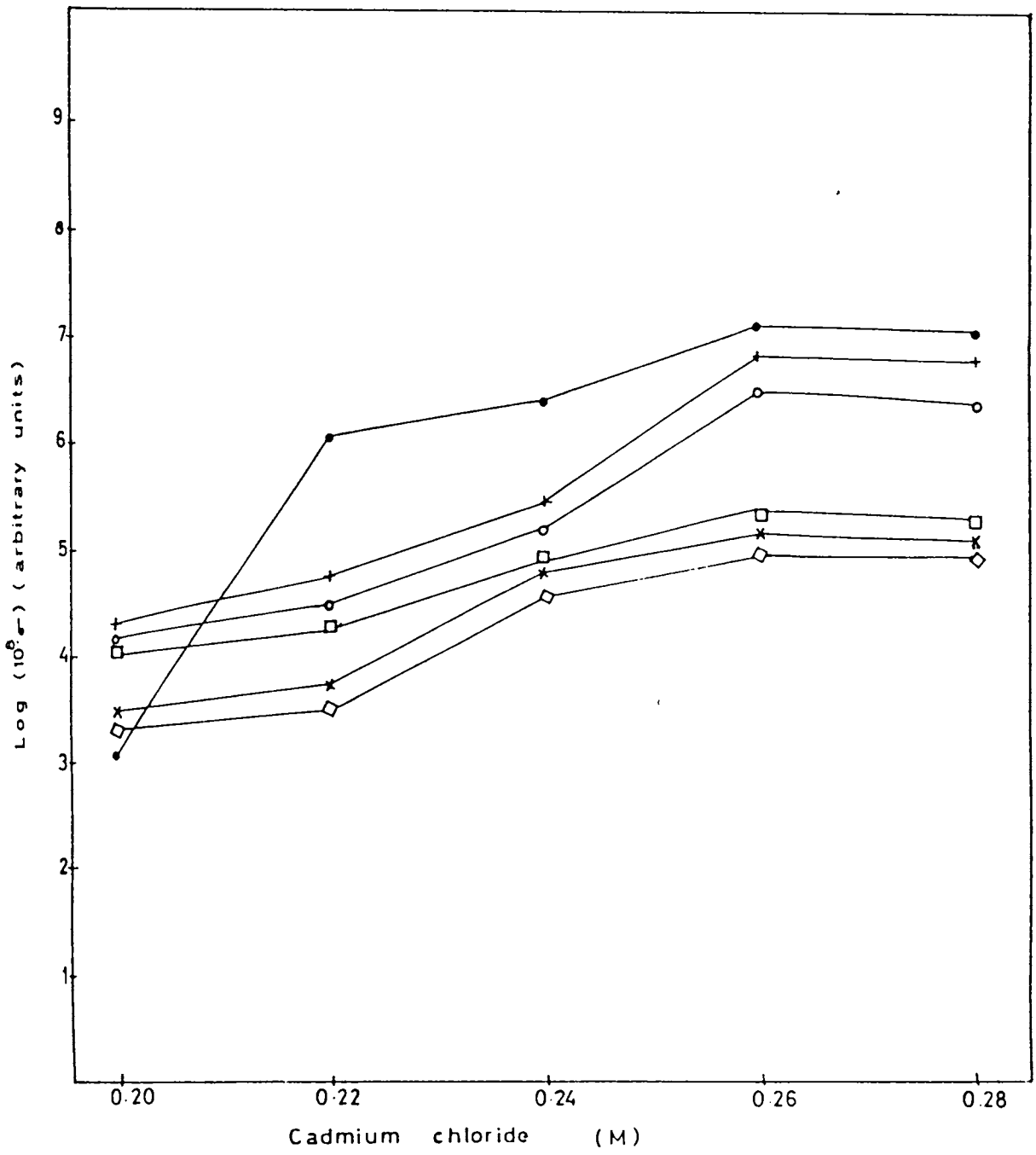

Fig. 6.2 (b) : Variation of conductivity as a function of concentration of Cadmium Chloride for the films in vacuum at 303 K: (•) unannealed and annealed at (+) 373 K, (o) 423 K, (□) 473 K, (X) 523 K and (◇) 573 K.

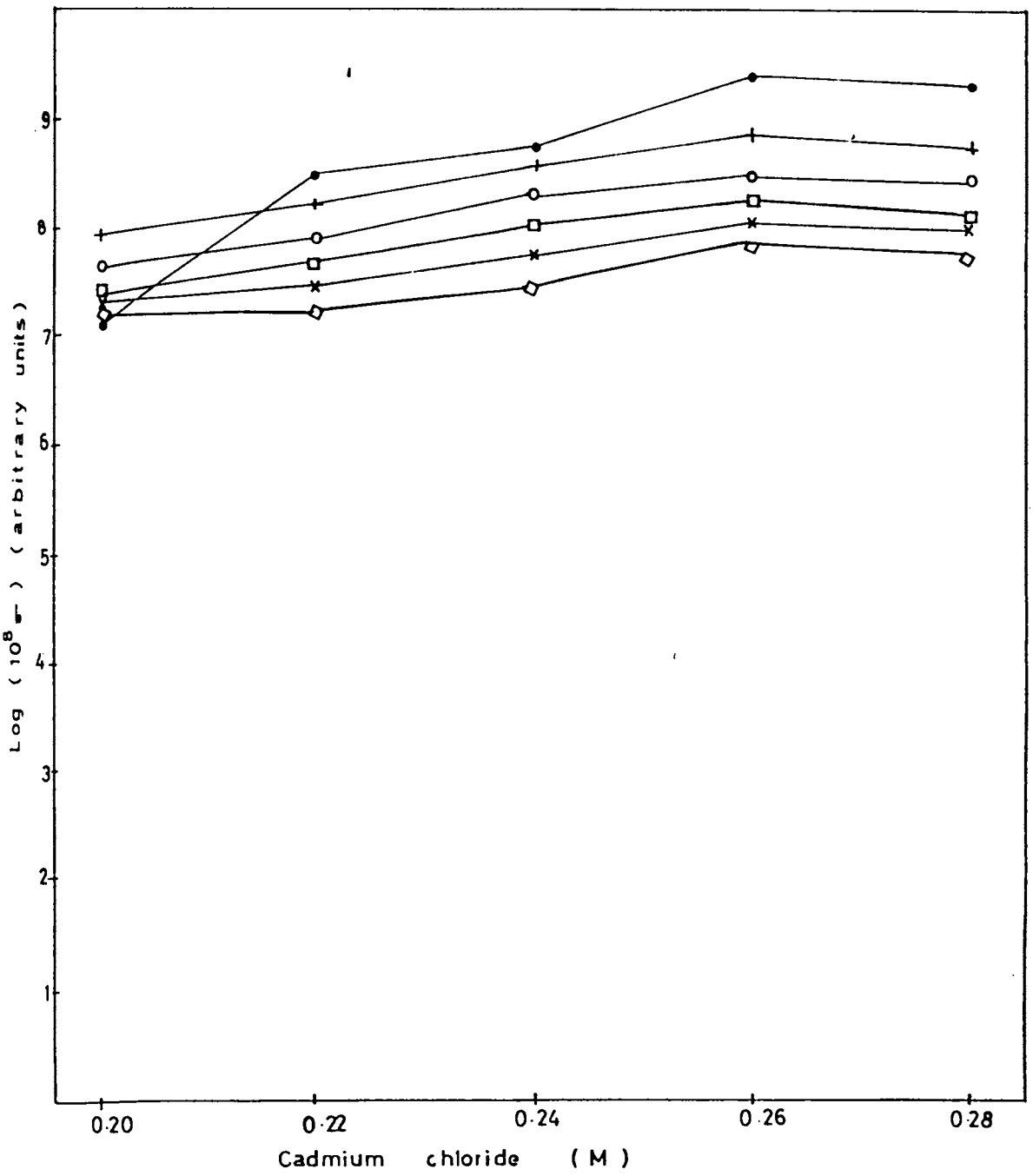

Fig 6.2 (c) : Variation of conductivity as a function of concentration of Cadmium Chloride for the films in vacuum at 423 K (•) unannealed and annealed at (+) 373 K, (o) 423 K, (□) 473 K, (X) 523 K and (◇) 573 K.

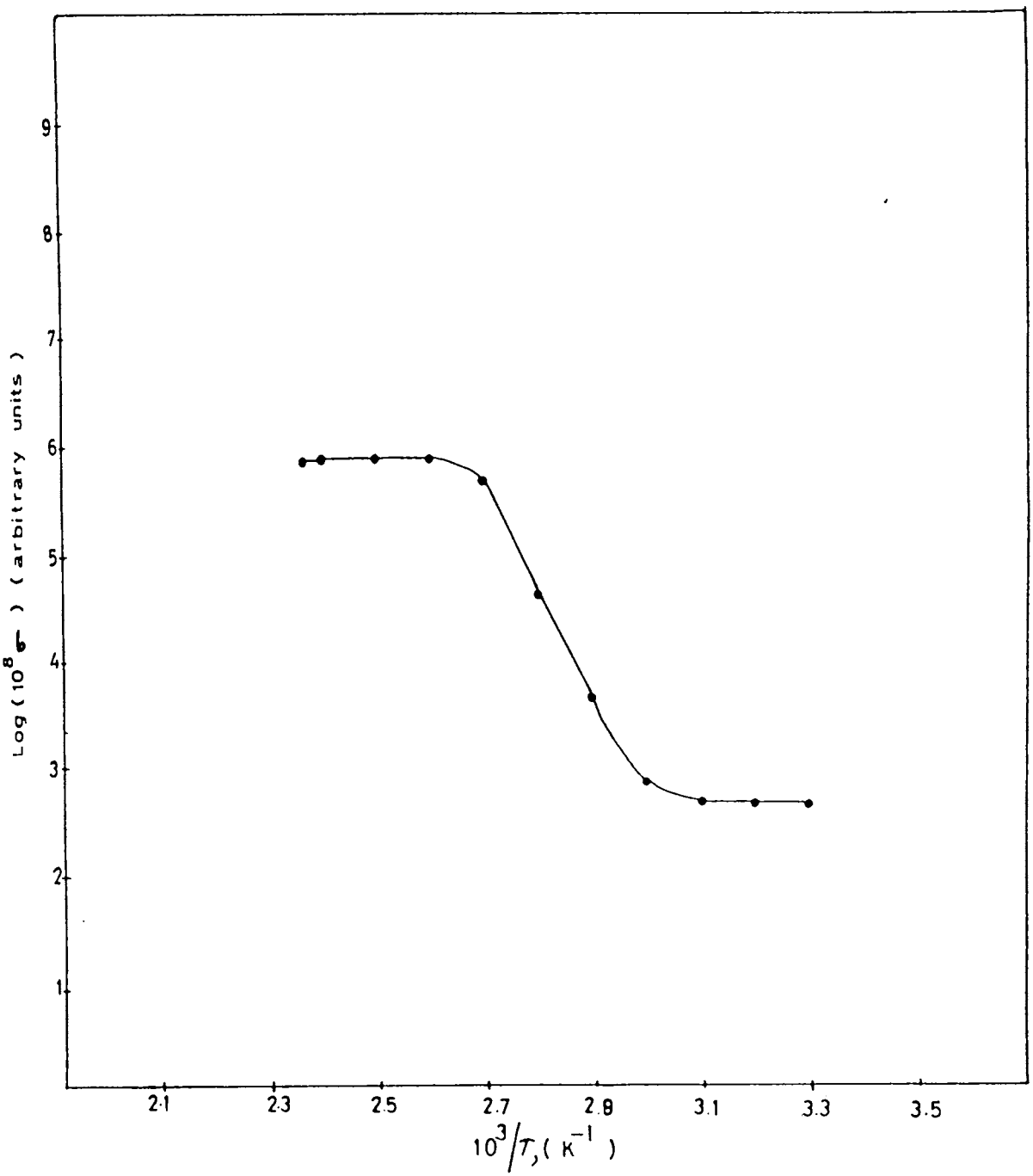

Fig 6.3 Plot of log ($10^8 \sigma$) against $10^3/T$ for the unannealed film A_1 in air.

unannealed film A_1. Similar result was also observed for other films. The figure indicates the presence of a trap level in the film. The values of the activation energy obtained for various films are presented in Table 6.2. When the conductivity of the films was measured in air, the occupation of defects by oxygen atoms produced new trap centres. The activation energy of the carriers is found to be ~ 2 eV for the film A_1 in air irrespective of annealing temperature and this shows that the carriers are liberated from this trap level [22]. The trap centre observed at ~ 0.90 eV in the films A_2 to A_5 is attributed to the chemisorbed oxygen surface state. This value was also reported by Mark [23] for thin insulating CdS crystals. The conductivity was also measured in air at 303 and 423K on films A_1 to A_5 prepared from different concentrations of cadmium chloride (0.20 to 0.28 M) and 0.20M thiourea and are plotted as shown in Figs. 6.4 (a) and 6.4 (b) respectively. When the concentration of cadmium chloride is increased from 0.20M to 0.22M, the conductivity is found to be increased. This is due to the increase in the number of donors. The effect can aslo be clearly seen from Table 6.2. The conductivity of the films containing higher cadmium contents is not affected on annealing. The values of conductivity of unannealed films obtained from the measurements in vacuum and air are given in Table 6.3. The decrease in the value of conductivity of the films in air is due to the difficulty in thermal excitation of the charge carriers. But the conductivity is increased when the samples are heated in vacuum. This is caused by the increase in the carrier concentration as a result of the desorption of oxygen from the film.

Table 6.2 The values of activation energy obtained from the conductivity measurements of the films in air.

Sample	Activation energy in the temperature range at 336-370K (eV)
A_1	
Unannealed	1.990
Annealed (573K)	2.000
A_2	
Unannealed	0.920
Annealed (573K)	0.910
A_3	
Unannealed	0.910
Annealed (573K)	0.900
A_4	
Unannealed	0.900
Annealed (573K)	0.920
A_5	
Unannealed	0.930
Annealed (573K)	0.910

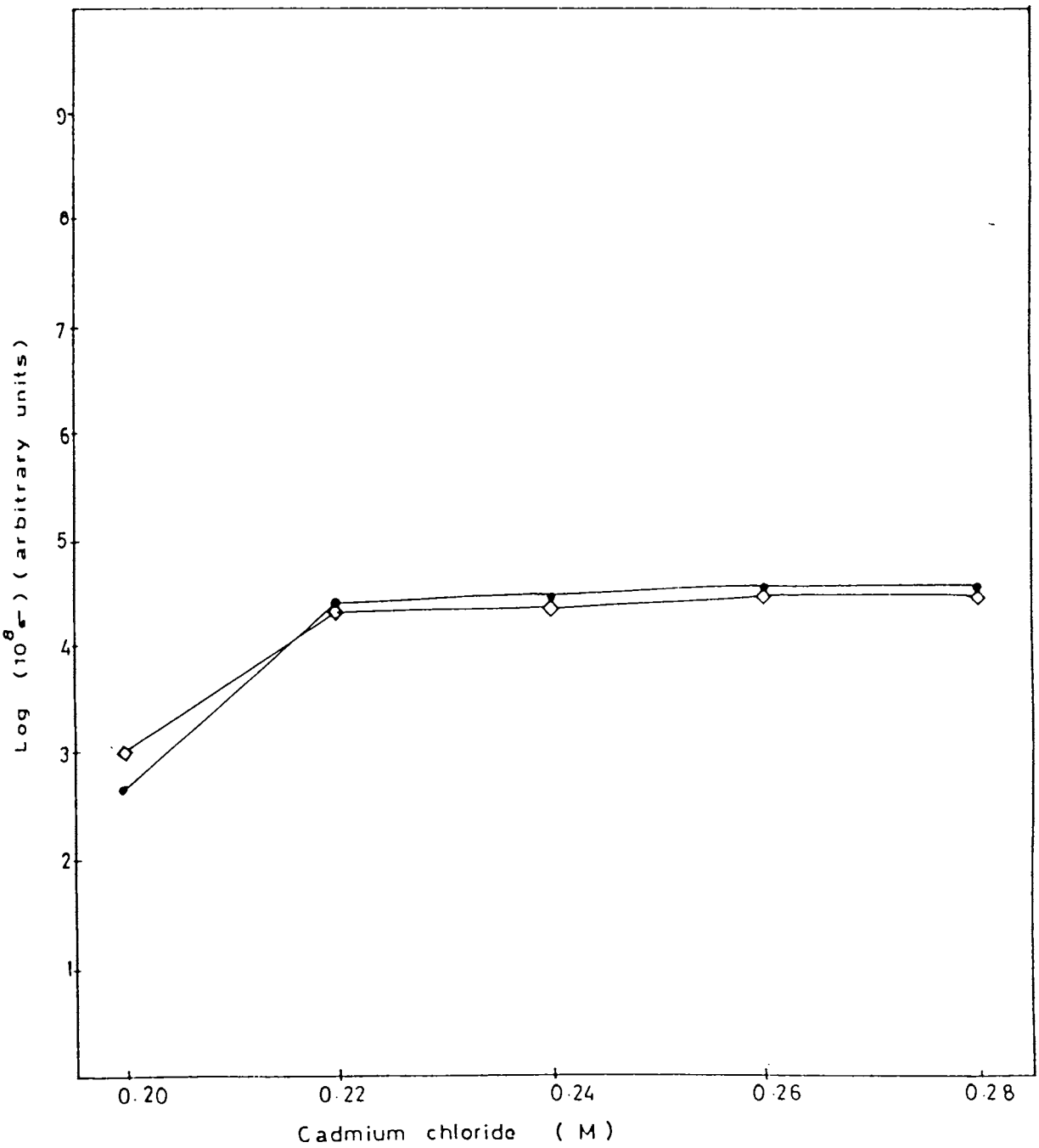

Fig 6.4 (a) : Variation of conductivity as a function of concentration of Cadmium Chloride for the films in air at 303 K : (•) unannealed and annealed at (◇) 573K.

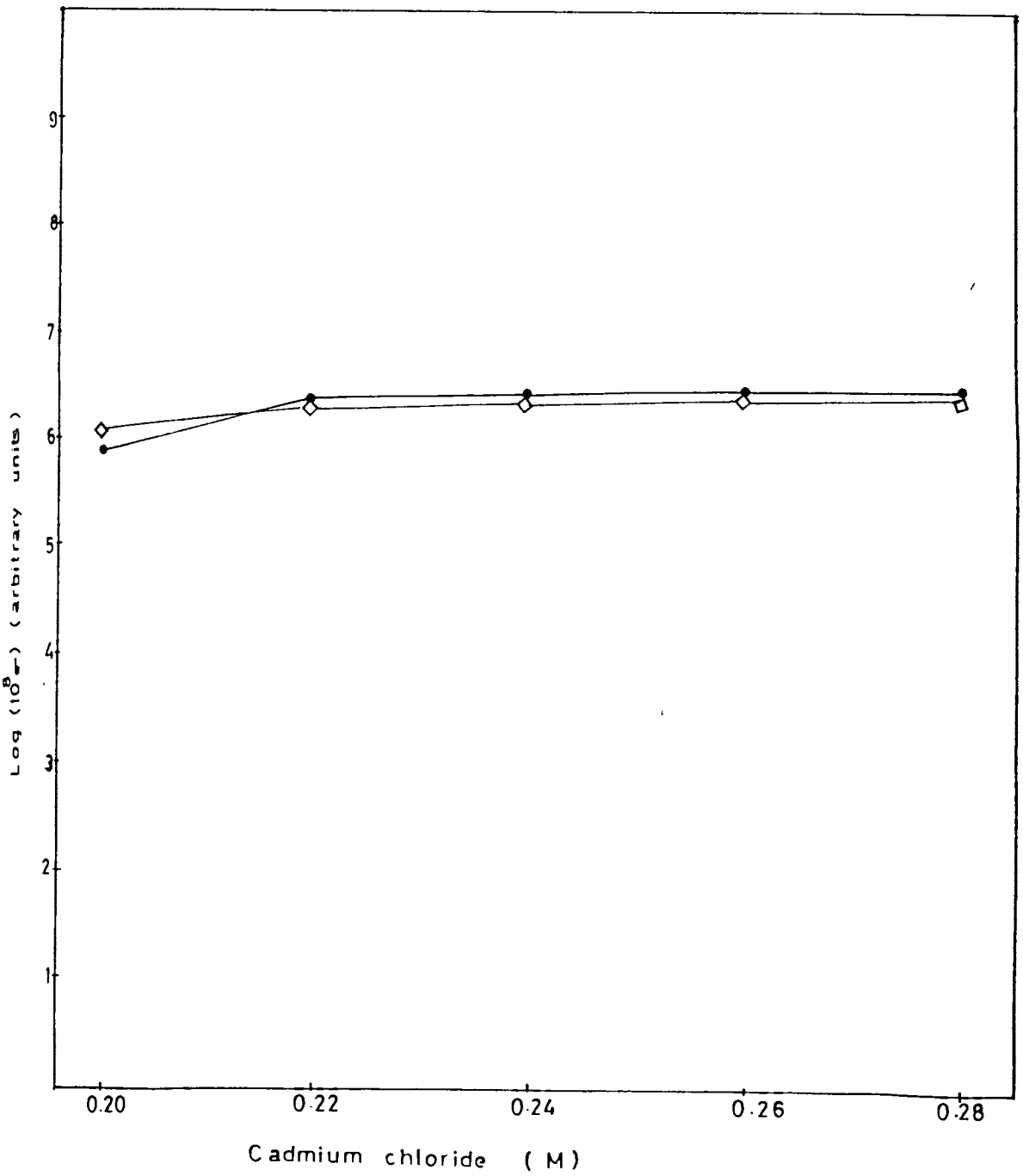

Fig 6.4 (b) : Variation of conductivity as a function of concentration of Cadmium Chloride for the films in air at 423 K : (•) unannealed and annealed at (◇) 573 K.

Table 6.3 The values of conductivity of unannealed films

Sample	Conductivity at room temperature in different ambients	
	Vacuum (Ω^{-1} m^{-1})	Air (Ω^{-1} m^{-1})
A_1	1.30×10^{-5}	5.0×10^{-6}
A_2	1.12×10^{-2}	2.82×10^{-4}
A_3	2.51×10^{-2}	3.16×10^{-4}
A_4	1.26×10^{-1}	3.55×10^{-4}
A_5	1.13×10^{-1}	3.56×10^{-4}

6.4 CONCLUSION

Electrical conduction mechanism is studied in thin films of CdS prepared from different concentrations of cadmium chloride by the spray pyrolysis method. The dark conductivity of the films in vacuum is found to be lower at 100K. But it increases with temperature and becomes a maximum at 423 K. Several discrete trap centres are identified in the films. The conductivity increases as the concentration of cadmium chloride increases from 0.20M to 0.26M. The higher conductivity values observed in films annealed at 373 K is associated with the maximum number of carrier generation. The presence of sulphur interstitials is responsible for the low value of conductivity of the unannealed film A_1. The magnitude of the conductivity and activation energy are sensitive to the heat treatment in air. The annealing temperature has negligible influence on the conductivity of the films at higher cadmium contents. The conductivity of the films in air is lower than that in vacuum.

6.5 REFERENCES

[1] G. Doucas, Vacuum 22 (1973) 651.

[2] R.W. Buckeley and J. Woods, J. Phys. D.6 (1973) 1084.

[3] L. Magafas, A.N. Anagnostopoulos and J.G. Antonopoulos, Phys. Stat. Solidi (a)·111 (1989) K 175.

[4] P.H. Wendland, J. Opt. Soc. Amer. 52 (1962) 581·

[5] W.C. Boesman and G.G. Avis, Transaction of the Tenth National Vacuum Symposium of the American Vacuum Society, New York, 1963.

[6] J.R. Clarke and J.E. Greene, J. Vac. Sci. Technol. 18 (1981) 382,

[7] F. Ei Akkad and M.A. Naby, Sol. Energy. Mater. 18 (1989) 151·

[8] D.C. Cameron, W. Duncan and W.M. Tsang, Thin Solid Films 58 (1979) 61.

[9] A. Yoshikawa and Y. Sakai, Jon. J. Appl. Phys. 15 (1976) 1861·

[10] V.P. Panov, I.I. Polezhaev and G.D. Sizova, Sov. Phys. Semicond. 10 (1976) 1202.

[11] J. Bougnot, M. Perotin, J. Marucchi, M. Sirkis and M.Savelli, 12th IEEE Photovaltaic Specialists Conference, New York, 1976.

[12] Y.Y. Ma and R.H. Bube, J. Electrochem. Soc. 124 (1977) 1430.

[13] B.K. Gupta, O.P. Agnihotri and A. Raza, Thin Solid Films 48 (1978) 153.

[14] R.H. Bube, J. Chem. Phys, 23 (1955) 18.

[15] J. Nishimura, Jpn. J. Appl. Phys. I, Regul. Pap. Short Notes 30 (1991) 537.

[16] J. Woods and K.H. Nicholas, Brit. J. Appl. Phys. 15 (1964) 1361.

[17] A.G. Valyomana, K.P. Vijayakumar and C. Purushothaman, J. Mater. Sci. Lett. 9 (1990) 1025.

[18] J.S. Sharman, Solid State Electron. 8 (1965) 17.

[19] N.Susa, H. Watanage and M. Wada, Jap. J. Appl. Phys. 15 (1976) 2365.

[20] D. Shaw and R.C. Whelan, Phys. Stat. Solidi 36 (1969) 705.

[21] W. Van Gool and G. Diemer, Luminescence of organic and inorganic materials, Eds. H.P. Kallman and G.M. Spruch (Wiley,New York,1962)

[22] A.G. Valyomana, K.P. Vijayakumar and C. Purushothaman, J. Mater. Sci. Lett.11 (1992) 616.

[23] P. Mark, J. Phys. Chem. Solids 25 (1964) 911.

7 PHOTOCONDUCTIVITY AND LIFETIME STUDIES OF CdS THIN FILMS

7.1 INTRODUCTION

Photoconductivity and life time studies of thin films provide information on the mechanism of generation and recombination of charge carriers. Several workers have reported the photoconduction mechanism of CdS films prepared by various techniques [1-7]. Korashy and Stirn[8] studied the photoconductivity of these films prepared by spray pyrolysis method. They achieved a resistivity of 10^7 Ohm Cm and a light to dark conductivity ratio of up to 10^6 in these films with 0.05 mole concentration $CdCl_2$ to thiourea ratio 1:2, and substrate temperature 235°C. Gupta et al [9] found maximum photosensitivity in these films prepared using higher concentration of thiourea. The investigations on the lifetime of CdS films have been done by a few authors [10,11]. However there is no sufficient data in the literature related to the interpretation of photoconductivity and lifetime of sprayed CdS films in terms of the existence of trap centers caused by the presence of slight excess of cadmium or other impurities. Hence in view of the research interest to understand the trapping mechanism of carriers, an attempt has been made to investigate the photoconductivity and lifetime studies of these films prepared by spray pyrolysis method. Particular attention has also been given to understand the effect of wavelength, heating temperature, and annealing on the measurements of films containing different cadmium contents.

7.2 EXPERIMENTAL

CdS films A_1 to A_5 were prepared from different concentrations of cadmium chloride (0.20 to 0.28M) and 0.2M thiourea for the present

investigations. The films were annealed in air at temperatures in the range 373 - 573 K. Aluminium electrodes were deposited by vacuum evaporation on the surface of the films. The measurements were carried out in vacuum and air using a metallic chamber as described in chapter4. During the measurements, the temperature of the films were controlled by the current applied to the heater from a stabilized voltage source. The samples were held at the desired temperature for a sufficiently long time before the measurements were made.

7.3 RESULTS AND DISCUSSION

7.3.1 Photoconductivity measurements

The photoconductivity of the films were measured in vacuum in the temperature range 100 - 423 K for different wavelengths. Fig.7.1 shows the dependence of photoconductivity (σ) as a function of wavelength for the unannealed film A_1. It is seen that, for temperatures upto 352 K, the photoconductivity is increased sharply, but at high temperatures, no significant increase in its value is observed. The impurity centres are frozen at low temperatures and hence free charge carriers are trapped in the impurity levels. This explains the low magnitude of photoconductivity at 100 K. But as temperature increases, thermal energy which supplies the ionizing energy for the excitation of carriers from the impurity level increases. Hence the carriers are increased and higher conductivity values are observed at high temperatures.

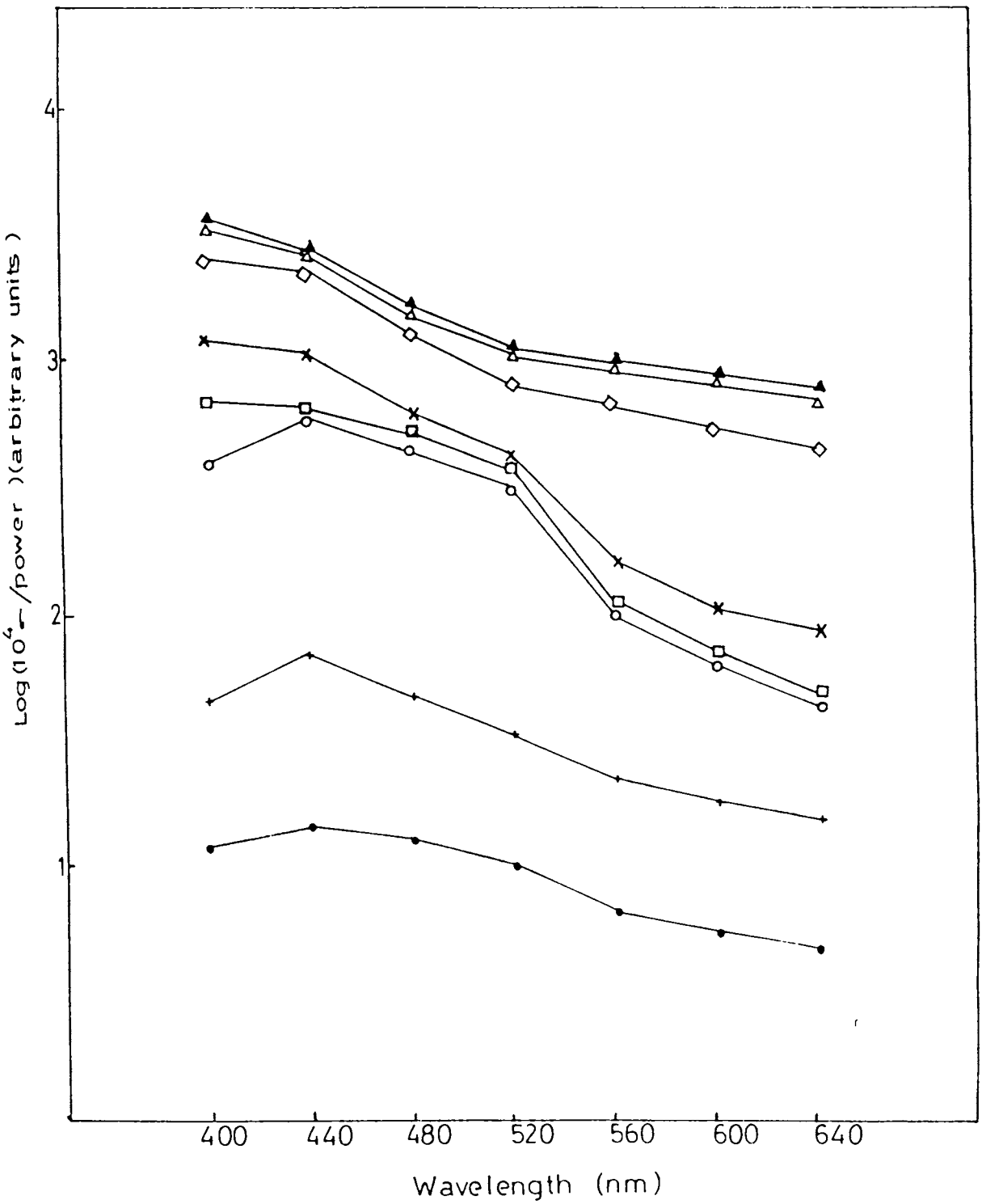

Fig 7.1 : Plot of log ($10^4 \sigma_{in\ vacuum}$/Power) against wave length for the unannealed film A_{11} for different temperatures: (•) 100 K, (+) 224 K, (o) 303 K, (□) 328 K, (x) 352 K, (◇) 366K, (△) 400 K and (▲) 423 K.

The conductivity curves obtained at 100 K (Figs.7.2 to 7.6) are respectively similar to that obtained at 303 K. (Figs. 7.7 to 7.11). Also it is interesting to note that for each film, the photoconductivity observed at 303 K is higher than that at 100 K. It is observed that the photoconductivity decreases as the wavelength increases from 400 to 640 nm. The photon energy $\sim$ 3 eV (energy corresponds to the wavelength of light centered at 400 nm) is sufficient for the photo-ionization of the centers. Hence the free carriers produced at this wavelength increases. As the wavelength increases from 400 to 640nm, the number of photoexcited carriers decreases rapidly and hence the photoconductivity is decreased.

During the present study it has been observed that the annealing of the films have significant effect on the photoconductivity. The results obtained during the measurements at 303 K are explained as follows. The photoconductivity of the films annealed at 373 K shows higher value compared to that obtained for film annealed at higher temperatures. The higher conductivity values observed in these films are due to the generation of higher number of carriers. Moreover, these films have no structural imperfections.

Another observation is that the photoconductivity of the films A_1 to A_3 decreases with annealing temperature and becomes a minimum at 473 K . The trapping of carriers is responsible for the reduction in photoconductivity at the annealing temperature 473K. The carrier

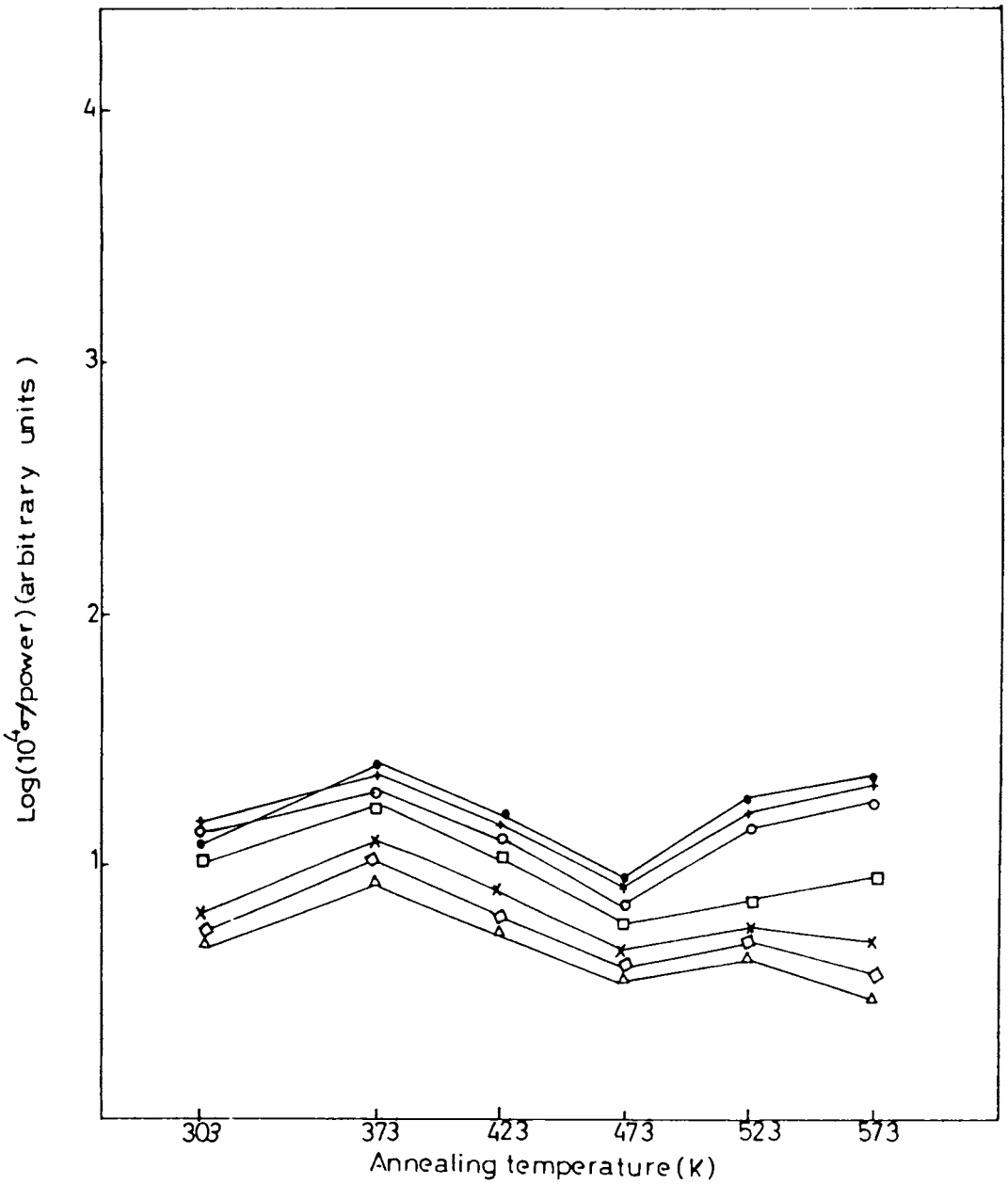

Fig 7.2 : Plot of log ($10^4\sigma$ /power) against annealing temperature at 100 K in vacuum for the film A_1 at different wavelengths: (•) 400 nm (+) 440 nm, (o) 480 nm, (□) 520 nm, (x) 560 nm, (◊) 600 nm and (Δ) 640 nm.

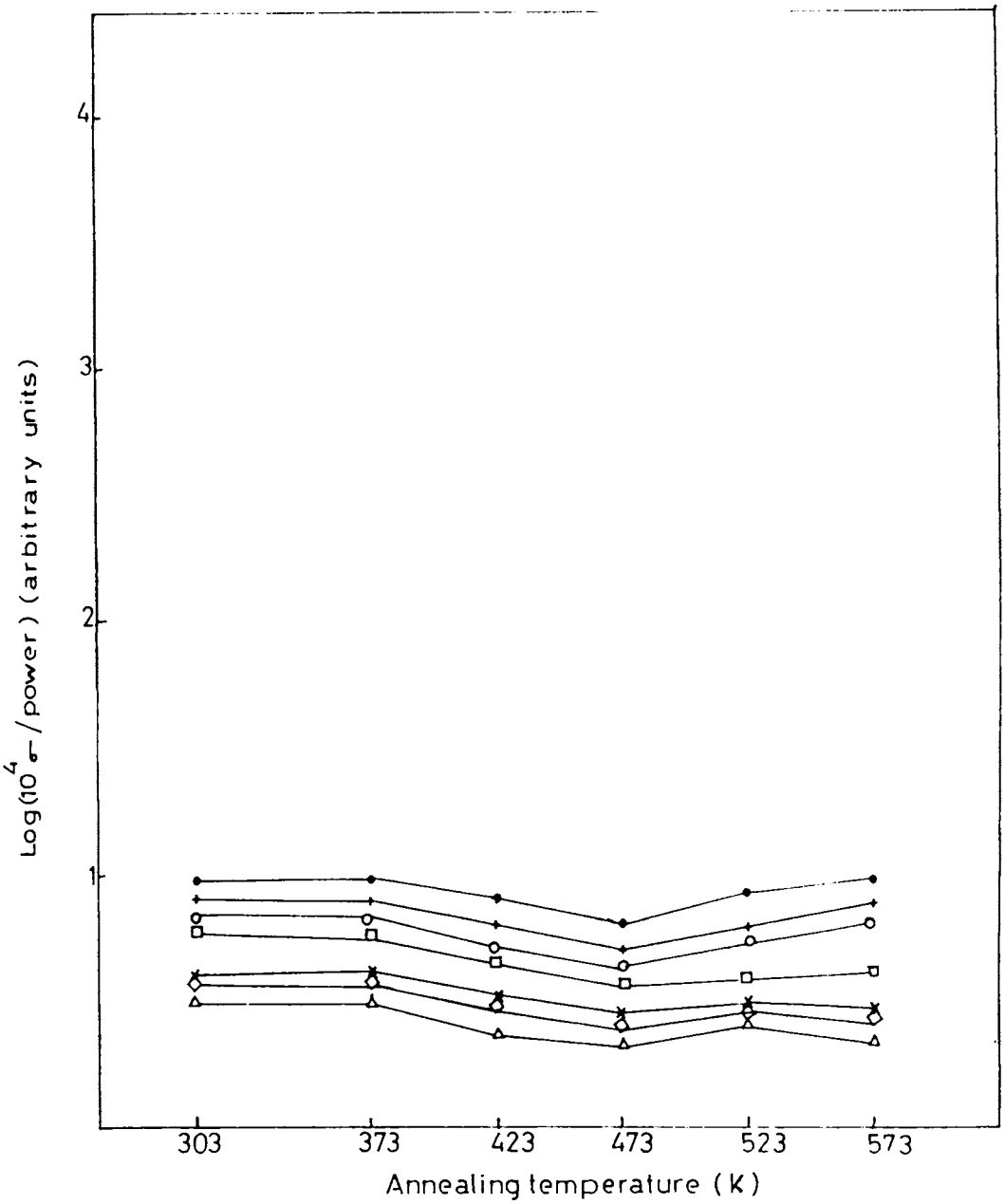

Fig 7.3 : Plot of log ($10^4\sigma$ /power) against annealing temperature at 100 K in vacuum for the film A_2 at different wavelengths: (•) 400 nm, (+) 440 nm, (o) 480 nm, (□) 520 nm, (x) 560 nm, (◇) 600 nm and (△) 640 nm.

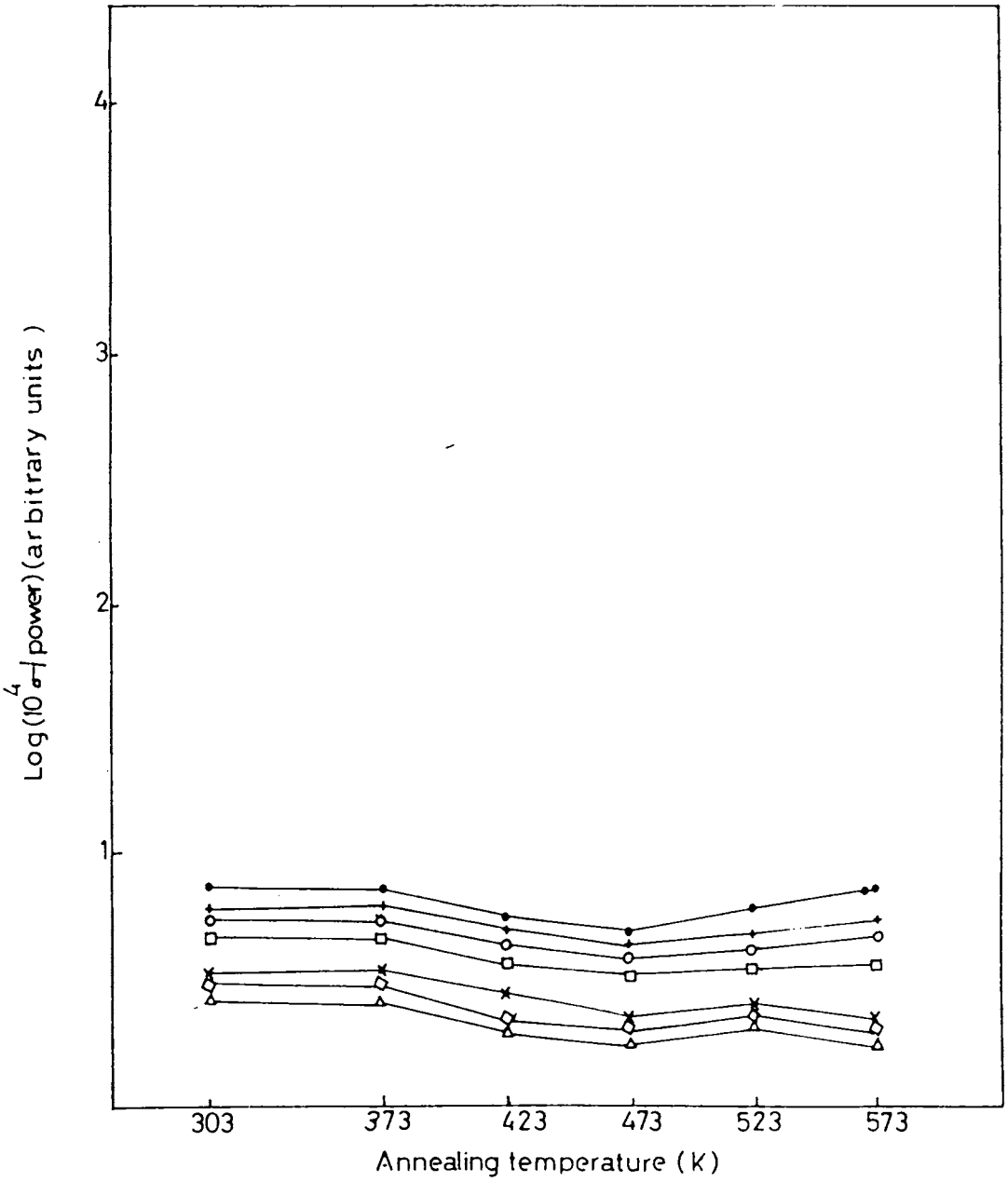

Fig 7.4 : Plot of log ($10^4\sigma$ /power) against annealing temperature at 100 K in vacuum for the film A_3 at different wavelengths: (•) 400nm, (+) 440 nm, (o) 480 nm, (□) 520 nm. (x) 560 nm, (◇) 600 nm, and (△) 640 nm.

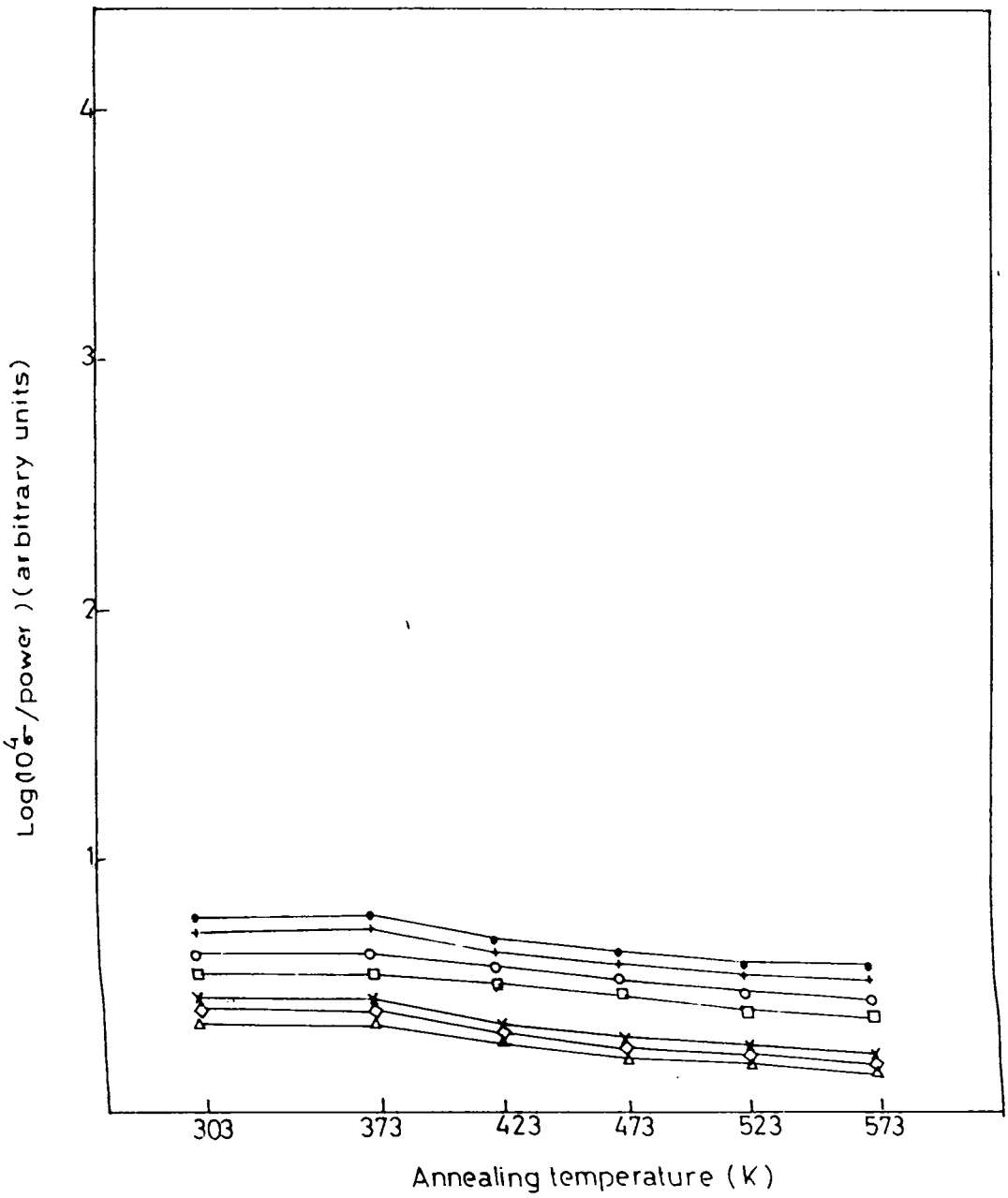

Fig 7.5 : Plot of log ($10^4\sigma$/power) against annealing temperature at 100 K in vacuum for the film A_4 at different wavelengths: (•) 400nm, (+) 440 nm, (o) 480 nm, (□) 520 nm (x) 560 nm, (◇) 600 nm and (△) 640 nm.

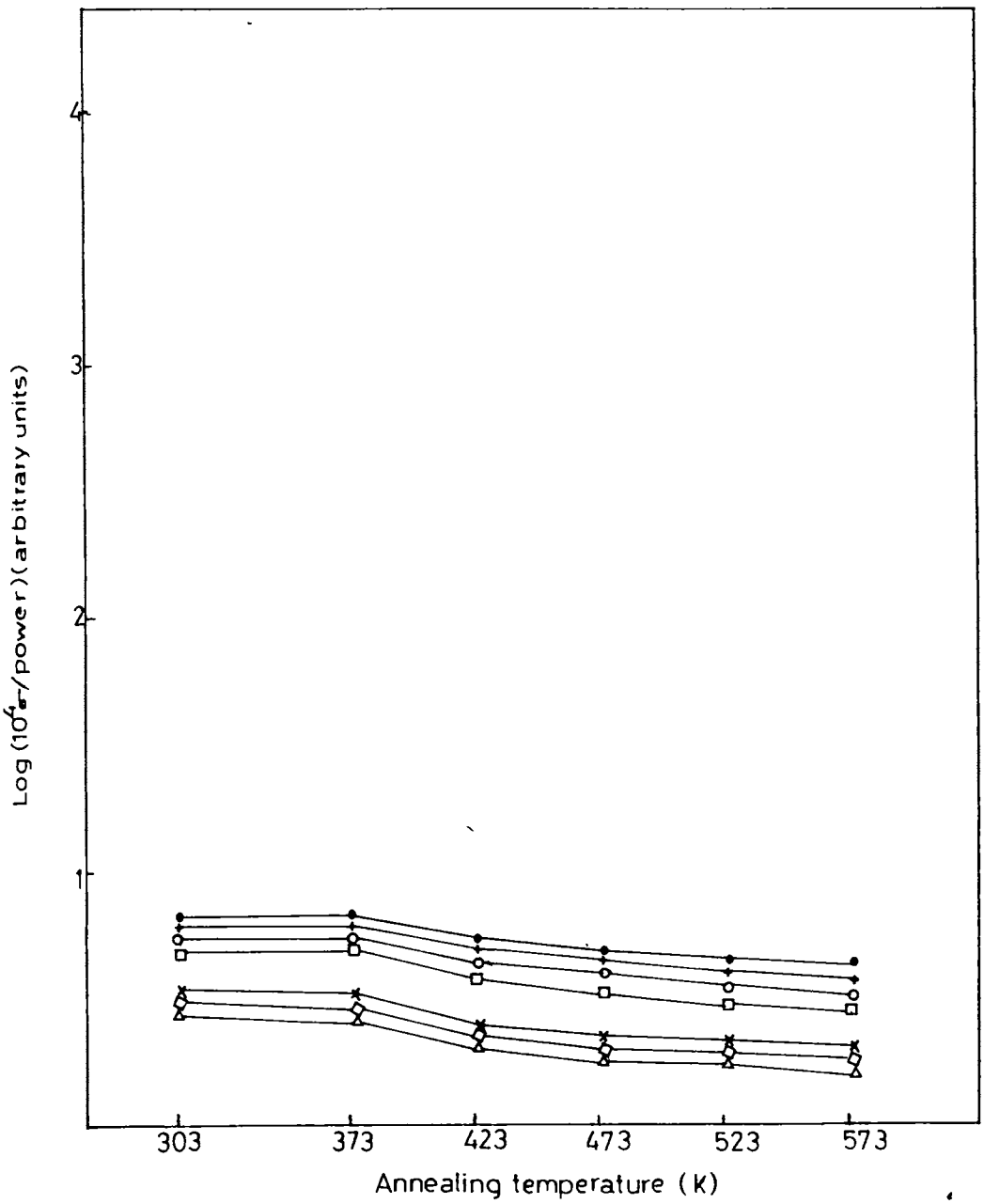

Fig 7.6 : Plot of log ($10^4\sigma$/power) against annealing temperature at 100 K in vacuum for the film A_5 at different wavelengths: (•) 400nm, (+) 440 nm, (o) 480 nm, (□) 520 nm, (x) 560 nm, (◇) 600 nm and (△) 640nm.

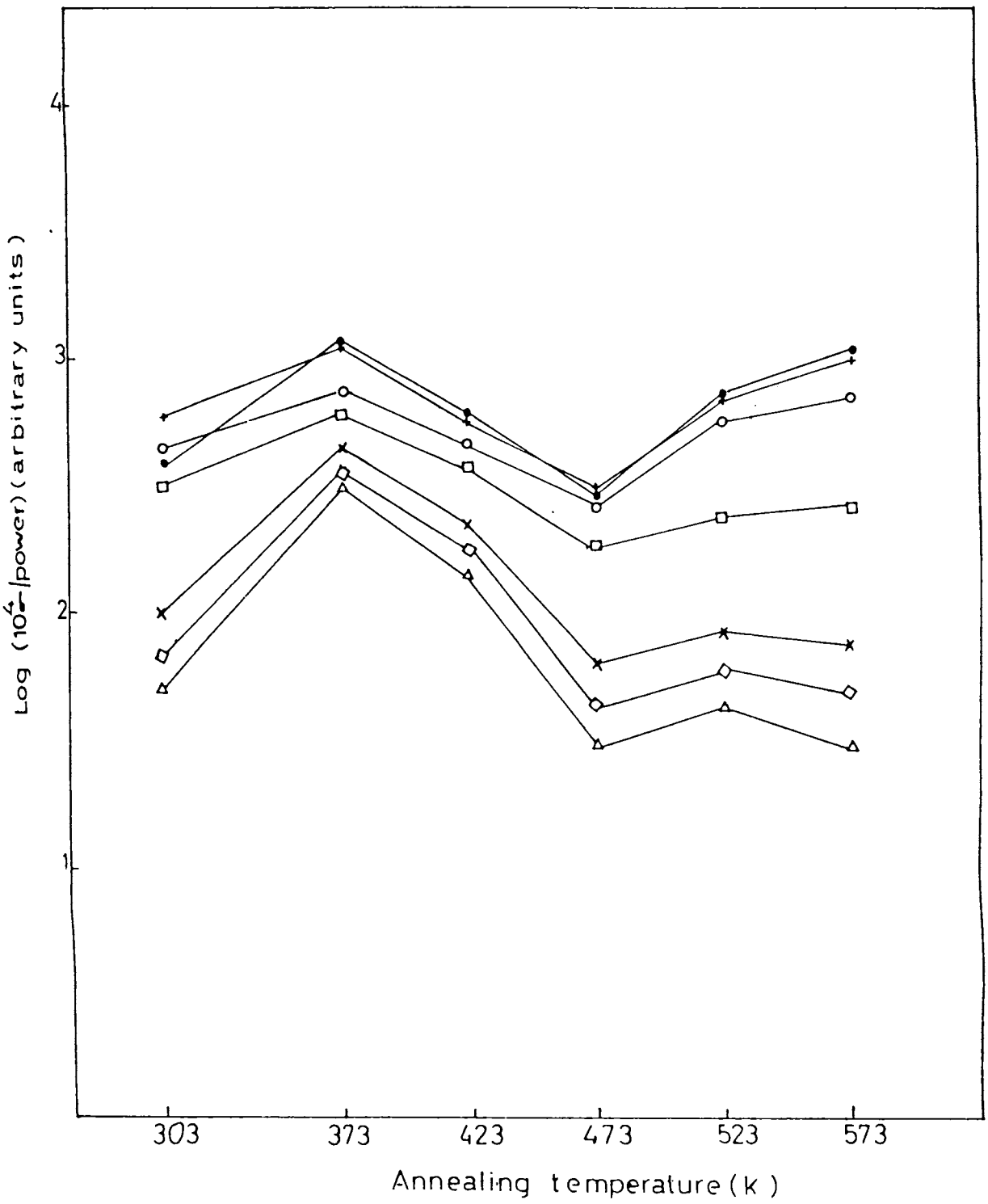

Fig 7.7 : Plot of log ($10^4\sigma$/Power) against annealing temperature at 303 K in vacuum for the film A_1 at different wavelengths: (•) 400 nm, (+) 440 nm, (o) 480 nm, (□) 520 nm, (x) 560 nm, (◇) 600 nm and (△) 640 nm.

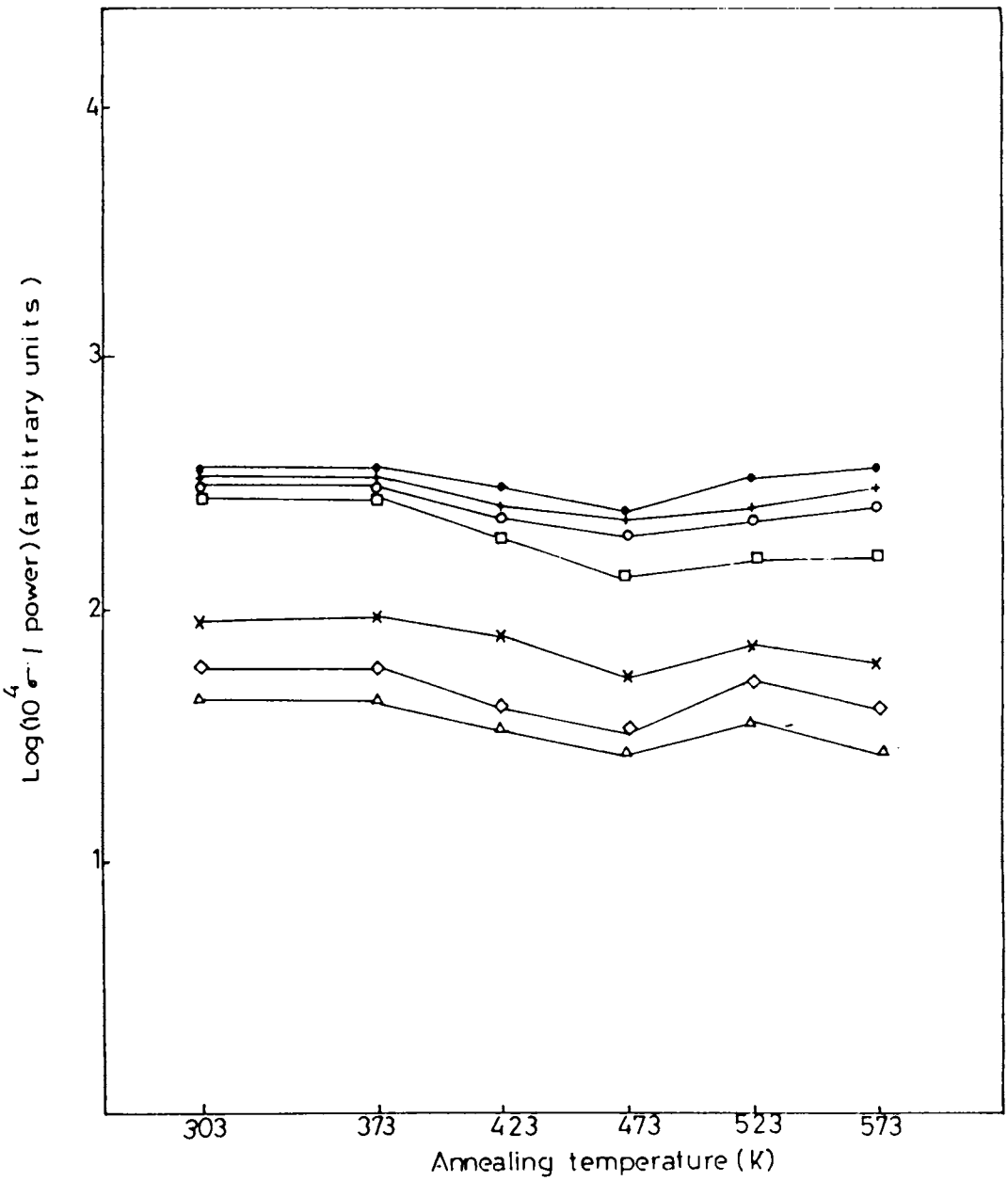

Fig 7.8 : Plot of log ($10^4 \sigma$ /power) against annealing temperature at 303 K in vacuum for the film A_2 at different wavelengths: (•) 400 nm, (+) 440 nm, (o) 480 nm, (□) 520 nm, (x) 560 nm, (◇) 600 nm and (△) 640 nm.

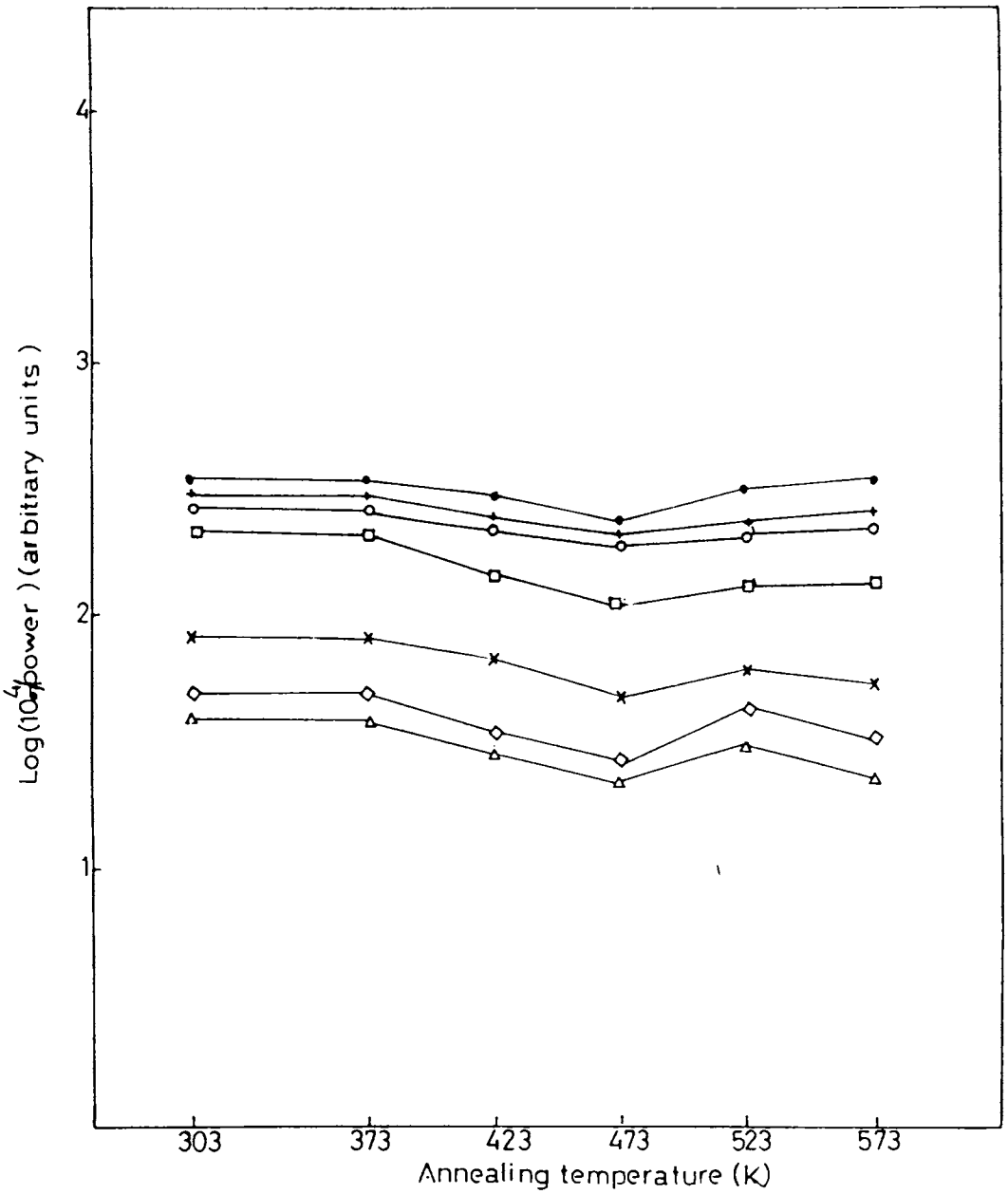

Fig 7.9 : Plot of log ($10^4\sigma$/power) against annealing temperature at 303 K in vacuum for the film A_3 at different wavelengths: (•) 400 nm, (+) 440 nm, (o) 480 nm, (□) 520 nm, (x) 560 nm, (◇) 600 nm and (△) 640 nm.

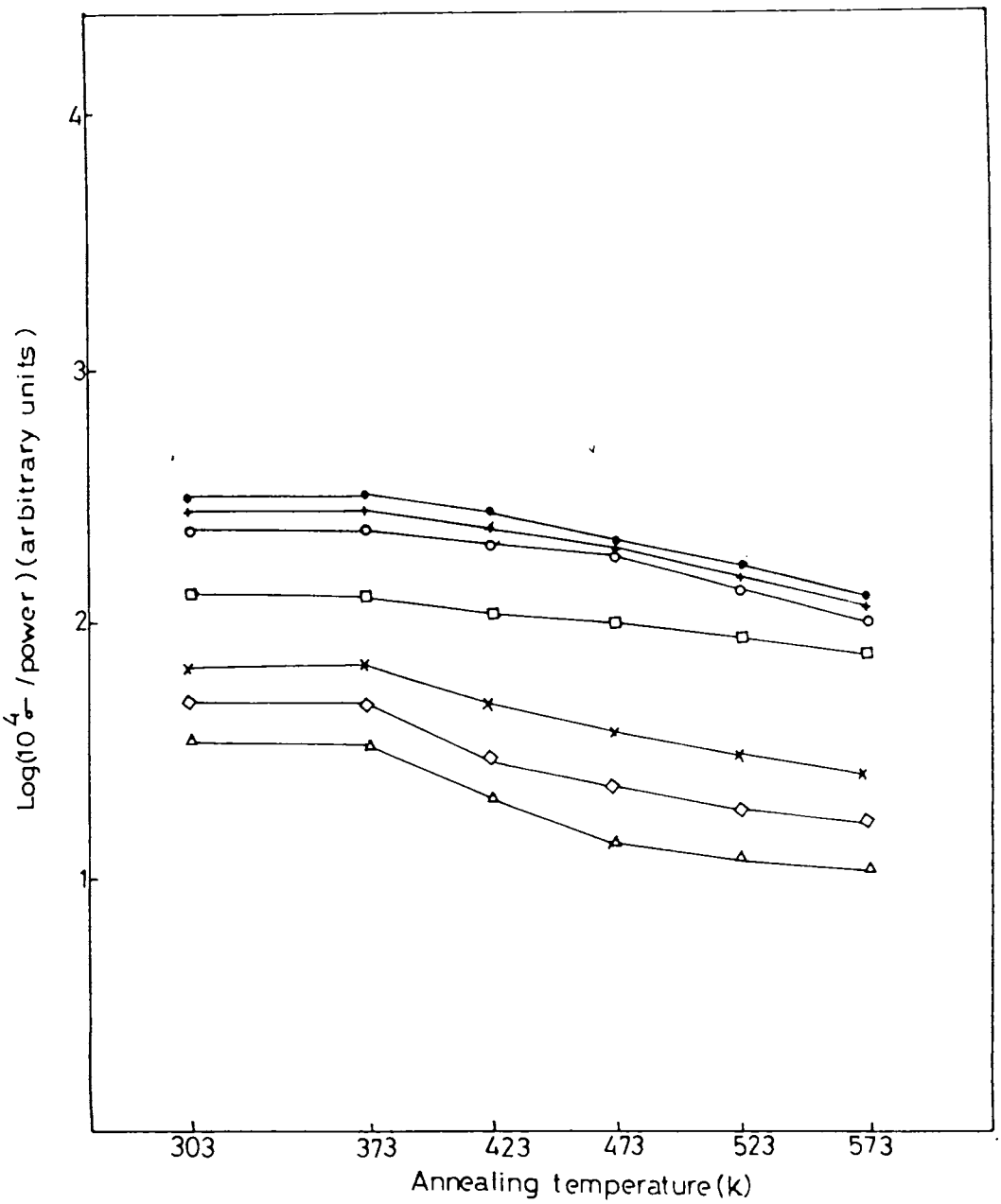

Fig 7.10 : Plot of log ($10^4\sigma$ /power) against annealing temperature at 303 K in vacuum for the films A_4 at different wavelengths: (•) 400nm, (+) 440 nm, (o) 480 nm, (□) 520 nm, (x) 560 nm, (◇) 600 nm and (Δ) 640nm.

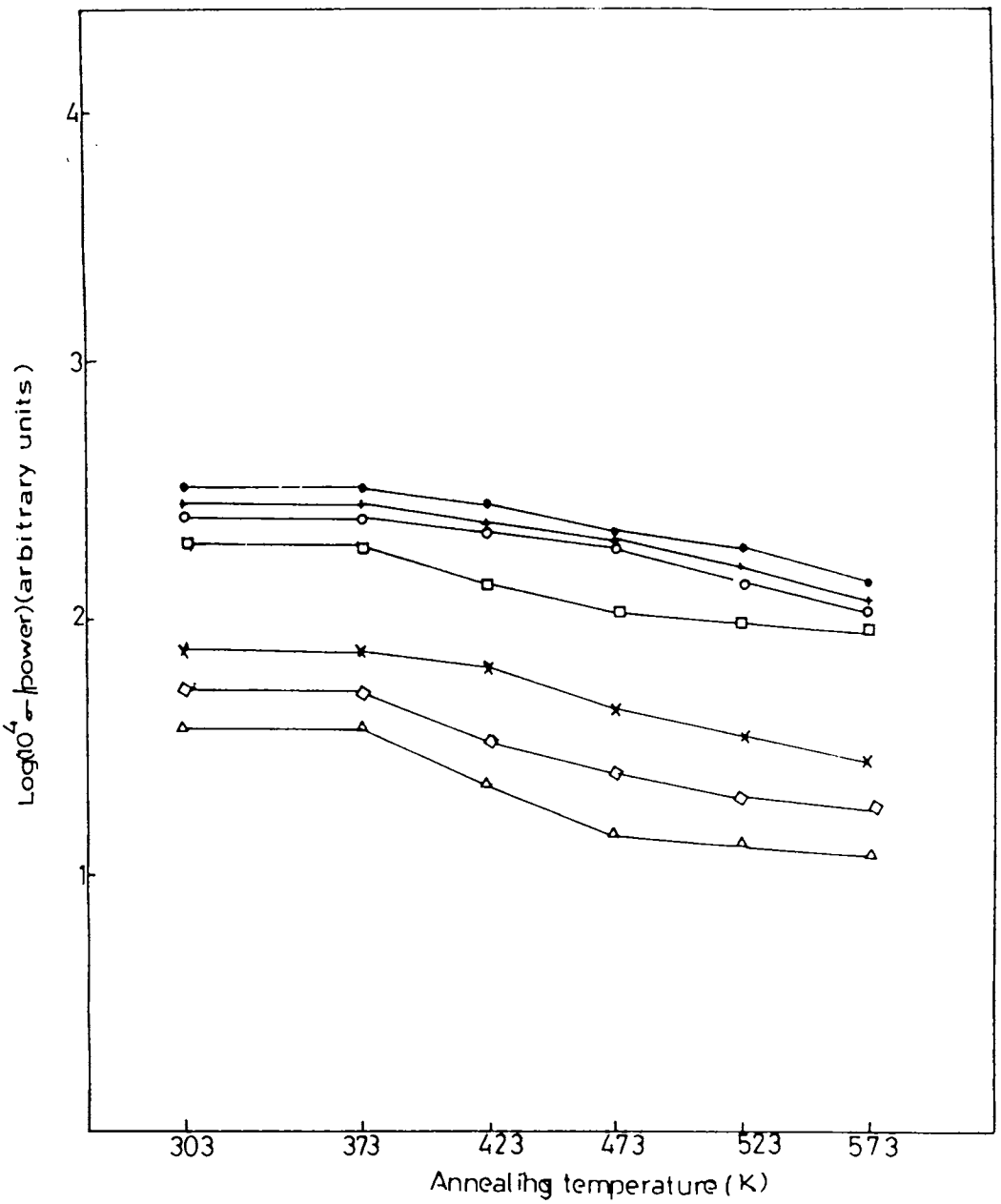

Fig 7.11 : Plot of log ($10^4\sigma$ /power) against annealing temperature at 303 K in vacuum for the film A_5 at different wavelengths: (•) 400 nm, (+) 440 nm, (o) 480 nm, (□) 520 nm, (x) 560 nm, (◇) 600 nm and (△) 640 nm.

generation is also reduced considerably. The photoconductivity of the films A_1 to A_3 annealed above 523 K has a pronounced effect on the wavelengths in the range 400 to 640 nm. The above results can be clearly observed in Figs. 7.7 to 7.9. The magnitude of photoconductivity is found to be increased for wavelengths in the range 400 to 520 nm. This may be due to the reduction in traps in the films and this in turn leads to an increase in the number of carriers of higher energy [12]. The photoconductivity decreases abruptly at wavelength $>$ 520nm for the films annealed above 523 K. The probability of the trapping of the carriers by the traps or defects present in these films may be the reason for the decrease in photoconductivity at higher wavelengths. On annealing the films A_4 and A_5 above 373 K, the probability of trapping of carriers is so high that the carriers will be released slowly. This fact is most indicative of the decrease in photoconductivity of these films annealed above 373 K (Figs. 7.10 and 7.11).

The results obtained from the conductivity measurements of the films at higher heating temperatures were analysed to study the influence of these temperatures on the release of trapped carriers. Fig. 7.12 shows the variation of photoconductivity with temperature for film A_1 annealed at 373 K. Since there is not much influence in photoconductivity with wavelength, it is clear that the trapping of carriers does not occur in this film. Similar result is obtained for the films A_2 to A_5 annealed at 373 K. It should be noted that, photoconductivity is increased for all wavelengths due to the release of charge carriers from traps during the heating of the films A_1 to A_3 annealed

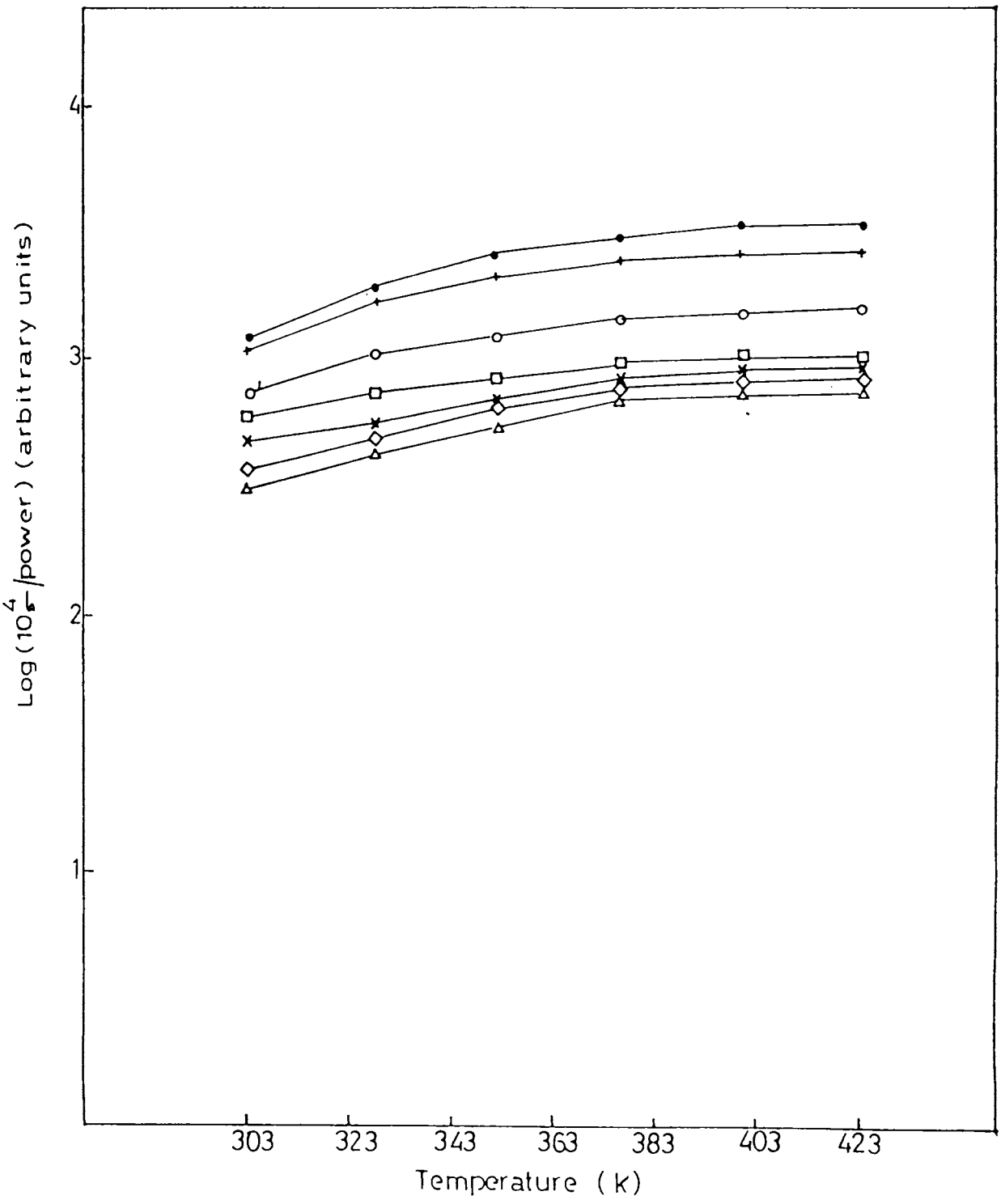

Fig 7.12 : Plot of log ($10^4\sigma$ /Power) against temperature of film A_1 in vacuum, annealed at 373 K for different wavelengths: (•) 400 nm, (+) 440 nm, (o) 480 nm, (□) 520 nm, (x) 560 nm, (◇) 600 nm and (△) 640 nm.

at 473 K. The typical characteristics obtained for the film A_1 is shown in Fig. 7.13. The considerable increase in photoconductivity observed in this figure indicates that a greater density of carriers are trapped at low heating temperatures (at or below 303 K). The photoconductivity of the film A_1 annealed at 573 K (Fig. 7.14) does not show any variation with wavelength upto 480 nm indicating no trapping. But there is considerable rise in conductivity for this film at higher wavelengths due to the release of charge carriers from the traps as this film is heated. This effect is found to be similar for films A_2 and A_3 annealed at 573 K.

The variation of photoconductivity with heating temperature for the films A_4 and A_5 annealed at 423 K is found to be similar for those annealed at higher temperatures. The results obtained for these films annealed at 423 K are shown in Figs. 7.15 and 7.16. The decrease in photoconductivity is observed due to the recombination of carriers taking place at higher temperatures. The free carrier density is decreased for all wavelengths. At higher wavelengths, the photoconductivity is decreased to a greater extent (Fig. 7.16) due to the phenomenon of surface recombination. But at lower wavelengths, recombination of carriers takes place deep inside the film.

Figs. 7.17 to 7.21 show the results of the photoconductivity studies of the films in air. The effect of annealing temperature on the photoconductivity of the films A_2 to A_5 (Figs. 7.18 to 7.21) at 303 K is respectively similar to that in vacuum (Figs 7.8 to 7.11).

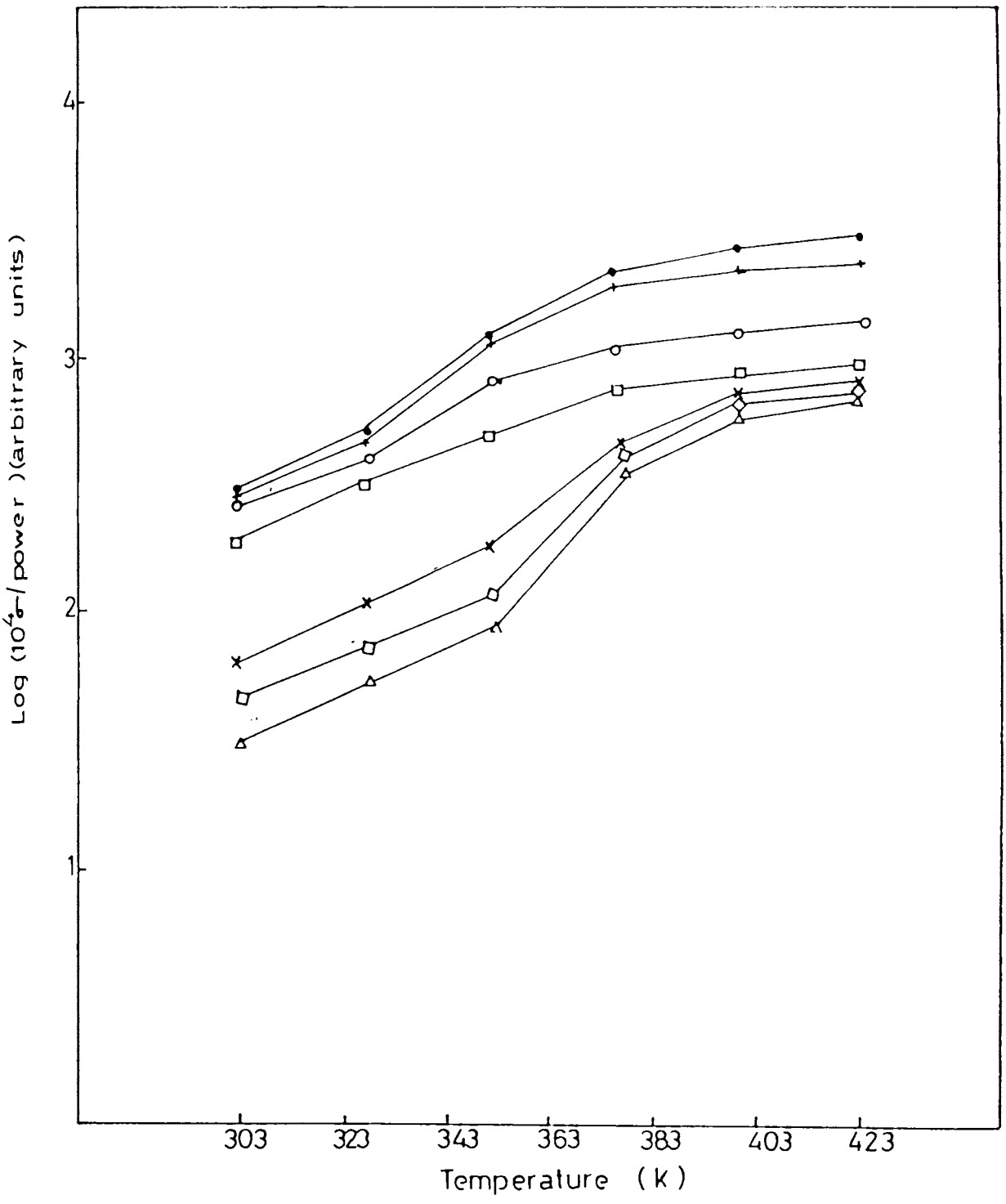

Fig 7.13 : Plot of log ($10^4\sigma$/power) against temperature of film A_1 in vacuum, annealed at 473 K for different wavelengths: (•) 400 nm, (+) 440 nm, (o) 480 nm, (□) 520 nm, (x) 560 nm, (◊) 600 nm and (△) 640 nm.

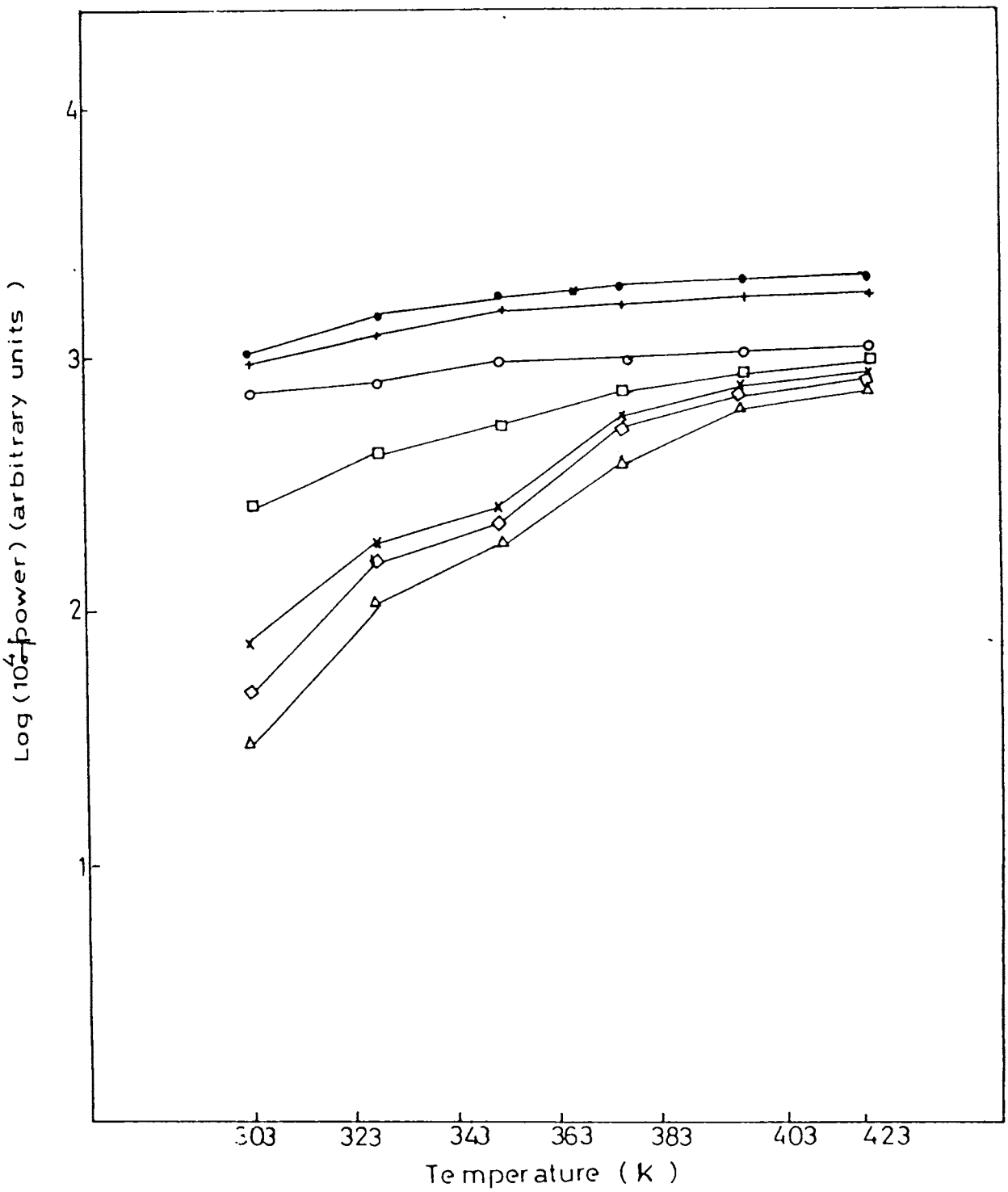

Fig 7.14 : Plot of log ((10^4 σ/power) against temperature of film A_1 in vacuum, annealed at 573 K for different wavelengths: (•) 400 nm, (+) 440 nm, (o) 480 nm, (□) 520 nm, (x) 560 nm, (◇) 600 nm and (△) 640 nm.

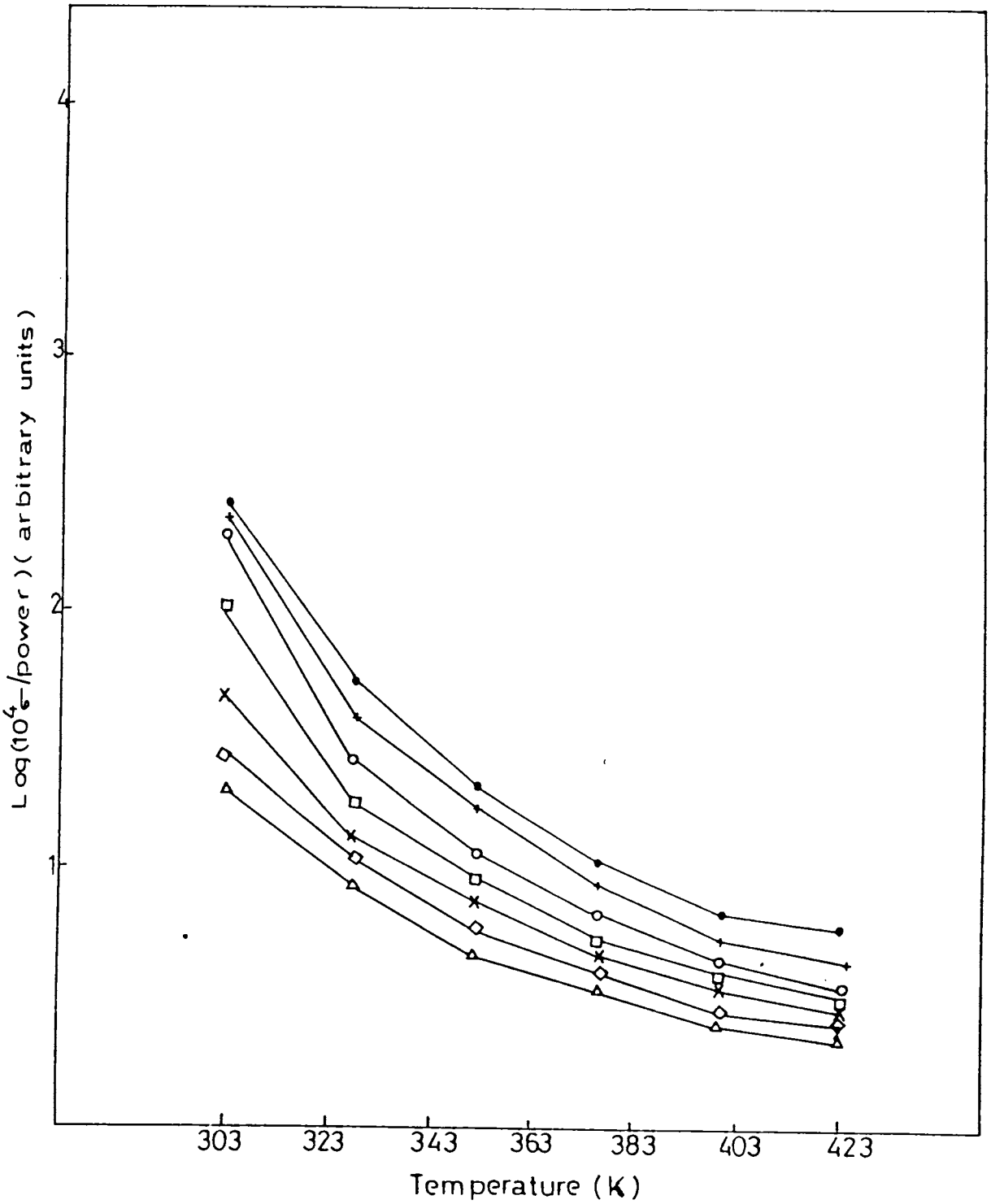

Fig 7.15 : Plot of log $(10^4\sigma$ /power) against temperature of film A_4 in vacuum, annealed at 423 K for different wavelengths: (•) 400 nm, (+) 440 nm, (o) 480 nm, (□) 520 nm, (x) 560 nm, (◇) 600 nm and (Δ) 640 nm.

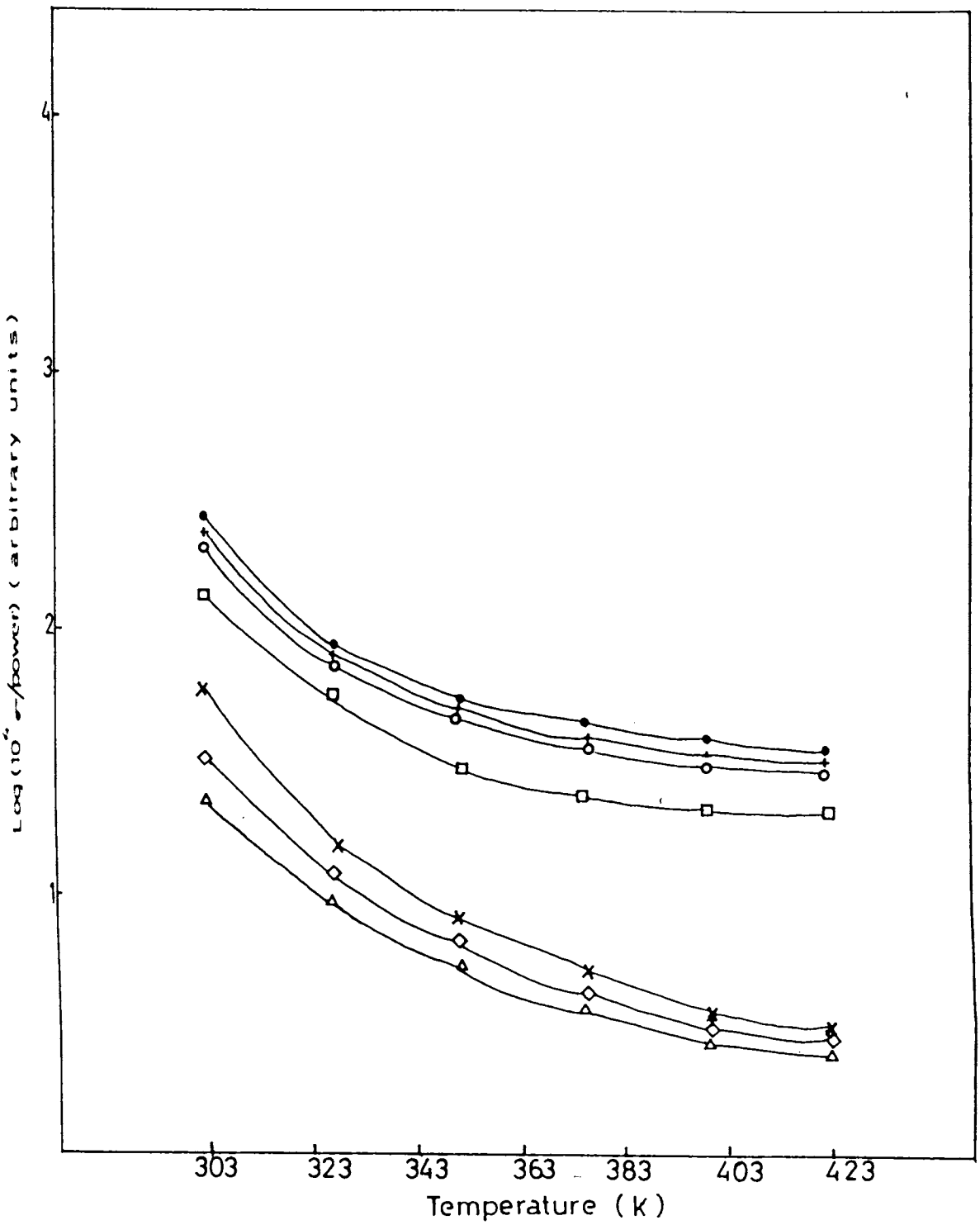

Fig 7.16 : Plot of log ($10^4\sigma$ /power) against temperature of film A_5 in vacuum, annealed at 423 K for different wavelengths: (•) 400 nm, (+) 440 nm, (o) 480 nm, (□) 520nm, (x) 560 nm, (◇) 600 nm and (△) 640 nm.

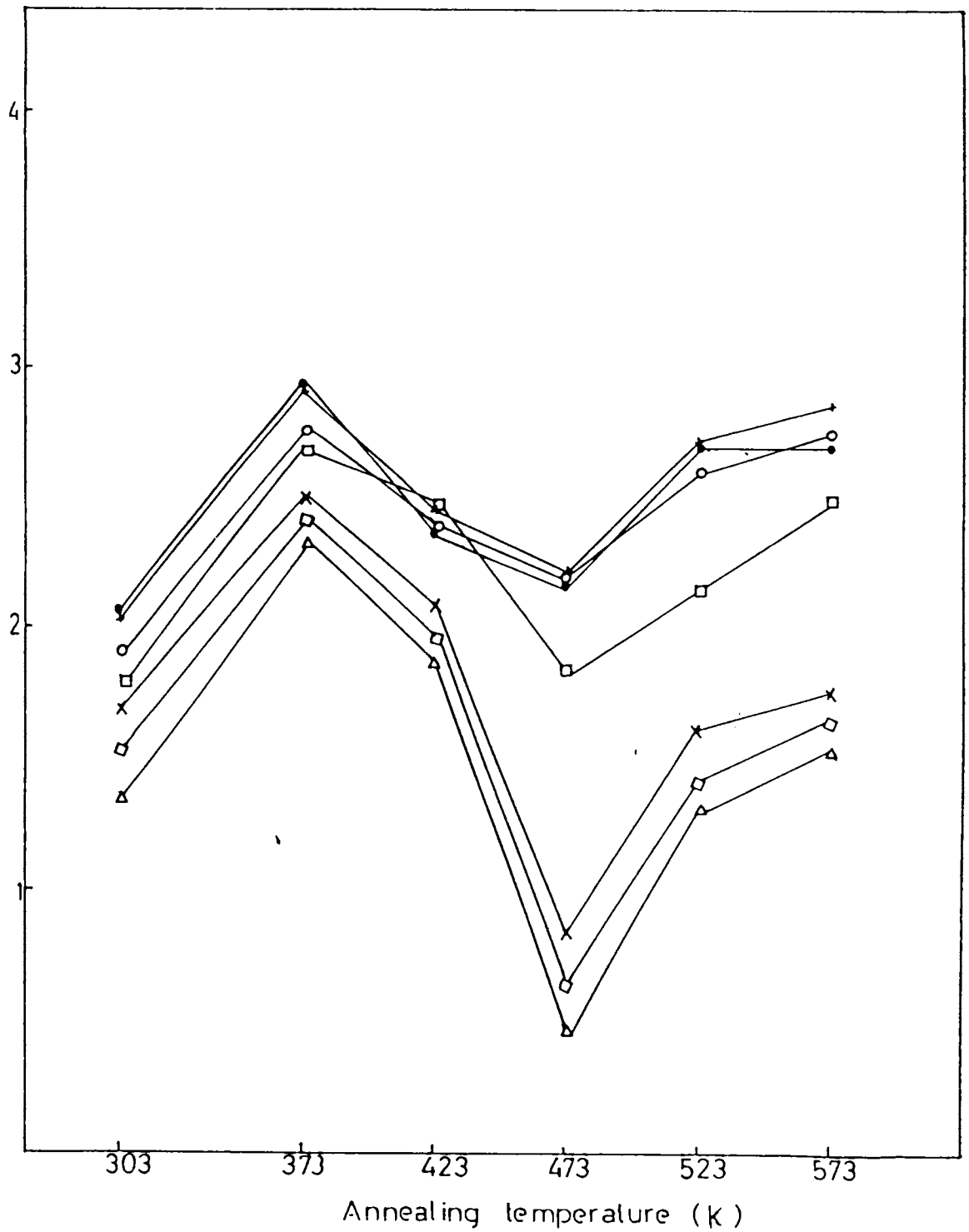

Fig 7.17 : Plot of log ($10^4\sigma$ /power) against annealing temperature at 303 K in air for the film A_1 at different wavelengths: (•) 400 nm, (+) 440 nm, (o) 480 nm, (□) 520 nm, (x) 560 nm, (◇) 600 nm and (△) 640 nm.

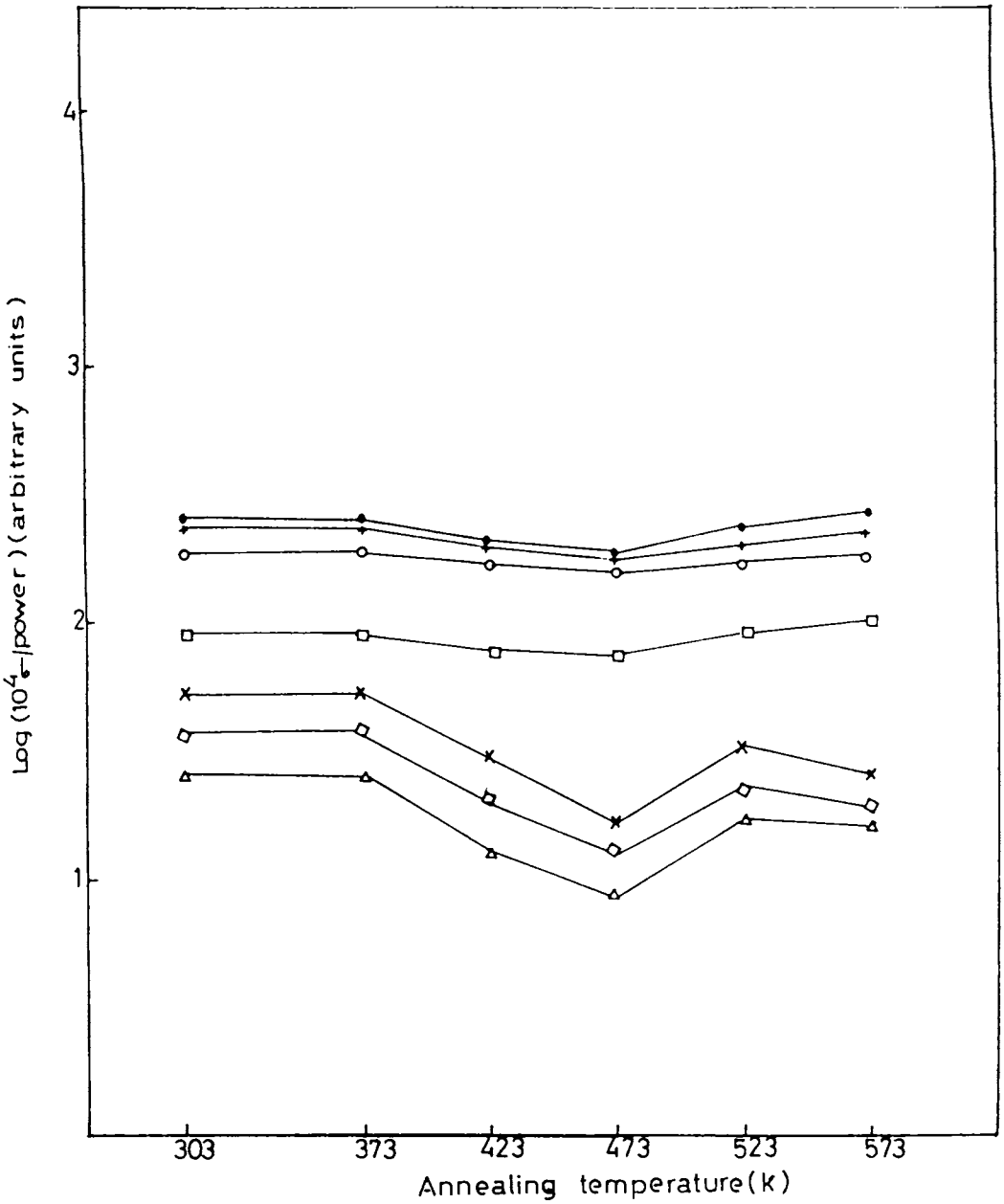

Fig 7.18 : Plot of log ($10^4\sigma$/power) against annealing temperature at 303 K in air for the film A_2 at different wavelengths: (•) 400 nm, (+) 440 nm, (o) 480 nm, (□) 520 nm, (x) 560 nm, (◇) 600 nm and (△) 640 nm.

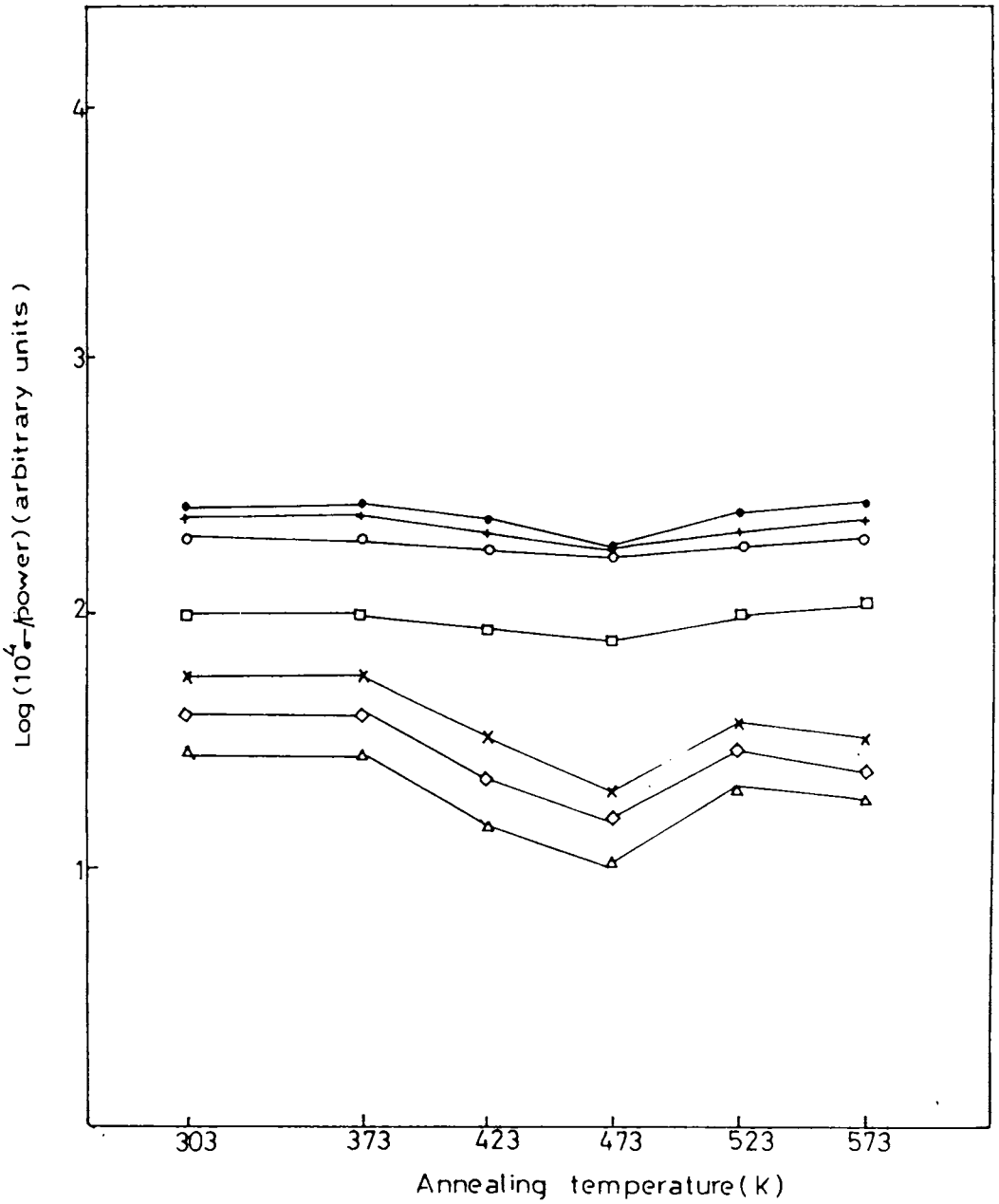

Fig 7.19 : Plot of log ($10^4\sigma$/power) against annealing temperature at 303 K in air for film A_3 at different wavelengths: (•) 400 nm, (+) 440 nm, (o) 480 nm, (□) 520 nm, (x) 560 nm, (◇) 600 nm and (△) 640 nm.

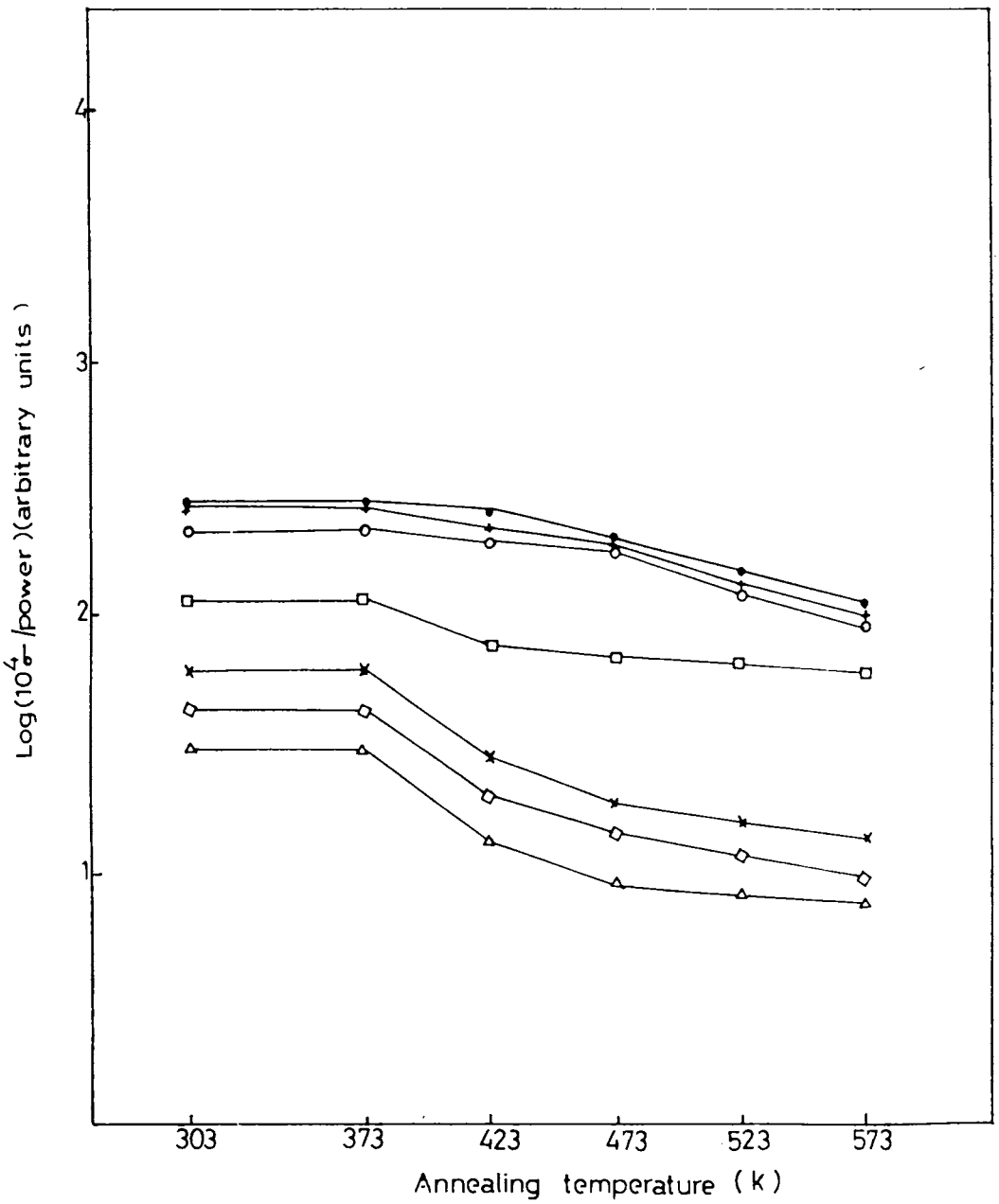

Fig 7.20 : Plot of log ($10^4\sigma$/power) against annealing temperature at 303 K in air for the film A_4 at different wavelengths: (•) 400 nm, (+) 440 nm, (o) 480 nm, (□) 520 nm, (x) 560 nm, (◇) 600 nm and (△) 640 nm.

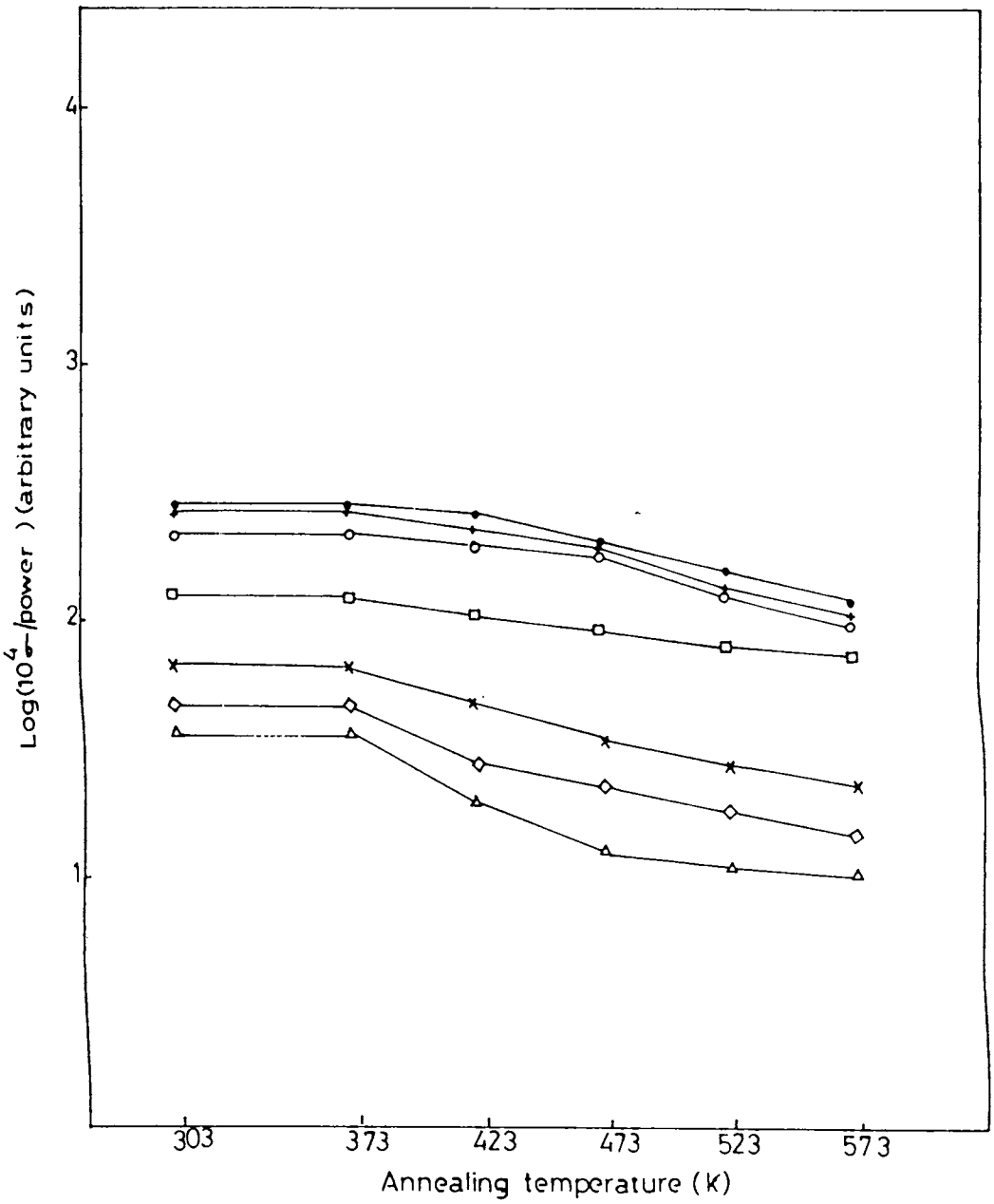

Fig 7.21 : Plot of log ($10^4\sigma$/power) against annealing temperature at 303 K in air for the film A_5 at different wavelengths: (•) 400 nm, (+) 440 nm, (o) 480 nm, (□) 520 nm, (x) 560nm, (◊) 600 nm and (Δ) 640 nm.

However the dependence of photoconductivity on the annealing temperature of the film A_1 for the wavelength in the range 400 - 640 nm in air and vacuum is different. It is clear that for the film A_1, there is similar trend in the photoconductivity variation in air (Fig. 7.17) and vacuum (Fig. 7.7) with annealing temperature upto 473 K. However the photoconductivity of this film annealed above 523 K is found to be strongly ambient dependent. The photoconductivity showed a small increase as the annealing temperature increased above 523 K irrespective of the wavelength when the measurement is carried out in air [13]. This result implies that the presence of air or oxygen affects the trap level in CdS films.

Comparing the results of photoconductivity measurements of films in vacuum and air, it can be inferred that photoconductivity of films is profoundly affected by the ambient conditions. The photoconductivity of films in air is found to be lower than that in vacuum. This can be explained by the fact that, photoconductivity is sensitive to the intake of oxygen in the films. This indicates that, oxygen has a significant influence on the photoconductivity of films.

7.3.2 Lifetime measurements

The lifetime measurements were carried out in the films containing different cadmium contents at wavelengths 400, 520 and 640 nm. The variation of lifetime (τ) with inverse temperature for the unannealed film A_1 is shown in Fig. 7.22. At low temperature, the carriers are

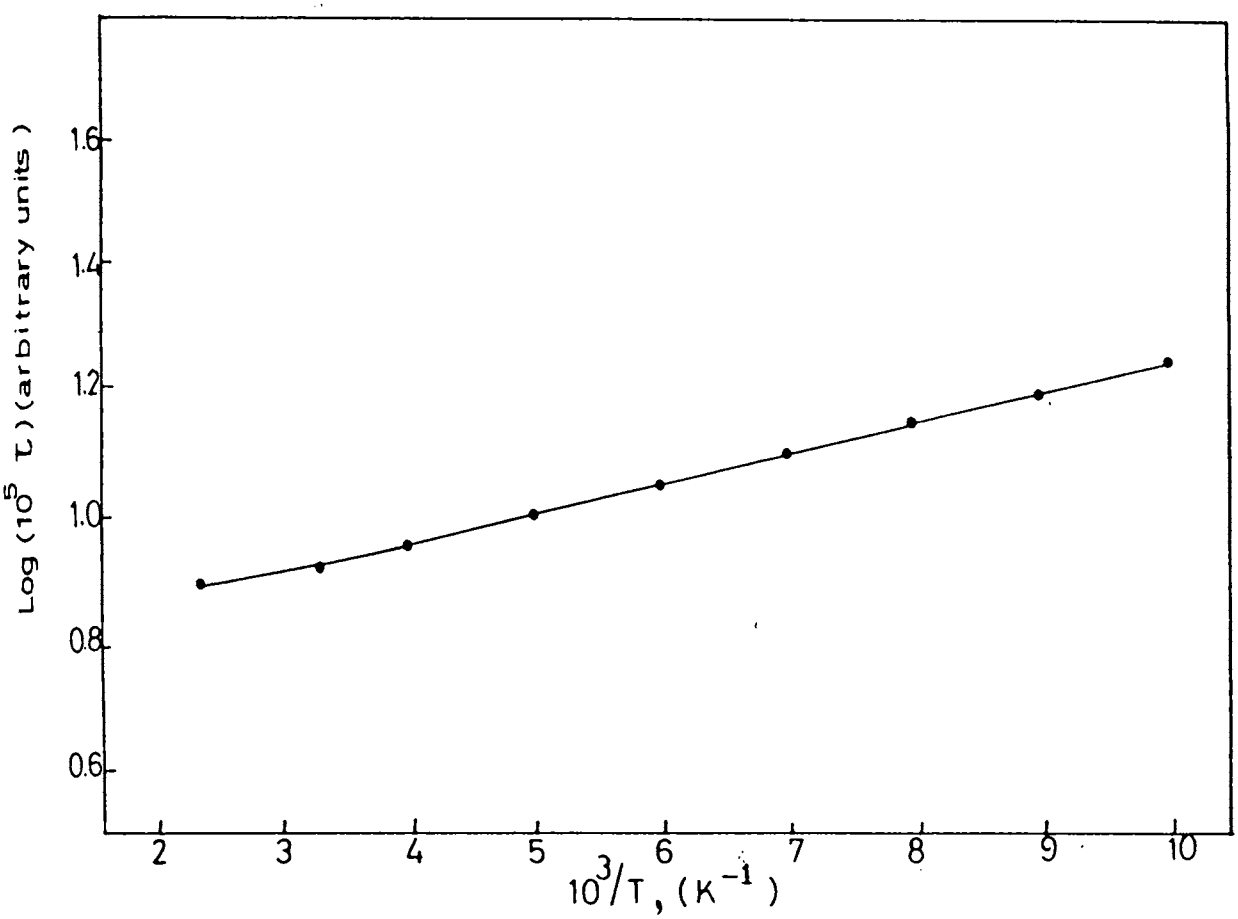

Fig 7.22 : Plot of log ($10^5 \tau$) against $10^3/T$ for the unannealed film A_1 in vacuum at 400 nm.

trapped on the frozen impurity levels and hence the lifetime is increased. As temperature is raised, thermal activation dominates and within a very small time carriers from the trap level are released. This give rise to a drop in lifetime of carriers at the heating temperature 423K.

The lifetime of carriers were determined (Table 7.1) from the measurements in vacuum at room temperature (303K). It is seen that, the lifetime at 400 nm is less than that at 640 nm. At higher wave lengths, photoexcited carriers are readily trapped to produce higher value of lifetime. This indicates that the traps are filled or emptied by optical excitation. The high value of lifetime obtained for the annealed (373K) films A_1 to A_5 reflects the fact that they contain lesser number of imperfections. The lifetime can be controlled by controlling the density of traps in the films. Films A_1 to A_3 annealed at 473K has a low value of lifetime. This results when there is an increase in the density of traps that influence the behaviour of free carriers. At 400 nm, the excess concentration of carriers is large for these films annealed above 523 K. The number of carriers produced by the light at wavelength 640 nm is small due to the capture of carriers by the centres. As a result, lifetime is increased. A decrease in the value of lifetime is observed for the films A_4 and A_5 annealed above 373 K.

The value of lifetime is increased at 100 K. As temperature increases above 303 K, life time decreases for all films. Life time of carriers in films A_4 and A_5 annealed above 373 K entirely depends on recombination kinetics. As the heating temperature increases above 303K,

Table 7.1 The values of lifetime obtained from the measurements of the films in vacuum at different temperatures

Sample	100K $\tau \times 10^{-4}$ sec at			303K $\tau \times 10^{-4}$ sec at			423K $\tau \times 10^{-4}$ sec at		
	400nm	520nm	640nm	400nm	520nm	640nm	400nm	520nm	640nm
A_1									
Unannealed	1.737	2.691	5.011	0.851	1.621	2.137	0.793	1.513	1.862
Annealed(373K)	2.089	3.235	5.370	0.977	1.778	2.344	0.891	1.621	2.089
Annealed(423K)	1.819	3.019	5.248	0.870	1.698	2.238	0.812	1.584	1.995
Annealed(473K)	1.621	2.398	4.365	0.794	1.380	1.862	0.724	1.288	1.621
Annealed(523K)	1.995	2.630	4.570	0.954	1.548	1.949	0.870	1.445	1.698
Annealed(573K)	1.905	2.511	4.786	0.912	1.479	2.041	0.831	1.348	1.778
A_2									
Unannealed	1.547	2.453	4.677	0.811	1.478	1.861	0.756	1.380	1.621
Annealed(373K)	1.548	2.454	4.678	0.812	1.479	1.862	0.757	1.381	1.622
Annealed(423K)	1.288	2.238	3.801	0.724	1.348	1.513	0.660	1.258	1.348
Annealed(473K)	1.202	1.949	3.548	0.691	1.148	1.412	0.645	1.070	1.258
Annealed(523K)	1.479	2.137	3.981	0.794	1.288	1.584	0.741	1.202	1.412
Annealed(573K)	1.412	2.041	4.265	0.758	1.230	1.698	0.691	1.122	1.479

Contd....

Contd.. Table 7.1

Sample	100K τ x10^{-4} sec at			303K τx10^{-4} sec at			423K τ x10^{-4} sec at		
	400nm	520nm	640nm	400nm	520nm	640nm	400nm	520nm	640nm
A_3									
Unannealed	1.412	2.290	4.265	0.794	1.348	1.737	0.724	1.230	1.513
Annealed(373K)	1.413	2.291	4.267	0.795	1.349	1.738	0.725	1.232	1.514
Annealed(423K)	1.000	1.995	3.162	0.691	1.258	1.412	0.645	1.174	1.258
Annealed(473K)	0.954	1.698	3.019	0.781	1.071	1.348	0.616	1.000	1.202
Annealed(523K)	1.380	1.905	3.630	0.758	1.202	1.479	0.691	1.122	1.318
Annealed(573K)	1.288	1.819	3.981	0.724	1.148	1.584	0.676	1.071	1.380
A_4									
Unannealed	1.258	2.040	4.073	0.776	1.288	1.621	0.707	1.202	1.412
Annealed(373K)	1.260	2.041	4.075	0.777	1.290	1.623	0.708	1.203	1.413
Annealed(423K)	0.933	1.778	2.691	0.660	0.676	0.691	0.602	0.588	0.575
Annealed(473K)	0.831	1.479	1.995	0.630	0.645	0.660	0.588	0.575	0.562
Annealed(523K)	0.776	1.258	1.778	0.602	0.616	0.630	0.575	0.562	0.549
Annealed(573K)	0.707	1.202	1.698	0.575	0.588	0.602	0.562	0.537	0.524
A_5									
Unannealed	1.38	2.290	4.897	0.794	1.318	1.659	0.724	1.230	1.445
Annealed(373K)	1.40	2.291	4.898	0.795	1.319	1.660	0.725	1.231	1.446
Annealed(423K)	0.954	2.137	4.570	0.691	0.724	0.776	0.660	0.630	0.602
Annealed(473K)	0.870	1.862	4.265	0.660	0.691	0.741	0.630	0.602	0.588
Annealed(523K)	0.831	1.584	3.630	0.630	0.660	0.707	0.616	0.588	0.562
Annealed(573K)	0.758	1.513	2.630	0.602	0.630	0.660	0.588	0.562	0.537

the trapped carriers at low temperature is disappeared due to the recombination, which takes place at high temperatures.

The values of lifetime of carriers determined for the films heat treated in air are listed in Table 7.2. The influence of wavelength and heating temperature on lifetime is similar to that observed in vacuum. Due to the effect of oxygen impurities incorporated in the films during air heat treatment, the values of lifetime obtained during the measurements are found to be less compared to that in vacuum. Moreover, carriers generated by the photoexcitation are trapped by the oxygen impurities.

7.4 CONCLUSION

The photoconductivity measurements were carried out in CdS film in vacuum and air as a function of wavelength, cadmium contents and annealing temperature. Films A_1 to A_5 annealed at 373 K are found to have maximum photoconductivity in vacuum. Due to the trapping of carriers, minimum photoconductivity is observed for the films A_1 to A_3 annealed at 473 K. On annealing the films A_1 to A_3 above 523K, the photoconductivity is increased at 400 nm, whereas it is decreased at 640 nm.. A decrease in the photoconductivity is observed for the films A_4 to A_5 annealed above 373K. The effect of heating on the photoconductivity of the films from 303 to 423 K shows that trapping of carriers does not occur in the films annealed at 373 K. The decrease in photoconductivity observed for the films A_4 to A_5 annealed above

Table 7.2 The values of lifetime obtained from the measurements of the films in air at different temperatures

Sample	303K $\tau \times 10^{-4}$ sec at			423K $\tau \times 10^{-4}$ sec at		
	400nm	520nm	640nm	400nm	520nm	640nm
A_1						
Unannealed	0.524	0.794	1.023	0.501	0.741	0.933
Annealed(373K)	0.758	1.258	1.659	0.691	1.148	1.479
Annealed(423K)	0.616	1.174	1.548	0.588	1.122	1.412
Annealed(473K)	0.549	0.851	0.933	0.524	0.776	0.831
Annealed(523K)	0.707	1.122	1.445	0.660	1.071	1.318
Annealed (573K)	0.676	1.071	1.348	0.630	1.023	1.174
A_2						
Unannealed	0.690	1.148	1.348	0.630	1.047	1.148
Annealed(373K)	0.691	1.149	1.350	0.631	1.049	1.149
Annealed(423K)	0.588	0.954	1.096	0.549	0.870	1.000
Annealed(473K)	0.562	0.870	1.047	0.530	0.831	0.977
Annealed(523K)	0.660	1.071	1.174	0.588	1.000	1.071
Annealed(573K)	0.630	1.023	1.258	0.562	0.954	1.096

Contd ...

Contd...Table 7.2

Sample	303K			423K		
	400nm	520nm	640nm	400nm	520nm	640nm
A_3						
Unannealed	0.724	1.202	1.412	0.660	1.096	1.202
Annealed(373K)	0.725	1.203	1.413	0.661	1.098	1.204
Annealed(423K)	0.630	1.047	1.174	0.562	0.933	1.047
Annealed(473K)	0.575	0.933	1.096	0.537	0.870	1.000
Annealed(523K)	0.691	1.148	1.258	0.616	1.047	1.122
Annealed(573K)	0.660	1.096	1.318	0.588	1.000	1.148
A_4						
Unannealed	0.741	1.230	1.479	0.676	1.148	1.288
Annealed(373K)	0.744	1.231	1.480	0.677	1.149	1.289
Annealed(423K)	0.645	0.660	0.676	0.588	0.562	0.549
Annealed(473K)	0.602	0.630	0.660	0.562	0.549	0.537
Annealed(523K)	0.575	0.602	0.616	0.549	0.524	0.512
Annealed(573K)	0.549	0.562	0.575	0.537	0.512	0.501
A_5						
Unannealed	0.758	1.258	1.548	0.691	1.174	1.348
Annealed(373K)	0.761	1.260	1.550	0.692	1.175	1.349
Annealed(423K)	0.660	0.707	0.741	0.630	0.616	0.575
Annealed (473K)	0.630	0.660	0.707	0.602	0.575	0.562
Annealed(523K)	0.588	0.616	0.676	0.575	0.549	0.537
Annealed(573K)	0.562	0.588	0.616	0.549	0.524	0.512

373 K is due to the recombination of carriers. Photoconductivity of the films in air is found to be less than that in vacuum. This is due to the fact that, photoconductivity in sensitive to the intake of oxygen in the films. The lifetime of photogenerated carriers depends on several parameters such as annealing temperature, cadmium content and ambient conditions. The results obtained from the present investigation in vacuum at room temperature indicates that photoconductivity and lifetime of the films containing higher cadmium contents is relatively lower than that of the film A_1.

7.5 REFERENCES

[1] M. Bohacek, E. Fryba, F. Khol and V. Rosicka, Proc. of the 5th Czechoslavakia Conf. on electronics and vacuum physics, Czechoslovakia, 1972.

[2] P.A. Viktor, V.V. Zotov, S.A. Korepanov and V.V.Serdyuk, Inorg. Mater. 19 (1983) 155.

[3] M. Takeuchi, Y. Sakagawa and H.Nagasaka, Thin Solid Films 33 (1976) 89

[4] C.E. Weitzel and L.K. Monteith, Surf. Sci: 24 (1974) 438

[5] M.J.B. Thomas, J. Electrochem. Soc. 106 (1959) 964.

[6] R. Krupa and A. Wrzesinskai, Acta. Phys. Pol.A, A53 (1978) 675

[7] N. Croitoru and S. Jakobson, Thin Solid Films 56 (1979) L5.

[8] A.M.E. Korashy and R.J. Stirn,Egypt. J. Solids 7 (1985) 8.

[9] B.K. Gupta, O.P. Agnihotri and A. Raza, Thin Solid Films 48 (1978) 153.

[10] Z. Porada and E. Schabowska, Thin Solid Films 66 (1980) L,55

[11] J. Ebothe, Colloq. Phys. C-6 (1989) 176

[12] A.G. Valyomana, K.P. Vijayakumar and C.Purushothaman, J. Mater. Sci. Lett. 9 (1990) 1025

[13] A.G. Valyomana, K.P. Vijayakumar and C. Purushothaman, J.Mater. Sci. Lett. 11 (1992) 616.

8 IONIC THERMOCURRENT AND THERMALLY STIMULATED CURRENT STUDIES OF CdS THIN FILMS

8.1 INTRODUCTION

Ionic thermocurrent (ITC) method is a powerful tool for the investigation of impurity-vacancy (I-V) complexes in semiconducting compounds. The ITC studies of alkali halide crystals have been reported by many authors [1-5]. However, no data is reported in the literature regarding the ITC characteristics of sprayed CdS films.

Thermally stimulated current (TSC) studies of CdS crystals have been done by a few workers [6-9]. Kitamura [10] performed the TSC measurements of sintered CdS films and observed a TSC peak at room temperature. But no systematic investigation on electron trapping in these films using the TSC technique has been made yet. Therefore it was intended to carry out a detailed study on the TSC measurements for getting full information on the nature of the trap levels in sprayed CdS films.

This chapter presents the ITC and TSC studies of CdS films prepared by spray pyrolysis method. The effect of various activation parameters like field strength, poling temperature and poling time on the ITC peak of CdS films have been investigated for the first time. Special attention has been given to examine the influence of annealing temperature and cadmium contents on the ITC and TSC peaks. The values of activation energy required for the reorientation of (I-V) complexes and the capture cross section of the observed electron traps are also estimated.

8.2 EXPERIMENTAL

CdS films A_1 to A_5 were prepared by spray pyrolysis method as already described in Chapter 5. The films were annealed in air for 30 min in a glass chamber with provision for temperature measurement and heating. Electrical contacts were made by depositing aluminium electrodes [$\sim$ 2000 Å] on the surface of the films using vacuum evaporation technique. The ITC and TSC measurements were made in an evacuated metallic cell as described in Chapter 4. Several heating and cooling cycles were done to obtain reproducible results. For the ITC measurements, the samples were subjected to a dc field of 1-3 KV/cm at the poling temperature in the range 303-425 K for a poling time of 1-10 min. The field was switched off after cooling the film to liquid nitrogen temperature. On reaching the lowest temperature, the film was heated at a constant rate of 0.06 K/Sec and the current was measured using an electrometer. In the case of TSC measurements, the film was cooled down to the liquid nitrogen temperature and subjected to optical excitation by a tungsten halogen lamp for 2-15 min. After removing the optical source, the film was heated at a constant rate of 0.06 K/Sec. The current through the film was then measured with the field applied (1-5 KV/cm). The trap depth and capture cross section of electron traps were evaluated as described in Chapter 3.

8.3 RESULTS AND DISCUSSION

8.3.1 ITC Measurements

The ITC measurements were carried out on unannealed and annealed films in the temperature range 100-450 K. The spectra recorded for the films containing various cadmium contents after applying a field of 1 KV/cm for 1 min at 303 K are shown in Figs. 8.1 to 8.5. A peak centered around 363 K is observed for all films. This is due to the reorientation of (I-V) complexes as can be observed in the case of certain alkali halides [1]. The origin of the (I-V) complexes can be interpreted in terms of the presence of chlorine and the nature of defects occuring during the film formation. The addition of certain impurities create vacancies or interstitials in a lattice. Change in the spray rate during deposition also introduces defects (vacancies) into the film. Therefore it is possible to create lattice vacancies associated with these impurities in which they form (I-V) complexes.

The ITC spectra obtained for the film A_1 prepared from 0.20 M cadmium chloride and 0.20 M thiourea as a function of poling field are illustrated in Fig. 8.6. The inset shows the variation of the current maximum with the applied field. The height of the peak is found to vary linearly with the poling field. This is attributed to the increase in number of dipoles oriented at higher poling fields. Fig. 8.7 shows the effect of poling temperature on the ITC peaks of the film A_1 and the inset shows the respective variation of current maximum with the poling temperature. The decrease in

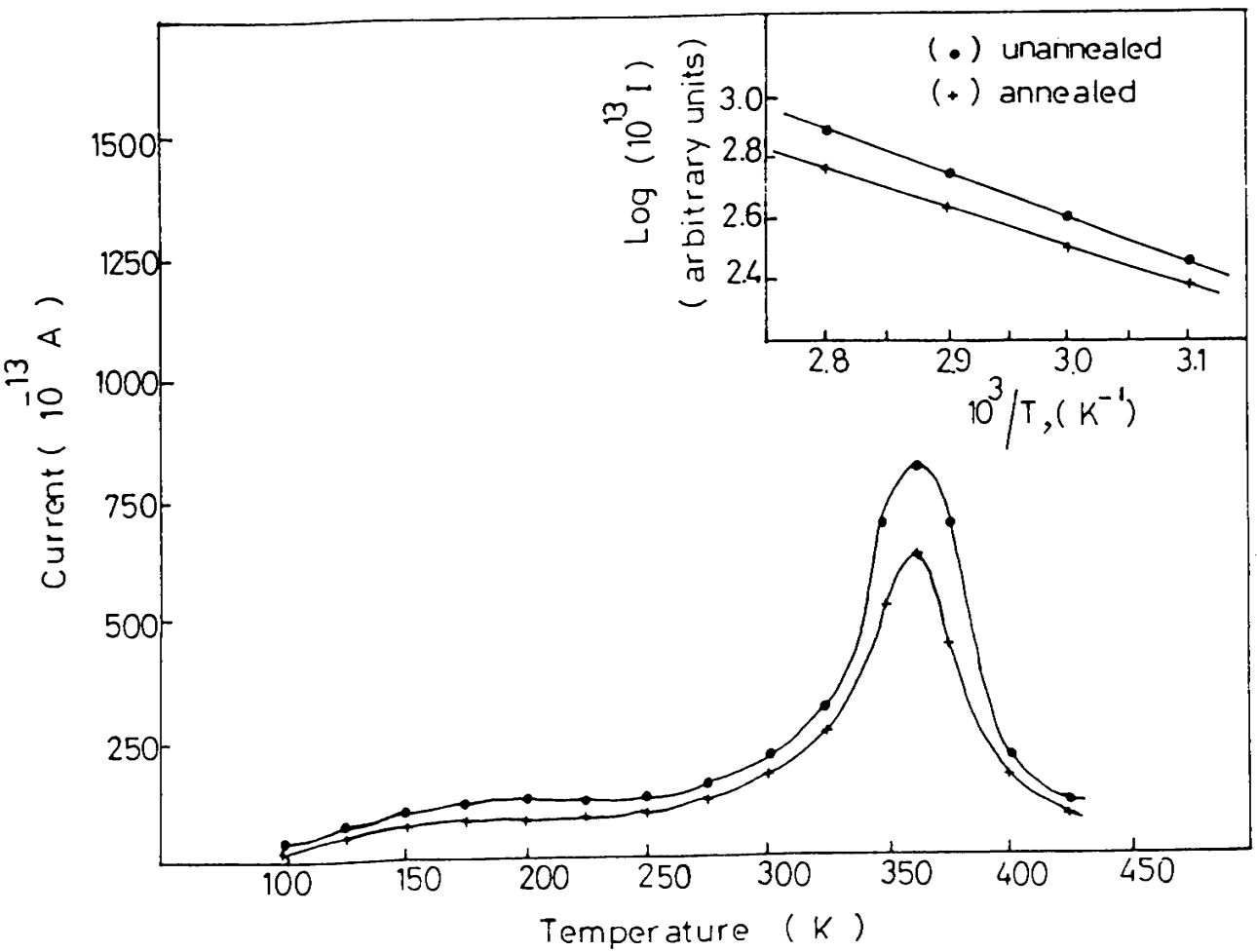

Fig. 8.1: ITC spectrum of the film A_1 (.) unannealed and (+) annealed at 573 K. The inset shows the plot of log (10^{13} I) against $10^3/T$.

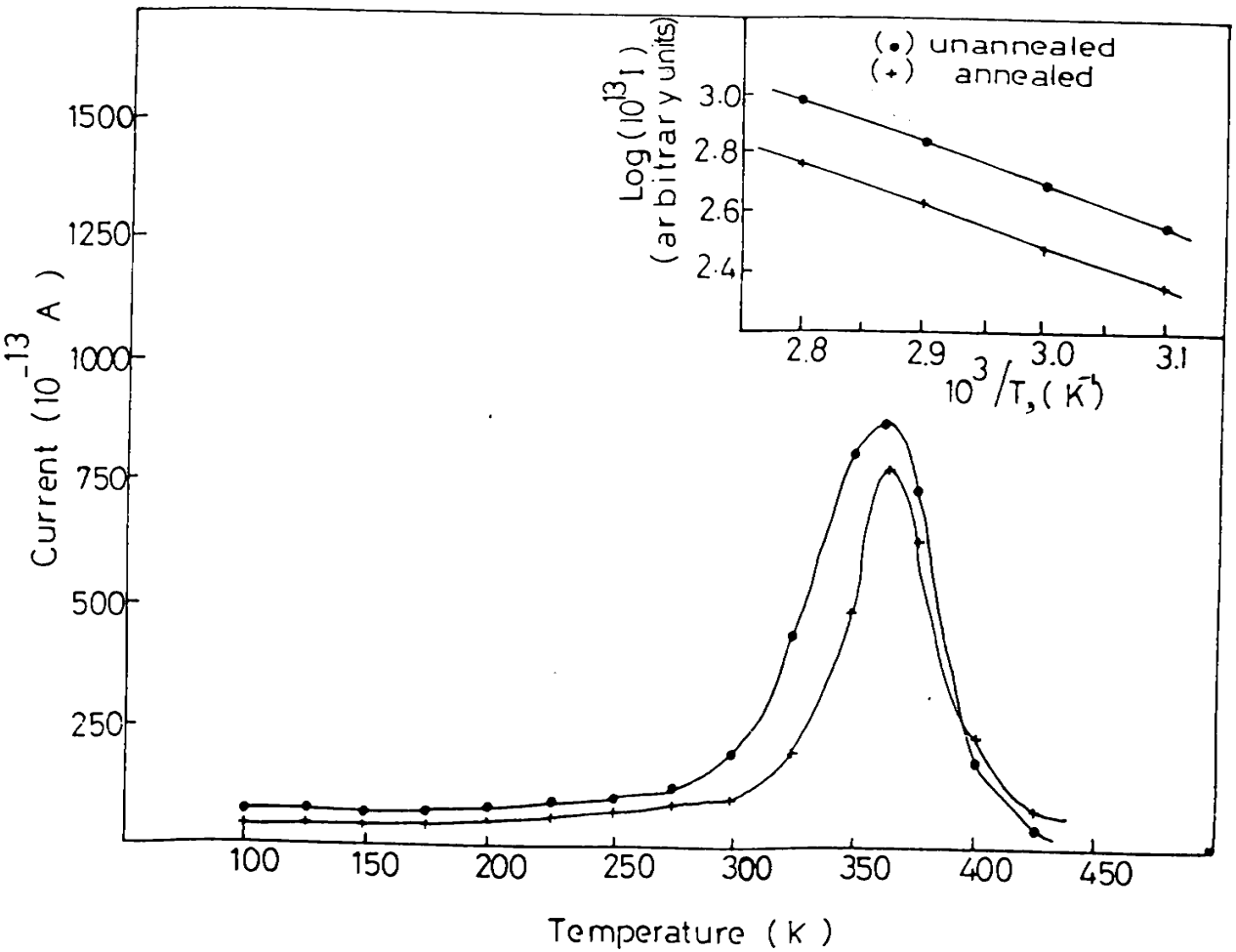

Fig 8.2 : ITC spectra of the film A_2 (•) unannealed and (+) annealed at 573 K. The inset the plot of log (10^{13} I) against $10^3/T$.

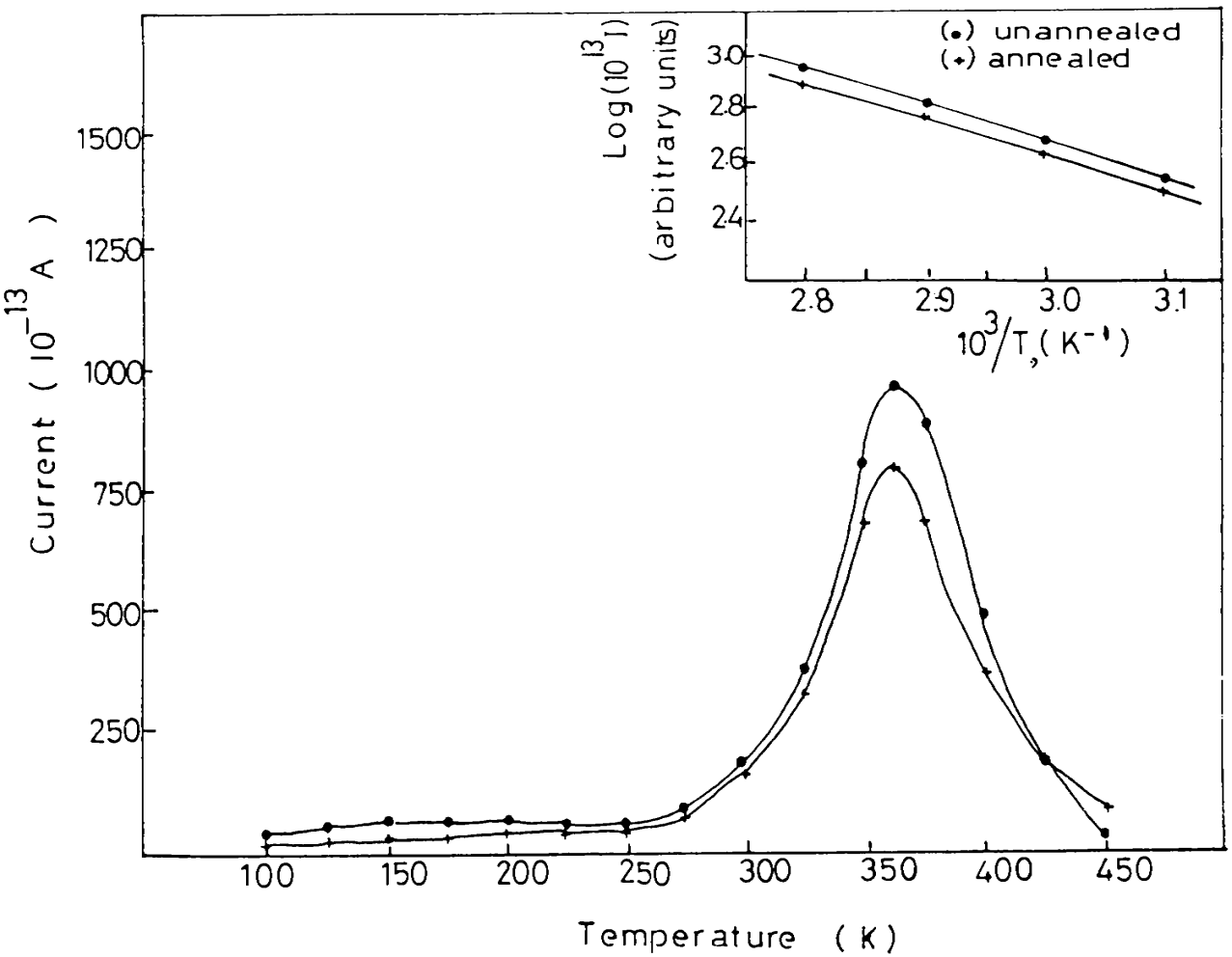

Fig 8.3 : ITC spectra of the film A_3 (•) unannealed and (+) annealed at 573 K. The inset shows the plot of log (10^{13}I) against $10^3/T$.

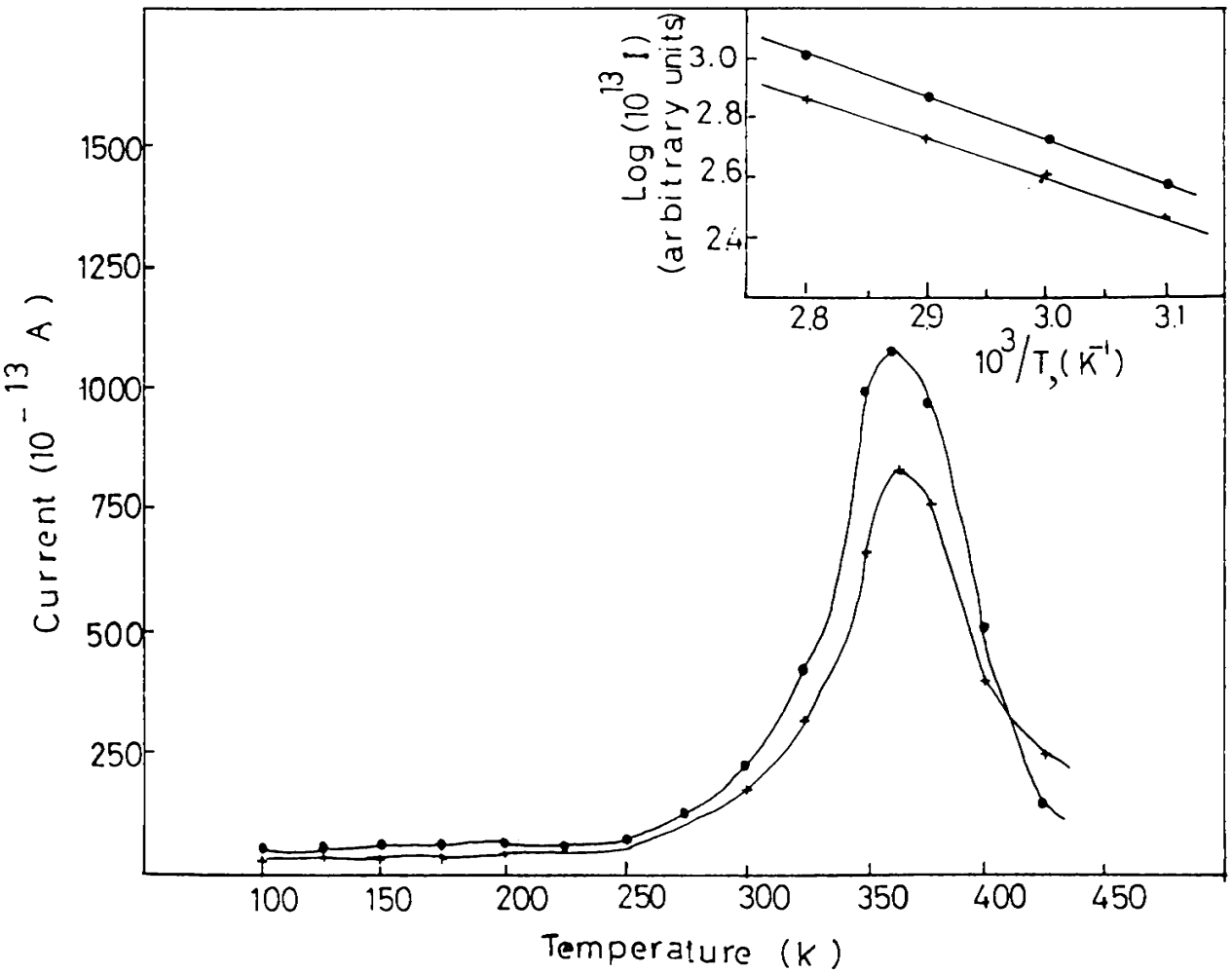

Fig 8.4 : ITC spectra of the film A_4 (•) unannealed and (+) annealed at 573 K. The inset shows the plot of log (10^{13}I) against $10^3/T$.

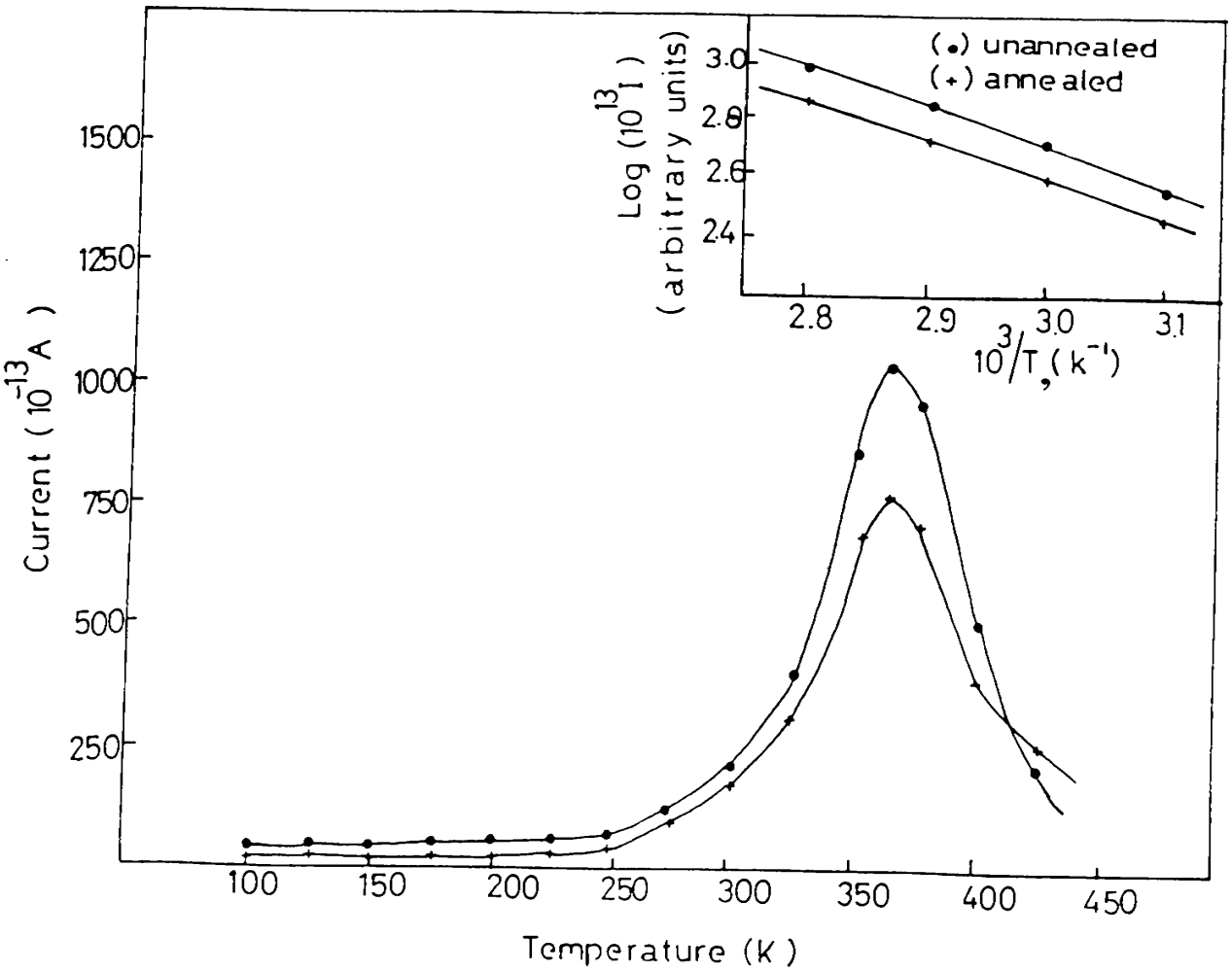

Fig 8.5 : ITC spectra of the film A_5 (•) unannealed and (+) annealed at 573 K. The inset shows the plot of log (10^{13}I) against $10^3/T$.

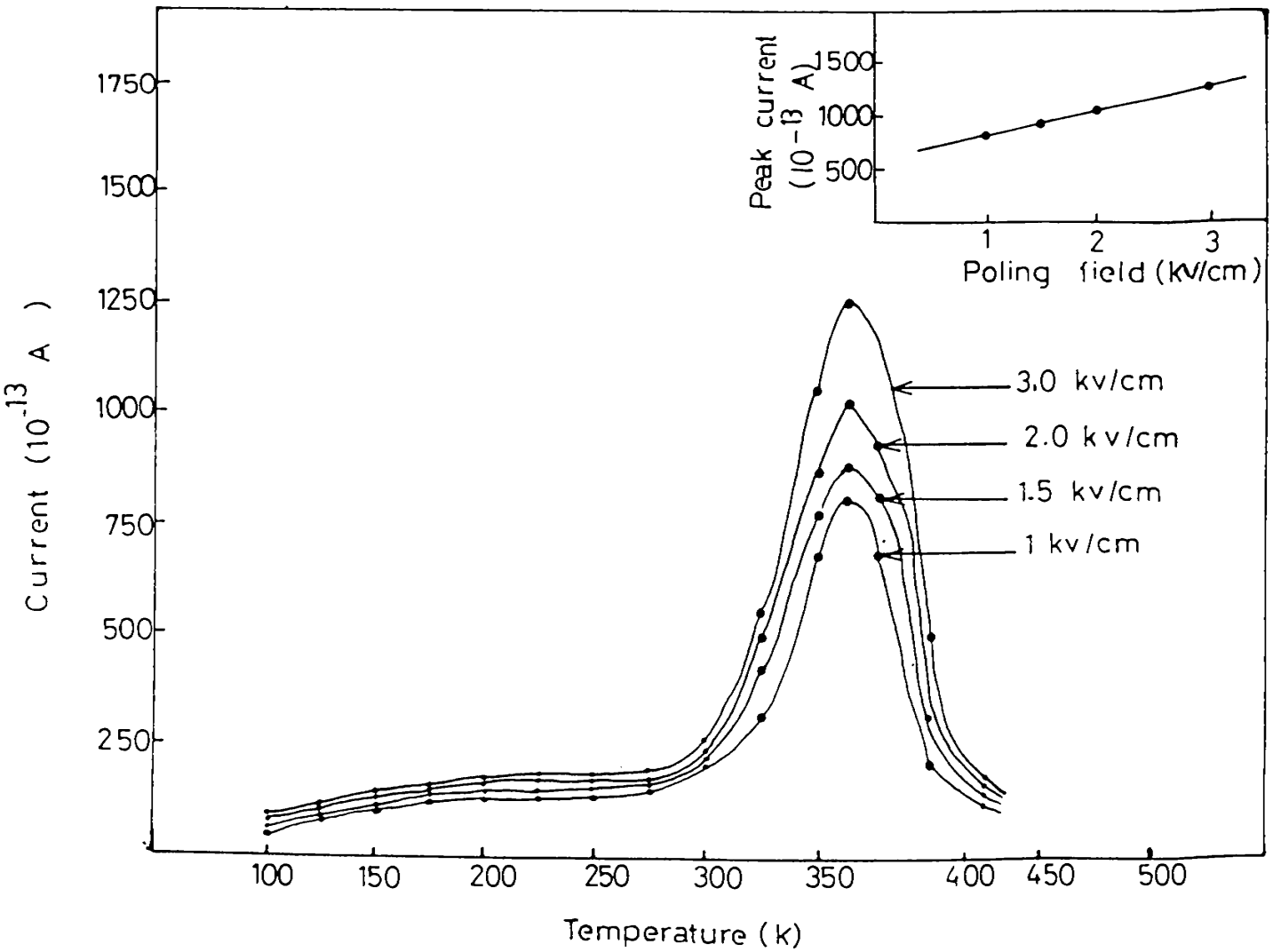

Fig 8.6 : Dependence of the ionic thermocurrent for the unannealed film A_1 at different poling fields. The inset shows the plot of peak height against poling field.

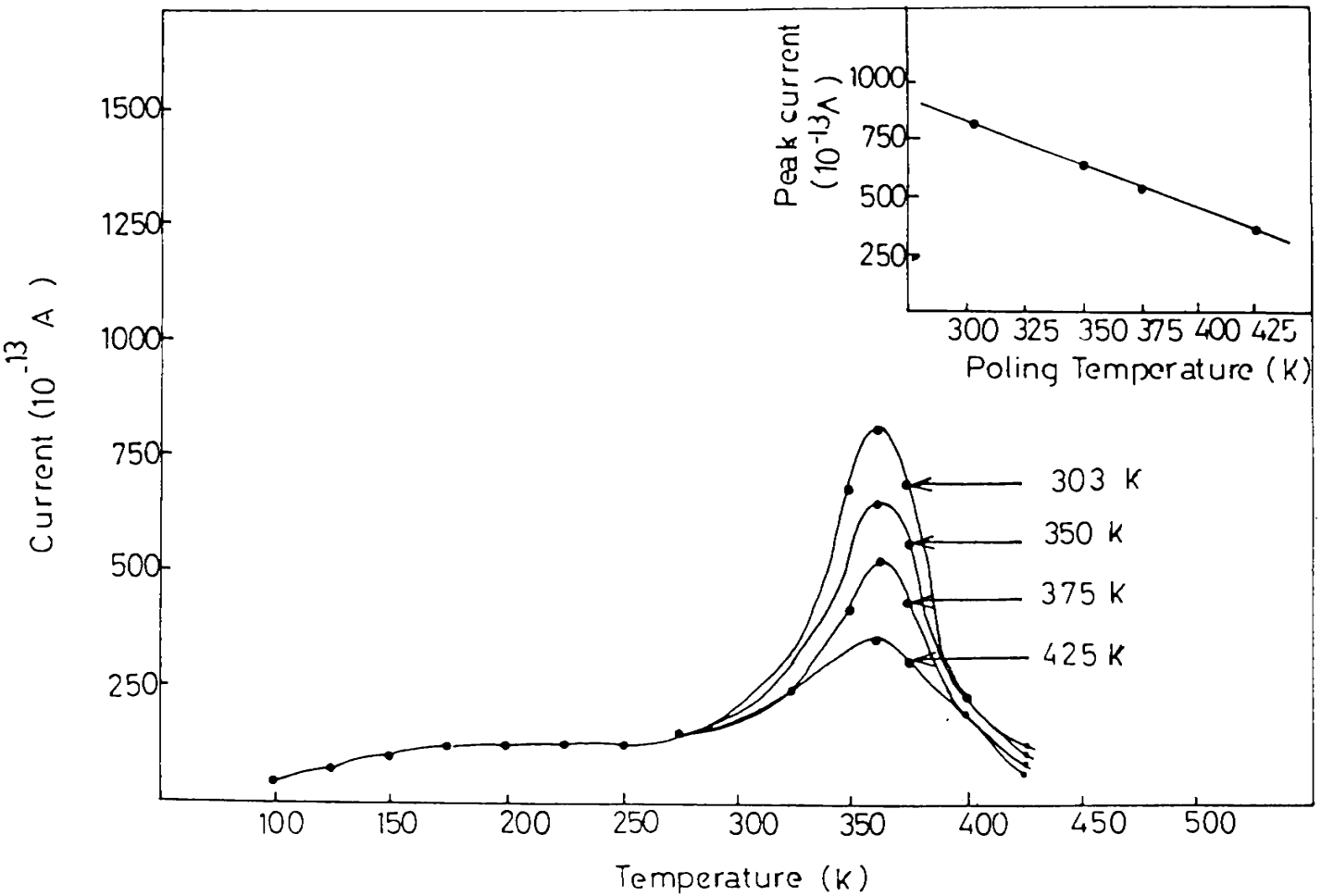

Fig 8.7 : Dependence of the ionic thermocurrent for the unannealed film A_1 at different poling temperatures. The inset shows the plot of peak height against poling temperature.

peak height with increase in poling temperature is due to the dissociation of the (I-V) complexes. The effect of poling time on the variation of the ITC peak of the film A_1 is depicted in Fig. 8.8. The magnitude of the peak increases with poling time (Inset of Fig.8.8). The polarization of the (I-V) dipoles is extremely sensitive to the poling time and more number of dipoles are oriented with the increase in poling time.

During the present investigations, it has been found that the effect of poling field, poling temperature and poling time on the ITC peaks are similar for all films containing different cadmium contents.

Fig. 8.9 shows the effect of cadmium chloride concentration on the height of ITC peaks. It is found that the height of the peak first increases, reaches a maximum and then slowly decreases. The increase in peak height has been attributed to the presence of higher chlorine content in the films. For the annealed films, the magnitude of peak is found to be less than that of unannealed films. This is due to the dissociation of (I-V) dipoles.

The values of activation energy required for the reorientation of (I-V) dipoles can be estimated from the initial rise method. The slope of the inset of Figs. 8.1 to 8.5 gives the values of activation energy and are presented in Table 8.1. The increase in the value of activation energy is characteristic of the additional energy required

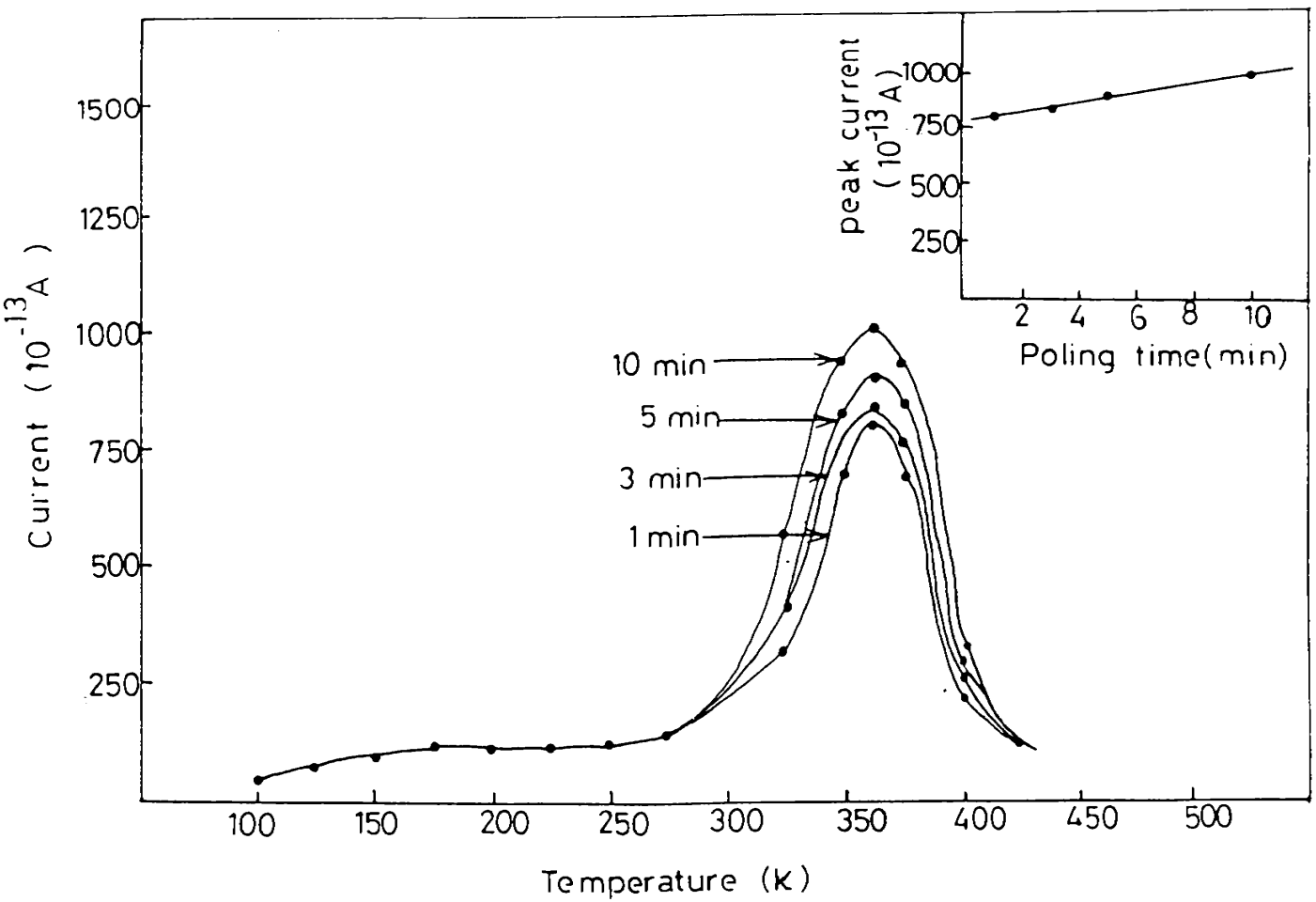

Fig 8.8 : Dependence of the ionic thermo current for the unannealed film A_1 at different poling time. The inset shows the plot of peak height against poling time.

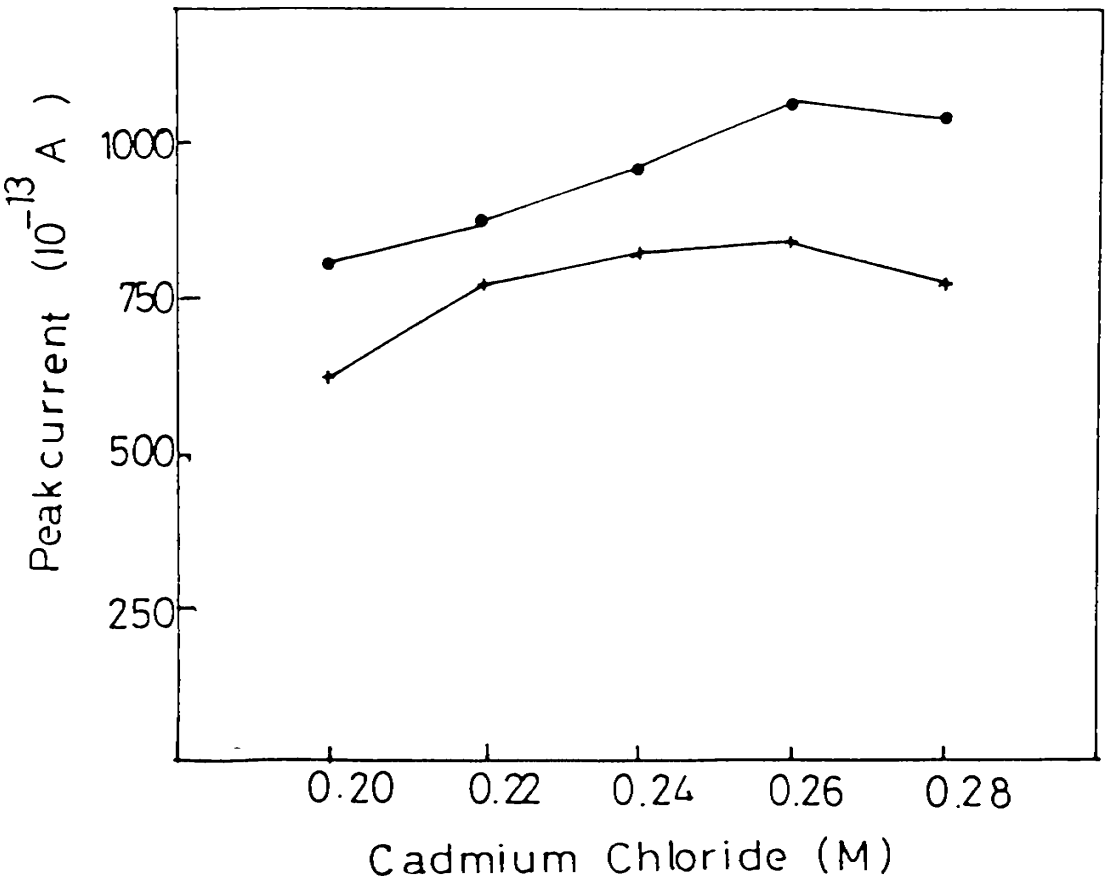

Fig 8.9 : Plot of ionic thermocurrent against cadmium chloride concentration for the films (•) unannealed and (+) annealed at 573 K.

Table 8.1 The values of activation energy obtained from the ITC spectra of CdS films.

Sample	Activation energy (eV)
A_1	
Unannealed	0.283
Annealed (573 K)	0.261
A_2	
Unannealed	0.285
Annealed (573 K)	0.263
A_3	
Unannealed	0.288
Annealed (573 K)	0.265
A_4	
Unannealed	0.290
Annealed (573 K)	0.268
A_5	
Unannealed	0.287
Annealed (573 K)	0.264

for the higher number of (I-V) dipoles in CdS films [11].

8.3.2 TSC Measurements

Figs. 8.10 to 8.14 show the TSC spectra recorded for the CdS films of various cadmium contents. In all cases, the spectra exhibit three prominent TSC peaks represented by A, B and C. The temperature corresponding to the peaks (Tm) is found to be dependent on the cadmium contents. It is clear from Fig. 8.10 that the current maximum of the peak A for the film A_1 annealed at 373 K is slightly shifted, to the lower temperature region as compared to the unannealed film. The values of activation energy (E) of trap levels, capture cross section and Tm for all the films are given in Tables 8.2 to 8.4. It is seen from Fig. 8.11 that the height of the peak A obtained for the film A_2 prepared from 0.22 M cadmium chloride and 0.20 M thiourea annealed at 573 K is lower than that of unannealed film. In the case of film A_3 prepared from 0.24 M cadmium chloride and 0.20 M thiourea, the peak A is situated at 117 K with a trap depth of 0.046 eV and the peak B is at 256 K with the trap depth of 0.235 eV. The peak C is situated at 406 K and the trap depth is 0.81 eV. The TSC peaks are found to be independent of annealing temperature (Fig. 8.12). When the concentration of cadmium chloride is increased to 0.26 M, the spectra of the prepared film possess three peaks A, B and C at temperatures 105 K, 265 K and 407 K respectively (Fig. 8.13). These peaks are also found to be independent of the annealing temperature. It is clear from Figs. 8.10

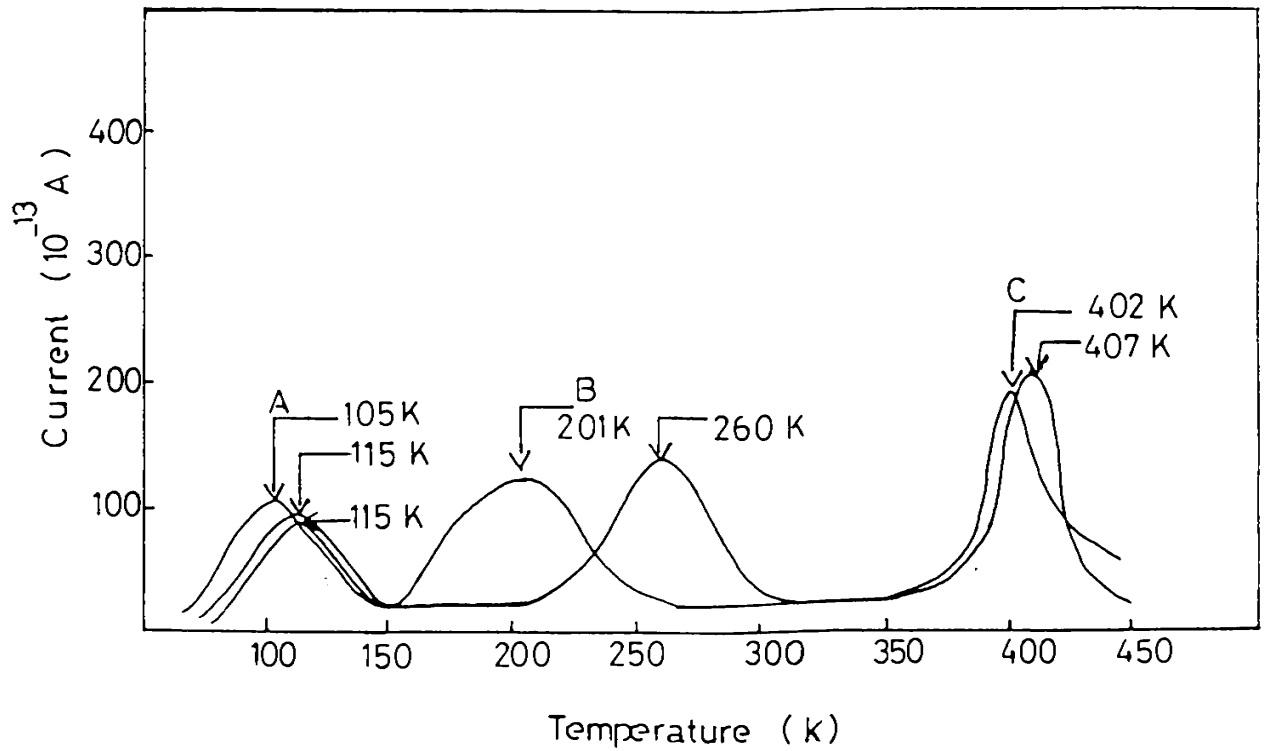

Fig 8.10 : TSC spectra of the film A_1.

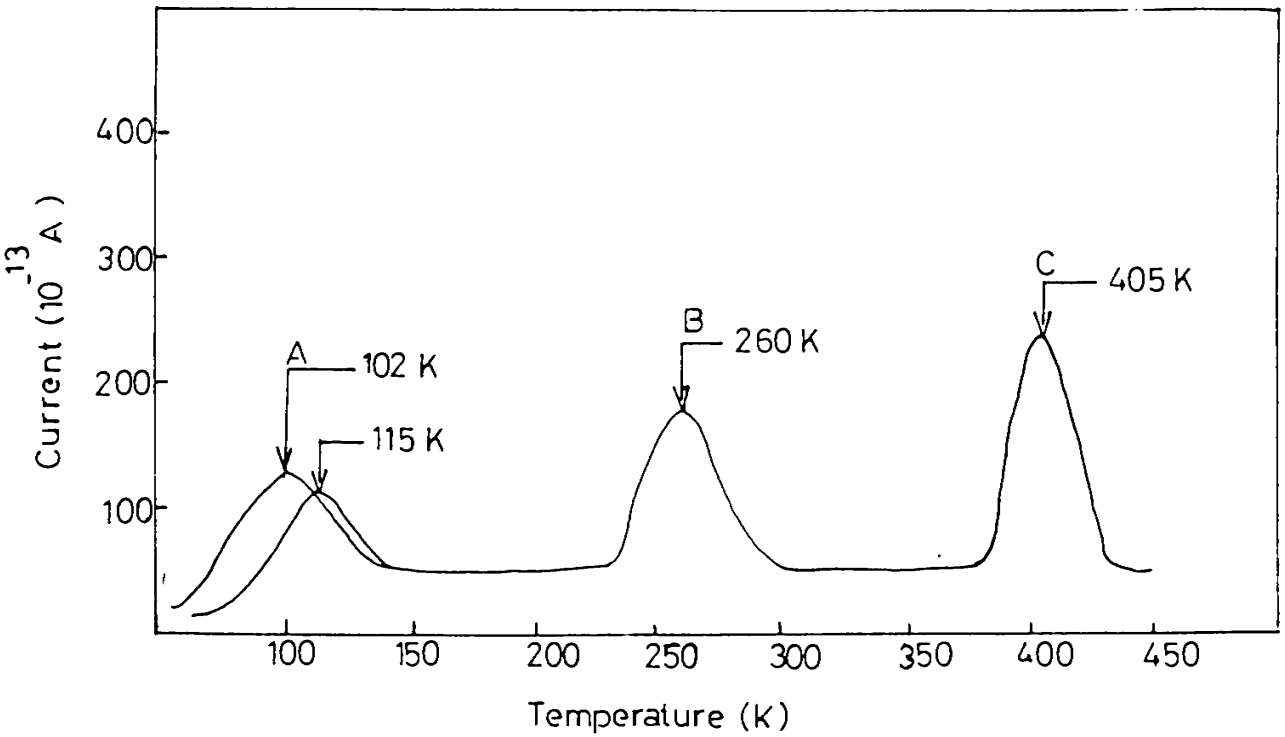

Fig 8.11 : TSC spectra of the film A_2.

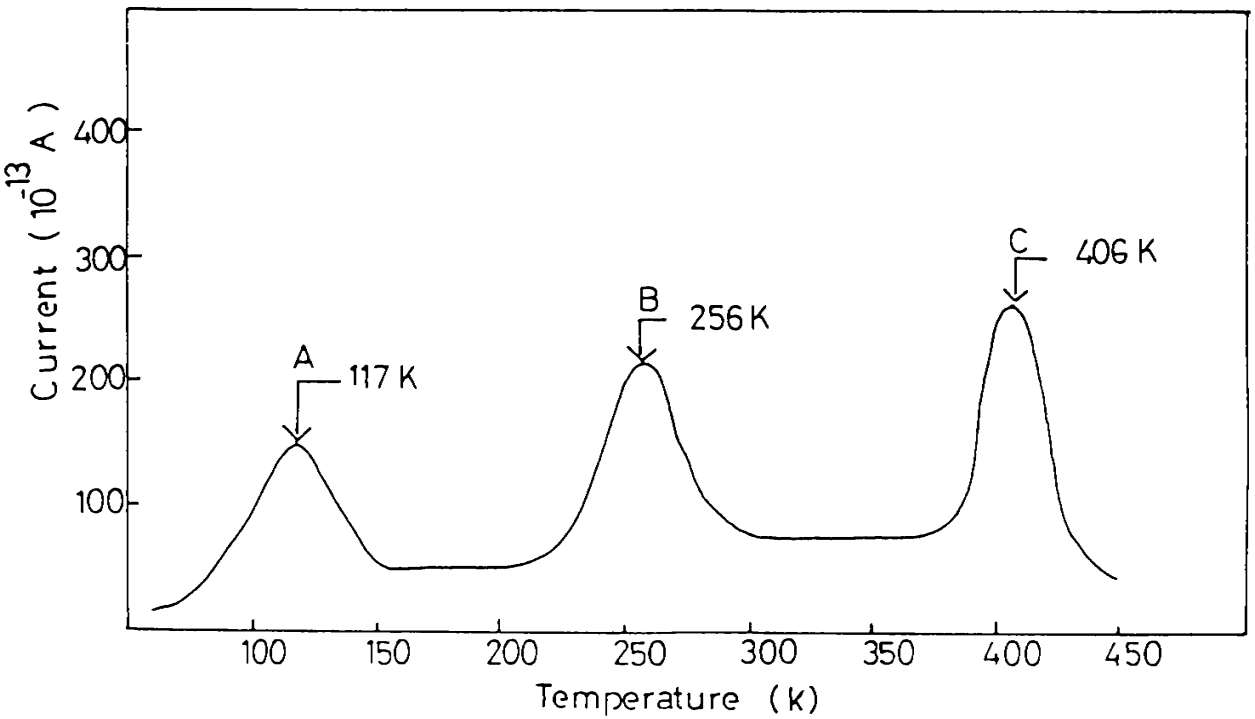

Fig 8.12 : TSC spectrum of the film A_3.

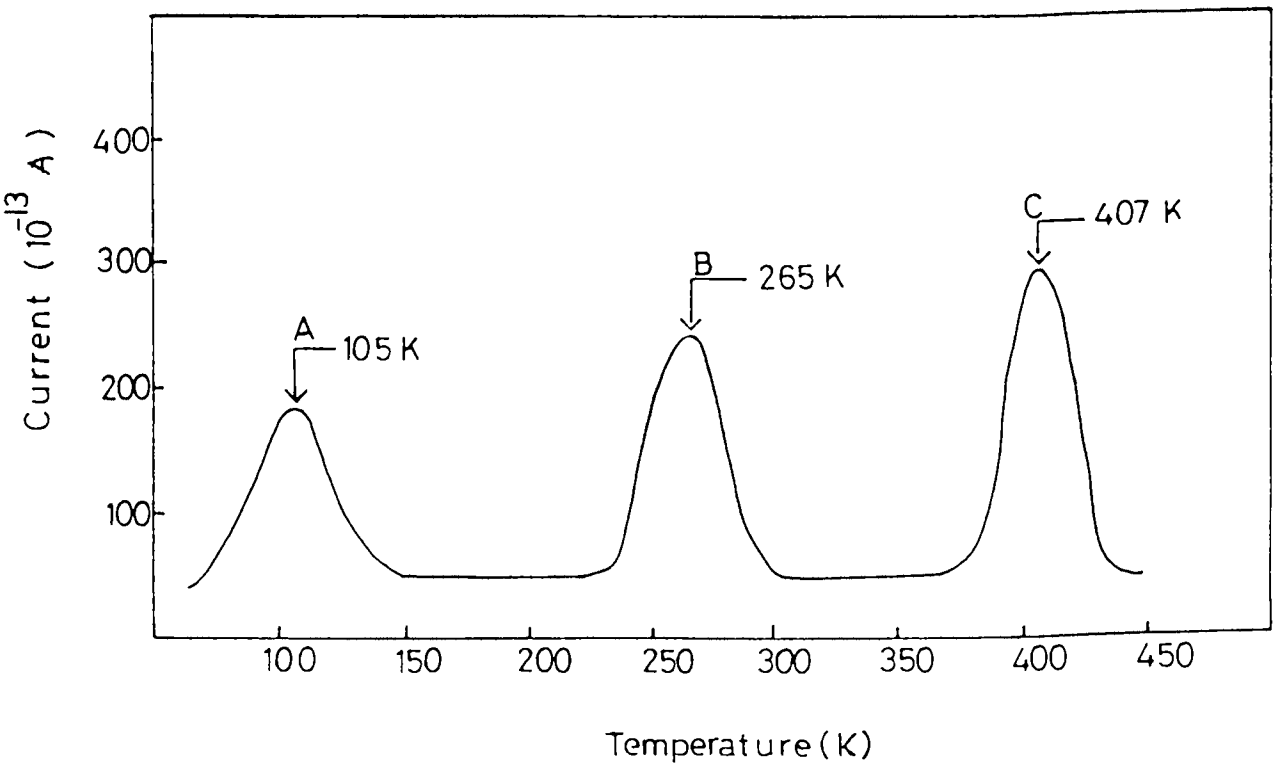

Fig 8.13 : TSC spectrum of the film A_4.

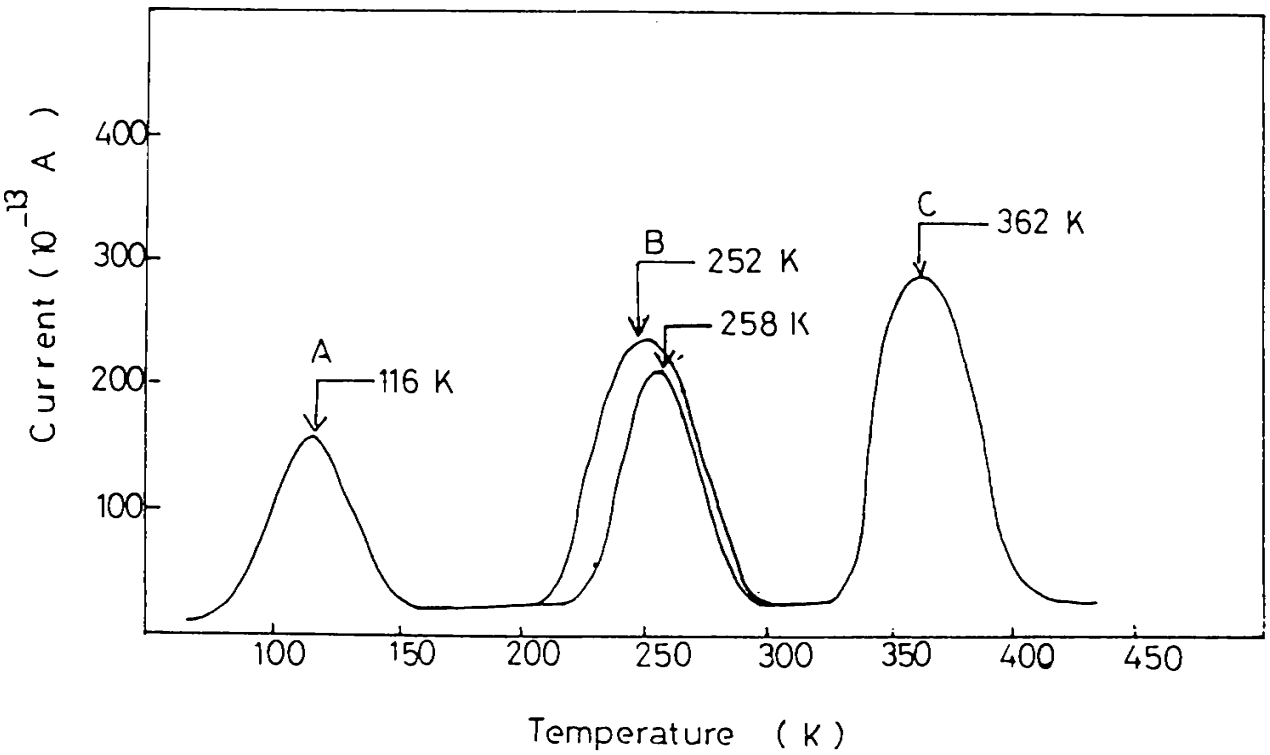

Fig 8.14 : TSC spectra of the film A_5.

Table 8.2 The values of various parameters obtained for the Peak A of TSC spectra of CdS films

Sample	Tm (K)	E (eV)	Capture Cross section (Cm^2)
A_1			
Unannealed	115	0.047	2.82×10^{-27}
Annealed (373K)	105	0.038	1.59×10^{-27}
Annealed (423K)	115	0.049	3.82×10^{-27}
Annealed (473K)	"	"	"
Annealed (523K)	"	"	"
Annealeld (573K)	"	"	"
A_2			
Unannealed	102	0.031	7.00×10^{-28}
Anneale d (373K)	"	"	"
Annealed (423K)	115	0.050	4.00×10^{-27}
Annealed (473K)	102	0.031	7.00×10^{-28}
Annealed (523K)	115	0.050	4.00×10^{-27}
Annealed (573K)	"	"	"

Contd.....

Contd...Table 8.2

Sample	Tm (K)	E (eV)	Capture Cross section (Cm^2)
A_3			
Unannealeld	117	0.046	2.23×10^{-27}
Annealed (373K)	"	"	"
Annealed (423K)	"	"	"
Annealeld (473K)	"	"	"
Annealed (523K)	"	"	"
Annealed (573K)	"	"	"
A_4			
Unannealed	105	0.036	1.20×10^{-27}
Annealed (373K)	"	"	"
Annealed (423K)	"	"	"
Annealed (473K)	"	"	"
Annealed (523K)	"	"	"
Annealed (573K)	"	"	"

Contd....

Contd.... Table 8.2

Sample	Tm (K)	E (eV)	Capture Cross section (Cm^2)
A_5			
Unannealed	116	0.051	4.31×10^{-27}
Annealed (373K)	"	"	"
Annealed (423K)	"	"	"
Annealed (473K)	"	"	"
Annealed (523K)	"	"	"
Annealed (573K)	"	"	"

Table 8.3 The values of various parameters obtained for the Peak B of TSC spectra of CdS films

Sample	Tm (K)	E (eV)	Capture Cross section (Cm^2)
A_1			
Unannealed	201	0.100	5.51×10^{-27}
Annealed (373K)	260	0.243	1.26×10^{-24}
Annealed (423K)	"	"	"
Annealed (473K)	"	"	"
Annealed (523K)	"	"	"
Annealed (573K)	"	"	"
A_2			
Unannealed	260	0.250	1.78×10^{-24}
Annealed (373K)	"	"	"
Annealed (423K)	"	"	"
Annealed (473K)	"	"	"
Annealed (523K)	"	"	"
Annealed (573K)	"	"	"

Contd...

Contd... Table 8.3

Sample	Tm (K)	E (eV)	Capture Cross section (Cm^2)
A_3			
Unannealed	256	0.235	1.04×10^{-24}
Annealed (373K)	"	"	"
Annealed (423K)	"	"	"
Annealed (473K)	"	"	"
Annealed (523K)	"	"	"
Annealed (573K)	"	"	"
A_4			
Unannealed	265	0.269	3.44×10^{-24}
Annealed (373K)	"	"	"
Annealed (423K)	"	"	"
Annealed (473K)	"	"	"
Annealed (523K)	"	"	"
Annealed (573K)	"	"	"

Contd.....

Contd.... Table 8.3

Sample	Tm (K)	E (eV)	Capture Cross section (Cm^2)
A_5			
Unannealed	252	0.220	5.70×10^{-25}
Annealed (373K)	"	"	"
Annealed (423K)	"	"	"
Annealed (473K)	"	"	"
Annealed (523K)	258	0.260	3.36×10^{-24}
Annealed (573K)	"	"	"

Table 8.4 The Values of various parameters obtained for the Peak C of TSC spectra of CdS films

Sample	Tm (K)	E (eV)	Capture Cross section (Cm^2)
A_1			
Unannealed	407	1.020	1.78×10^{-16}
Annealed (373K)	"	"	"
Annealed (423K)	"	"	"
Annealed (473K)	"	"	"
Annealed (523K)	402	0.850	1.62×10^{-18}
Annealed (573K)	"	"	"
A_2			
Unannealed	405	0.808	3.80×10^{-19}
Annealed (373K)	"	"	"
Annealed (423K)	"	"	"
Annealed (473K)	"	"	"
Annealed (523K)	"	"	"
Annealed (573K)	"	"	"

Contd....

Contd... Table 8.4

Sample	Tm (K)	E (eV)	Capture Cross section (Cm^2)
A_3			
Unannealed	406	0.810	3.79×10^{-19}
Annealed (373K)	"	"	"
Annealed (423K)	"	"	"
Annealed (473K)	"	"	"
Annealed (523K)	"	"	"
Annealed (573K)	"	"	"
A_4			
Unannealed	407	0.810	3.57×10^{-19}
Annealed (373K)	"	"	"
Annealed (423K)	"	"	"
Annealed (473K)	"	"	"
Annealed (523K)	"	"	"
Annealed (573K)	"	"	"

Contd.....

Contd... Table 8.4

Sample	Tm (K)	E (eV)	Capture Cross section (Cm^2)
A_5			
Unannealed	362	0.426	1.90×10^{-23}
Annealed (373K)	"	"	"
Annealed (423 K)	"	"	"
Annealed (473K)	"	"	"
Annealed (523K)	"	"	"
Annealed (573K)	"	"	"

to 8.14 that the magnitude of the peak height increases as the concentration of cadmium chloride increases from 0.20 to 0.26 M, and on further increase in the concentration a slight decrease in the magnitude is observed. Figs. 8.15 and 8.16 depict the variation of the height of TSC peaks with biasing field and excitation time for the film A_1. It is seen that the peak height increases with excitation time and biasing field.

During the TSC measurements, certain conditions are to be satisfied: the conduction and valence bands must be independent, trap levels must initially be completely filled, there must be equilibrium between the conduction band and the traplevels and the retrapping process must be slow. In the present case, the results obtained are in accordance with these conditions. When the traps are emptied, the currents are found to be very low and TSC peaks are fairly well resolved for all the CdS films studied. The temperature corresponding to the current maxima is different for various samples. The trap depth obtained from the TSC curves show a shift in value with that reported by Woods and Nicholas [12] in CdS crystals. This variation is not necessarily associated with any deficiencies in the theories underlying the various proposed models but rather is the result of inherent practical difficulties.

The trapping of impurities during the formation of CdS f ıs has significant influence on the TSC measurements and their effect is more predominent at low temperatures. The TSC peak obtained

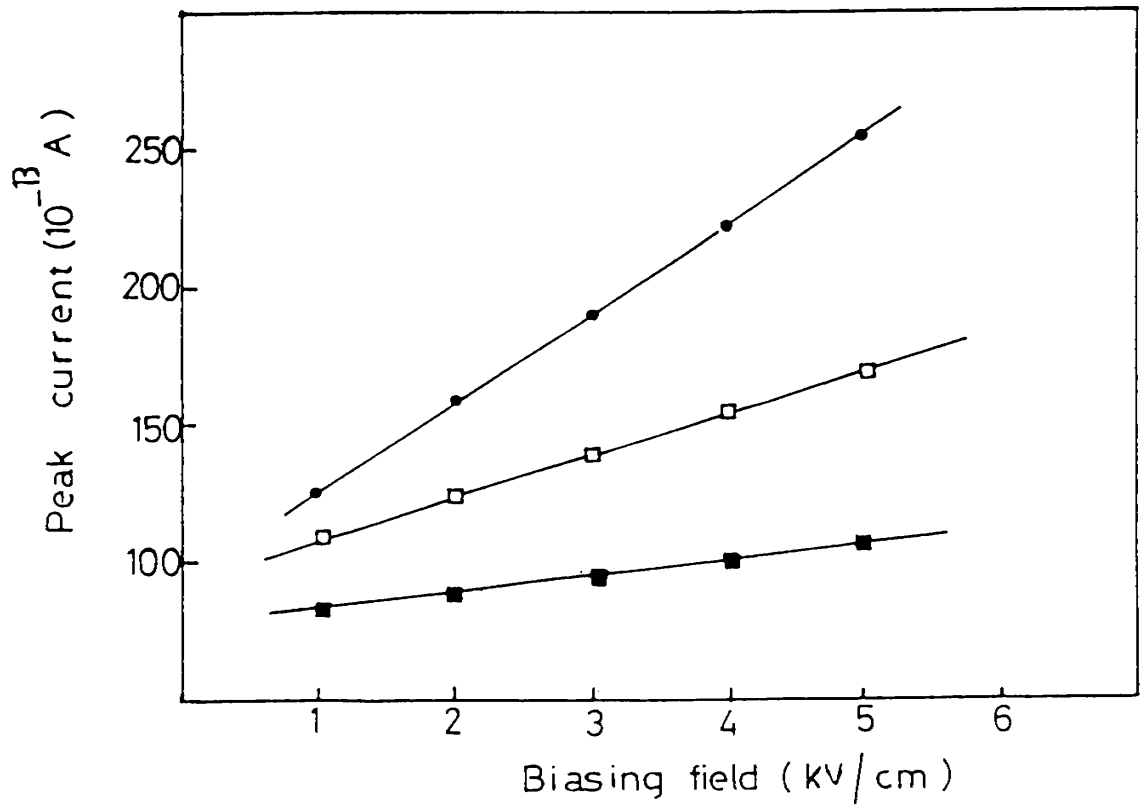

Fig 8.15 : Plot of peak height against biasing field for the film A_1 annealed at 573 K for the peaks: (■) A, (□) B and (•) C.

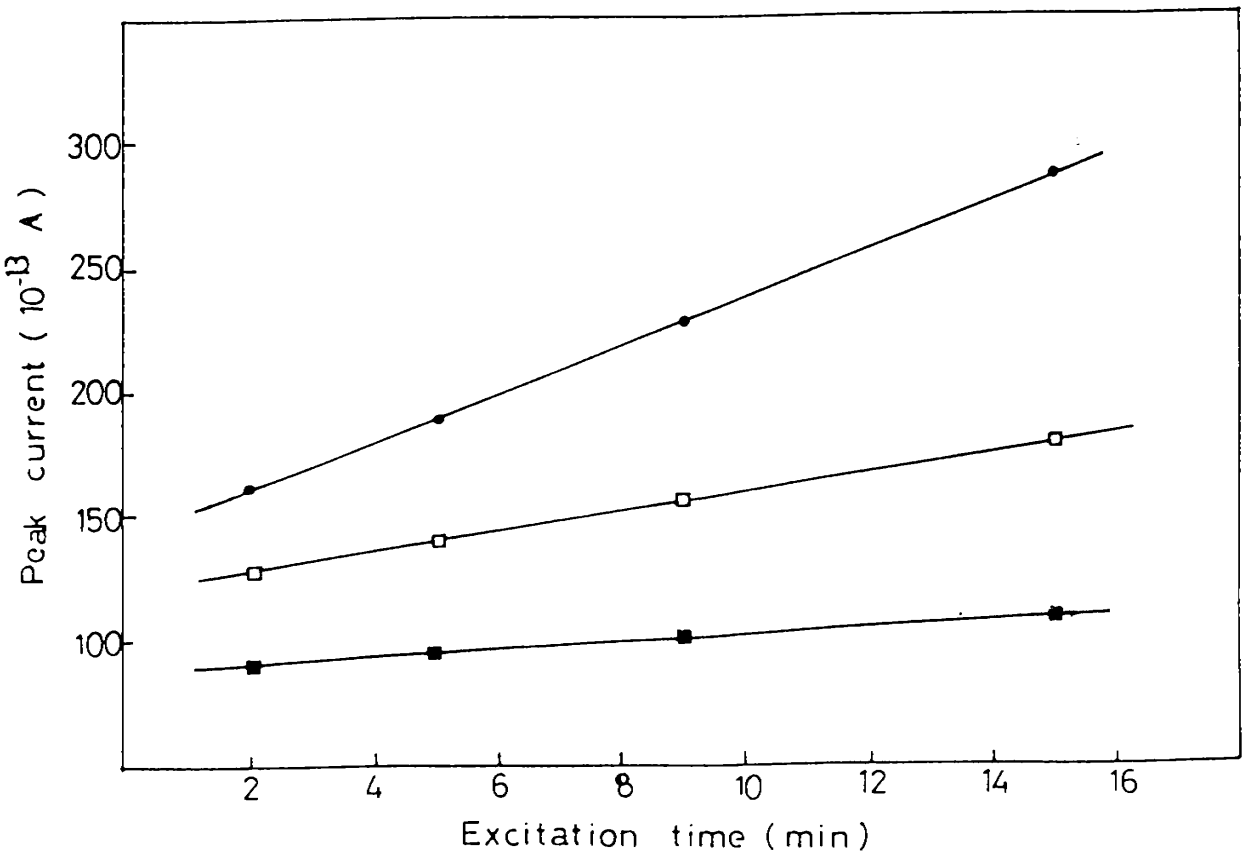

Fig 8.16 : Plot of peak height against excitation time for the film A_1 annealed at 573 K for the peaks: (■) A, (□) B and (•) C.

with the activation energy of $\sim$ 0.03 eV can be attributed to the trapping of chlorine in the film. The peak A observed in the films with a level of $\sim$ 0.05 eV is attributed to the sulphur vacancies. The peak observed in the film with the trap depth $\sim$ 0.1 eV indicates the presence of sulphur interstitials. This result agrees with that obtained from the dark conductivity studies of CdS films [13]. Since the value of trap depth of $\sim$ 0.25 eV is same for all films, it is concluded that they are probably characteristic of aggregates of sulphur vacancies. Woods and Nicholas [12] suggested that the trap levels in CdS crystals appearing at 0.41 and 0.83 eV are complexes of associated cadmium and sulphur vacancies in nearest neighbour sites. The TSC peaks obtained in the high temperature region thus confirm the existence of cadmium and sulphur vacancy complexes. In the present investigation, the trap levels were observed at $\sim$ 0.4 and $\sim$ 0.8 eV (Table 8.2).

The magnitude of the TSC peaks also depends on the concentration of cadmium chloride. The TSC peak of the film A_5 prepared from 0.28 M cadmium chloride and 0.20 M thiourea shows a decrease in magnitude. This may be due to the low donor concentration in the films. It is thus clear that both annealing temperature and cadmium content play an important role in the origin of the traps found in the CdS films [14].

8.4 CONCLUSION

The ITC spectra obtained for the CdS films show a prominent peak at 363 K. The peak is formed due to the formation of (I-V) dipoles. The peak height is found to vary linearly with poling field, poling temperature and poling time. Ionic thermocurrent of annealed films is found to be lower than that of unannealed films. The activation energy values obtained for unannealed and annealed films show a slight variation in their magnitudes. The increase in activation energy values with increase in concentration of cadmium chloride is characterized by the higher content of chlorine ions trapped in the films.

The temperature corresponding to the TSC peaks depends on the cadmium contents in the film. The peak height increases with biasing field and excitation time. The trap levels are identified from the TSC analysis and their origin is discussed. From the results obtained, it can be ascertained that TSC technique is a powerful method for the determination of traps in semiconducting materials.

8.5 REFERENCES

[1] J.E. Strutt and E. Lilley, Phys. Stat. Sol. (a) 33 (1976) 229.

[2] R. Capelletti and E. De Benedetti, Phys. Rev. 165 (1968) 981.

[3] S. Unger and M.M. Perlman, Phys. Rev. B. 10 (1974) 3692.

[4] J.S. Dryden, J. Phys. Soc. Japan, Suppl. 18 (1963) 129.

[5] G.M. Sessler, Topics in Applied Physics, Vol. 33 (Springer - Verlag, Heidelberg 1980).

[6] E. Vateva and I. Georgieva, Sov. Phys. Semicond. 8 (1974) 361.

[7] Yu. M. Shirshov, V.A. Tyagai, O.V. Snitko and V.D. Yarinovskii, Fiz. Tekh. Poluprovodnikov, 1 (1967) 1553.

[8] A.P. Trofimenko, G.A. Fedorus and M.K. Sheinkman, Fiz. Tverd. Tela. 5 (1963) 1805.

[9] K. Kirov and V. Zhelev, C.R. Acad. Bulg. Sci. 17 (1964) 989.

[10] S. Kitamura, J. Phys. Soc. Japan 15 (1960) 1697.

[11] A.G. Valyomana and C. Purushothaman (Communicated)

[12] J.Woods and K.H. Nicholas, Brit. J. Appl. Phys. 15 (1964) 1361.

[13] A.G. Valyomana, K.P. Vijayakumar and C. Purushothaman, J. Mater. Sci. Lett. 9 (1990) 1025.

[14] A.G. Valyomana and C. Purushothaman (Communicated).

9

PREPARATION OF Cu_xS THIN FILMS

9.1 INTRODUCTION

Copper sulphide (Cu_xS) is a semiconducting compound belonging to I-VI group. Investigations of Cu_xS have stimulated continuous interest both because of its variety of properties [1-7] and because of the many applications in semiconducting devices [8-15]. Cu_xS in the bulk form is known to exist in different stable phases at room temperature [16]. The distinct room-temperature phases are the orthorhombic chalcocite (x=1.995-2.000), djurleite (x=1.93-1.96) and digenite (x= 1.765 - 1.79). The characterization of orthorhombic chalcocite Cu_2S have been studied by several authors [17-22]. The studies on the tetragonal phase have also been reported [23, 24]. Janosi [25] has investigated the structure of Cu_2S and reported that it had a tetragonal unit cell.

Cu_xS as a material, particularly in thin film form has received particular attention since the discovery in 1954 by Reynolds et al.[26] The preparation of Cu_xS films by vacuum evaporation technique have been reported by several authors [27 - 31]. Arjona et al. [29] prepared polycrystalline thin films of Cu_xS by vacuum evap ration and carried out the structure identification and optical properties. Couve et al [30] have also fabricated Cu_xS layers by vacuum evaporation technique and done the measurements on the resistivities and optical transmission of the layers. The methods of characterization of evaporated layers of Cu_xS have also been described by Rezig et al. [31]. Bretzner and Martinuzzi [32] have prepared Cu_2S

films by flash deposition method and determined the spectral variations of the absorption coefficient. The coexistence of direct and indirect transitions had been confirmed, for which the width vlues of the prohibited band were 1.7 and 1.05 eV respectively. Reports on the preparation of thin films of Cu_xS by the activated reactive evaporation were also found in the literature [33]. A few works were also reported on these films prepared by the sputtering methods [34-39]. Engelken and Mc Cloud [40] have electrodeposited thin films of $Cu_{2-x}S$ and $Cu_{1+x}S$ at temperatures from 21° to 120°C and studied the material characterization by X-ray diffraction. The films were grown on a variety of substrates including indium tin oxide, tin coated glasses, graphite etc. The formation of Cu_2S thin films by an electrochemical procedure was reported by Garcia - Camarero et al.[41] The deposition of Cu_xS films by spray pyrolysis method were also reported [42]. But only a few reports were seen on the preparation of Cu_xS films by the chemical bath deposition technique[43,44].

In this chapter the preparation of Cu_xS thin films by chemical bath deposition technique and annealing are described. The X-ray analysis of the films and the examination of surface features by an optical microscope have been investigated. The results of absorption spectrum recorded and the differential scanning calorimetric studies performed in these films are also included.

9.2 EXPERIMENTAL

During the present investigation, chemical bath deposition method was employed for the deposition of Cu_xS films. A chemical bath was constituted from 0.5 M solution of copper chloride, 10 ml triethanolamine, 25% ammonia solution and 1 M solution of thiourea and distilled water. The deposition process consists of the following steps. 10 ml of triethanolamine was added to 10 ml 0.5 M copper chloride in a pre-cleaned beaker. This will promote the formation of a pale blue precipitate. This precipitate is completely dissolved by the addition of 10 ml of ammonia and the solution becomes deep blue in colour. 10 ml 1M thiourea was added to the resultant solution and then maintained at room temperature without stirring. Later the precleaned ordinary glass slides (7.5 x 1.2 cm) were dipped carefully in the solution. After a deposition time of about 2½ h, the slides were taken out, rinsed with distilled water and dried. The films obtained were uniform, smooth and possess good adhesion to the substrate. Inorder to study the dependence of electrical characteristics on copper and sulphur contents, films were prepared by changing the volume of copper chloride and thiourea solution. The film obtained from the bath constituting 10 ml 0.5M copper chloride, 10ml triethanolamine, 10ml ammonia and 10ml 1M thiourea is referred to as B_1. Similar representation was made for all other films [Table 9.1]. The freshly prepared films are annealed by using a vacuum chamber as described in Chapter 4.

Table 9.1 Designation of Cu_xS Films prepared using different bath compositions

Sample	Bath composition
B_1	10ml 0.5 M Copper Chloride, 10ml triethanolamine, 10ml ammonia, 10ml 1M thiourea.
B_2	30ml 0.5M Copper Chloride, 10ml triethanolamine, 10ml ammonia, 10ml 1 M thiourea
B_3	50ml 0.5 M Copper Chloride, 10ml triethanolamine, 10ml ammonia, 10ml 1M thiourea.
B_4	70ml 0.5 M Copper chloride, 10ml triethanolamine, 10ml ammonia, 10ml 1M thiourea
B_5	90ml 0.5 M Copper chloride, 10ml triethanolamine, 10ml ammonia, 10ml 1 M thiourea
B_6	10ml 0.5 M Copper chloride, 10ml triethanolamine, 10ml ammonia, 30ml 1 M thiourea.
B_7	10ml 0.5 M Copper chloride, 10ml triethanolamine, 10ml ammonia, 50ml 1 M thiourea
B_8	10ml 0.5 M Copper chloride, 10ml triethanolamine, 10ml ammonia, 70ml 1 M thiourea
B_9	10ml 0.5 M Copper chloride, 10ml triethanolamine, 10ml ammonia, 90ml 1 M thiourea.

The surfaces of the films were observed using a Union Versamet-2 metallographic microscope. X-ray diffraction patterns were recorded by means of an X-ray diffractometer with CuKα radiation. The absorption spectrum of films was taken in the wavelength range 400 -1500nm by means of a U-3410 Hitachi spectrophotometer. Differential scanning calorimetric data have been taken on the film at a scanning rate of 5°C/min during heating using a Perkin - Elmer Delta Series Differential Scanning Calorimeter (model DSC-7).

9.3 RESULTS AND DISCUSSION

The films under vacuum annealing for different temperatures prevent structural degradation and remains stable. But annealing of the films in air at higher temperatures produce surface roughness. In Fig. 9.1, the microscopic view of the film annealed at 473K is shown, where the cracks developed are clearly seen. No such pattern is observed for the films annealed in vacuum under similar conditions. Hence in the present study, vacuum annealing is preferred than air annealing of the films. The X-ray diffraction pattern of the film is shown in Fig 9.2. The results obtained are found to be in good agreement with that reported in the literature for djurleite phase [45]. Fig. 9.3 shows the absorption spectrum of the film. The band gap of the film evaluated from this spectrum is about 1.796 eV. The observed value of the band gap is typical of djurleite phase [46]. The DSC spectra recorded for the films in the temperature range 80°C to 120°C with a scanning rate of 5°C/min are

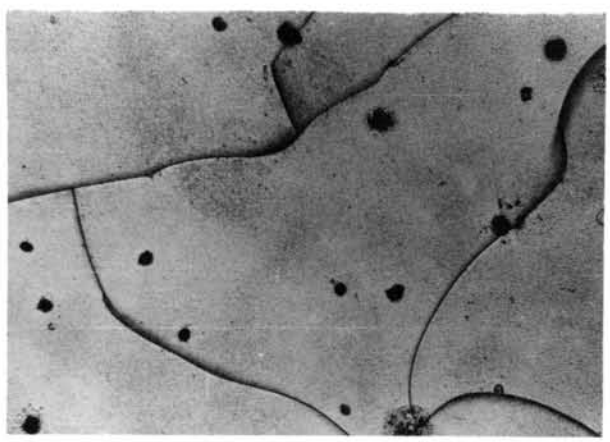

Fig. 9.1: Photograph showing the surface of the film annealed in air at 473 K. (X100)

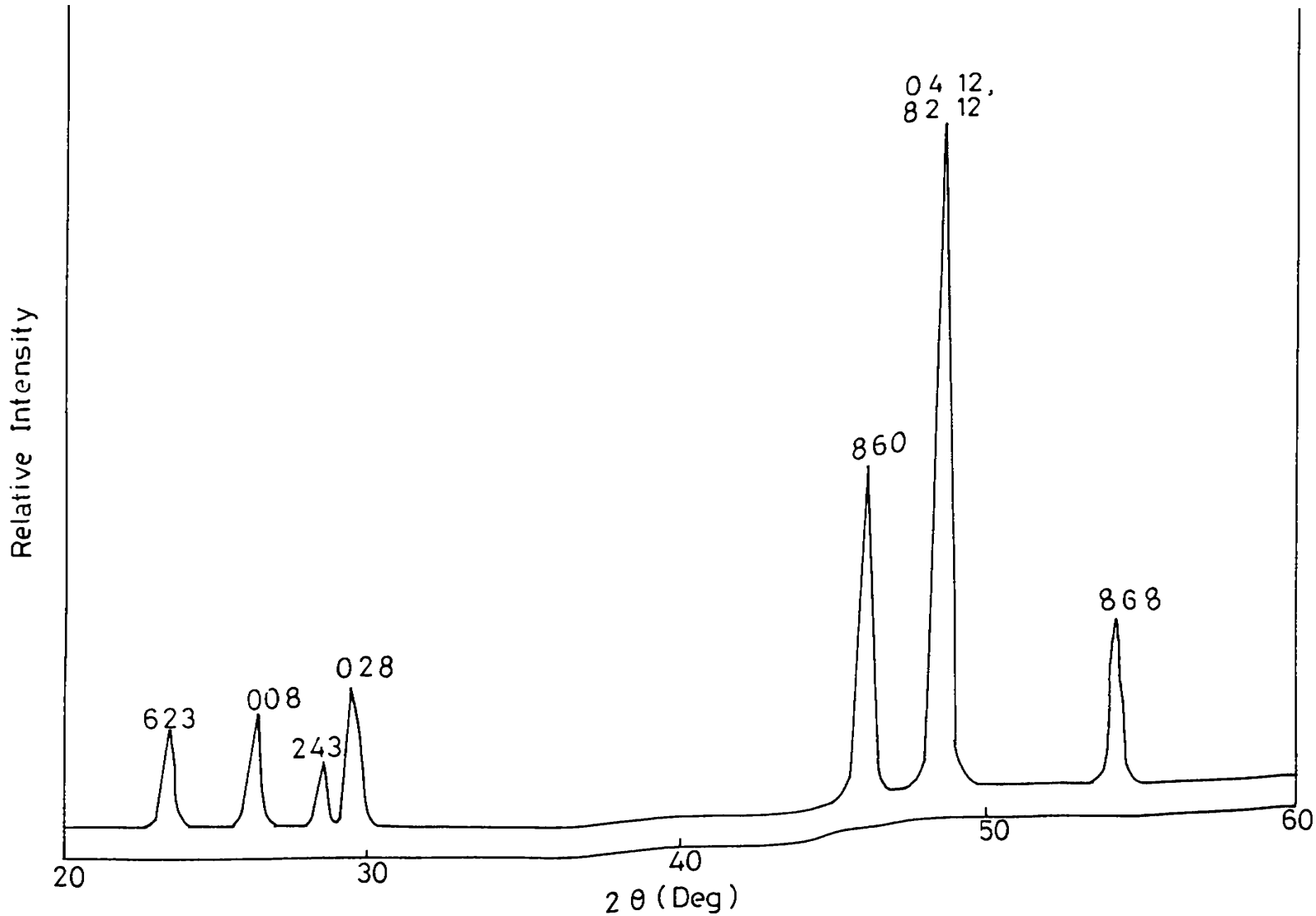

Fig. 9.2: X-ray diffraction pattern of the film.

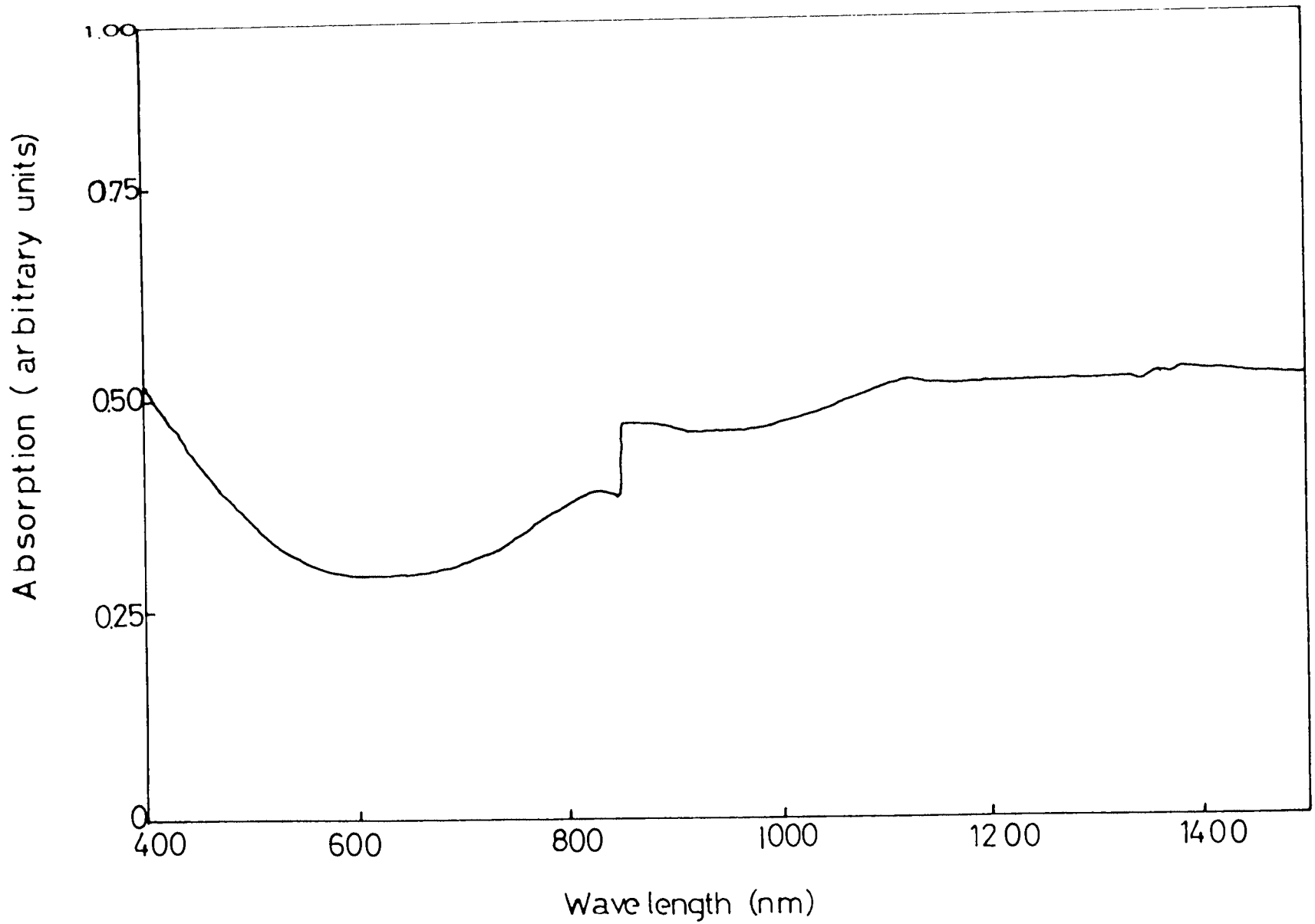

Fig. 9.3: Absorption spectrum of the film.

depicted in Figs. 9.4 to 9.6 . A variation in the heat flow indicative of the occurence of phase transition in Cu_xS films is observed in all cases. The phase transition temperature determined from the DSC spectra of the films B_1, B_5 and B_9 are 102.125°C, 102.292°C and 97.125°C respectively.

9.4 CONCLUSION

Cu_xS thin films were prepared by the chemical bath deposition technique using different volume compositions of copper chloride and thiourea. The surfaces of the films annealed in air are not smooth. X-ray diffraction studies are used to identify the prominent lines in the film. The band gap evaluated from the absorption spectrum is 1.796 eV. From these analysis, it is found that the prepared film corr-esponds to the djurleite phase. The occurence of phase transition was studied from the DSC analysis.

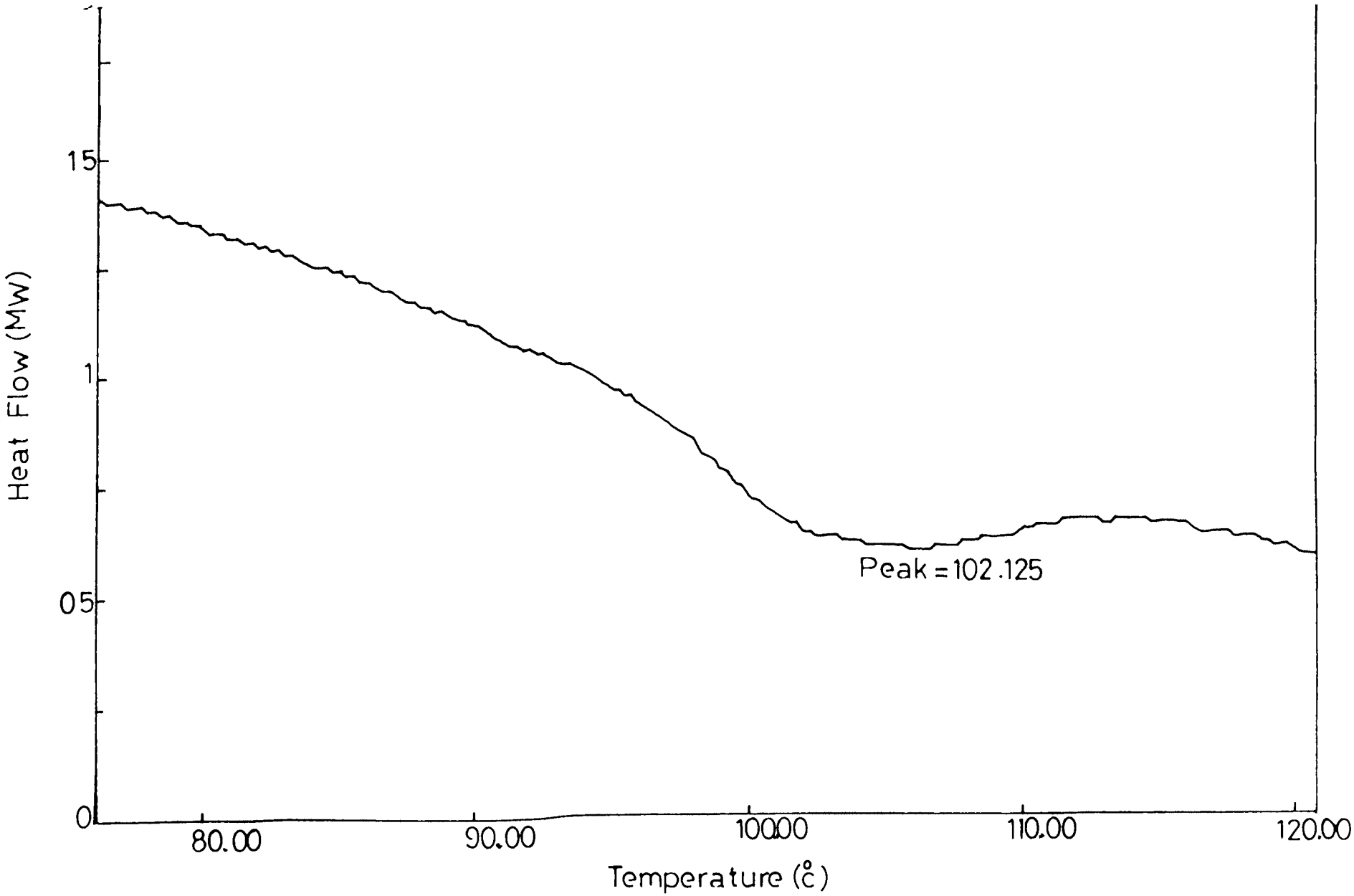

Fig. 9.4: DSC spectrum of the film B_1.

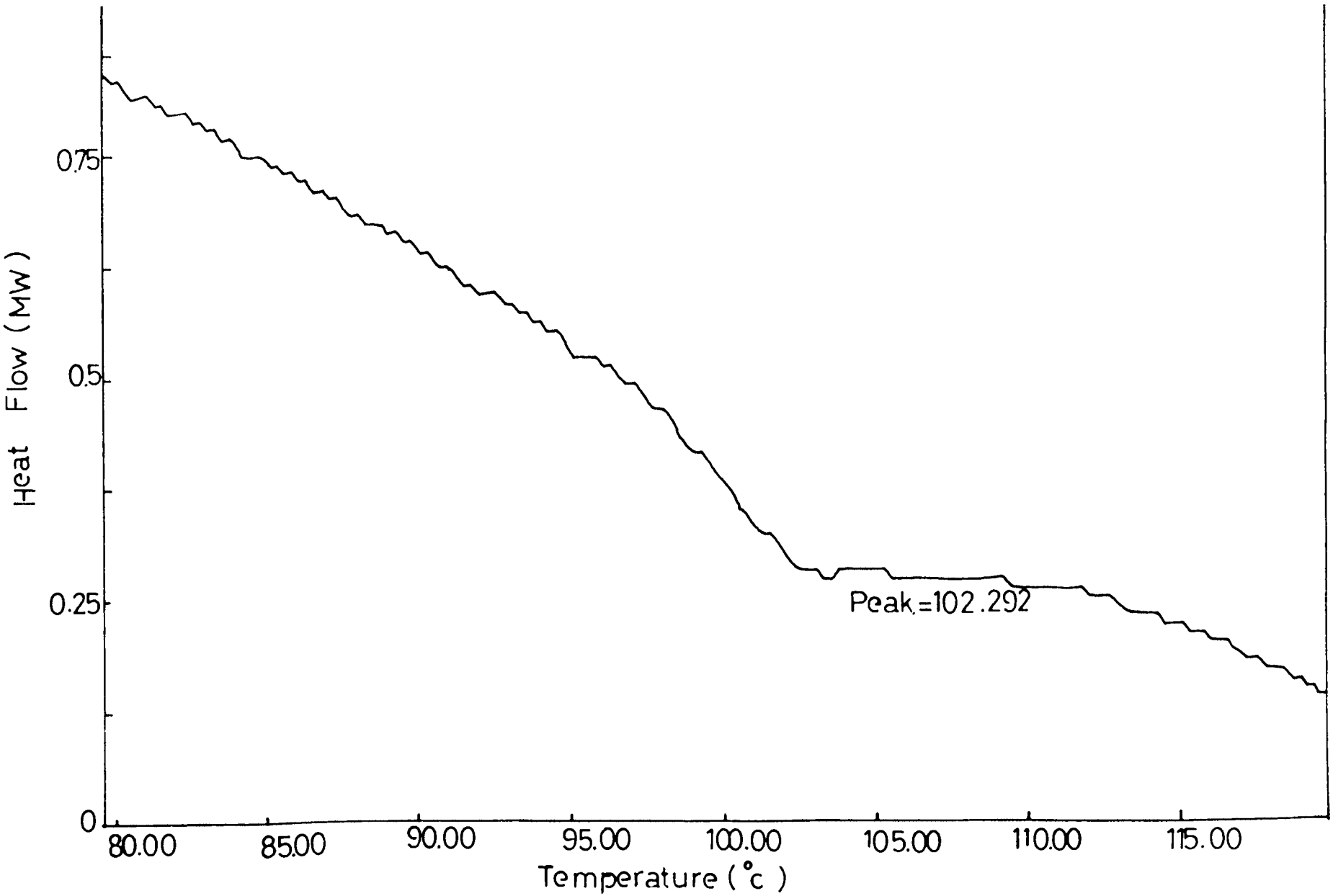

Fig. 9.5: DSC spectrum of the film B_5.

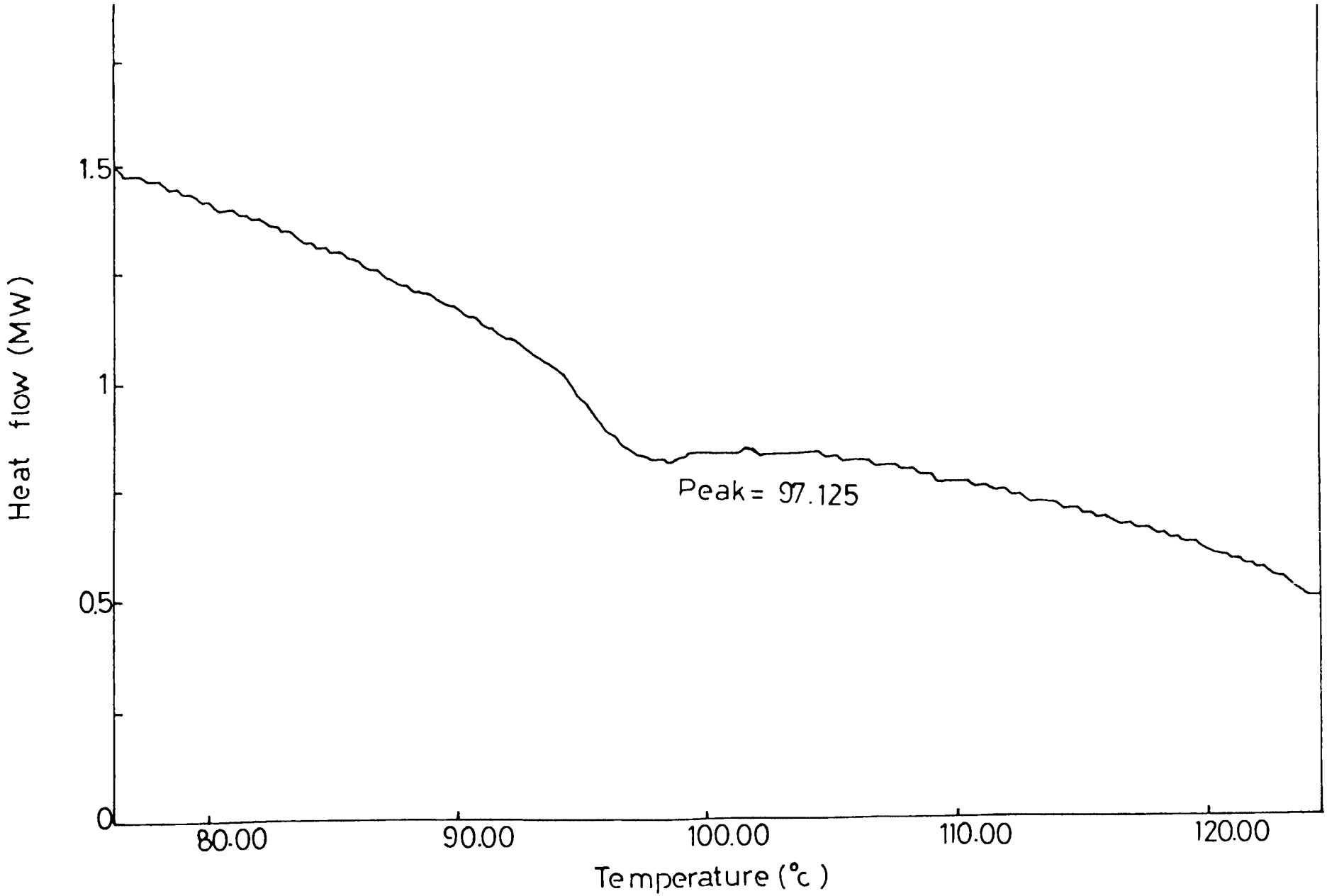

Fig. 9.6: DSC spectrum of the film B_9.

9.5 REFERENCES

[1] E. Hirahara, J.Phys. Soc. Japan. 2 (1947) 211.

[2] N. Nakayama, J. Phys. Soc. Japan 25 (1968) 290

[3] R. Marshall and S.S. Mitra, J. Appl. Phys. 36 (1965) 3882.

[4] M. Reinhold and H. Mohrung, Z. Phys. Chem. B 38 (1938) 221

[5] E. Hirahara, J. Phys. Soc. Japan. 6 (1951) 422

[6] S. Miyatani and Y. Suzuki, J.Phys.Soc.Japan 8 (1953) 660.

[7] K. Okamoto, Jpn. J. Appl Phys. 8 (1969) 718

[8] K.W. Boer, Phys. Stat. Solidi (a) 40 (1977) 355.

[9] G.H. Hewig, F. Pfisterer, H.W. Schock, W. Arndt and W.L.Bloss, Proc. 16th IEEE Photovoltaic Specialists Conf. New York, 1982 P. 713.

[10] F. Pfisterer and W.L. Bloss, Sol. Cells 12 (1984) 155.

[11] N. Nakayama, A. Gyobu and N. Morimoto, Jpn. J. Appl. Phys. 10 (1971) 1415

[12] W. Palz, J. Besson, T. Nguyen Duy and J. Vedel, Proc. 9th IEEE photovoltaic Specialist Conf, New York, 1972, P.91

[13] R.J. Mytton, Brit. J. Appl. Phys (J. Phys D) 1 (1968) 721

[14] S. Martinuzzi, Sol. Cells. 5 (1982) 243.

[15] L.D. Partain, P.S. McLeod, J.A. Duisman, T.M. Peterson, D.E. Sawyer and C.S. Dean, J.Appl. Phys. 54 (1983) 6708

[16] M. Savelli and J. Bougnot, Topics in Applied Physics, ed. B.O. Seraphin, Vol. 31, (Springer, Berlin, 1979) P.213

[17] M. Savelli and J. Bougnot, Topics. Appl. Phys. 31 (1979) 213

[18] W. Palz, J. Besson, N. Duy and J. Vedel, Proc. 10th IEEE Photovoltaic Specialists Conf., New York, 1973.

[19] T.S. De Velde and J. Dieleman, Philips Res. Rep.. 28 (1973) 573.

[20] T.S. De Velde and J. Dieleman, Philips Res. Rep. 28 (1973) 573.

[21] B.J. Moulder, Krist. Tech. 8 (1973) 825.

[22] M.J. Burger and W. Wunsch. Science 141 (1963) 276

[23] J.G. Vaissier and F.M. Roche, Mater Res. Bull. 11 (1976) 851.

[24] S. Djurle, Acta. Chem. Scand. 12 (1958) 1415

[25] A. Janosi, Acta. Cryst. 17 (1964) 311

[26] D.C. Reynolds, G. Leies, L.T. Antes and R.E. Marburger, Phys. Rev. 96 (1954) 533.

[27] B. Selle and J. Maege, Phys. Stat. Solidi. 30 (1968) K 153.

[28] H. Nimura, A. Atoda and T. Nakau, Jpn. J.Appl. Phys. 16 (1977) 403

[29] F. Arjona, E. Elizalde, E. Garcia - Camerero, A. Feu, B. Lacal, M. Leon, J. Llabres and F. Rueda, Sol. Energy. Mater. 1 (1979) 379.

[30] S. Couve, L. Gouskov, L. Szepessy, J. Vedel and E.Castel, Thin Solid Films 15 (1973) 223.

[31] B. Rezig, S. Duchemin and F. Guastavino, Sol. Energy. Mater. 2 (1979) 53

[32] J.F. Bretzner and S. Martinuzzi, C.R. Acad. Sci. B. 268 (1969) 1097.

[33] H.S. Randhawa, R.F. Bunshah, D.G. Brock, B.M. Basol and O.M. Statfsudd, Sol. Energy Mater. 6 (1982) 445

[34] E. Iborra, J. Santamaria, I. Martil, G. Gonzalez and F. Sanchez. Quesada, Vacuum. 37 (1987) 437.

[35] K. Radler, H. Frey, W. Muller, K.H. Schuller and J.Von Wienskowski, Thin solid films 59 (1979) 13

[36] E. Vanhoecke and M. Burgelman, Thin Solid Films 112 (1984) 97.

[37] J.A. Thornton, D.G. Cornog, W.W. Anderson, R.B. Halt and J.E. Phillips, Proc. 16th IEEE Photovoltaic Specialists Conf., New York, 1982. P. 737.

[38] A.D. Jonath, W.W. Anderson, J.A. Thornton and D.G. Cornog, J. Vac. Sci. Technol. 16 (1979) 200.

[39] G.A. Armantrout, D.E. Miller, K.E. Vindelev and T.G. Brown, J. Vac.Sci. Technol. 16 (1979) 212

[40] R.D. Engelken and H.E. Mc Cloud, J. Electrochem. Soc. 132 (1985) 567.

[41] E. Garcia - Camarero, F. Arjona, M. Leon and M.J. Nunez, J. Mater - Sci. 21 (1986) 4169.

[42] J.F. Jordan, Proc. 13th IEEE Photovoltaic Specialists Conf., New York, 1975, P. 508.

[43] R.N. Bhattacharya and P. Pramanik, Bull Mater Sci. 3 (1981) 403.

[44] P.K. Nair, M.T.S. Nair and J. Campos, Proc. SPIE, 823 (1987) 256.

[45] JCPDS: International Centre for Diffraction Data, USA,1978

[46] P.Massicot, Phys. Stat.Solidi (a) 11 (1971) 535

10

ELECTRICAL CONDUCTIVITY STUDIES OF Cu_xS THIN FILMS

10.1 INTRODUCTION

Electrical properties of copper sulphide (Cu_xS) films deposited by various techniques have been studied by many authors [1-5] Garcia - Camarero [6] prepared Cu_xS films on copper substrates by an electrochemical procedure and studied their electrical characteristics. The conductivity of these films has marked influence on various factors such as copper and sulphur contents , annealing temperature, ambient conditions etc. But no results on the conductivity of chemically bath deposited Cu_xS films have been reported related to the phase transition at higher temperatures.

This chapter deals with the electrical conductivity studies of chemically bath deposited Cu_xS films. Special attention has been given to analyse the dependence of copper and sulphur contents, annealing temperature and ambient conditions on the values of conductivity of these films. The anomalous behaviour of conductivity at high temperature has been explained with the results obtained from the differential scanning calorimetric studies. The values of activation energy have been evaluated and are reported here.

10.2 EXPERIMENTAL

Cu_xS films B_1 to B_9 used in the present investigations were prepared by chemical bath deposition technique using copper chloride, triethanolamine, ammonia and thiourea. The description of the sample designation is already presented in Table 9.1, Chapter 9.The samples were annealed in vacuum in the temperature range 373 - 573K

for 30 min. Thin silver electrodes were deposited on the surface of these films using vacuum evaporation technique at a pressure of 10^{-5} Torr. Details of the metallic cell, sample holder and temperature measurement have been described in Chapter 4. For electrical conductivity measurements, a voltage of 9V from a battery was applied across the film kept under vacuum conditions and the resulting current was measured . The experiment was also carried out in an air ambient. During the measurements, sufficient time was given for the current reading to stabilize and very reproducible results could be obtained on all the films studied. The activation energy for the hole conduction was also estimated.

10.3 RESULTS AND DISCUSSION

Electrical conductivity measurements as a function of temperature were monitored in vacuum and air on a number of films. Copper and sulphur contents in the films play an important role in determining the values of conductivity. Since these films exhibit phase transition, the present study has also been used to reveal this aspect.

Fig. 10.1 shows the variation of the conductivity in vacuum as a function of $10^3/T$ for the film B_1 prepared from 10ml 0.5M copper chloride, 10ml triethanolamine, 10ml ammonia and 10ml 1M thiourea. The measurements carried out on films B_2 to B_9 containing different copper and sulphur contents also show similar trends. As can be seen from the above figure, the conductivity tends to remain constant at low temperature (100-135K) and thereafter rises

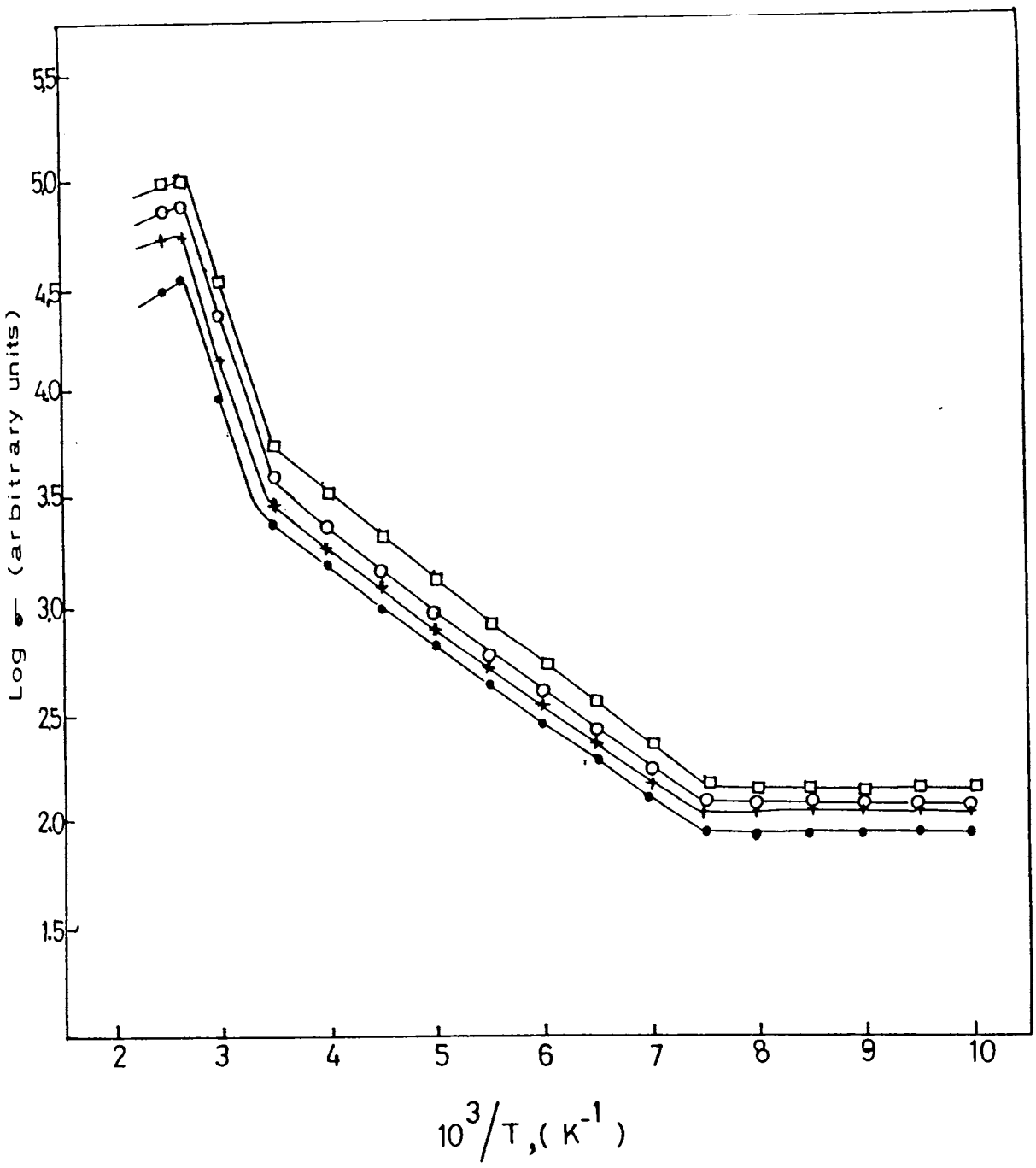

Fig 10.1 : Plot of log σ against $10^3/T$ for the film B_1 in vacuum: (•) unannealed and annealed at (+) 373 K, (o) 473 K and (□) 573 K.

slowly in the temperature range 135 - 303K. The film B_1 exhibits an exponential increase in conductivity upto 375K and after wards decreases very gradually. In copper sulphide films, the P-type conductivity is due to the presence of copper vacancies which act as acceptors and give rise to free holes. Thus the process of conduction in the present case is predominantly hole conduction. The hole density increases very slowly with the temperature upto 303K, then it increases rapidly and decreases above 375K. For temperatures upto 375K, ionization of acceptor states causes conductivity to increase. But the electrical conductivity shows an anomalous change at 375K. This is due to the fact that the films undergo phase transition at high temperatures. This was confirmed from the DSC spectrum of the film B_1 (Fig.9.4, Chapter 9).

The values of activation energy deduced from the conductivity measurements of the films are given in Table 10.1. Since the increase in conductivity with temperature is determined mainly from the corresponding change in the hole concentration, the values presented in this table correspond to the activation energy of acceptor levels. The values of activation energy obtained for the film B_6 annealed at 373K are consistent with that reported in the literature [5,7].

The electrical properties of the films are found to vary with change in copper and sulphur contents. Figs. 10.2 (a) to 10.2 (d) show the conduction characteristics in vacuum of the films B_1 to B_5 prepared from different volume compositions of copper chloride. The result is found to be similar for all measurements at 135, 303, 343 and 370K. The conductivity is found to be high for the film B_1. The decrease in conductivity for the films B_2 to B_5 is caused probably by the increase of excess

Table 10.1 The values of activation energy obtained from the conductivity measurements of the films in vacuum.

Sample	Activation energy in the temperature range at 135-294K (eV)	303-370K (eV)
B_1		
Unannealed	0.070	0.347
Annealed (373K)	0.072	0.339
Annealed (473K)	0.074	0.364
Annealed (573K)	0.078	0.330
B_2		
Unannealed	0.062	0.306
Annealed (373K)	0.061	0.314
Annealed (473K)	0.064	0.364
Annealed (573K)	0.063	0.365
B_3		
Unannealed	0.064	0.314
Annealed (373K)	0.065	0.330
Annealed (473K)	0.063	0.331
Annealed (573K)	0.066	0.397

Contd....

Contd... Table 10.1

Sample	Activation energy in the temperature range at 135-294K (eV)	303-370K (eV)
B_4		
Unannealed	0.055	0.322
Annealed (373K)	0.052	0.347
Annealed (473K)	0.054	0.339
Annealed (573K)	0.053	0.380
B_5		
Unannealed	0.052	0.330
Annealed (373K)	0.054	0.339
Annealed (473K)	0.053	0.347
Annealed (573K)	0.055	0.346
B_6		
Unannealed	0.068	0.298
Annealed (373K)	0.070	0.405
Annealed (473K)	0.073	0.364
Annealed (573K)	0.072	0.347

contd....

Contd....Table 10.1

Sample	Activation energy in the temperature range at 135-294K (eV)	303-370K (eV)
B_7		
Unannealed	0.067	0.281
Annealed (373K)	0.068	0.347
Annealed (473K)	0.069	0.322
Annealed (573K)	0.070	0.298
B_8		
Unannealed	0.069	0.273
Annealed (373K)	0.066	0.314
Annealed (473K)	0.067	0.289
Annealed (573K)	0.065	0.265
B_9		
Unannealed	0.074	0.265
Annealed (373K)	0.078	0.289
Annealed (473K)	0.077	0.248
Annealed (573K)	0.079	0.264

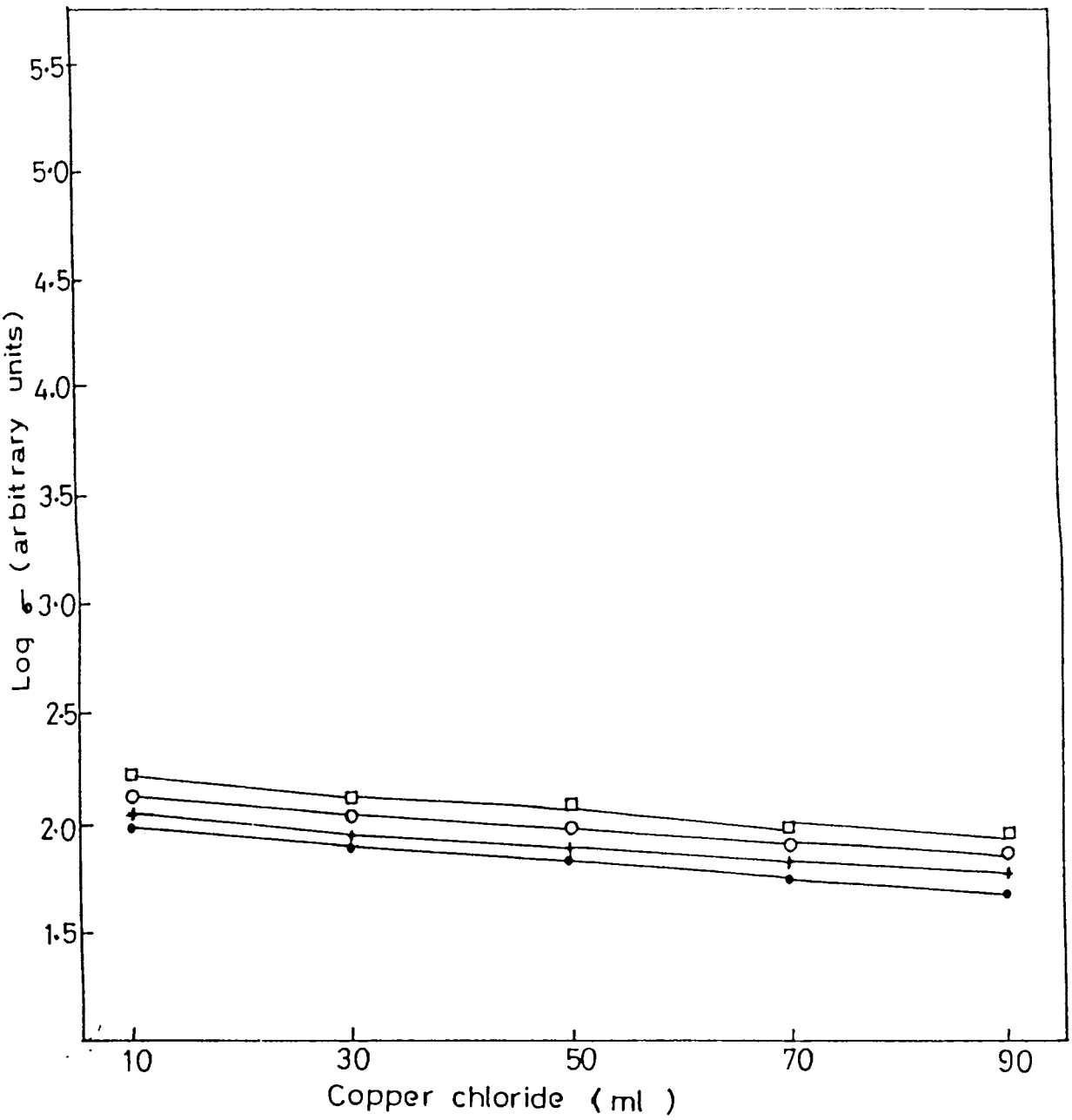

Fig 10.2 (a) : Variation of conductivity as a function of volume of copper chloride for the films in vacuum at 135 K: (•) unannealed and annealed at (+) 373 K, (o) 473 K and (□) 573 K.

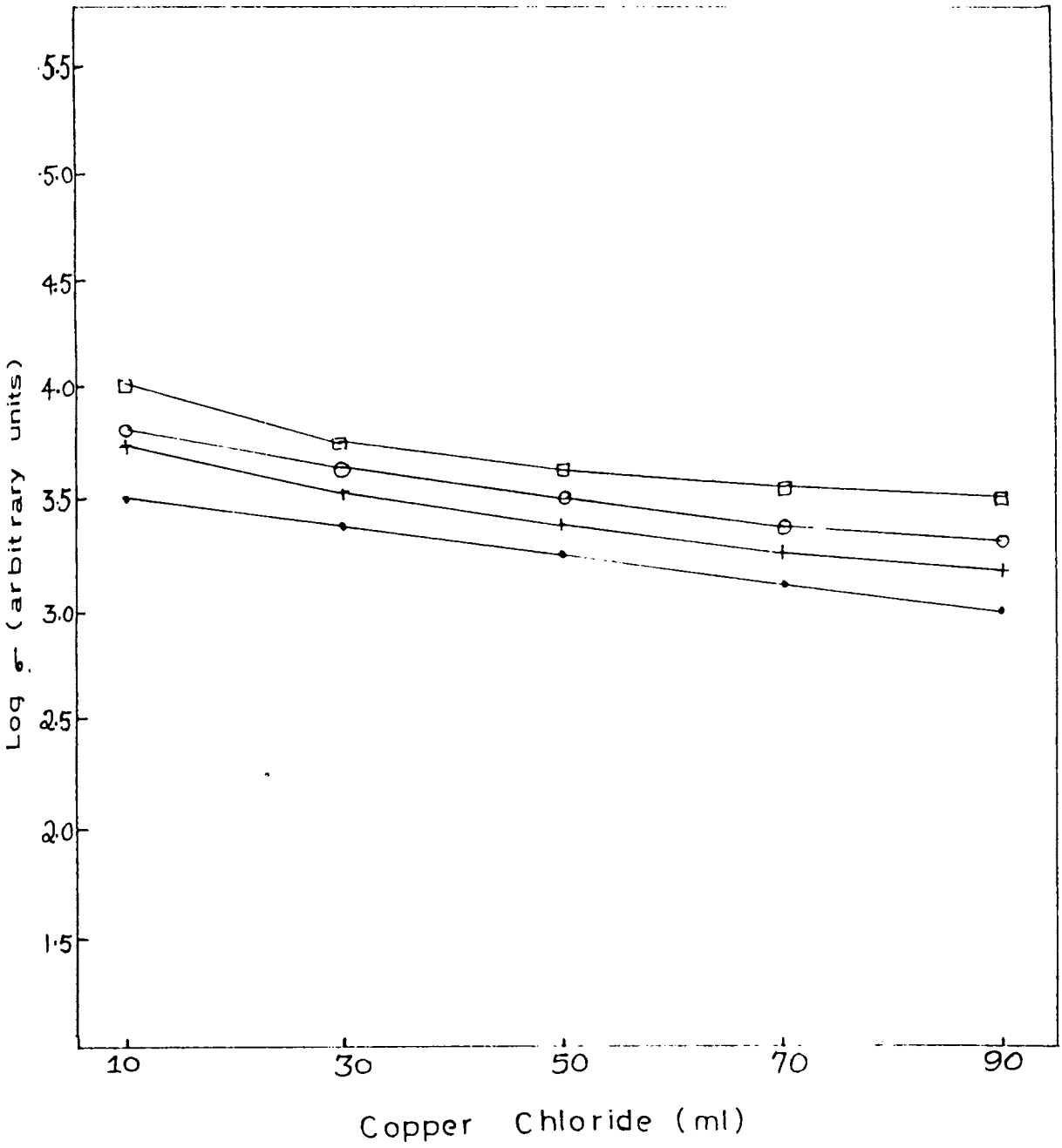

Fig 10.2 (b) : Variation of conductivity as a function of volume of copper chloride for the films in vacuum at 303 K: (•) unannealed and annealed at (+) 373 K, (o) 473 K and (□) 573 K.

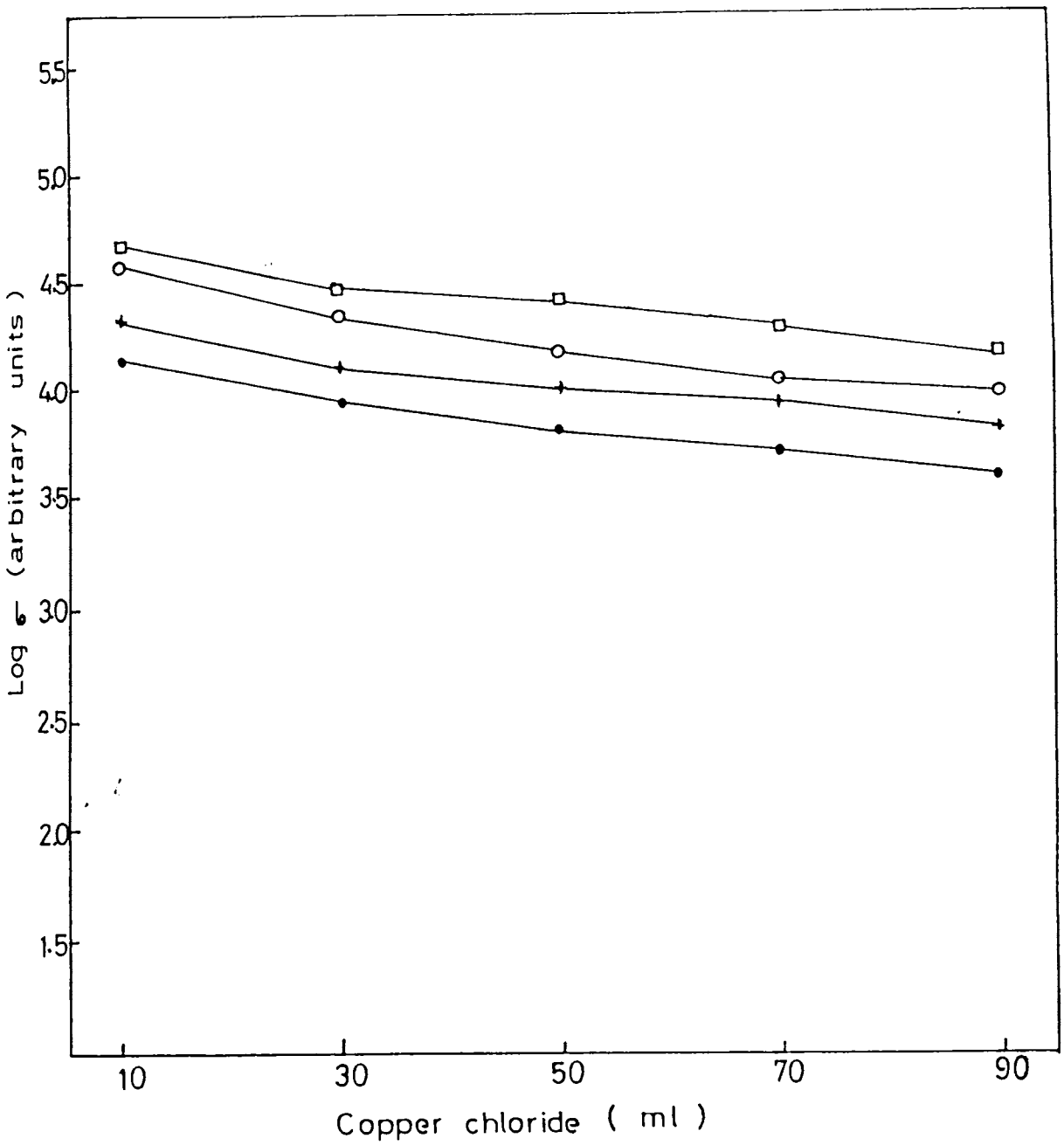

Fig 10.2 (c) : Variation of conductivity as a function of volume of copper chloride for the films in vacuum at 343 K: (•) unannealed and annealed at (+) 373 K, (o) 473 K and (□) 573 K.

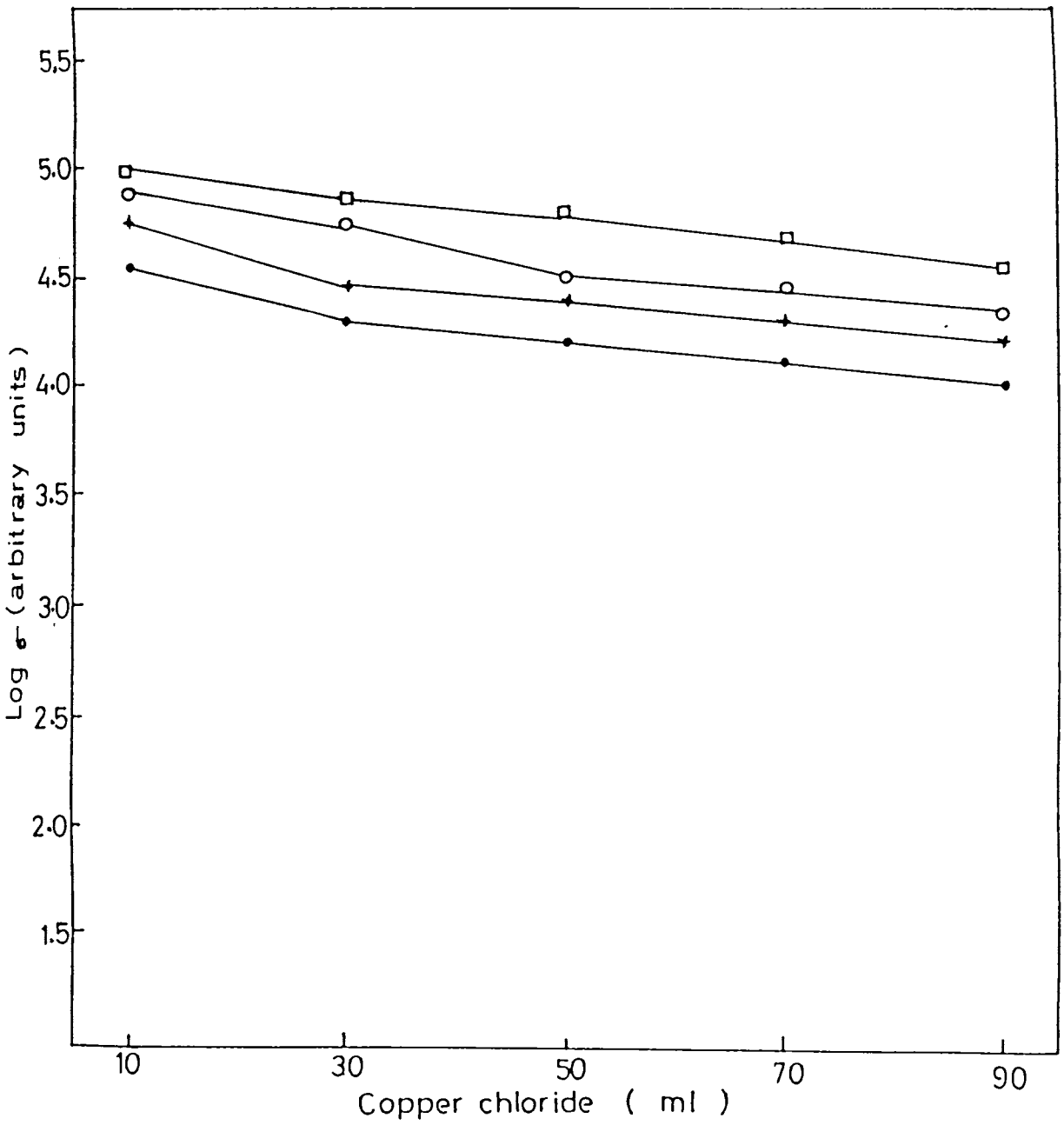

Fig 10.2 (d) : Variation of conductivity as a function of volume of copper chloride for the films in vacuum at 370 K: (•) unannealed and annealed at (+) 373 K, (o) 473 K and (□) 573 K.

: contents which decrease the number of copper vacancies in the

In the case of films prepared from different volume compositions
iourea also, the behaviour of conductivity [Figs. 10.3 (a) to
(d)] is similar for the measurements at all temperatures. A signi-
increase in conductivity is observed with increasing sulphur con-

This is caused by the increase in the carrier concentration.
results obtained are found to be in agreement with that reported
ilms prepared by physical methods [8-10]. The conductivity is
to be increased with annealing temperature. Also when the temper-
of measurements is increased from 135 to 370K, a relative rise
e value of conductivity is observed [11].

The temperature dependence of the conductivity of the films was measured in air. The result obtained for the film B_1 is shown
g. 10.4. The values of activation energy obtained from the measure-
s in air are summarized in Table 10.2. The behaviour of condu-
ty of the films B_1 to B_5 prepared from different volume compo-
ıs of copper chloride in air are shown in Figs. 10.5 (a) to 10.5(b).
result obtained for the films B_6 to B_9 prepared from different
ne compositions of thiourea are depicted in Figs.10.6 (a) to 10.6(b).
effect of annealing on the conductivity of these films is similar
ıat obtained from the measurement in vacuum.

The effect of heat treatment of the films on the conductivity
ir is compared to that in vacuum [Table 10.3]. Prolonged heating
ıe films in air leads to an increase in conductivity. Copper sulphide
s have a rigid sulphur sublattice with copper ions loosely bound

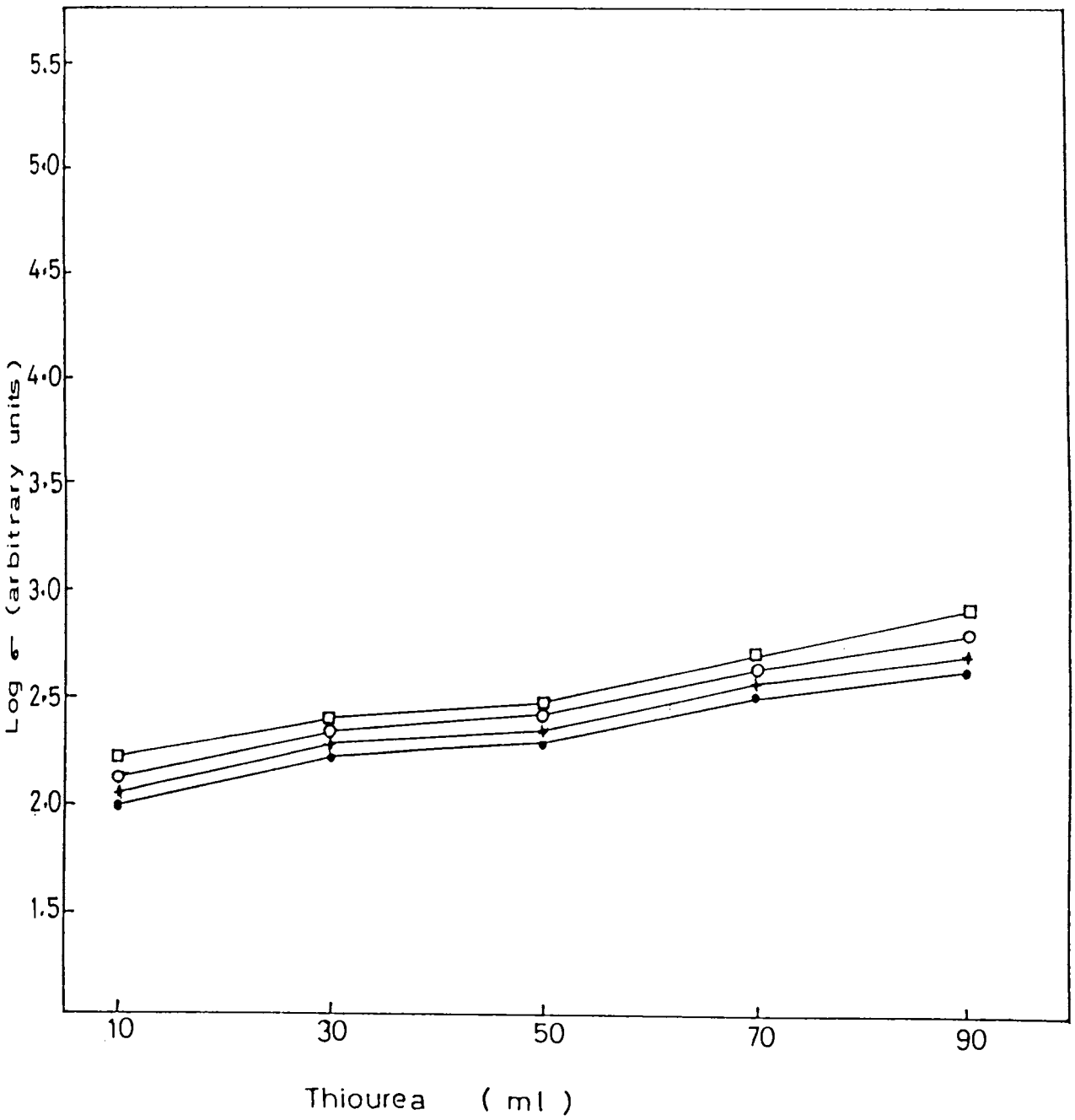

Fig 10.3 (a) : Variation of conductivity as a function of volume of thiourea for the films in vacuum at 135 K: (•) unannealed and annealed at (+) 373 K, (o) 473 K and (□) 573 K.

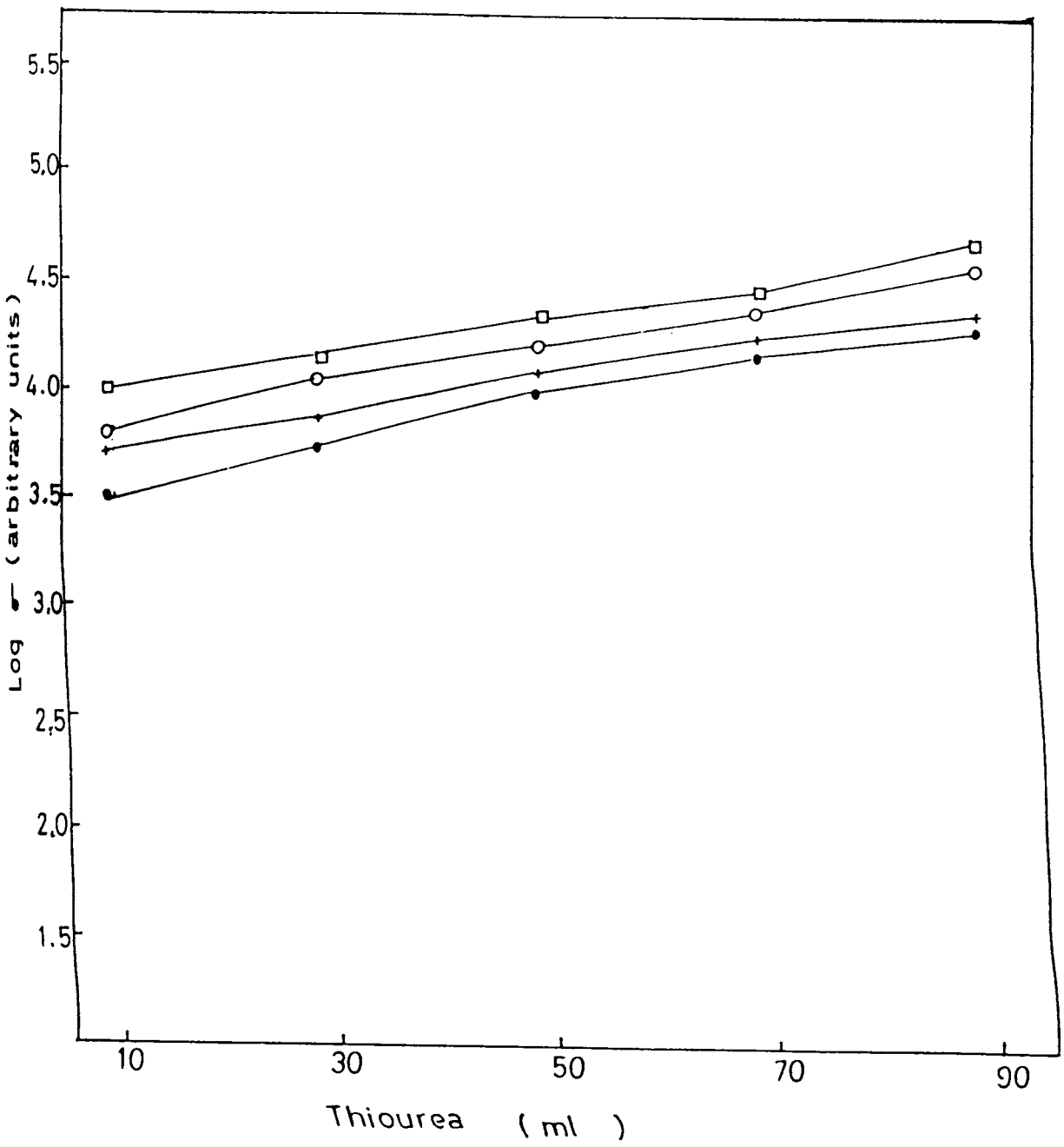

Fig 10.3 (b) : Variation of conductivity as a function of volume of thiourea for the films in vacuum at 303 K: (•) unannealed and annealed at (+) 373 K, (o) 473 K and (□) 573 K.

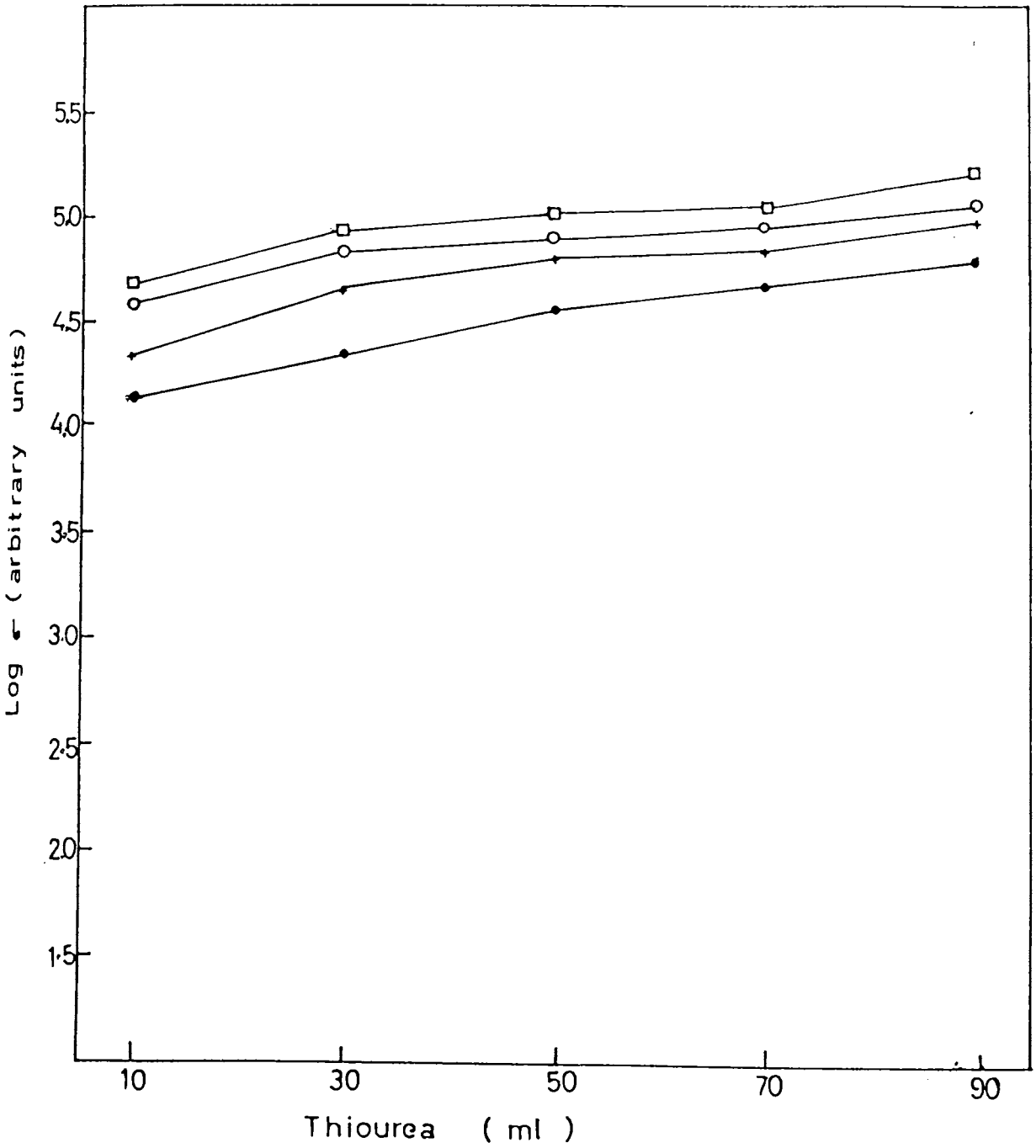

Fig 10.3 (c) : Variation of conductivity as a function of volume of thiourea for the films in vacuum at 343 K: (•) unannealed and annealed at (+) 373 K, (o) 473 K and (□) 573 K.

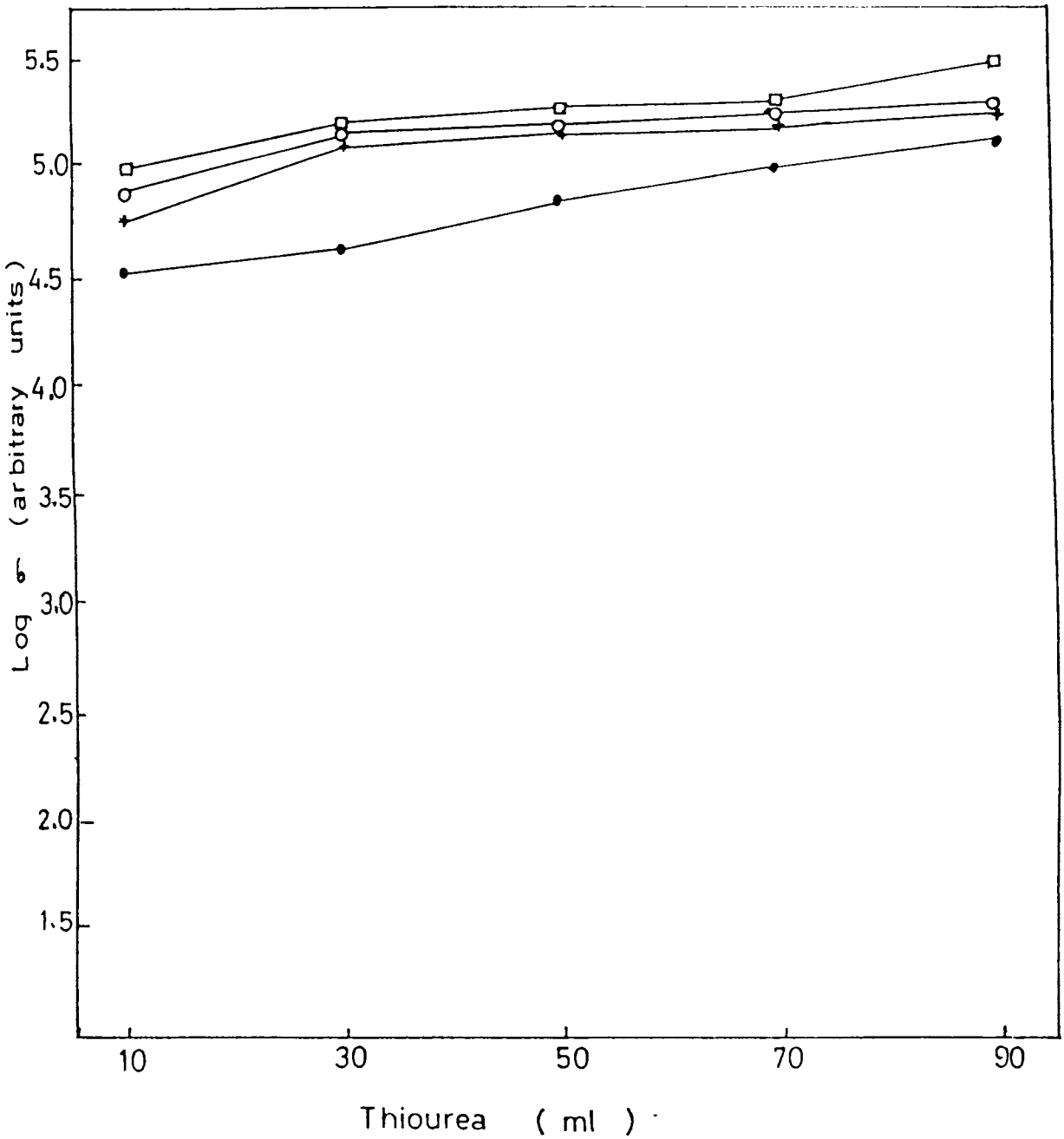

Fig 10.3 (d) : Variation of conductivity as a function of volume of thiourea for the films in vacuum at 370 K: (•) unannealed and annealed at (+) 373 K, (o) 473 K and (□) 573 K.

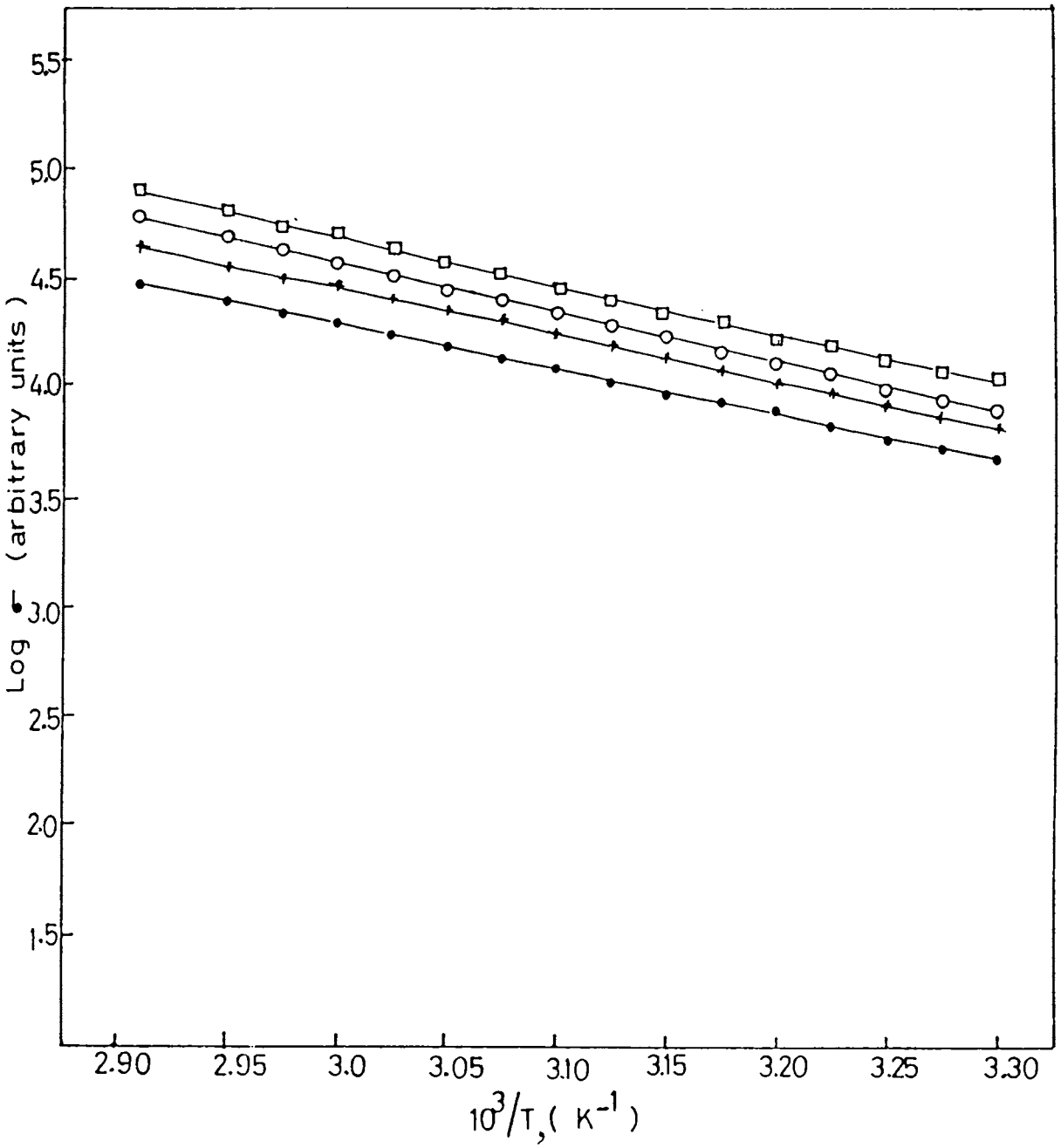

Fig 10.4 : Plot of log σ against $10^3/T$ for the film B_1 in air: (•) unannealed and annealed at (+) 373 K, (o) 473 K and (□) 573 K.

Table 10.2 The values of activation energy obtained from the conductivity measurements of the films in air.

Sample	Activation Energy in the Temperature Range at 303-343K (eV)
B_1	
Unannealed	0.394
Annealed (373K)	0.420
Annealed (473K)	0.458
Annealed (573K)	0.433
B_2	
Unannealed	0.445
Annealed (373K)	0.444
Annealed (473K)	0.446
Annealed (573K)	0.471
B_3	
Unannealed	0.470
Annealed (373K)	0.471
Annealed (473K)	0.484
Annealed (573K)	0.496

contd...

Contd...Table 10.2

Sample	Activation Energy in the temperature range at 303-343K (eV)
B_4	
Unannealed	0.496
Annealed (373K)	0.509
Annealed (473K)	0.497
Annealed (573K)	0.485
B_5	
Unannealed	0.508
Annealed (373K)	0.535
Annealed (473K)	0.509
Annealed (573K)	0.458
B_6	
Unannealed	0.407
Annealed (373K)	0.395
Annealed (473K)	0.394
Annealed (573K)	0.344

contd...

Contd...Table 10.2

Sample	Activation Energy in the temperature range at 303-343K (eV)
B_7	
Unannealed	0.369
Annealed (373K)	0.356
Annealed (473K)	0.331
Annealed (573K)	0.330
B_8	
Unannealed	0.406
Annealed (373K)	0.394
Annealed (473K)	0.382
Annealed (573K)	0.368
B_9	
Unannealed	0.408
Annealed (373K)	0.381
Annealed (473K)	0.318
Annealed (573K)	0.293

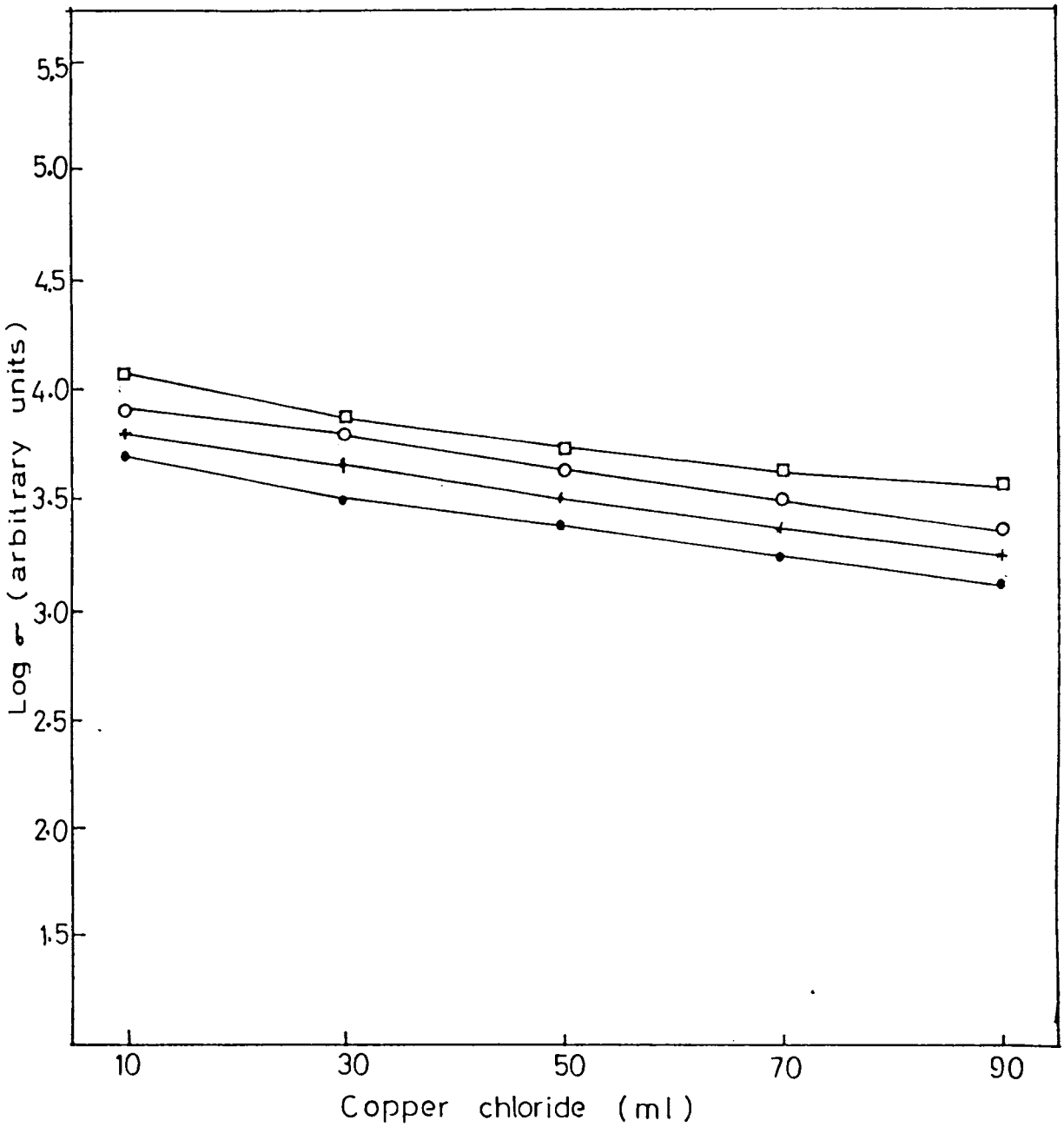

Fig 10.5 (a) : Variation of conductivity as a function of volume of copper chloride for the films in air at 303 K: (•) unannealed and annealed at (+) 373 K, (o) 473 K and (□) 573 K.

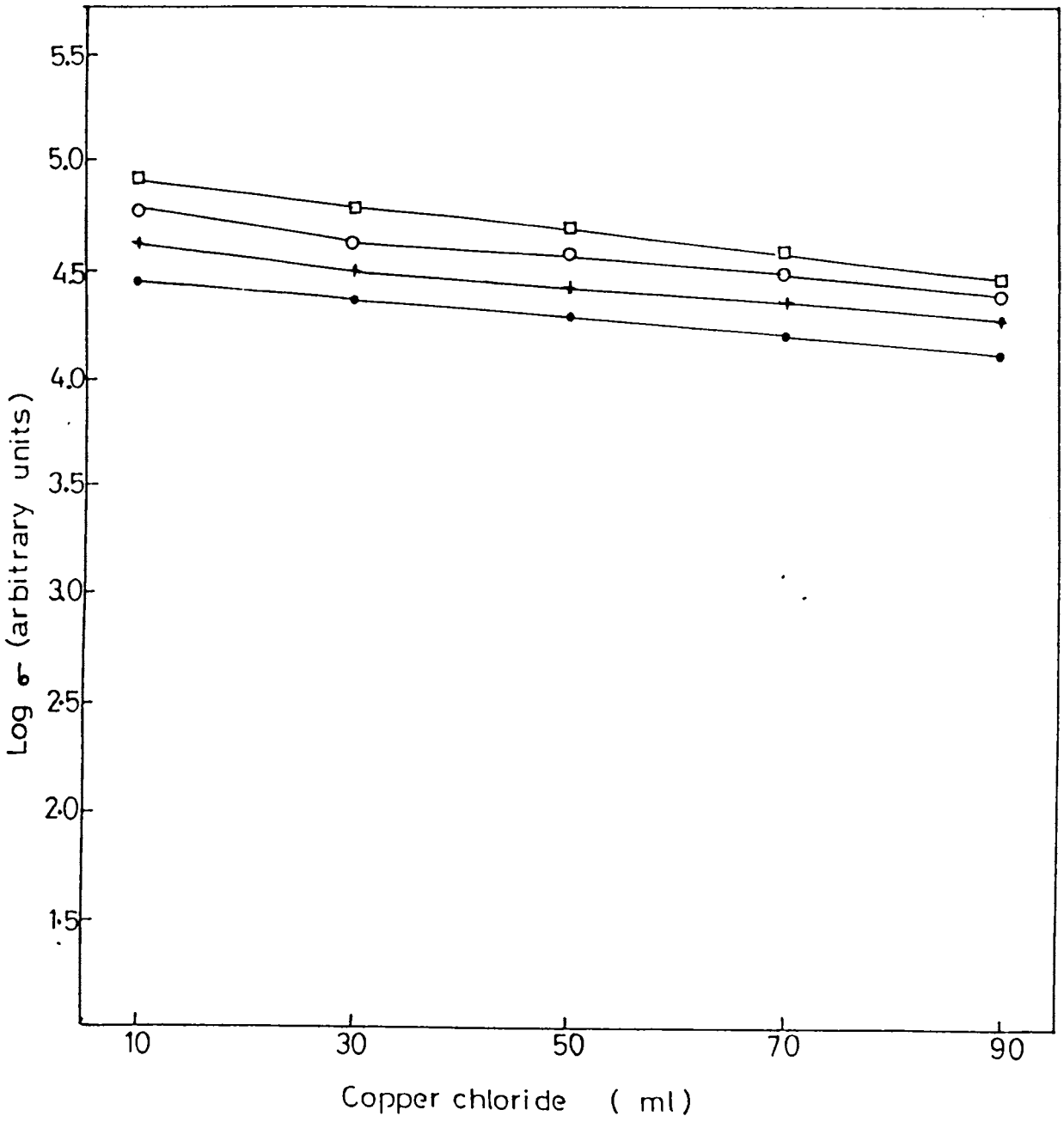

Fig 10.5 (b) : Variation of conductivity as a function of volume of copper chloride for the films in air at 343 K: (•) unannealed and annealed at (+) 373 K, (o) 473 K and (□) 573 K.

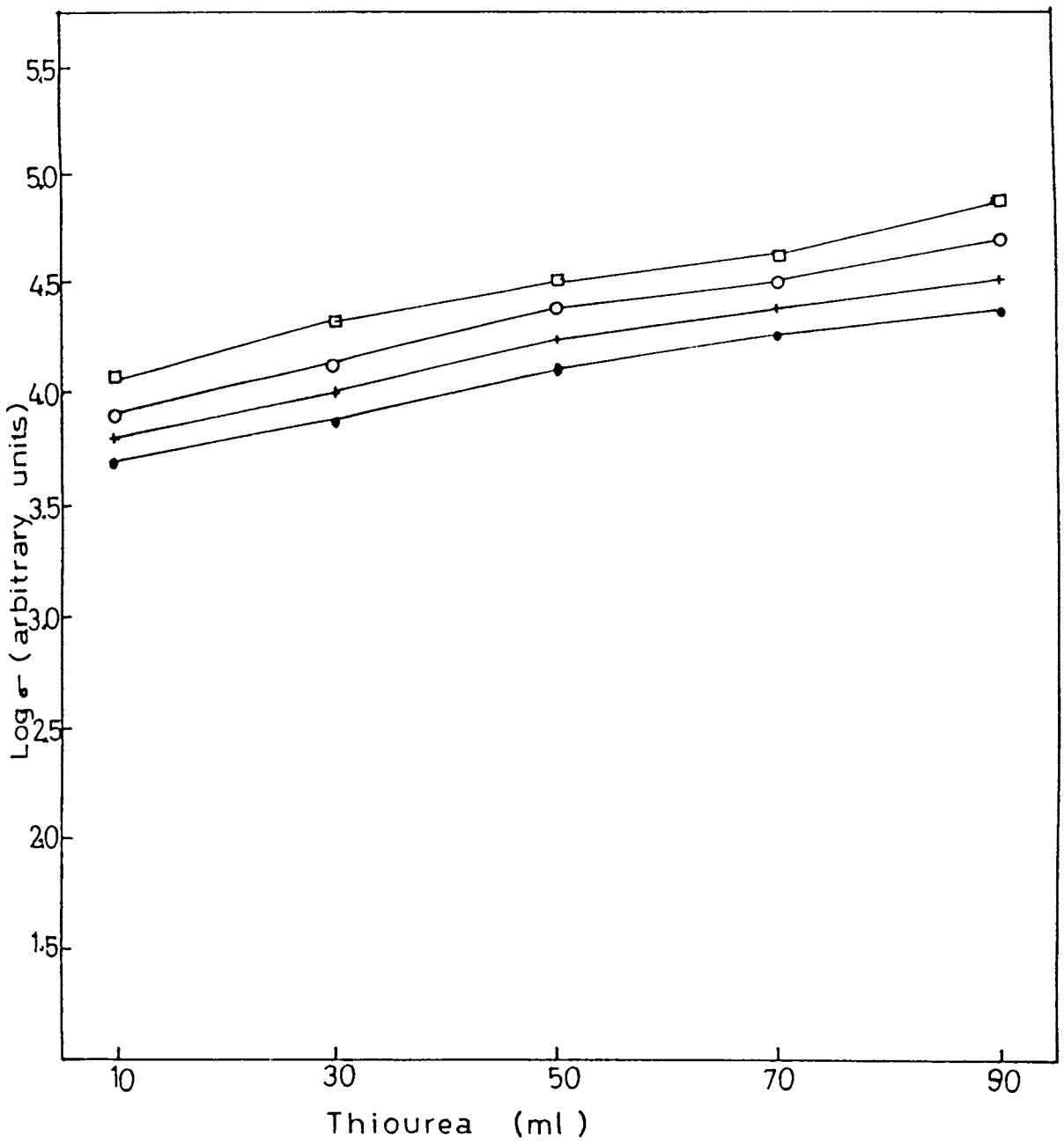

Fig 10.6 (a) : Variation of conductivity as a function of volume of thiourea for the films in air at 303 K: (•) unannealed and annealed at (+) 373 K, (o) 473 K and (□) 573 K.

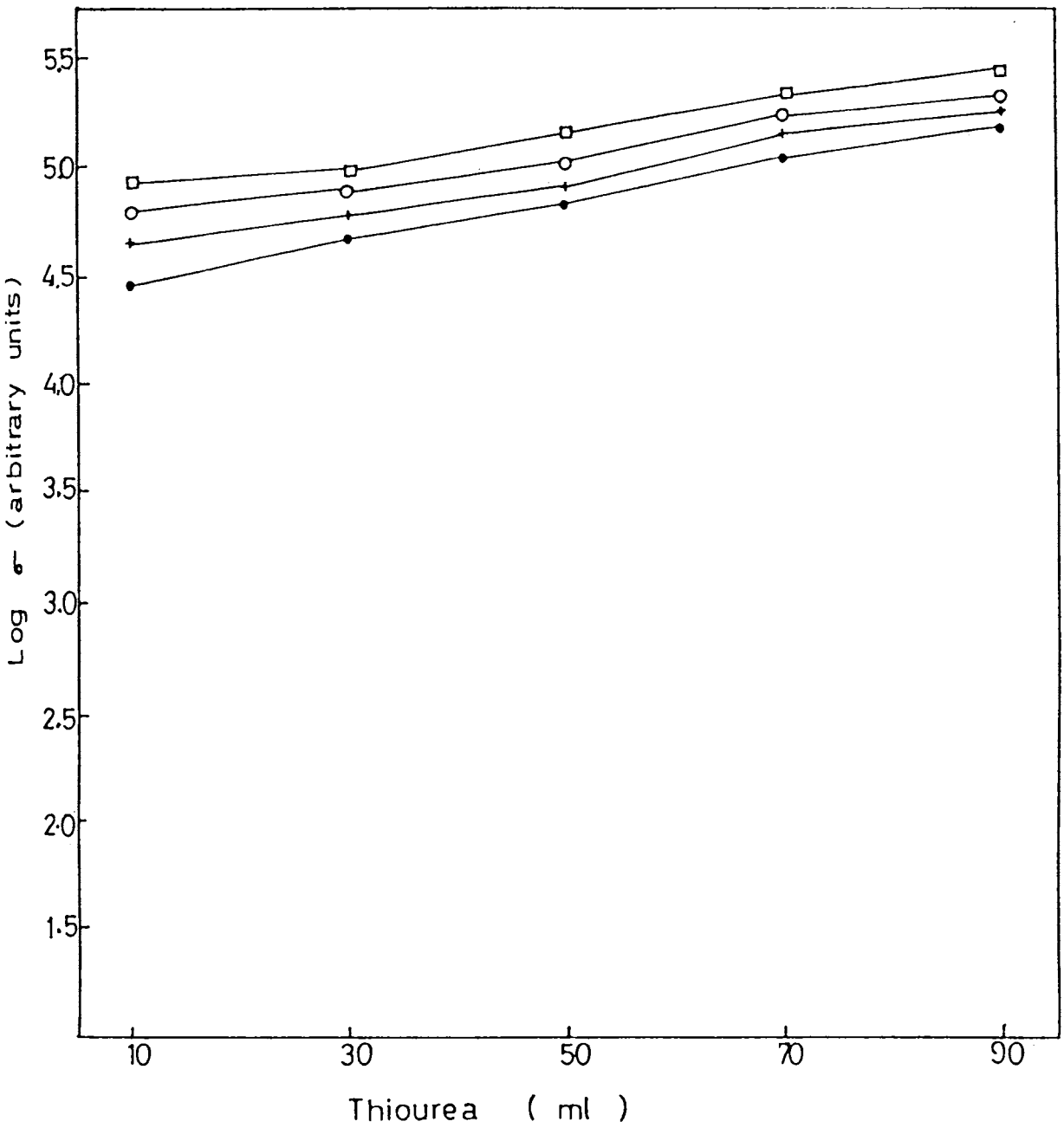

Fig 10.6 (b) : Variation of conductivity as a function of volume of thiourea for the films in air at 343 K: (•) unannealed and annealed at (+) 373 K, (o) 473 K and (□) 573 K.

Table 10.3 The values of conductivity of unannealed films

Sample	Conductivity at romm temperature in different ambients	
	Vacuum (Ω^{-1} m^{-1})	Air (Ω^{-1} m^{-1})
B_1	3.16×10^3	5.01×10^3
B_2	2.37×10^3	3.16×10^3
B_3	1.78×10^3	2.37×10^3
B_4	1.33×10^3	1.78×10^3
B_5	1.01×10^3	1.33×10^3
B_6	5.62×10^3	7.49×10^3
B_7	1.02×10^4	1.19×10^4
B_8	1.49×10^4	1.78×10^4
B_9	1.99×10^4	2.37×10^4

to the sulphur [12]. During the heating of the films in air, copper leaves the film and forms a surface oxide layer.

Removal of copper increases the copper vacancies and causes an increase in the majority carrier density. But the measurements in vacuum produced a substantial decrease in the value of conductivity.

10.4 CONCLUSION

Electrical conductivity measurements of copper sulphide films were carried out in vacuum and air. The observed increase in conductivity with temperature is essentially determined by an increase in the hole concentration. The films show an anomalous behaviour of conductivity at high temperatures. The values of activation energy are estimated both from the measurements in vacuum and air and the trap levels are identified. The results obtained in the films containing different copper and sulphur contents indicate that conductivity is decreased with increasing copper content whereas it is increased with sulphur content. The influence of annealing on conductivity of the films in air is similar to that obtained from the measurements in vacuum. It also appears that the films heated in air leads to an increase in the relative magnitude of conductivity.

10.5 REFERENCES

[1] E.Iborra, J. Santamaria, I. Martil, G. Gonzalez and F.S. Quesada, Vacuum 37 (1987) 437.

[2] E.Vanhoecke and M. Burgelman, Thin Solid Films 112 (1984) 97

[3] S.G. Ellis, J. Appl. Phys. 38 (1967) 2906

[4] S. Couve, L. Gouskov, L. Szepessy, J. Vedel and E.Castel, Thin Solid Films 15 (1973) 223

[5] B. Selle and J.Maege, Phys. Stat Solidi 30 (1968) K153

[6] E. Garcia-Camarero, F. Arjona, M.Leon and M.J. Nunez J.Mater. Sci. 21 (1986) 4169

[7] J.I. Leong and J.H. Yee, Appl. Phys. Lett. 35 (1979) 601.

[8] B. Rezig, S. Duchemin and F. Guastavino, Sol. Energy Mater.2 (1979) 53

[9] H.S. Randhawa, R.F. Bunshah, D.G. Brock, B.M. Basol and O.M. Staffsudd, Sol. Energy, Mater.6 (1982) 445

[10] J.A. Thornten, D.G. Cornog, W.W. Anderson, R.B.Hall and J.E. Phillips, Proc. 16th IEEE Photovoltaic Specialists Conf. New York, 1982.

[11] A.G. Valyom na and C.Purushothaman (Communicated)

[12] H.Evans, Nat. Phys. Sci. 232 (1971) 69.

11

THERMALLY STIMULATED CURRENT STUDIES OF Cu_xS THIN FILMS

11.1 INTRODUCTION

Several authors have employed the method of thermally stimulated currents (TSC) for studying the localized states in the semiconducting materials (1-6). But the TSC studies of Copper sulphide (Cu_xS) thin films have not been reported so far.

This chapter presents the investigations carried out in Cu_xS films using TSC technique. Influence of copper and sulphur contents and annealing temperature on the TSC peaks have been studied. The trap depth and capture cross section of the traps are determined. Attempts have also been made to understand the trapping mechanism of charge carriers in the film.

11.2 EXPERIMENTAL

Cu_xS films B_1 to B_9 were prepared by chemical bath deposition technique using different bath compositions as already described in Chapter 9. The samples were annealed in vaccum for 30 min. Silver electrodes were deposited over the films by vacuum evaporation and the measurements were carried out in a metallic cell under vacuum conditions as described in Chapter 4. The film was cooled down to low temperature where the probability of thermal release of carriers is negligible. It was then excited with a tungsten halogen lamp for 10 min. After switching off the halogen lamp the current through the film was monitored as a function of temperature

with the field applied. The heating rate employed was 0.06 K/Sec. As the temperature of the sample increases, the initial trapped carriers are released to produce a current in the presence of applied field. The trap parameters were determined as described in Chapter 3.

11.3 RESULTS AND DISCUSSION

In the present work, TSC spectra were recorded on films B_1 to B_5 prepared from different volume compositions of copper chloride (10 ml to 90 ml) and on films B_6 to B_9 prepared from different volume compositions of thiourea (30 ml to 90 ml). Figs. 11.1 to 11.5 represent the TSC spectra of unannealed and annealed (573 K) films B_1 to B_5. The spectra obtained by exciting the films for a period of 10 min and a biasing field of 3 KV/cm show two prominent TSC peaks a and b. However the magnitude of the peak height, the temperature at which it occurs and the area covered by the peaks depend on the copper content in the films. From the figures, it is clear that the magnitude of the current for films annealed at 573 K is higher than that of unannealed films. A slow decrease of peak current is observed at increasing copper contents (Fig.11.6). The TSC spectra of the films containing different sulphur contents are shown in Figs 11.7 to 11.10 . The magnitude of current

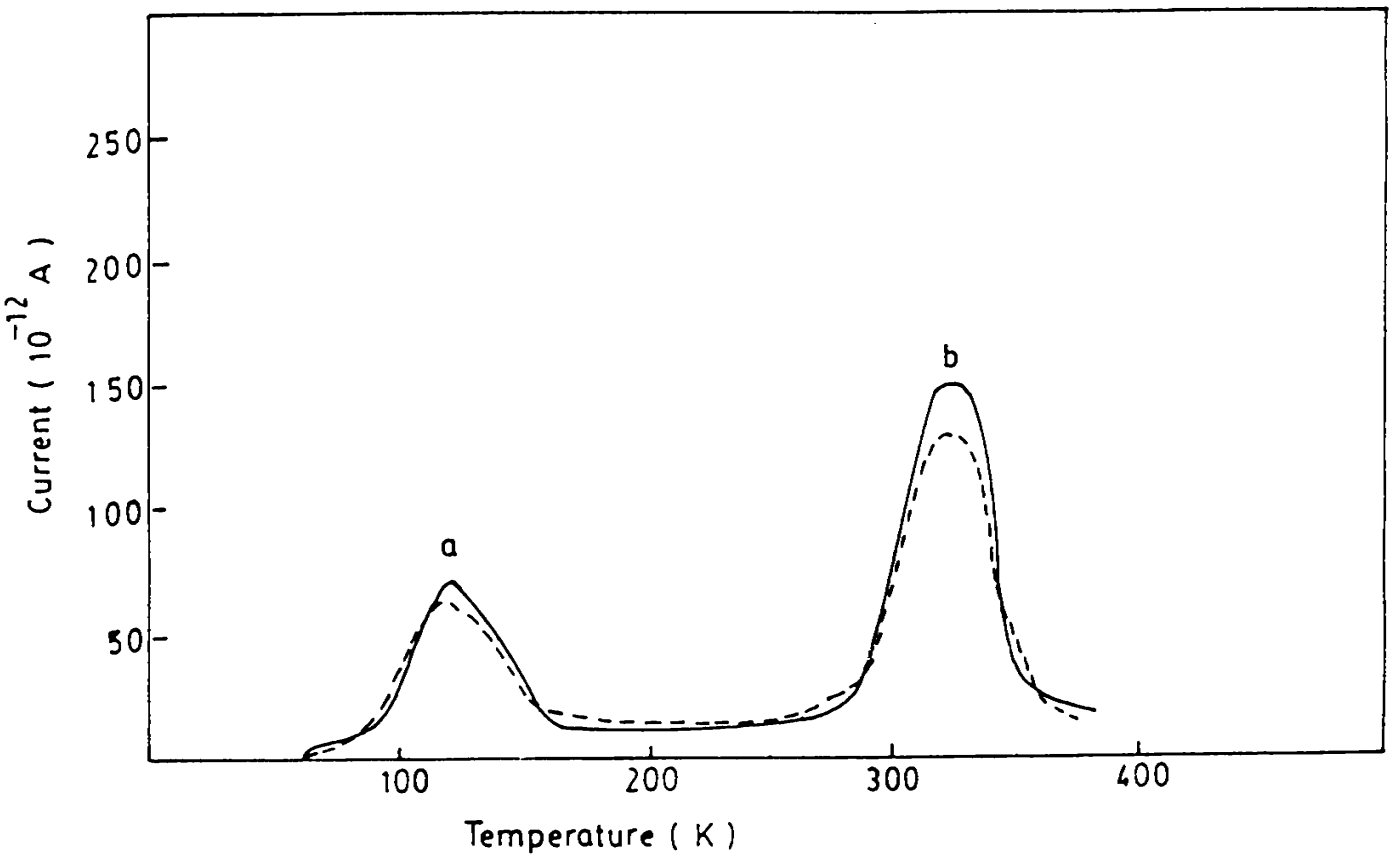

Fig. 11.1 TSC spectra of the film B_1: (.....) unannealed and (——) annealed at 573 K.

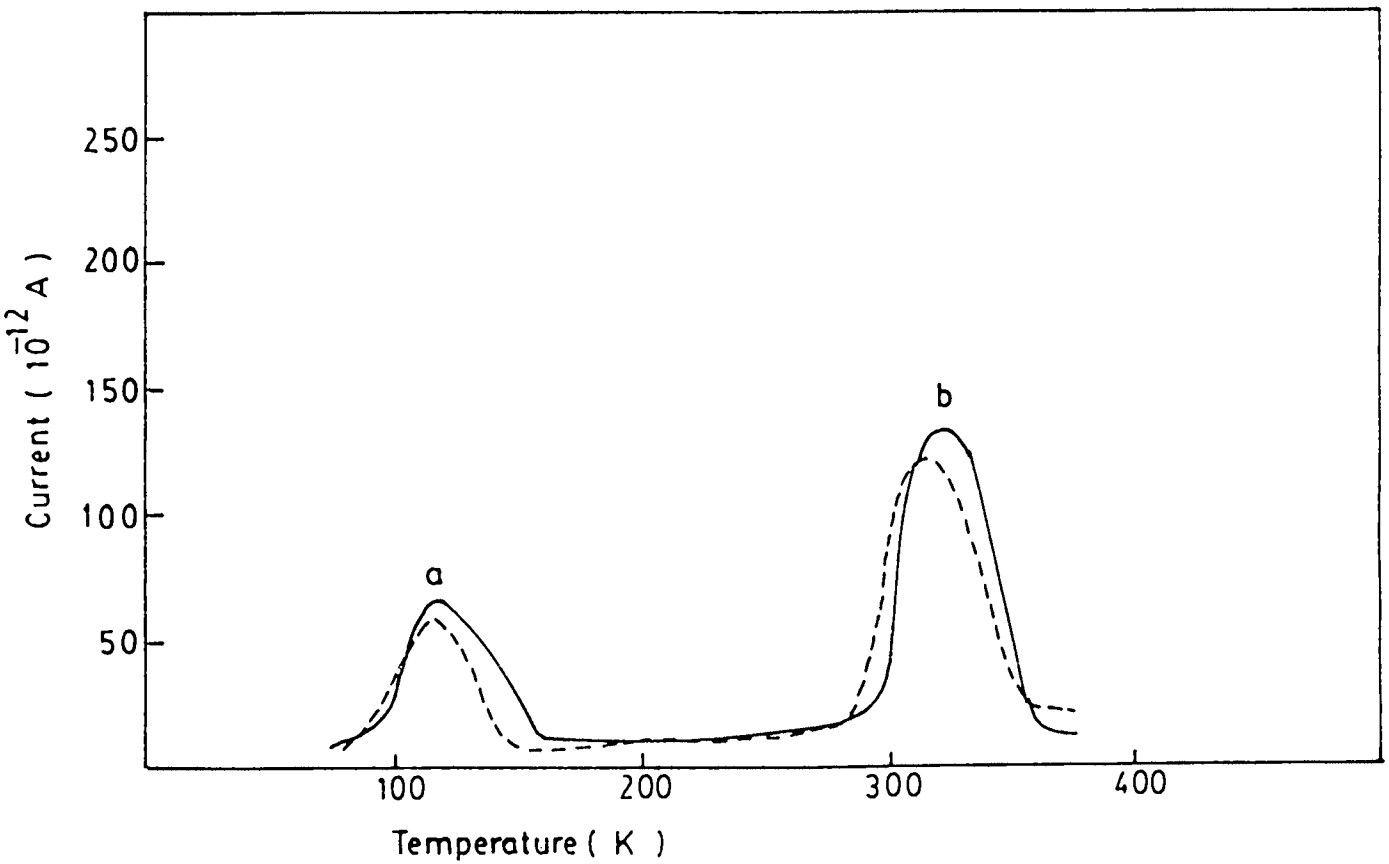

Fig. 11.2 TSC spectra of the film B_2: (.....) unannealed and (_____) annealed at 573 K.

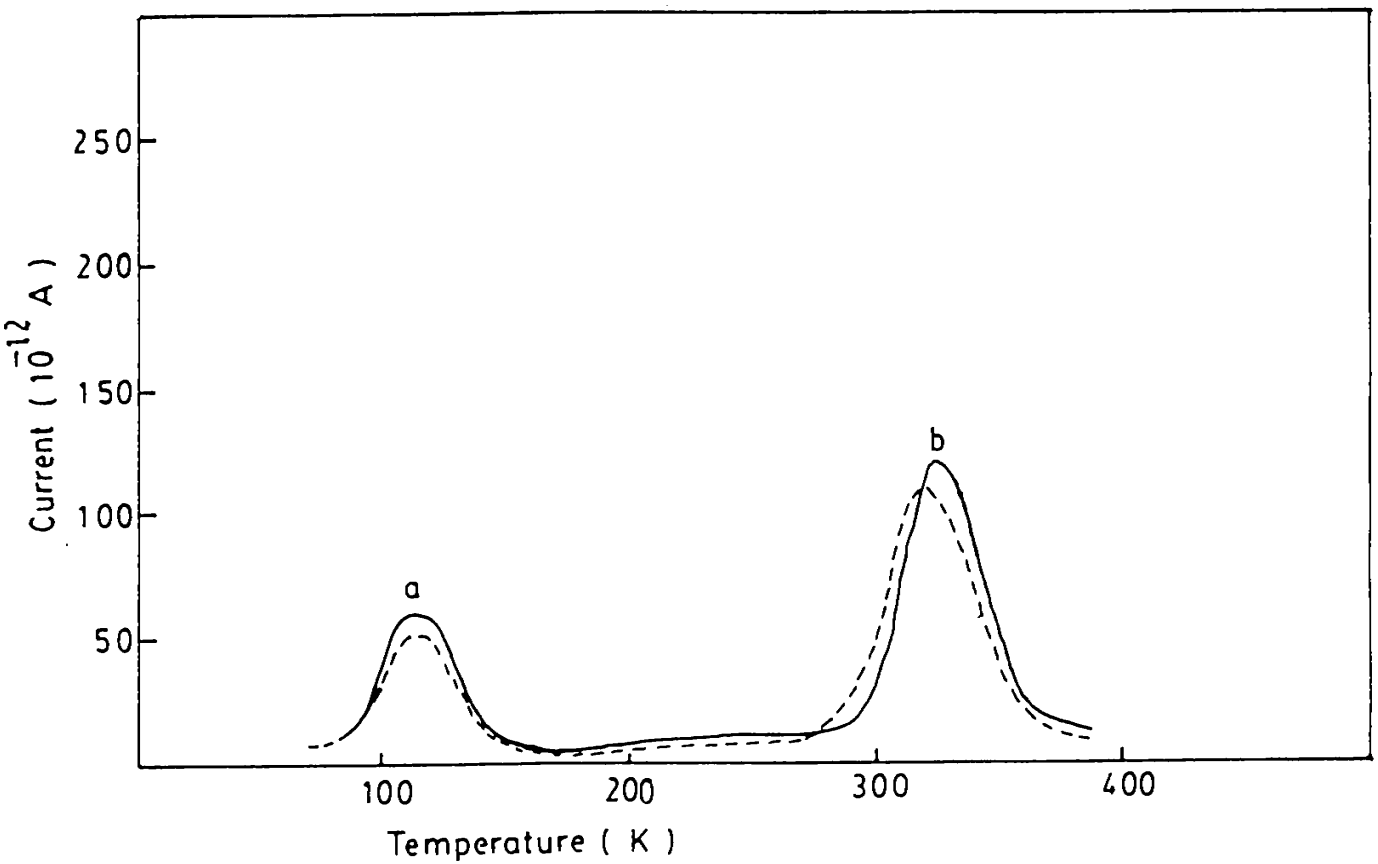

Fig. 11.3 TSC sepctra of the film B_3: (.....) unannealed and (_____) annealed at 573 K.

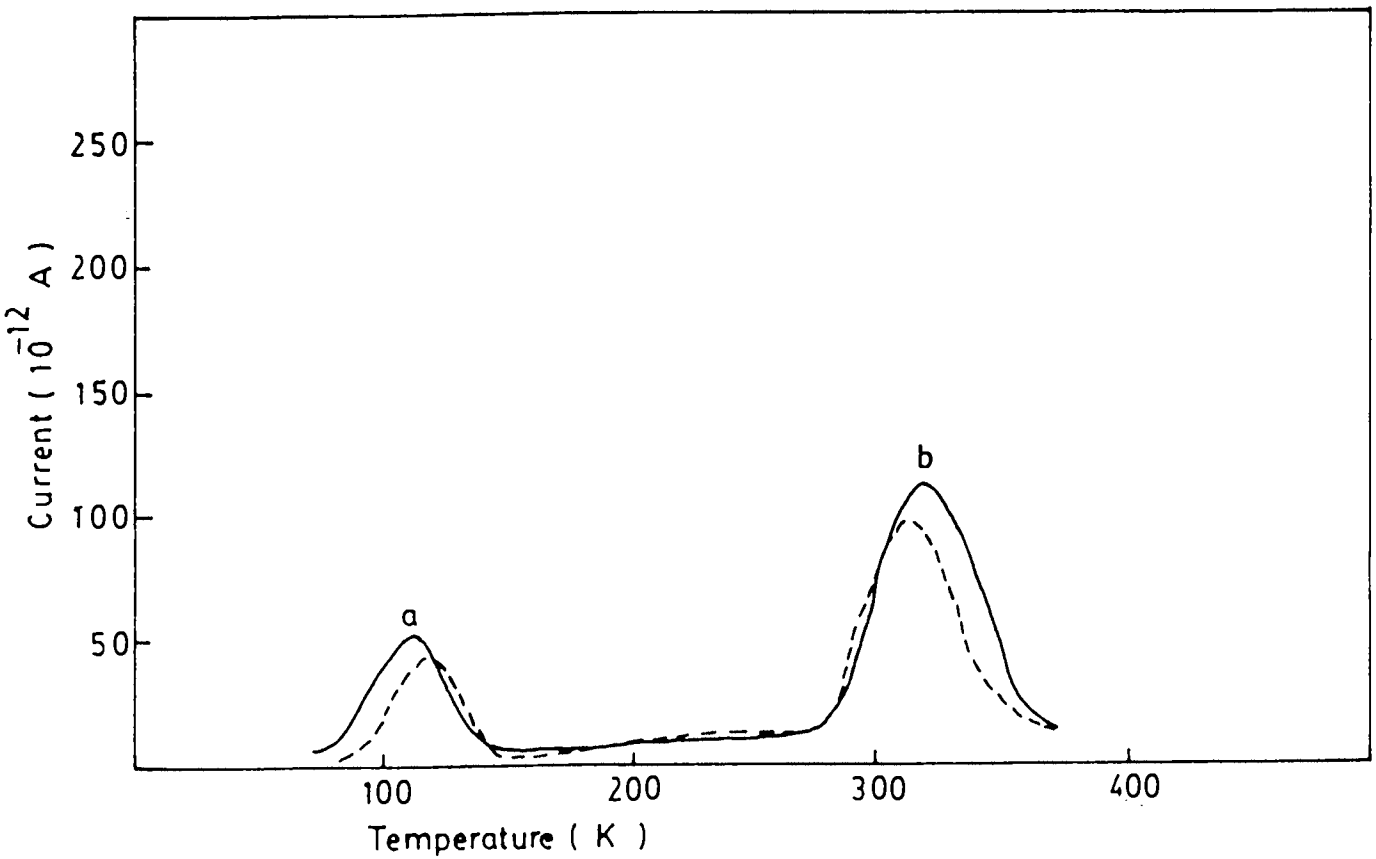

Fig. 11.4 TSC spectra of the film B_4: (.....) unannealed and (_____) annealed at 573 K.

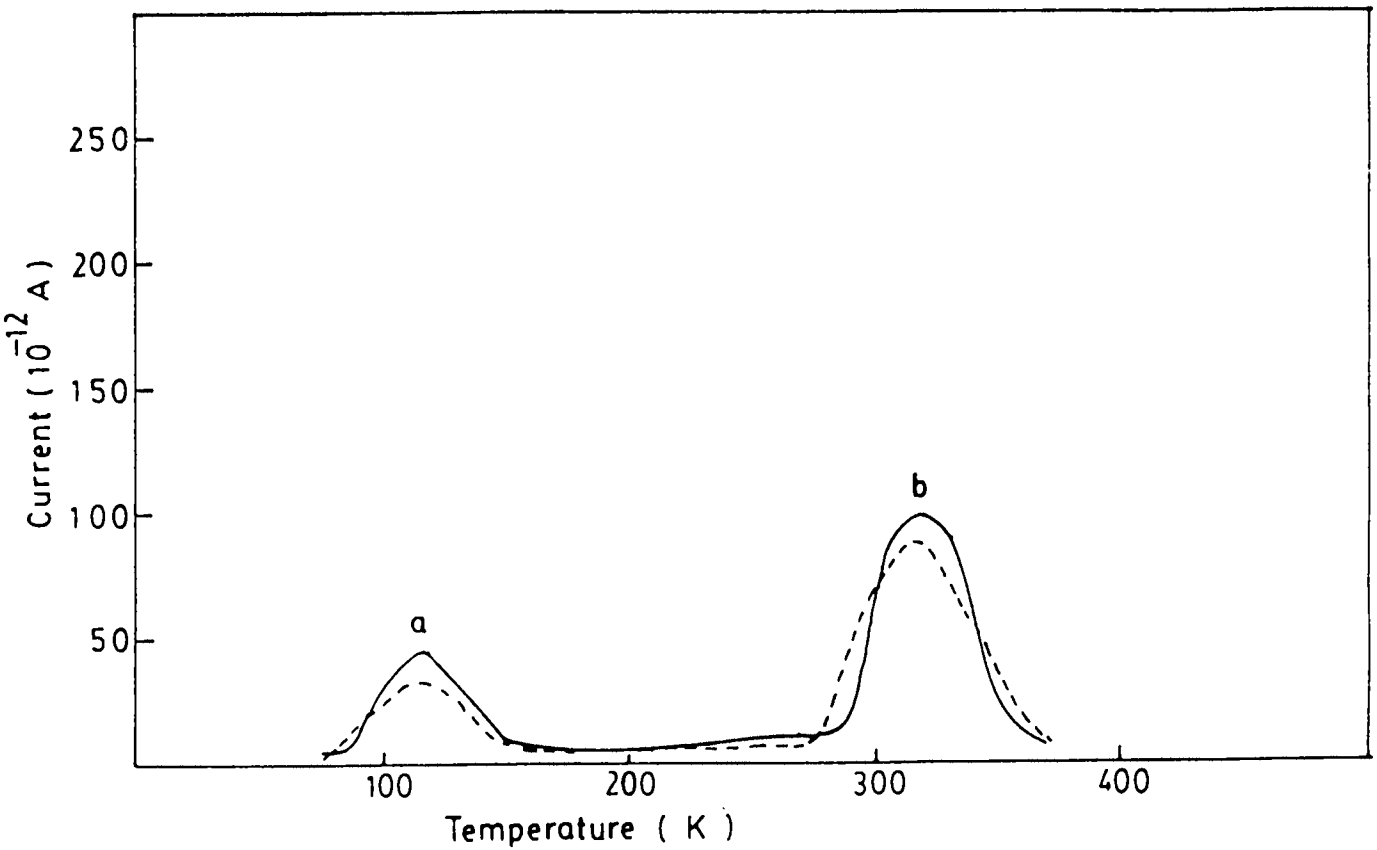

Fig. 11.5 TSC spectra of the film B_5: (.....) unannealed and (_____) annealed at 573 K.

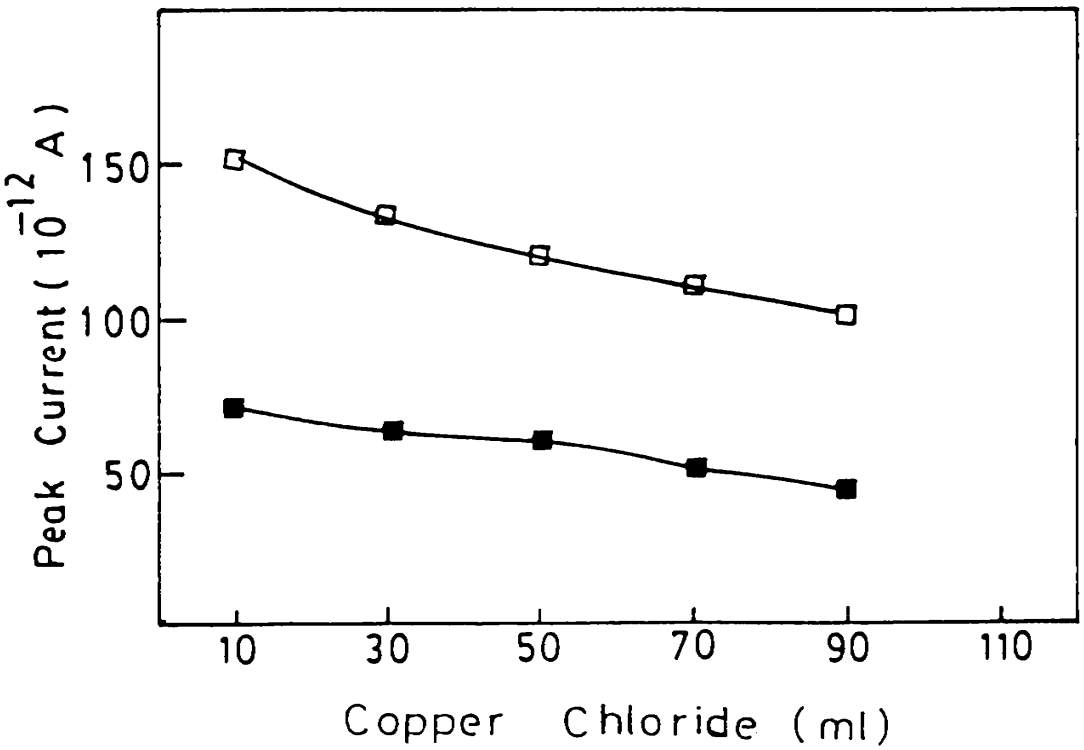

Fig. 11.6 Plot of peak height against volume of copper chloride for the films ~~films~~ annealed at 573 K for the peaks: (■) a and (□) b.

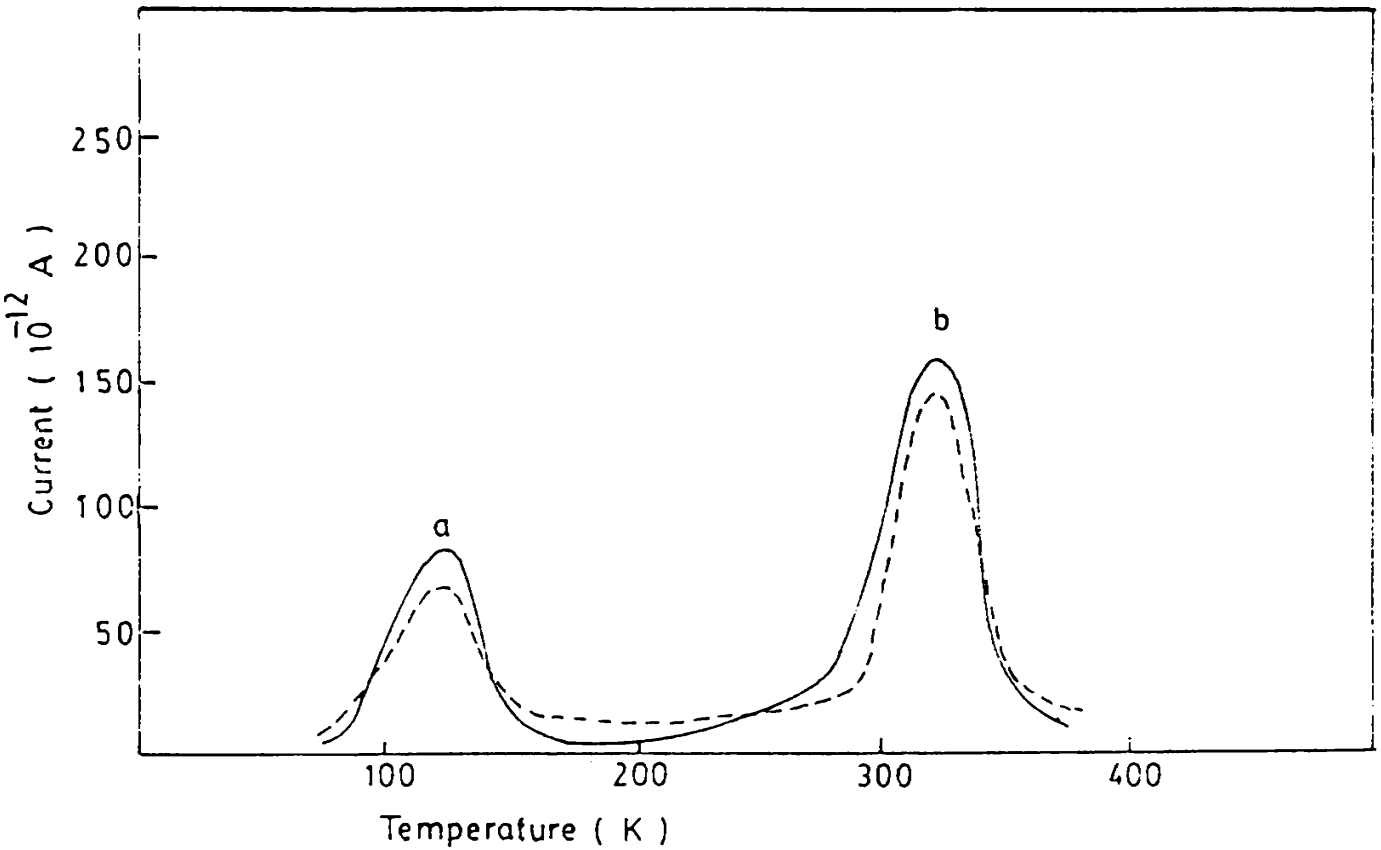

Fig. 11.7 TSC spectra of the film B_6: (.....) unannealed and (_____) annealed at 573 K.

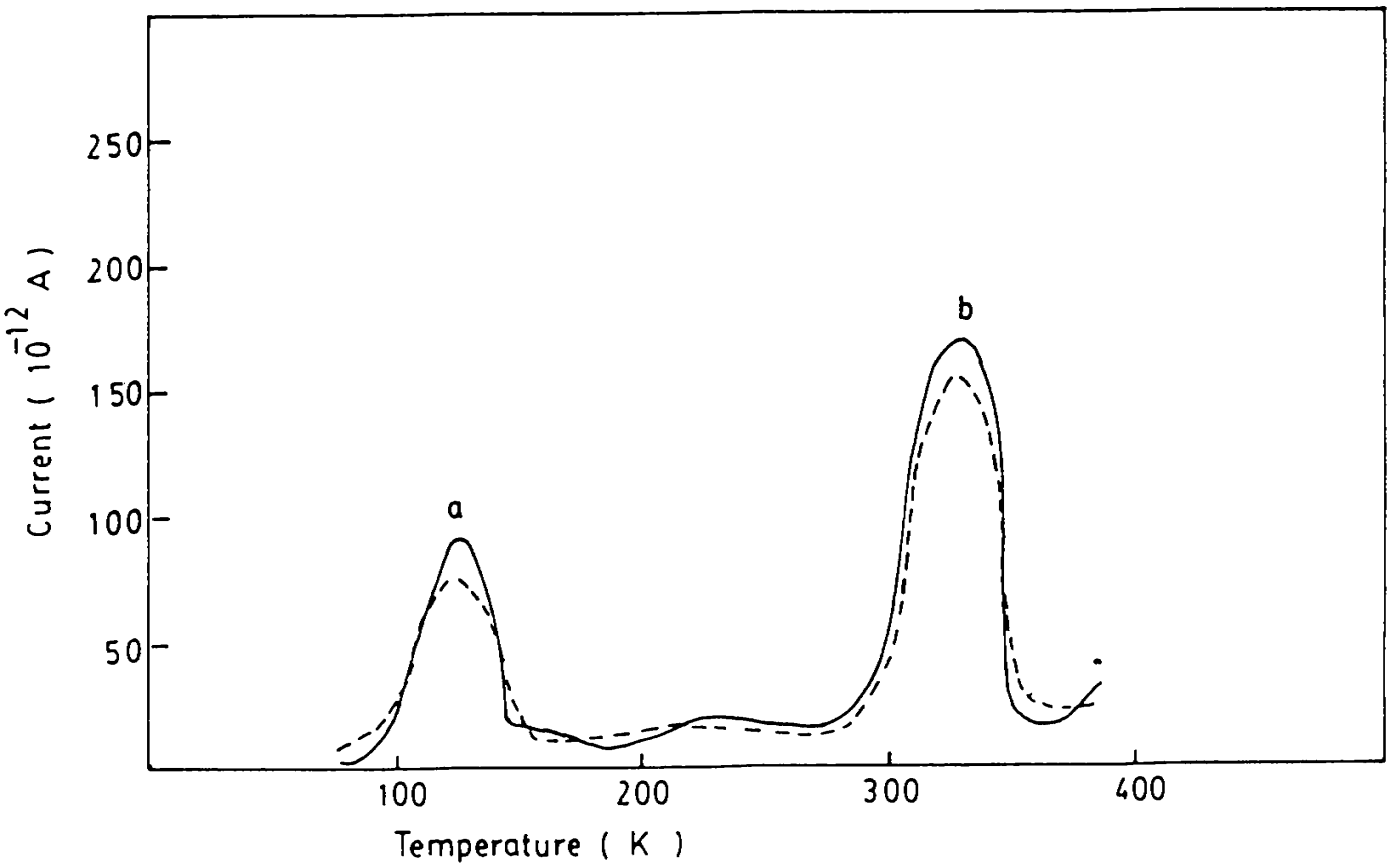

Fig. 11.8TSC sepctra of the film B_7: (.....) unannealed and (_____) annealed at 573 K.

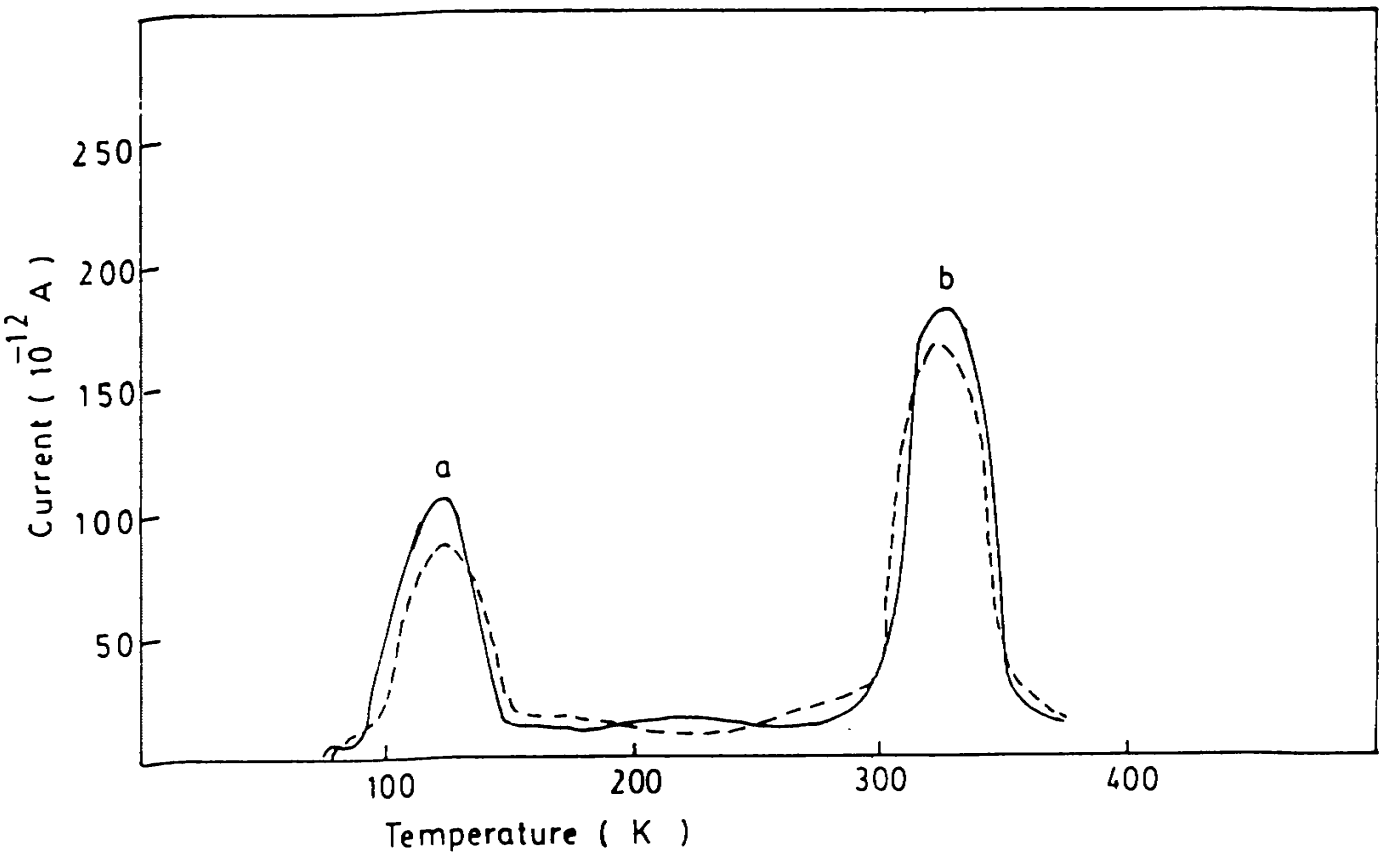

Fig. 11.9. TSC spectra of the film B_8: (.....) unannealed and (_____) annealed at 573 K.

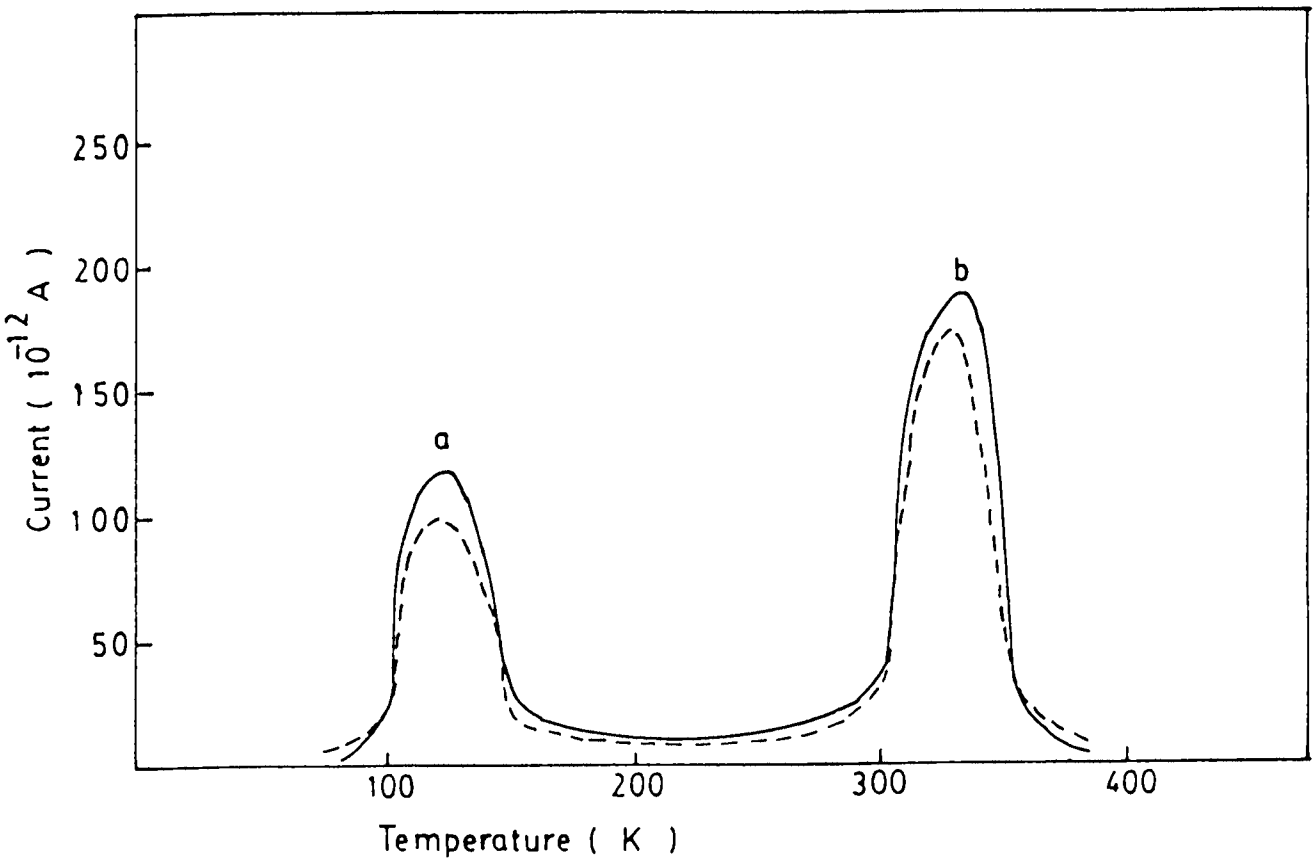

Fig. 11.10 TSC spectra of the film B_9: (.....) unannealed and (_____) annealed at 573 K.

is found to be lower for unannealed films. It is also noted that the peak current increases as the sulphur content increases (Fig. 11.11). Table 11.1 gives the values of activation energy, temperature corresponding to the current maxima and capture cross section.

The results obtained indicate that the distinct peaks observed in all samples are originated from a particular species of carriers. By considering the effect of annealing, copper and sulphur contents on the TSC peaks, it is clear that the origin of the peaks are related to the copper vacancies which act as acceptors and give rise to free holes, which in turn give rise to TSC peaks. The peak current is found to vary in accordance with the release of carriers from the trap levels present in the films.

The values of activation energy and the temperature corresponding to the current maxima of the peaks depends on the annealing temperature, copper and sulphur contents in the films [71]. The values of activation energy represent the various acceptor levels (copper vacancies) in the films.

In order to examine the influence of excitation time and biasing field on the magnitude of TSC peaks, the measurements have been performed on films by increasing the excitation time from 10 to 50 min and biasing field from 1 to 5 KV/cm. The height of the TSC peaks is found to vary linearly with biasing field and excitation time (Figs. 11.12 and 11.13). As the excitation time of the light

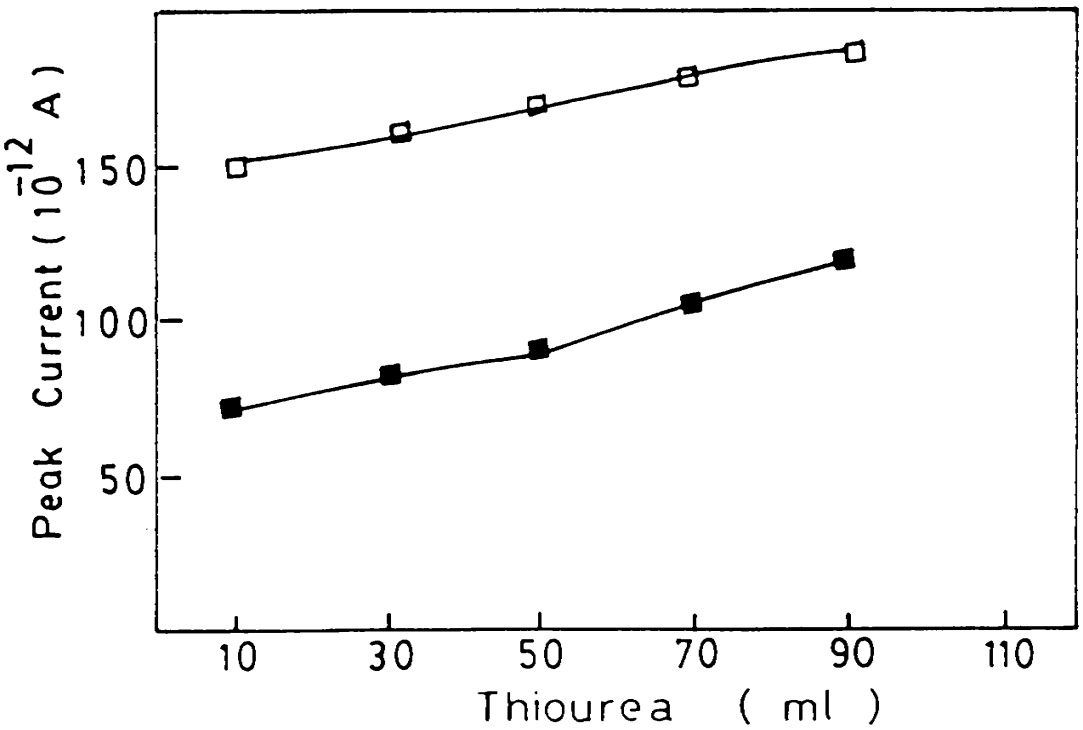

Fig. 11.11 Plot of peak height against volume of thiourea for the films annealed at 573 K. for the peaks: (■)a and (□)b.

Sample	Peak a			Peak b		
	Tm (K)	E (eV)	Capture Cross section (Cm^2)	Tm (K)	E (eV)	Capture cross section (Cm^2)
B_1						
Unannealed	117	0.048	2.80×10^{-27}	319	0.390	3.81×10^{-23}
Annealed(573K)	119	0.050	3.10×10^{-27}	321	0.403	5.70×10^{-23}
B_2						
Unannealed	116	0.056	7.80×10^{-27}	318	0.372	1.98×10^{-23}
Annealed(573K)	118	0.053	4.80×10^{-27}	324	0.402	4.71×10^{-23}

Contd.....

Contd...Table 11.1

Sample	Peak a			Peak b		
	Tm (K)	E (eV)	Capture Cross section (Cm^2)	Tm (K)	E (eV)	Capture Cross section (Cm^2)
B_3						
Unannealed	115	0.058	1.02×10^{-26}	318	0.396	5.07×10^{-23}
Annealed (573K)	"	0.056	8.30×10^{-27}	323	0.418	9.11×10^{-23}
B_4						
Unannealed	118	0.061	1.22×10^{-26}	316	0.366	1.73×10^{-23}
Annealed (573K)	114	0.058	1.13×10^{-26}	321	0.355	8.87×10^{-24}
B_5						
Unannealed	112	0.045	2.60×10^{-27}	316	0.290	8.44×10^{-25}
Annealed (573K)	116	0.048	3.00×10^{-27}	318	0.342	6.12×10^{-24}

Contd ...

Contd...Table 11.1

Sample	Peak a			Peak b		
	Tm (K)	E (eV)	Capture cross section (Cm^2)	Tm (K)	E (eV)	Capture cross section (Cm^2)
B_6						
Unannealed	120	0.050	3.40×10^{-27}	324	0.452	3.16×10^{-22}
Annealed (573K)	121	0.053	4.04×10^{-27}	324	0.412	6.90×10^{-23}
B_7						
Unannealed	123	0.056	5.04×10^{-27}	325	0.423	9.96×10^{-23}
Annealed (573K)	124	0.060	7.40×10^{-27}	327	0.419	7.71×10^{-23}
B_8						
Unannealed	123	0.059	7.20×10^{-27}	325	0.455	3.35×10^{-22}
Annealed (573K)	126	0.068	1.55×10^{-26}	329	0.491	1.03×10^{-21}
B_9						
Unannealed	123	0.061	8.80×10^{-27}	330	0.469	4.29×10^{-22}
Annealed (573K)	127	0.063	8.54×10^{-27}	332	0.487	7.40×10^{-22}

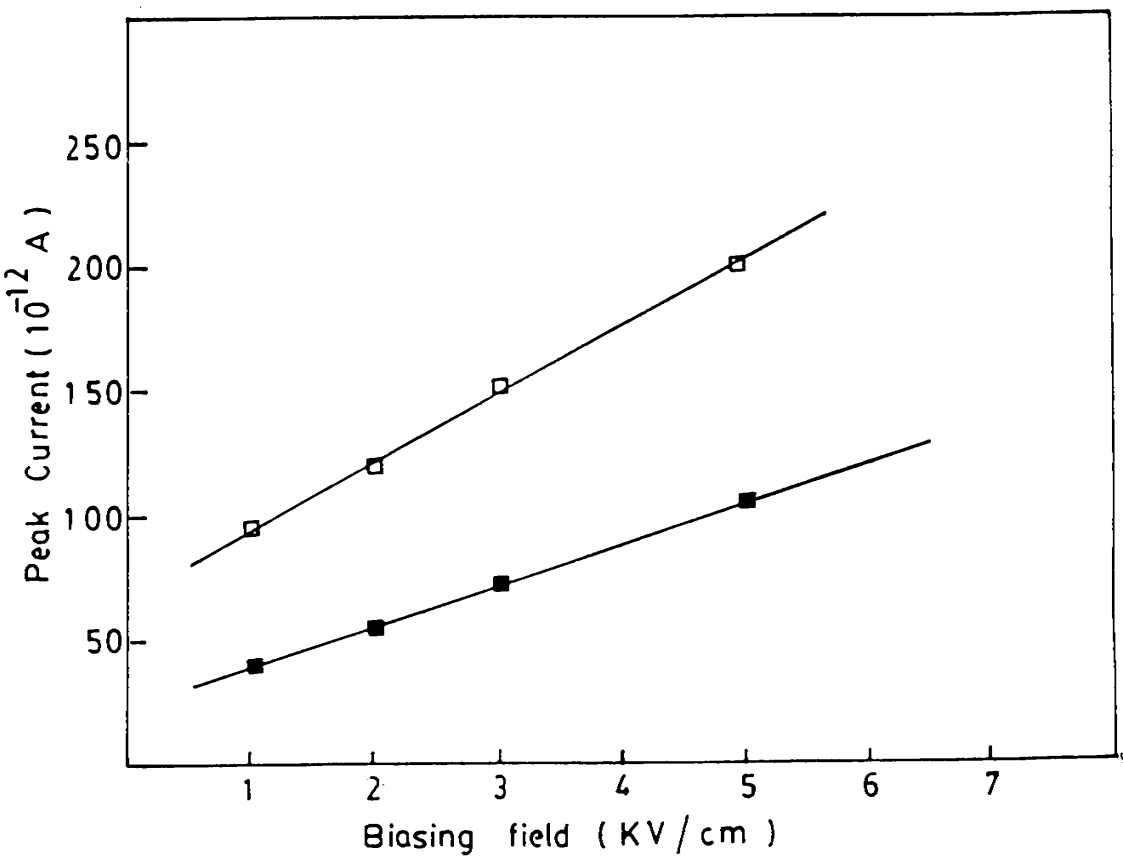

Fig. 11.12. Plot of peak height against biasing field for the film B_1 annealed at 573 K for the peaks; (■)a and (□)b.

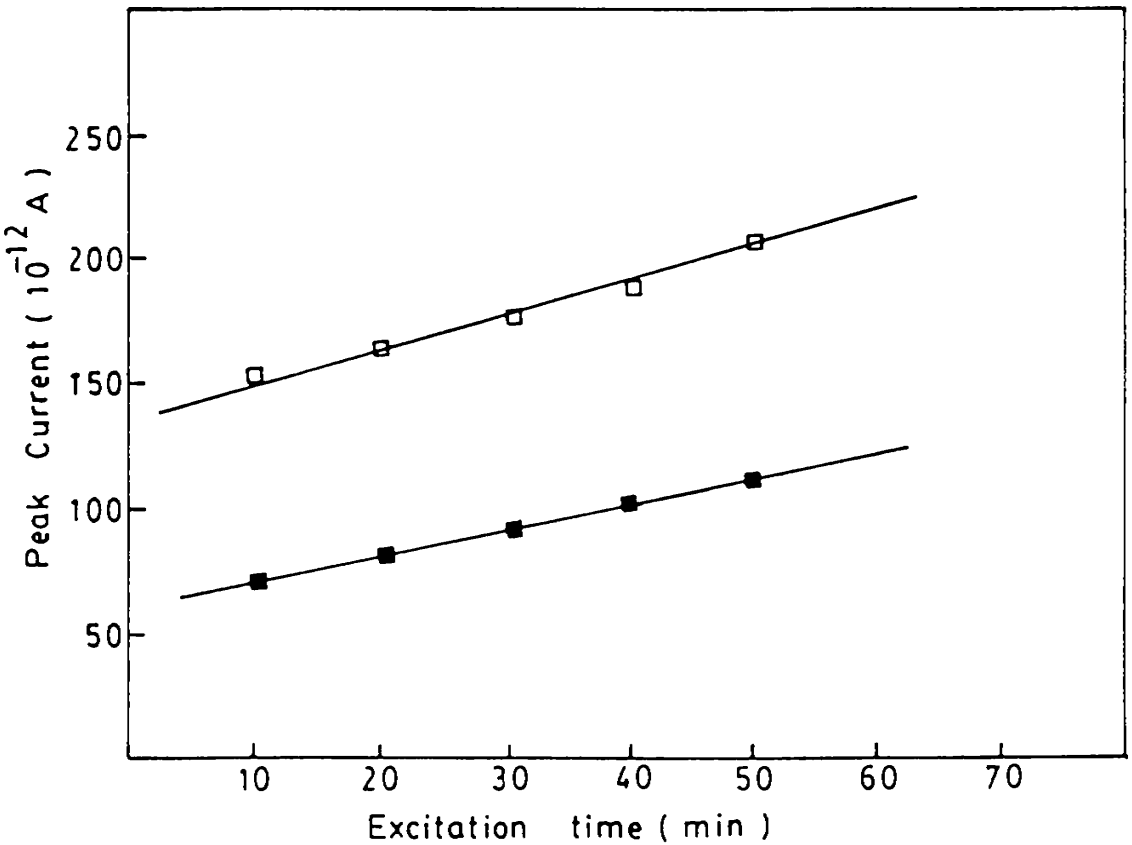

Fig. 11.13. Plot of peak height against excitation time for the film B_1 annealed at 573 K for the peaks (■)a and (□)b.

falling on the sample increases, the filling of the vacancies in the film also correspondingly increases. The peaks are then formed as a result of the excitation of carriers from the vacancy sites in the films. As the biasing field increases the peak height increases since more number of carriers are released.

11.4 CONCLUSION

The TSC spectra obtained for all films show two peaks a and b. The magnitude of the current is higher for the annealed samples compared to that of the unannealed samples. The peak height is found to be decreasing with increasing copper content whereas it is increasing with sulphur content. Also the current exhibits a linear relation with biasing field and excitation time. The origin of the peaks are related to the releasing of carriers from the shallow and deep acceptor states. The activation energy and capture cross section of the traps are also estimated from the TSC data.

11.5 REFERENCES

[1] R.H. Bube, Photoconductivity of Solids (Wiley, New York, 1960).

[2] S.G. Elkomos, M. Samimi, M. Hage-Ali, and P. Siffert, J.Appl. Phys. 57 (1985) 5313.

[3] P. Braunlich, P. Kelley and J.P. Fillard, in: Topics in Applied Physics, Vol. 37, ed. P. Braunlich (Springer-Verlag, Heidelberg, 1979).

[4] R.R. Haering and E.N. Adams, Phys. Rev. 117 (1960) 451.

[5] B.T. Kolomiets and T.F. Mazets, J. Non-Cryst. Solids 3 (1970) 46.

[6] R.A. Street and A.D. Yoffe, Thin Solid Films 11 (1972) 161.

[7] A.G. Valyomana and C. Puruthothaman (communicated).

12

PREPARATION AND CHARACTERIZATION OF $CuInSe_2$ THIN FILMS

12.1 INTRODUCTION

Copper indium selenide ($CuInSe_2$) belongs to I-III-VI group compounds and finds application in photovoltaic devices [1-4]. Several workers have reported the preparation and characterization of $CuInSe_2$ thin films by a number of methods [5-12]. But only a few reports are available regarding the preparation of these films by chemical deposition methods [13-15]. Bhattacharya [13] has prepared the films by the electroplating method. Also, Khare et al. [14] have used electrodeposition method for the same. The structural and electrical properties of the films prepared by the chemical bath deposition technique have been described by Murali [15]. He obtained P-type films of resistivity in the range 50-500 ohm cm depending on the deposition parameters. But detailed studies on the electrical conductivity of chemically deposited films have not been made yet.

Not much data has been seen reported on the electrical characteristics of the chemically deposited $CuInse_2$ films using the thermally stimulated current (TSC) technique, Datta et al. [16] have reported the TSC studies of $CuInSe_2$ films prepared by vacuum deposition technique. However, a very little information is avalable regarding the TSC studies of these films as a function of copper and selenium contents and annealing temperature. The electrical properties of $CuInSe_2$ films are strongly influenced by the presence of defects. Therefore it was intended to carry out measurements on the electrical conductivity and TSC of these films. The films have been characterized by X-ray analysis. The surface topographical features have also been examined. The optical absorption

has been studied in the spectral range 500-1500 nm to determine the band gap. The results of all these studies form the subject of this chapter.

12.2 EXPERIMENTAL

For the preparation of $CuInSe_2$ films, a composite layer of copper and indium was first deposited by using a vacuum system. The glass substrates were cleaned thoroughly by washing with cleaning solutions and then ultrasonically with doubly distilled water and acetone and finally dried. The precleaned glass substrates were inserted in the substrate holder. Molybdenum boats were used to evaporate the materials. After loading the system with one mole each of copper and indium, the chamber was evacuated to a pressure of 10^{-5} Torr. The substrates were heated and controlled to attain the required temperature (473K). At this temperature, stable composite layers of copper and indium were obtained. Inorder to deposit 2 moles of selenium, this layer was dipped into a solution containing appropriate amounts of selenium dioxide in dil. H_2SO_4 at room temperature. After rinsed with distilled water, the films were finally dried. In this case, the molarity of selenium dioxide employed was 2.01 M. The films containing different contents of copper and selenium were also prepared by changing the number of moles of Cu and molarity of selenium dioxide. In the present work, these films are represented as C_1, C_2, C_3, ...C_9, whose details are given in Table 12.1. The method of preparation of these films is similar to that reported in [17]. The films obtained are found to be P-type, when examined with hot probe method. Air annealing

Table 12.1 Designation of $CuInSe_2$ films

Sample	Reactants used for the preparation
C_1	1 mole copper, 1 mole indium, 2.01 M selenium dioxide solution.
C_2	1.02 mole copper, 1 mole indium, 2.01 M selenium dioxide solution.
C_3	1.04 mole copper, 1 mole indium, 2.01 M selenium dioxide solution.
C_4	1.06 mole copper, 1 mole indium, 2.01 M selenium dioxide solution.
C_5	1.08 mole copper, 1 mole indium, 2.01 M selenium dioxide solution.
C_6	1 mole copper, 1 mole indium, 2.03 M selenium dioxide solution.
C_7	1 mole copper, 1 mole indium, 2.05 M selenium dioxide solution.
C_8	1 mole copper, 1 mole indium, 2.07 M selenium dioxide solution.
C_9	1 mole copper, 1 mole indium, 2.09 M selenium dioxide solution.

treatments were carried out by using a glass chamber as described in Chapter 4.

X-ray diffraction studies were carried out with CuKα radiation. The surfaces of the films were observed in reflection using a Union Versamet - 2 metallographic microscope. The band gap of the film was determined from the absorption measurements in the spectral region 500 - 1500 nm using a U - 3410 Hitachi Spectrophotometer.

For obtaining good electrical contacts between the film and the electrodes, the surface of the film was coated with silver paint. The electrical conductivity measurements were carried out in the fabricated metallic cell as described in Chapter 4. For the TSC measurements, the samples were cooled down to a low temperature ($\sim$100 K). It was then excited using a tungsten halogen lamp for 5-30 min. After removing the light source, the sample was subjected to a heating rate of 0.06K/sec. With the biasing field in the range 1-5 KV/cm, the current was recorded as a function of temperature using an electrometer. The trap depth and capture cross section were evaluated as described in Chapter 3.

12.3 RESULTS AND DISCUSSION

During the present investigation, good quality films of $CuInSe_2$ were obtained. Fig. 12.1 is the photograph of the surface of a typical film. The X-ray diffractogram of the film is shown in Fig. 12.2. The diffraction lines are identified and the results obtained are found to be in good agreement with that reported for $CuInSe_2$[18].

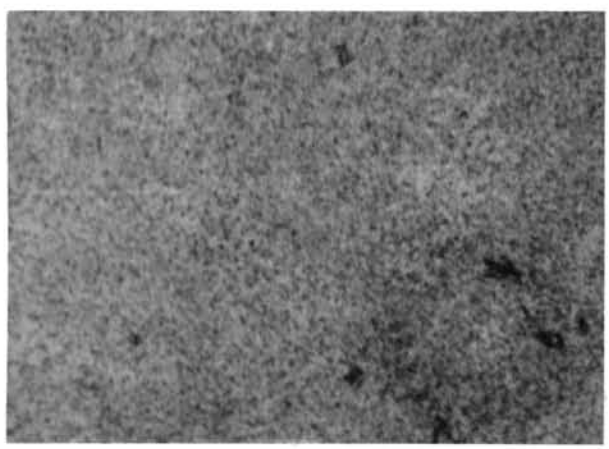

Fig. 12.1: Photograph showing the surface of film. (x100)

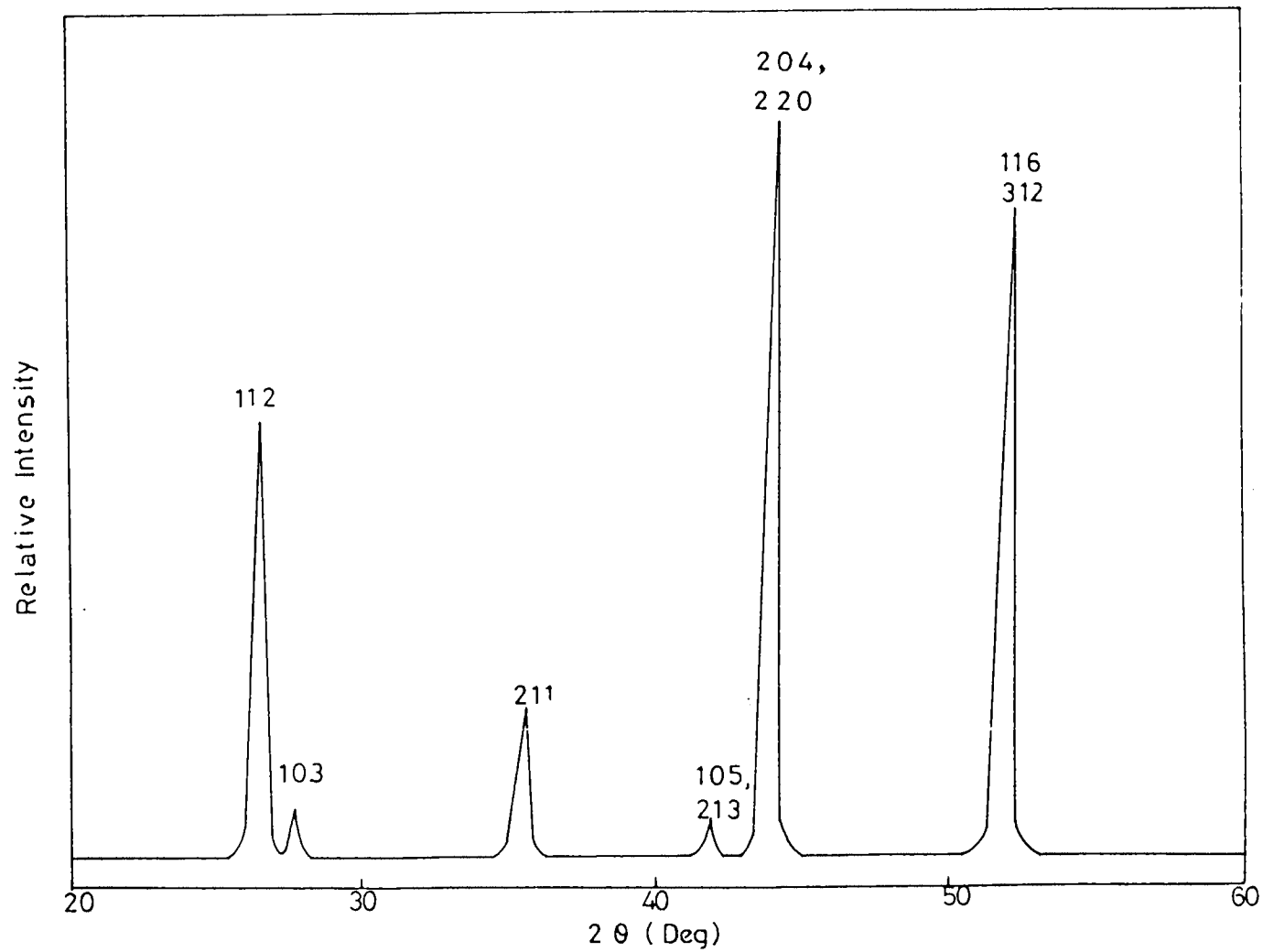

Fig. 12.2: X-ray diffraction pattern of the film.

Fig. 12.3 depicts the absorption spectrum of the film. The calculated value of band gap is 1.031 eV, which agreed well with that given in the literature [19].

12.3.1 Electrical Conductivity Measurements

The present investigation was undertaken with a view to study in detail the effect of ambient conditions, annealing temperature and copper and selenium contents on the conductivity of $CuInSe_2$ films. The activation energy of charge carriers was also determined.

The electrical conductivity σ has been measured in vacuum for different unannealed and annealed films as a function of temperature. Fig. 12.4 shows a typical log σ versus $10^3/T$ plot for the film C_1. The observed exponential dependence of σ upon temperature can be explained by the equation $\sigma = \sigma_0 \exp\left(-\frac{E}{kT}\right)$ where σ_0 is constant and E is the activation energy. For all films, the conductivity is found to increase slowly with temperature in the range 110 - 200 K while in the high temperature region, the conductivity is found to increase sharply with temperature. The activation energy obtained for the films (Table 12.2) represent the energy required for the excitation of charge carriers from various defect levels.

As the copper content increases, in the films the value of conductivity also increases and reaches a maximum for the film C_4. Whereas it decreases for the film C_5 [Figs. 12.5 (a) to 12.5(c)]. Excess copper is expected to provide acceptors if it sits on indium sites and hence an increase in the value of conductivity is observed. The decrease in the value of conductivity for the film C_5 is due to

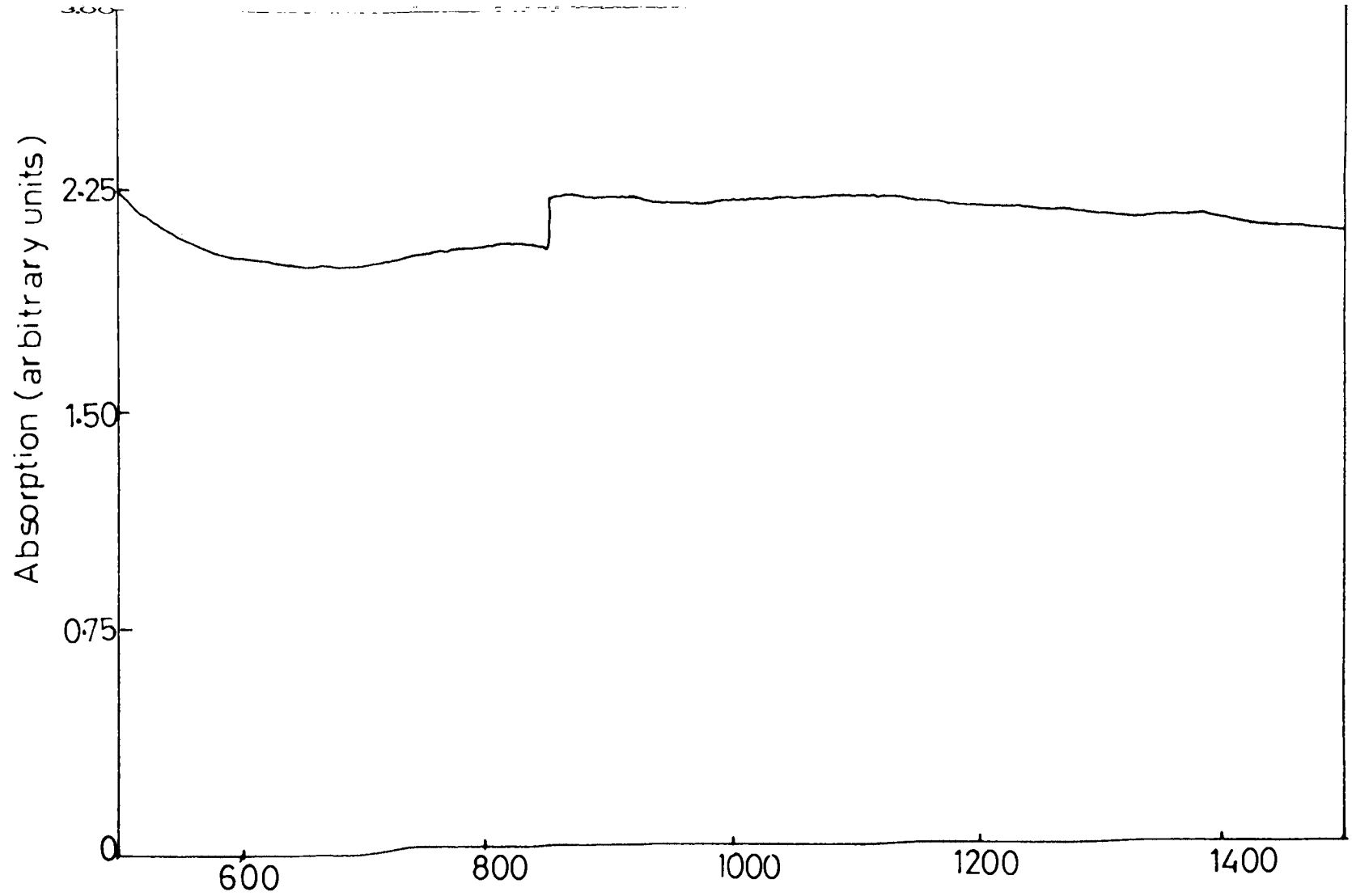

Fig. 12.3: Absorption spectrum of the film

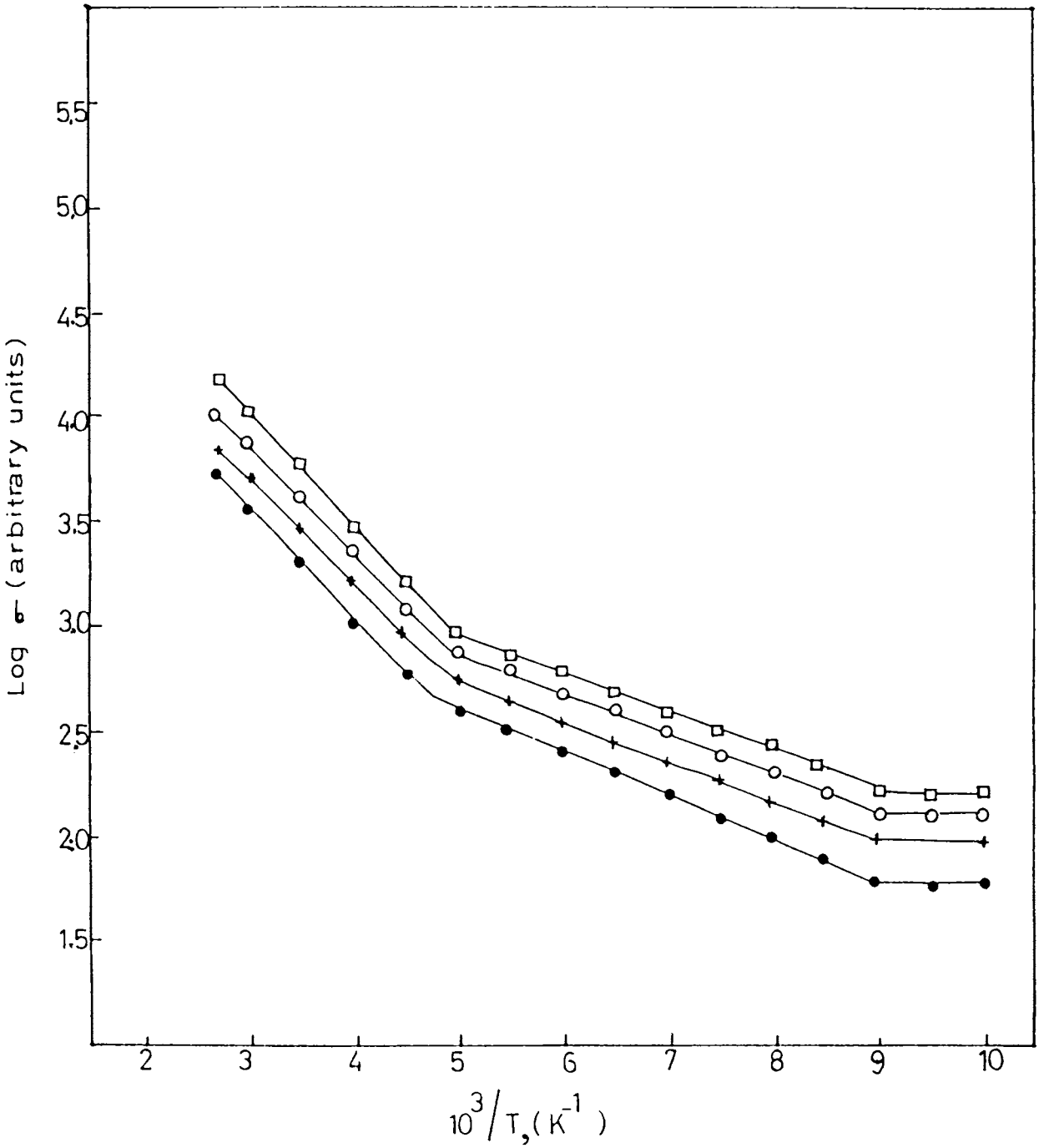

Fig 12.4 : Plot of log σ against $10^3/T$ for the film C_{14} in vacuum: (•) unannealed and annealed at (+) 373 K, (o) 473 K and (□) 573 K.

Table 12.2 The values of activation energy obtained from the conductivity measurements of the films in vacuum.

Sample	Activation energy in the temperature range at 110-200K (eV)	205-363K (eV)
C_1		
Unannealed	0.040	0.101
Annealed (373K)	0.036	0.103
Annealed (473K)	0.038	0.102
Annealed (573K)	0.037	0.105
C_2		
Unannealed	0.057	0.135
Annealed (373K)	0.055	0.133
Annealed (473K)	0.054	0.131
Annealed (573K)	0.053	0.121
C_3		
Unannealed	0.056	0.138
Annealed (373K)	0.055	0.132
Annealed (473K)	0.053	0.126
Annealed (573K)	0.054	0.121

contd...

Contd...12.2

Sample	Activation energy in the temperature range at	
	110-200K (eV)	205-363K (eV)
C_4		
Unannealed	0.073	0.098
Annealed (373K)	0.072	0.093
Annealed (473K)	0.069	0.096
Annealed (573K)	0.068	0.097
C_5		
Unannealed	0.027	0.151
Annealed (373K)	0.026	0.153
Annealed (473K)	0.025	0.152
Annealed (573K)	0.024	0.154
C_6		
Unannealed	0.025	0.114
Annealed (373K)	0.023	0.117
Annealed (473K)	0.021	0.119
Annealed (573K)	0.020	0.118

Contd...

Contd...Table 12.2

Sample	Activation energy in the temperature range at 110-200K (eV)	205-363K (eV)
C_7		
Unannealed	0.014	0.123
Annealed (373K)	0.013	0.121
Annealed (473K)	0.011	0.122
Annealed (573K)	0.012	0.124
C_8		
Unannealed	0.055	0.133
Annealed (373K)	0.054	0.131
Annealed (473K)	0.049	0.135
Annealed (573K)	0.048	0.121
C_9		
Unannealed	0.058	0.135
Annealed (373K)	0.057	0.126
Annealed (473K)	0.054	0.125
Annealed (573K)	0.053	0.124

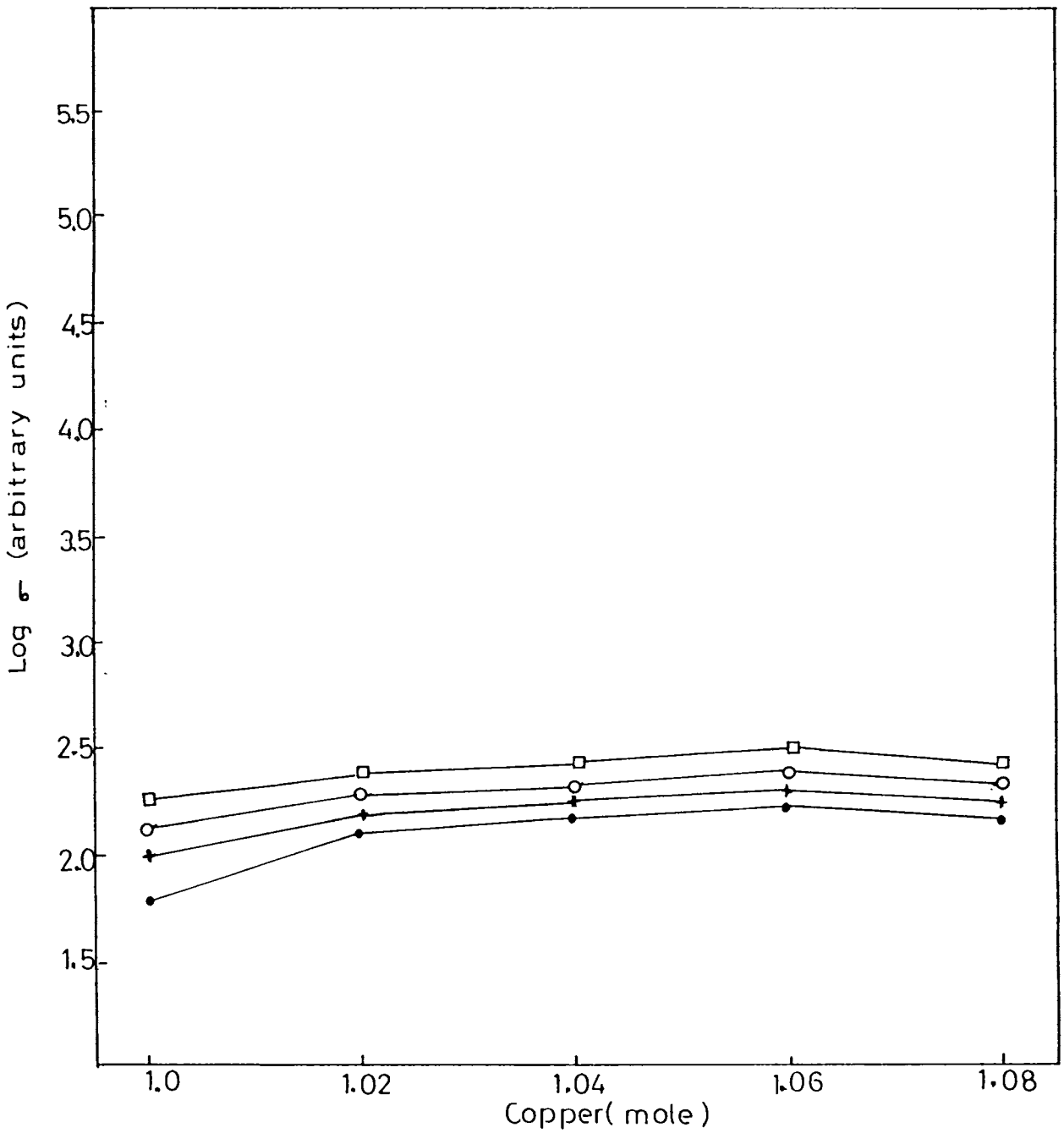

Fig 12.5 (a) Variation of conductivity as a function of number of moles of copper for the films in vacuum at 110 K: (•) unannealed and annealed at (+) 373 K, (o) 473 K and (□) 573 K.

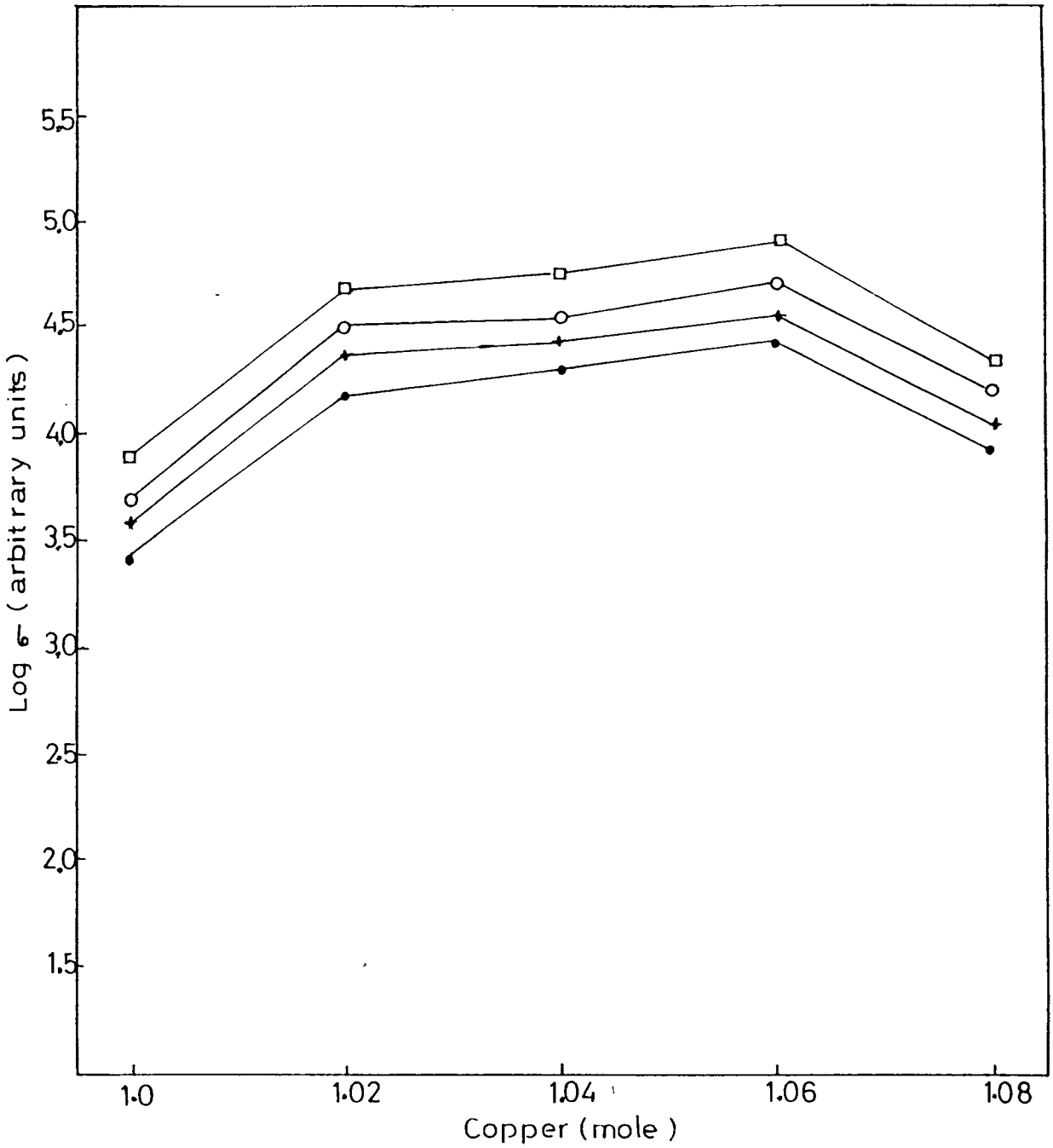

Fig 12.5 (b) : Variation of conductivity as a function of number of moles of copper for the films in vacuum at 303 K: (•) unannealed and annealed at (+) 373 K, (o) 473 K and (□) 573 K.

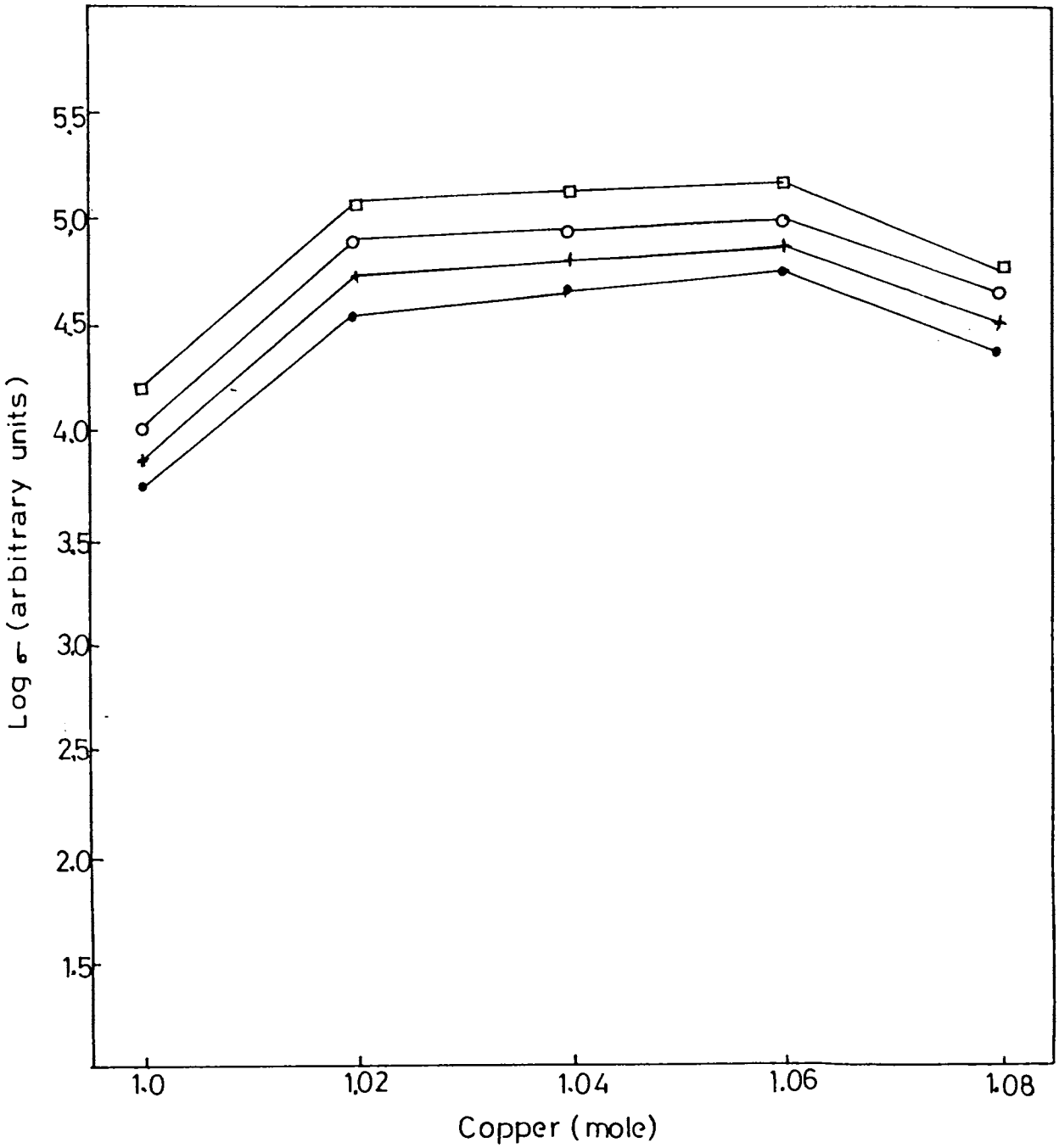

Fig 12.5 (c) : Variation of conductivity as a function of number of moles copper for the films in vacuum at 363 K: (•) unannealed and annealed at (+) 373 K, (o) 473 K and (□) 573 K.

the fact that excess copper in this film may fill its vacancies. Hence the concentration of acceptors (holes) decreases. During the annealing of films in air, oxygen will be incorporated and hence it affects the electrical properties of the films. In the present case, oxygen act as an acceptor and it increases the acceptor concentration. Hence annealing of the films in air causes the conductivity to increase irrespective of the copper contents in the film. The results obtained from the air annealing treatments are shown in Figs. 12.5 (a) to 12.5 (c). Films annealed at 373K have a low value of conductivity than that of films annealed at 573K. The slight adsorbed oxygen content in the films annealed at 373K can be removed easily during the measurements in vacuum while it becomes harder to desorb in the case of films annealed at elevated temperatures.

The significant decrease in the conductivity for the films C_6 and C_7. [Figs.12.6 (a) to 12.6 (c)] is due to the decrease in acceptor density. But the acceptor concentration is more for the films C_8 and C_9 and hence their conductivity is increased. This result is in agreement with that reported by Kokubun and Wada [20] on the evaporated films of $CuInSe_2$. When the temperature of annealing in air increases above 373K, the conductivity of the film C_6 increases slightly, owing to a very small increase in oxygen concentration. However the variation of conductivity with annealing temperature for the film C_7 is quite different. The conductivity of this film does not change significantly with annealing temperature. But for the films C_8 and C_9, the conductivity is remarkably increased on annealing.

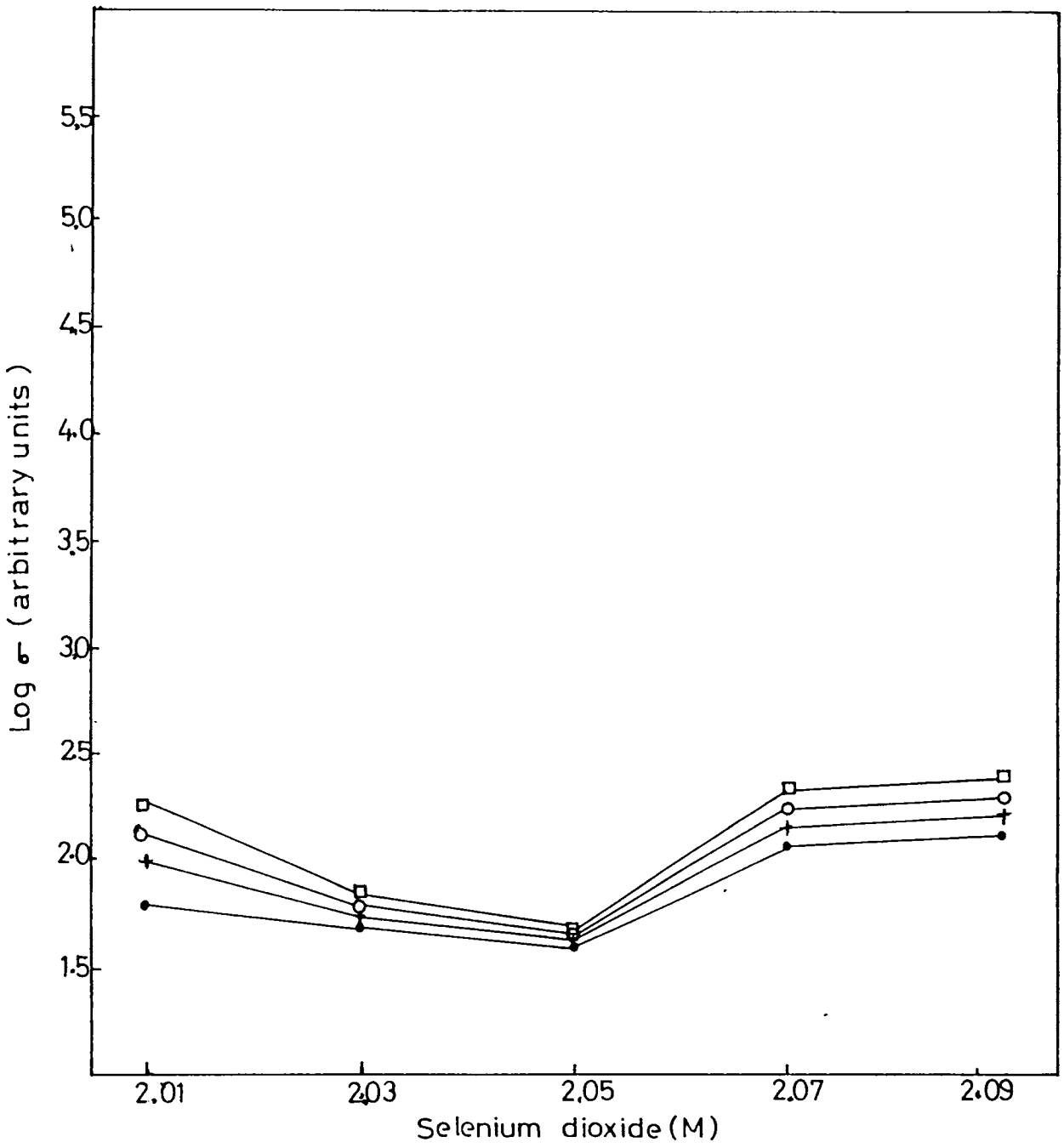

Fig 12.6 (a) : Variation of conductivity as a function of concentration of selenium dioxide for the films in vacuum at 110 K: (•) unannealed and annealed at (+) 373 K, (o) 473 K and (□) 573 K.

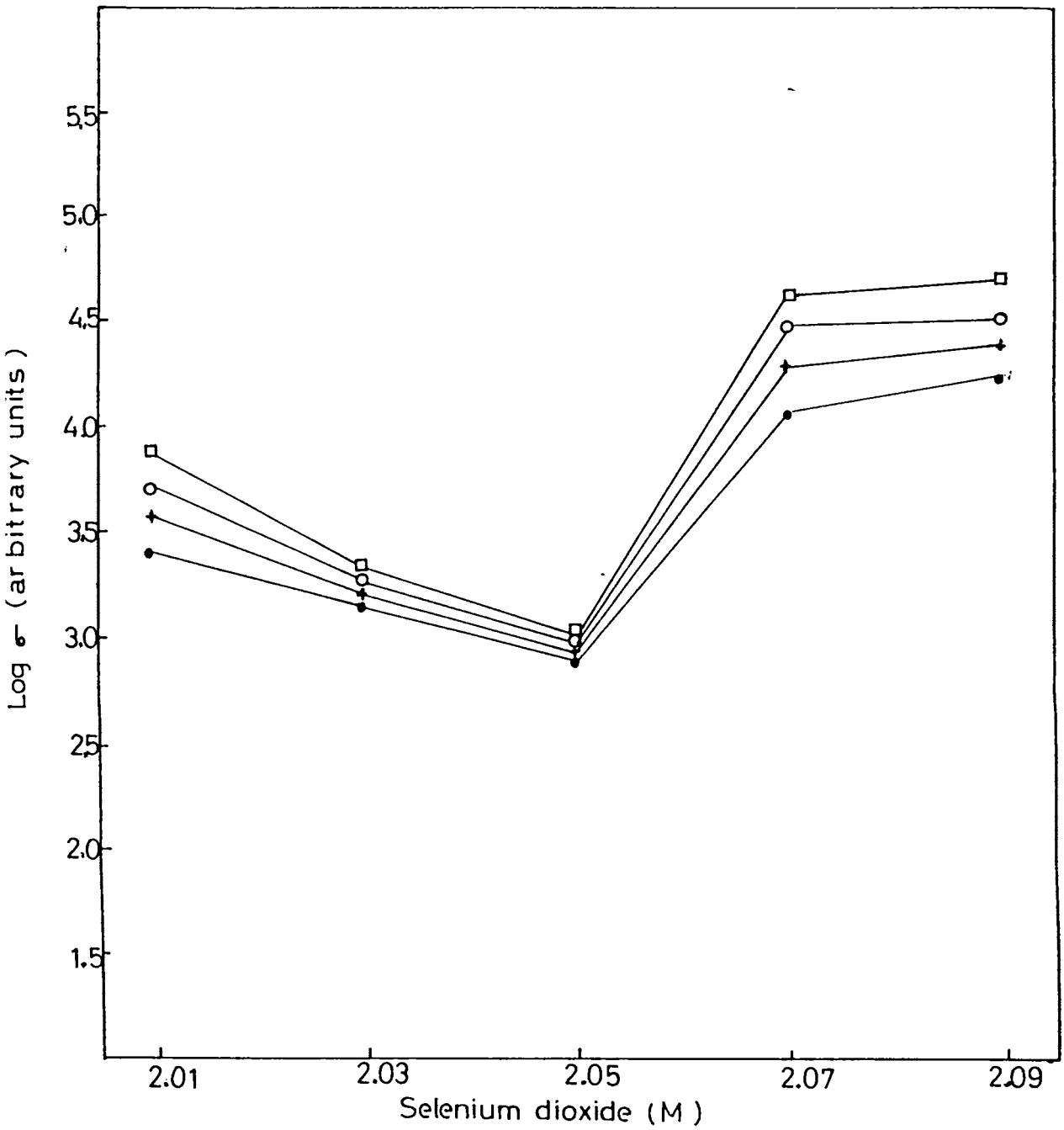

Fig 12.6 (b) : Variation of conductivity as a function of concentration of selenium dioxide for the films in vacuum at 303 K: (•) unannealed and annealed at (+) 373 K, (o) 473 K and (□) 573 K.

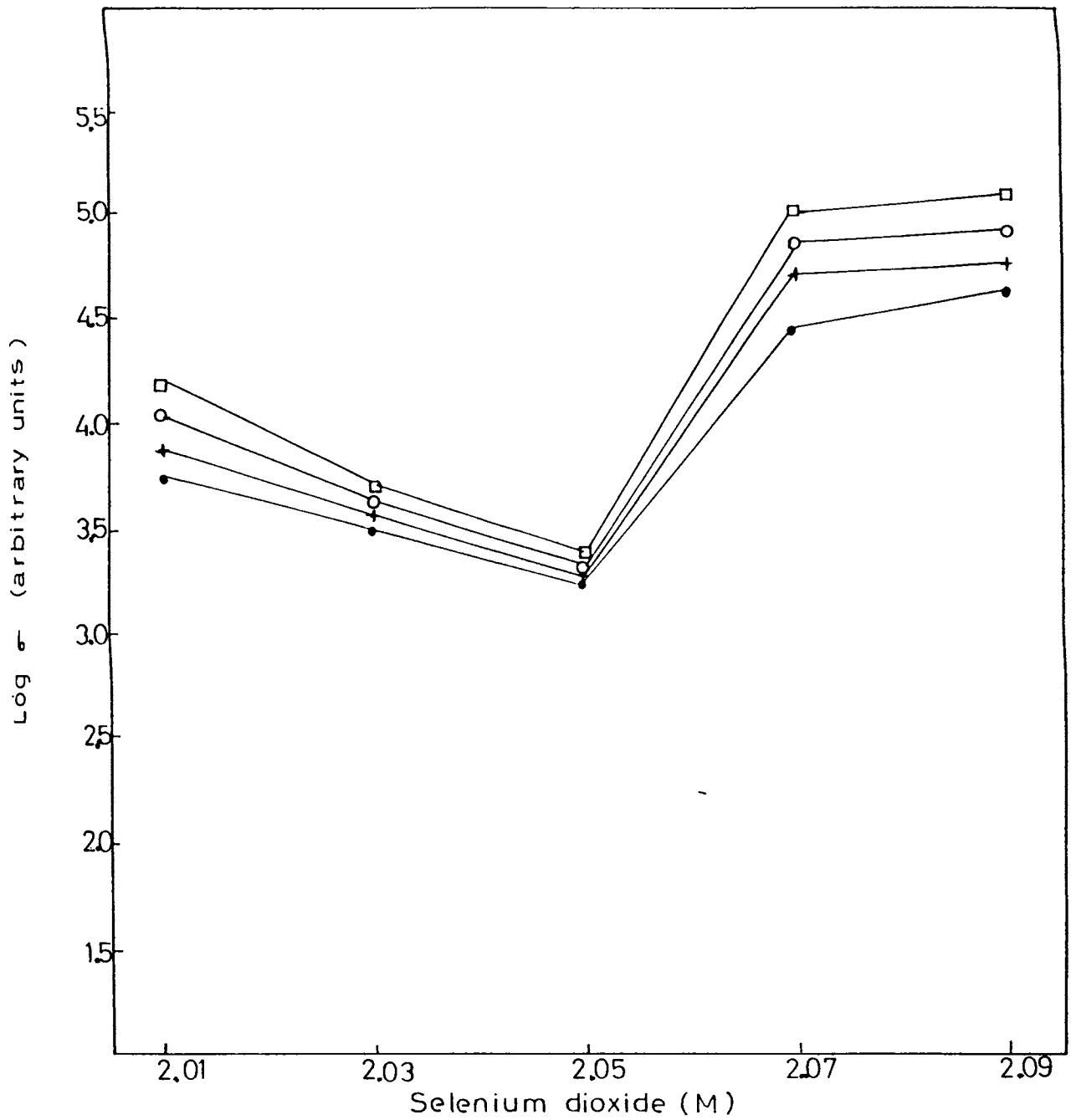

Fig 12.6 (c) : Variation of conductivity as a function of concentration of selenium dioxide for the films in vacuum at 363 K: (•) unannealed and annealed at (+) 373 K, (o) 473 K and (□) 573 K.

The temperature dependence of the electrical conductivity of the film C_1 in air is depicted in Fig. 12.7. It shows the typical behaviour, which is found to be similar to those obtained for all other films. The activation energy obtained from the conductivity measurements in air is given in Table 12.3.

The results of conductivity obtained on the films containing different copper contents are depicted in Figs. 12.8 (a) and 12.8(b). The conductivity of the film C_7 in air is increased rapidly for all annealing temperatures. [Figs. 12.9(a) and 12.9 (b)].

The magnitude of conductivity obtained from the measurements in air is higher than that in vacuum for all films. [Table 12.4]. The conductivity increase of films in air and the reversal in vacuum can be explained by the adsorption and desorption of oxygen at the film surface [21].

12.3.2 TSC Measurements

Inorder to understand the trapping mechanism of charge carriers, the TSC measurements were carried out on the films containing different copper and selenium contents in the temperature range 100 - 350K. Figs. 12.10 to 12.18 show the TSC spectra of the films C_1 to C_9 recorded with a biasing field of 3 KV/Cm after exciting for 5 min. The peaks are formed due to the release of the trapped carriers. The magnitude of the current is found to be higher for the peak b for all films. The films annealed at 573 K exhibit higher current than the unannealed films. A slight shift in the temperature corresponding to the current maximum(Tm

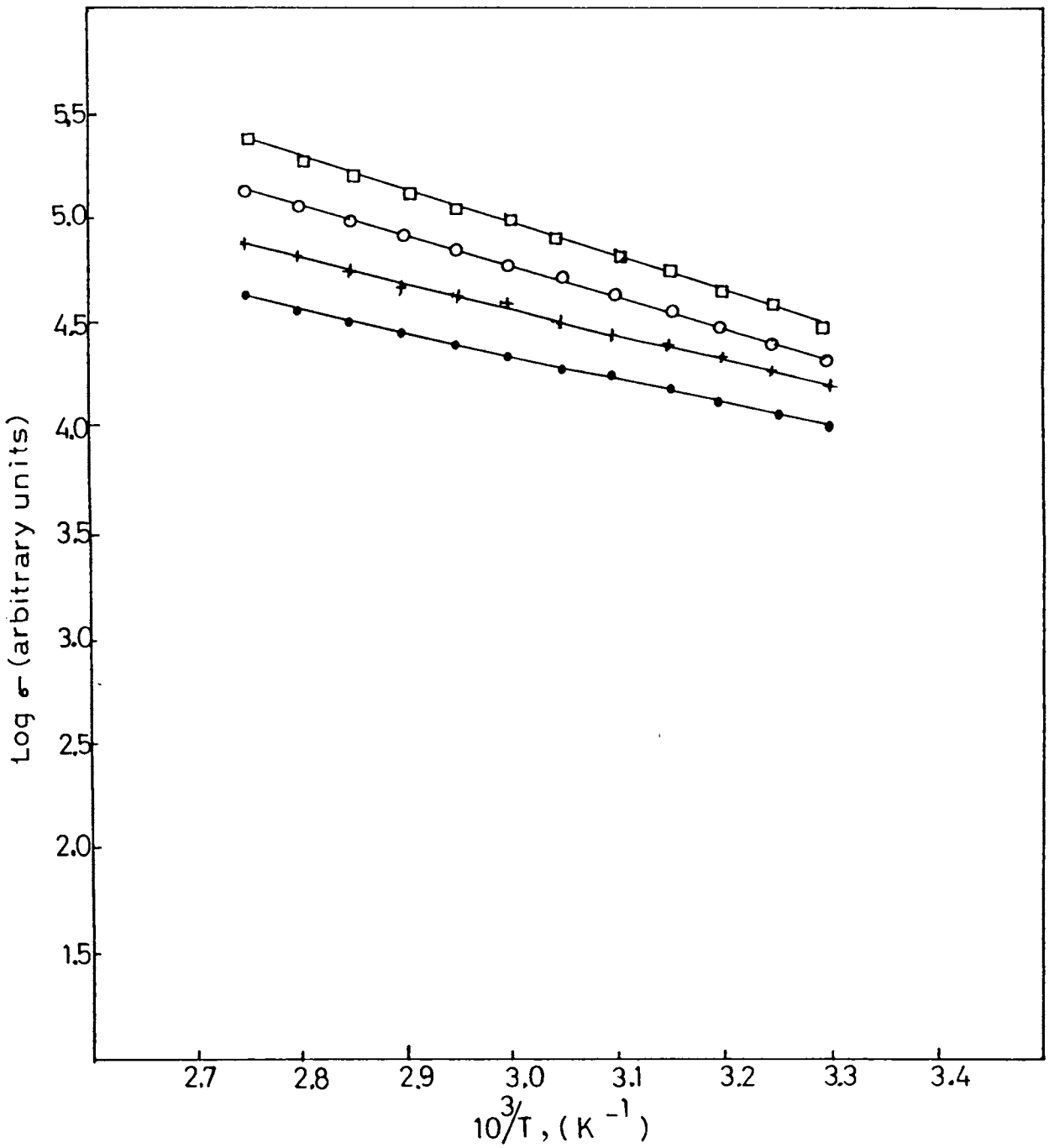

Fig 12.7 : Plot of log σ against $10^3/T$ for the film C_1 in air: (•) unannealed and annealed at (+) 373 K, (o) 473 K and (□) 573 K.

Table 12.3 The values of activation energy obtained from the conductivity measurements of the films in air.

Sample	Activation energy in the temperature range at 303-363K (eV)
C_1	
Unannealed	0.308
Annealed (373K)	0.274
Annealed (473K)	0.239
Annealed (573K)	0.214
C_2	
Unannealed	0.213
Annealed (373K)	0.238
Annealed (473K)	0.231
Annealed (573K)	0.215
C_3	
Unannealed	0.212
Annealed (373K)	0.239
Annealed (473K)	0.238
Annealed (573K)	0.205

Contd.... Table 12.3

Sample	Activation energy in the temperature range at 303-363K (eV)
C_4	
Unannealed	0.239
Annealed (373K)	0.256
Annealed (473K)	0.230
Annealed (573K)	0.197
C_5	
Unannealed	0.282
Annealed (373K)	0.275
Annealeld (473K)	0.240
Annealed (573K)	0.222
C_6	
Unannealed	0.231
Annealed (373K)	0.256
Annealed (473K)	0.230
Annealed (573K)	0.197

contd...

Contd.... Table 12.3

Sample	Activation energy in the temperature range at 303-363K (eV)
C_7	
Unannealed	0.214
Annealed (373K)	0.239
Annealed (473K)	0.231
Annealed (573K)	0.215
C_8	
Unannealed	0.205
Annealed (373K)	0.239
Annealed (473K)	0.238
Annealed (573K)	0.222
C_9	
Unannealed	0.206
Annealed (373K)	0.189
Annealed (473K)	0.188
Annealed (573K)	0.214

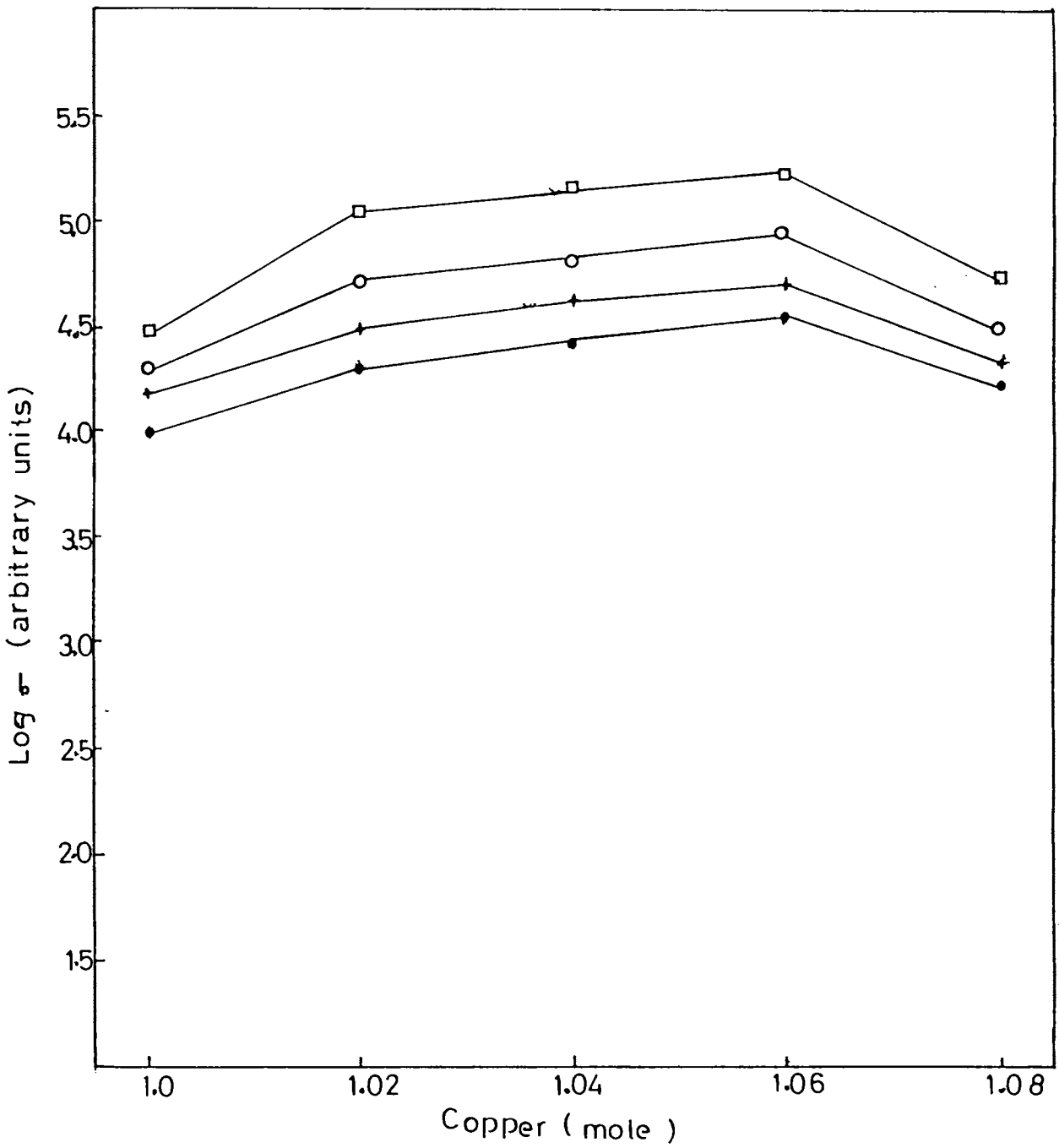

Fig 12.8 (a) : Variation of conductivity as a function of number of moles of copper for the films in air at 303 K: (•) unannealed and annealed at (+) 373 K, (o) 473 K and (□) 573 K.

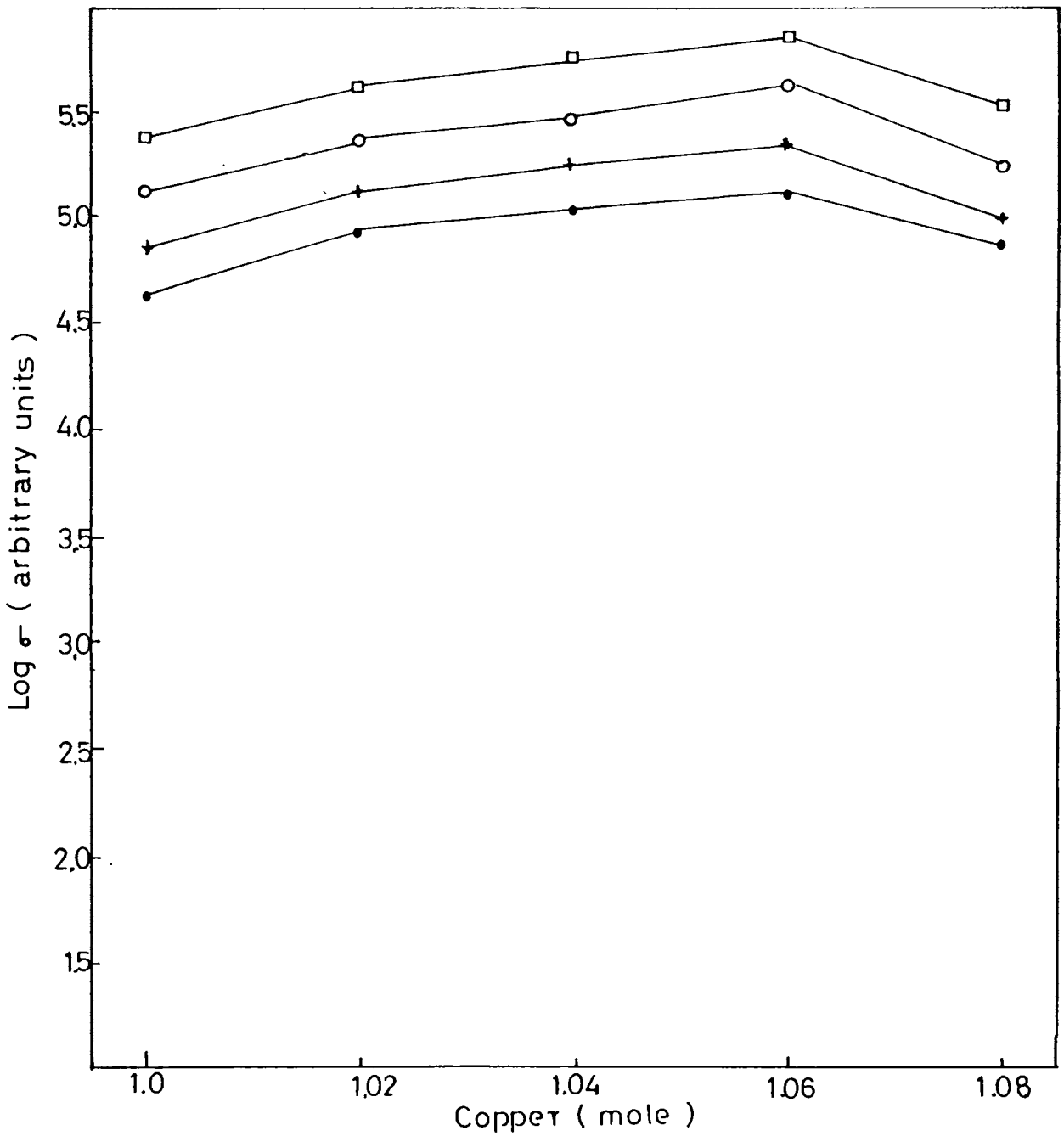

Fig 12.8 (b) : Variation of conductivity as a function of number of moles of copper for the films in air at 363 K: (•) unannealed and annealed at (+) 373 K, (o) 473 K and (□) 573 K.

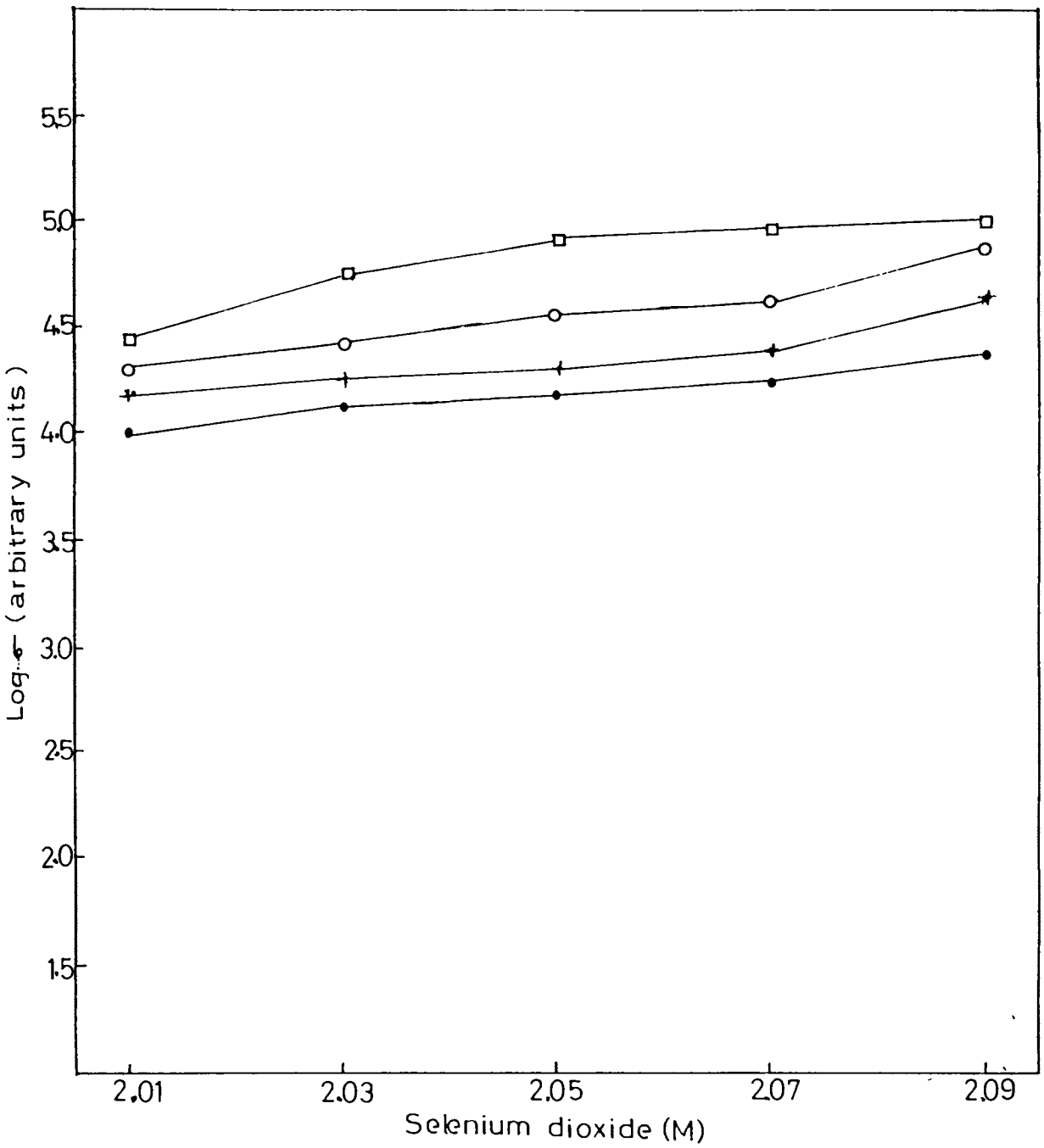

Fig 12.9 (a) : Variation of conductivity as a function of concentration of selenium dioxide for the films in air at 303 K: (•) unannealed and annealed at (+) 373 K, (o) 473 K and (□) 573 K.

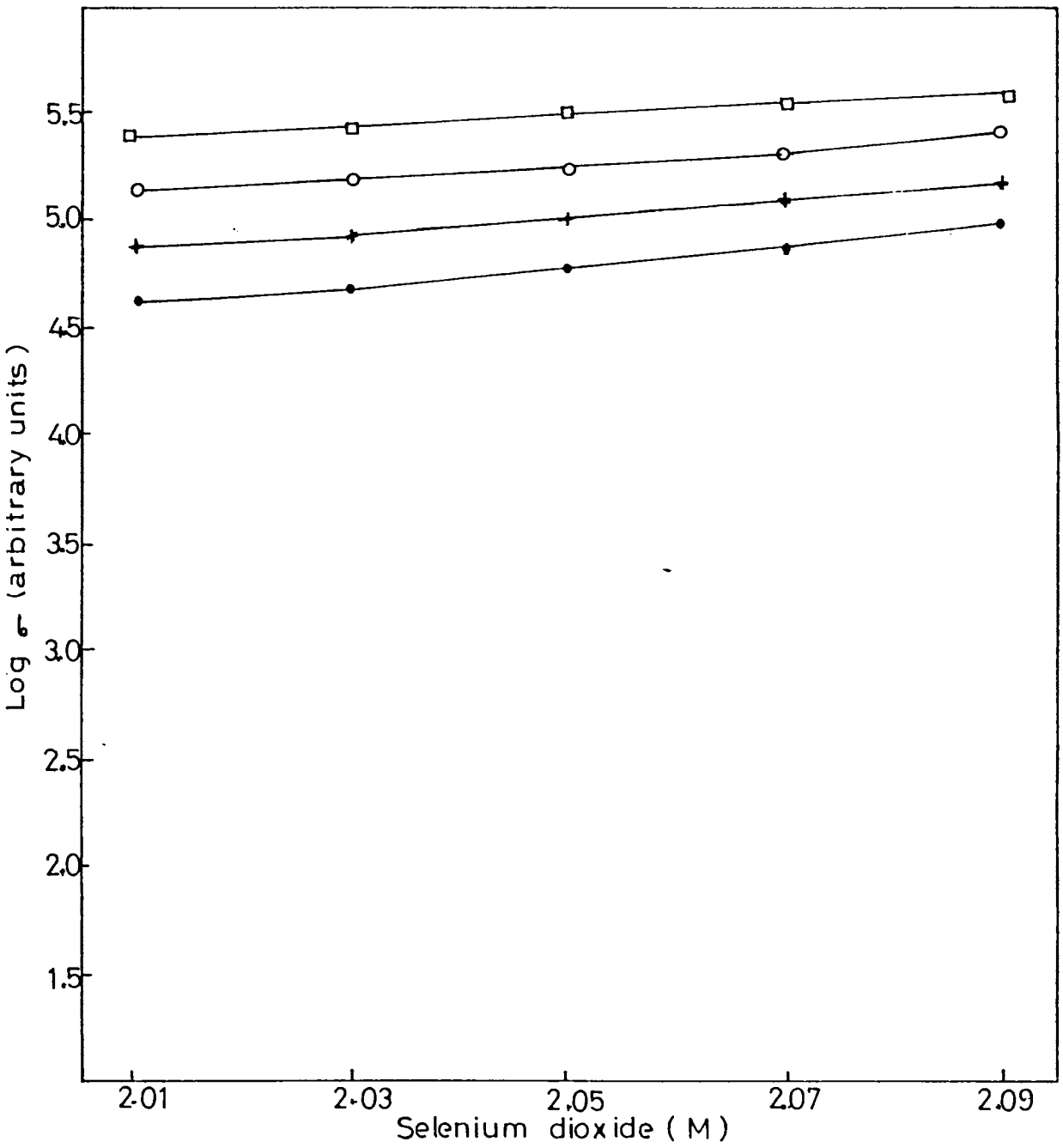

Fig 12.9 (b) : Variation of conductivity as a function of concentration of selenium dioxide for the films in air at 363 K. (•) unannealed and annealed at (+) 373 K, (o) 473 K and (□) 573 K.

Table 12.4 The values of conductivity of unannealed films

Sample	Conductivity at room temperature in different ambients	
	Vacuum (Ω^{-1} m^{-1})	Air (Ω^{-1} m^{-1})
C_1	2.66×10^3	1.01×10^4
C_2	1.49×10^4	1.98×10^4
C_3	1.99×10^4	2.65×10^4
C_4	2.82×10^4	3.55×10^4
C_5	8.41×10^3	1.68×10^4
C_6	1.41×10^3	1.33×10^4
C_7	7.94×10^2	1.48×10^4
C_8	1.19×10^4	1.77×10^4
C_9	1.78×10^4	2.37×10^4

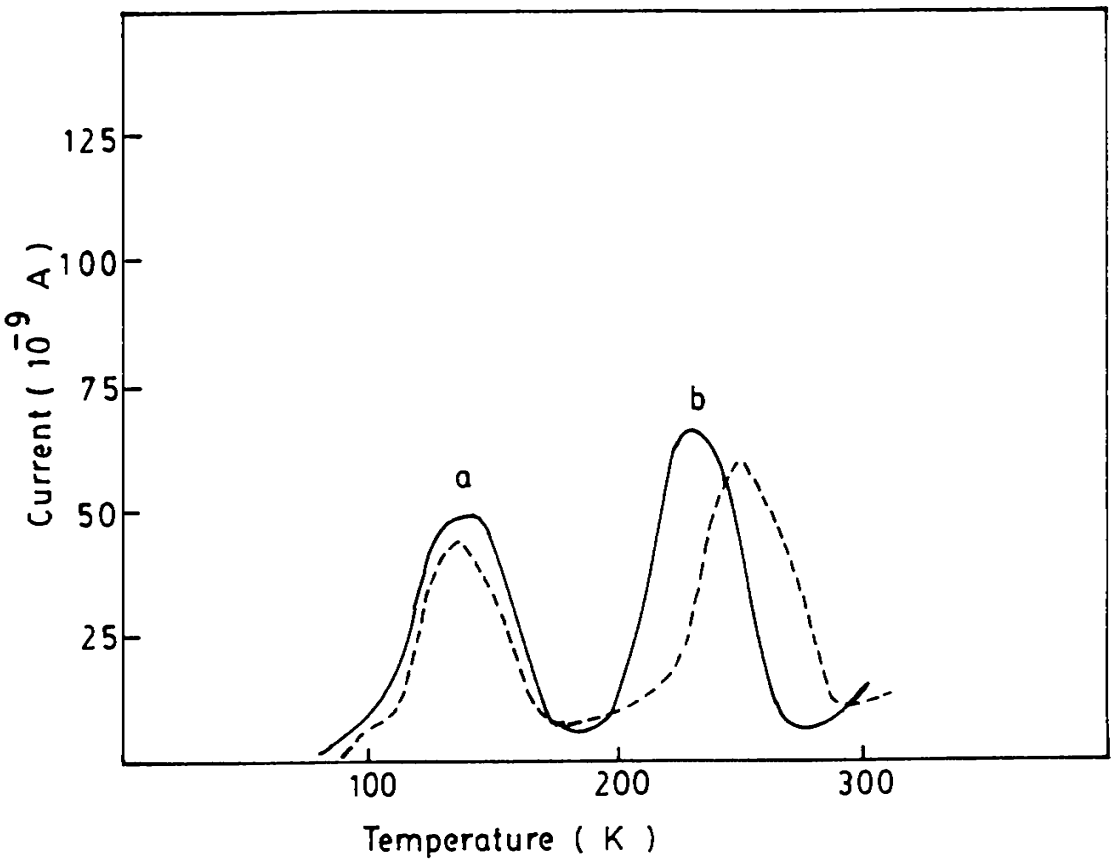

Fig 12.10 : TSC spectra of the C_I (.....) unannealed and (_____) annealed at 573 K.

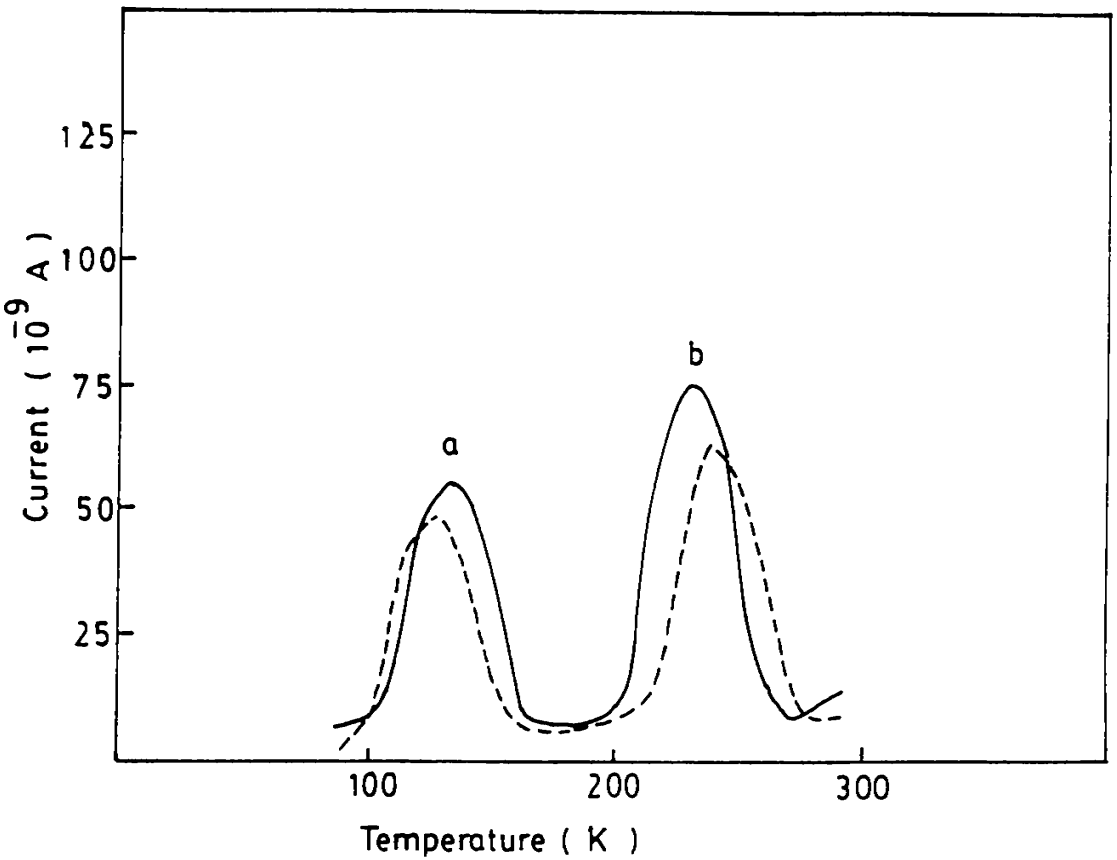

Fig 12.11 : TSC spectra of the film C_2 (.....) unannealed and (_____) annealed at 573 K.

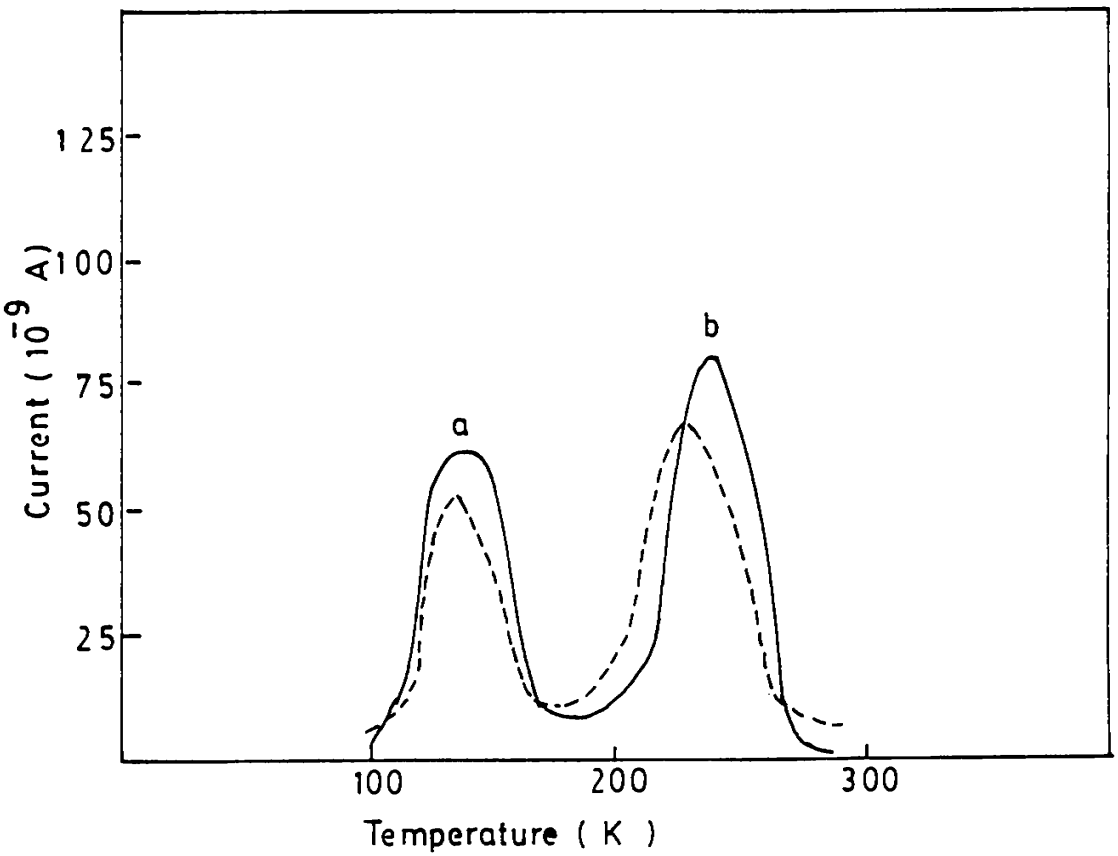

Fig 12.12 : TSC spectra of the C_3 (.....) unannealed and (_____) annealed at 573 K.

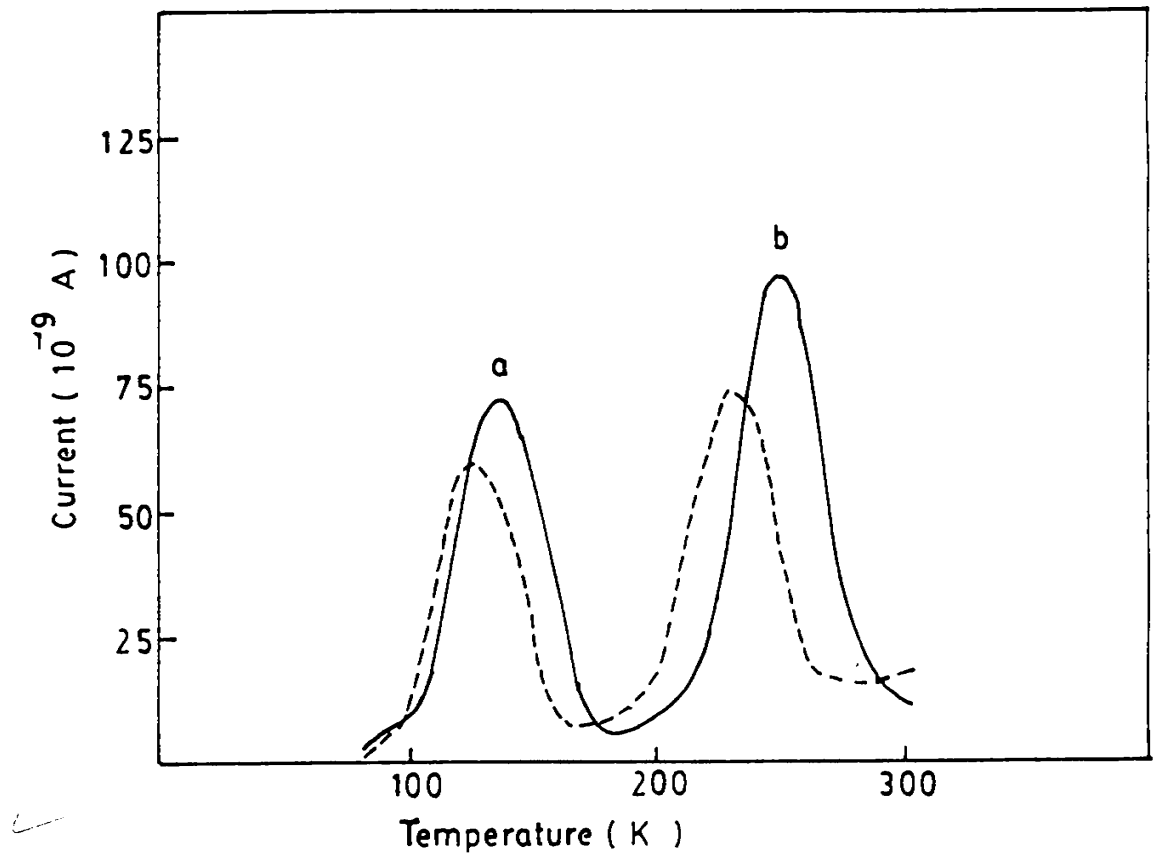

Fig 12.13 : TSC spectra of the film C_4 (.....) unannealed and (_____) annealed at 573 K.

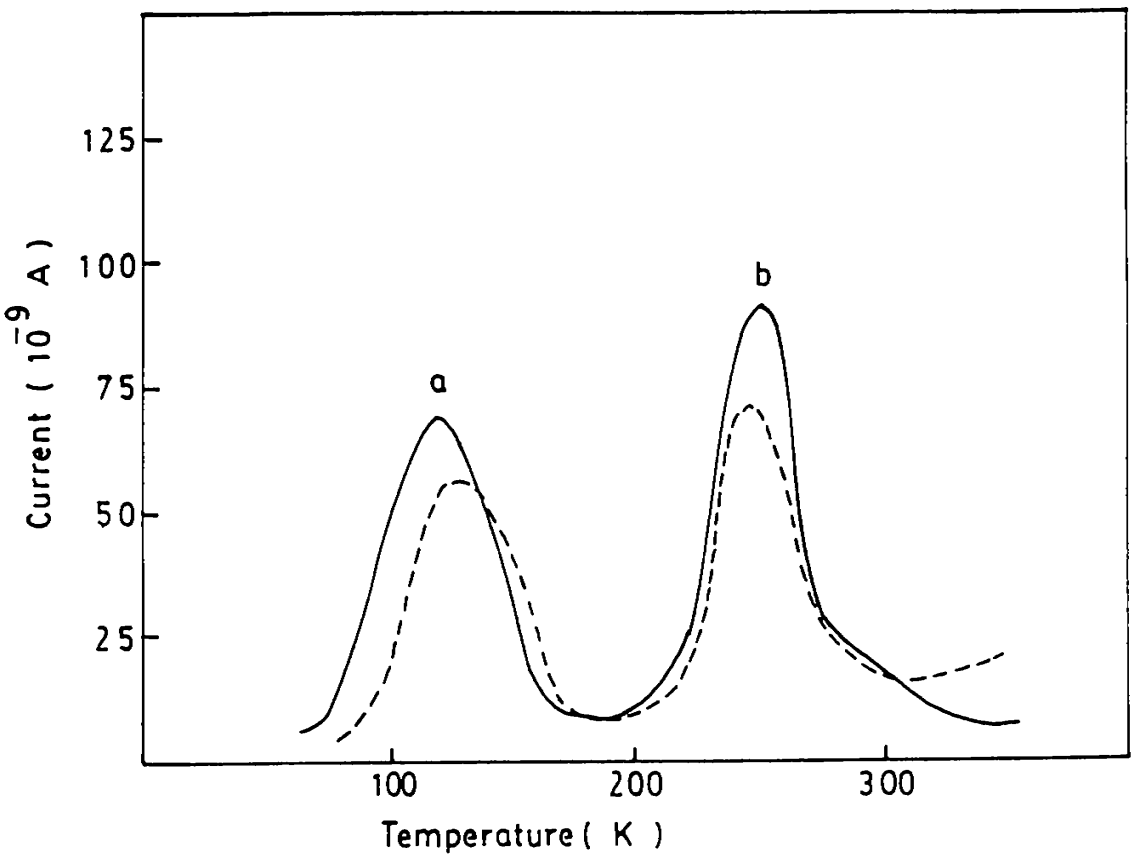

Fig 12.14 : TSC spectra of the film C_5 (.....) unannealed and (_____) annealed at 573 K.

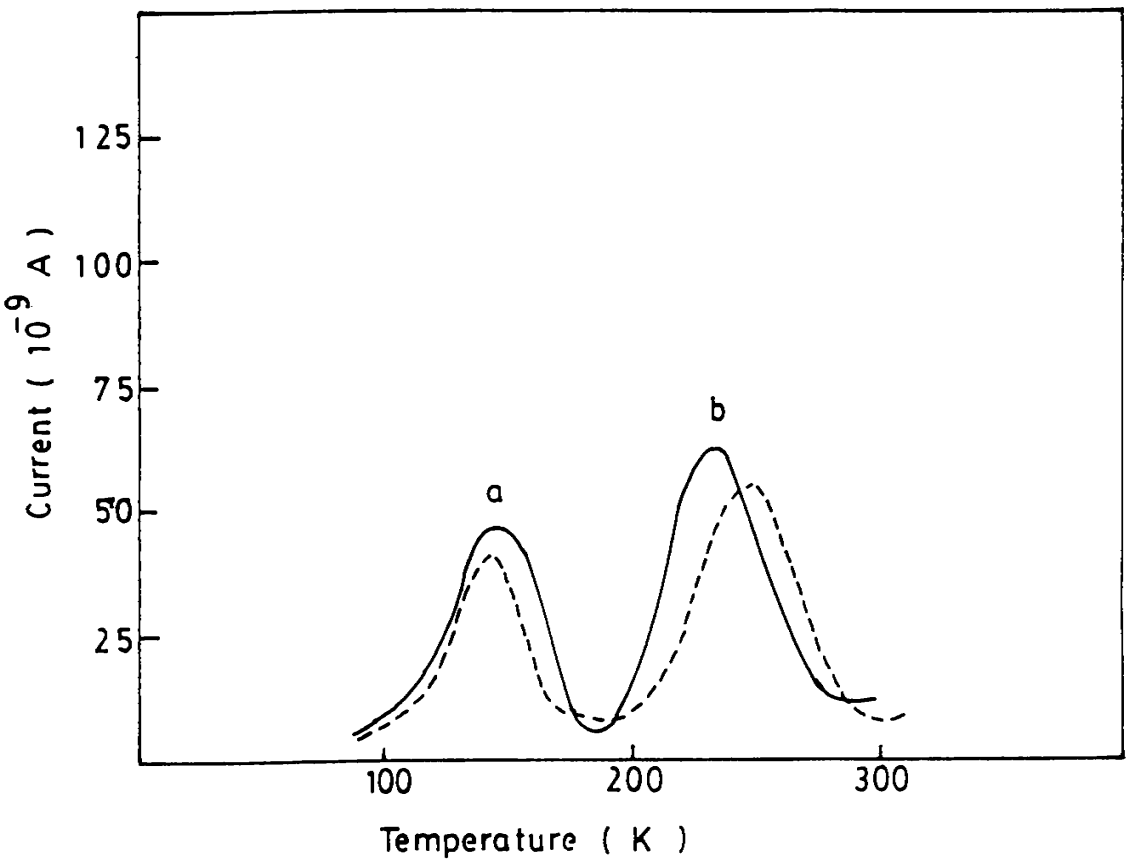

Fig 12.15 : TSC spectra of the film C_{60} (.....) unannealed and (_____) annealed at 573 K.

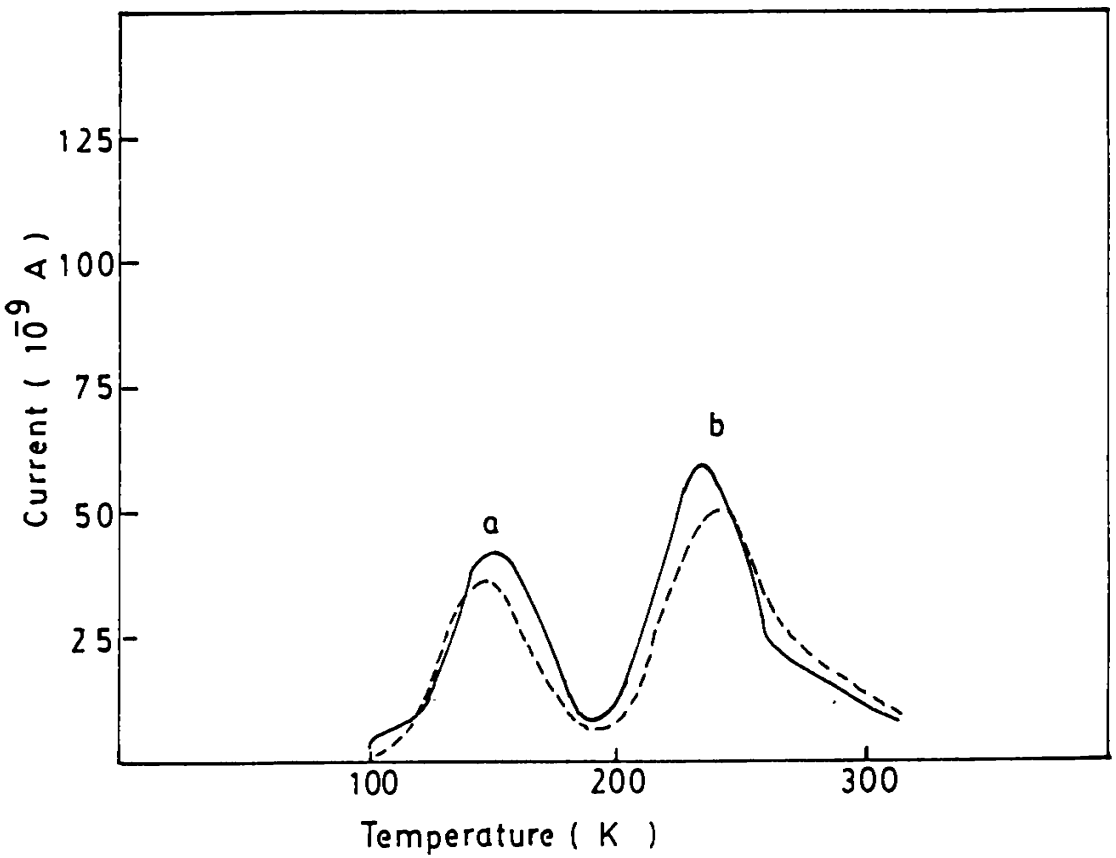

Fig 12.16 : TSC spectra of the film C_7 (....) unannealed and (_____) annealed at 573 K.

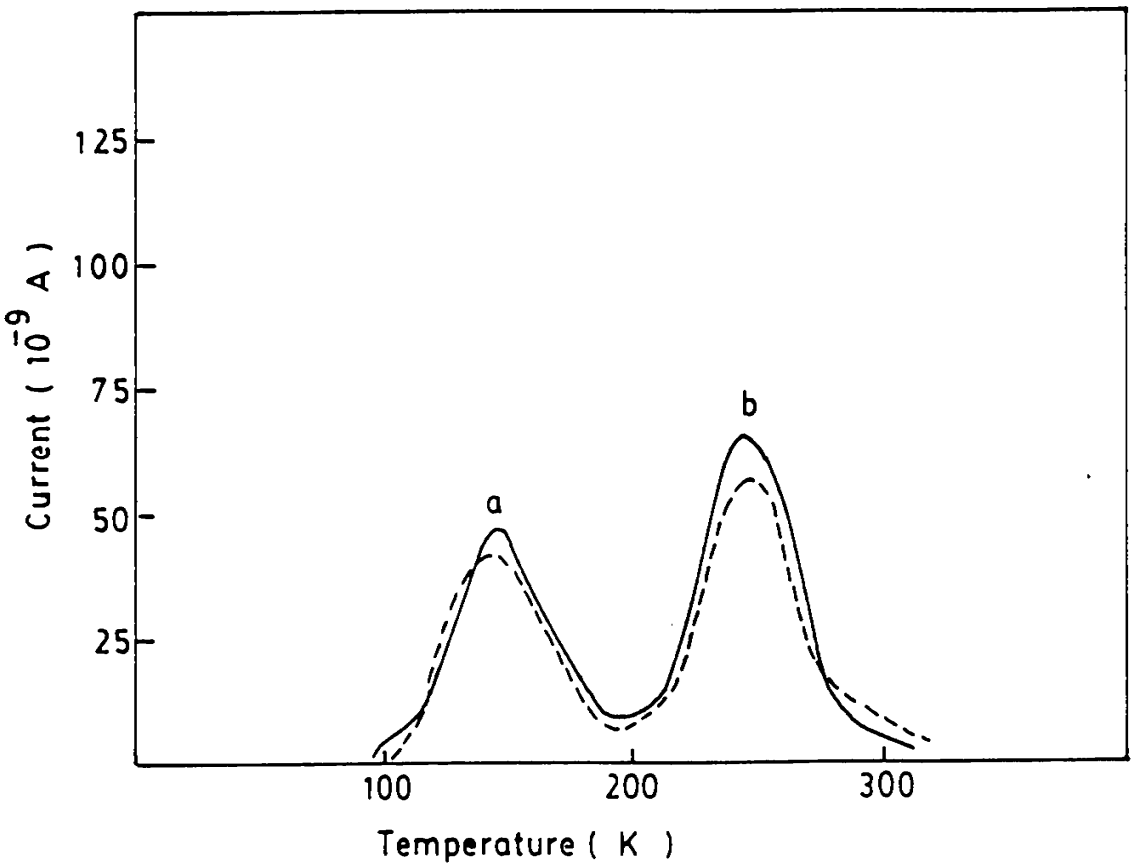

Fig 12.17 : TSC spectra of the film C_8 (.....) unannealed and (_____) annealed at 573 K.

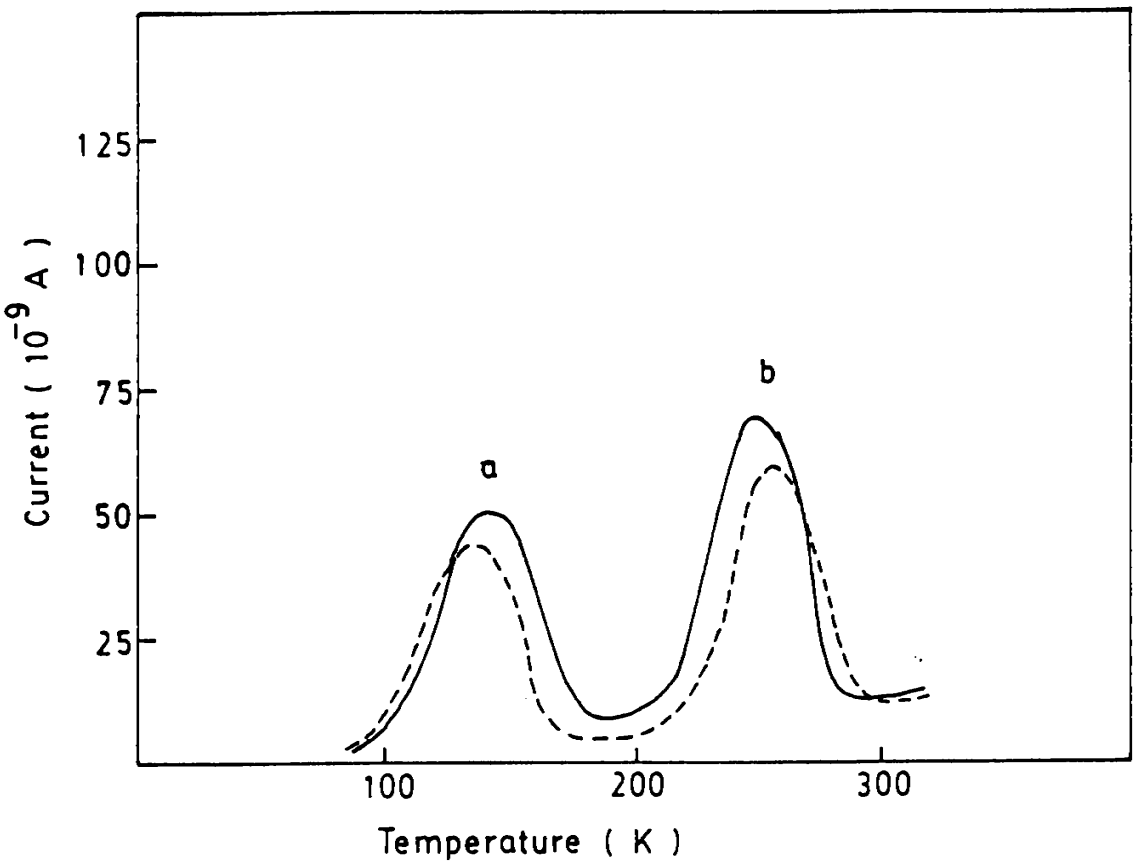

Fig 12.18 : TSC spectra of the film C_9 (....) unannealed and (_____) annealed at 573 K.

was also observed. The values of Tm, trap depth, capture cross section of the traps, etc are given in Table 12.5. It is seen from Fig 12.19 that the magnitude of the current increases with copper content, reaches a maximum value for the film C_4 and decreases thereafter. The peak height decreases as the selenium content increases and reaches a minimum value for the film C_7. [Fig. 12.20]. But for the films C_8 and C_9, an increase in the value of current is observed. Figs. 12.21 and 12.22 depict the variation of the peak height as a function of biasing field and excitation time. In both cases, the peak height is found to be increased linearly [22].

12.4 CONCLUSION

Thin films of $CuInSe_2$ containing different contents of copper and selenium have been prepared for studying their electrical characterization. The films are characterized by microscopic and XRD analysis. The value of band gap determined from the absorption spectrum is found to be 1.031 eV. The electrical characterization of the films indicate that the values of conductivity are influenced by the ambient conditions, annealing temperature and copper and selenium contents. The values of activation energy of charge carriers are determined for all films in vacuum and air.

The magnitude of thermally stimulated current depends on copper and selenium contents, annealing temperature, biasing field and excitation time. The peaks observed in all films are attributed to the release of carriers from the trap levels.

Table 12.5 The values of various parameters obtained from the TSC spectra of the films.

Sample	Peak a			Peak b		
	Tm (K)	E (eV)	Capture cross section (Cm^2)	Tm (K)	E (eV)	Capture cross section (Cm^2)
C_1						
Unannealed	139	0.0793	2.13×10^{-26}	251	0.208	3.41×10^{-25}
Annealed(573K)	142	0.075	1.18×10^{-26}	229	0.188	3.39×10^{-25}
C_2						
Unannealed	132	0.075	2.17×10^{-26}	244	0.238	2.26×10^{-24}
Annealed(573K)	137	0.072	1.18×10^{-26}	234	0.210	8.80×10^{-25}
C_3						
Unannealed	132	0.071	1.45×10^{-26}	229	0.188	3.39×10^{-25}
Annealed(573K)	139	0.072	3.17×10^{-26}	240	0.231	1.95×10^{-24}
C_4						
Unannealed	125	0.058	5.60×10^{-27}	230	0.198	5.62×10^{-25}
Annealed(573K)	136	0.061	4.15×10^{-27}	250	0.239	1.73×10^{-24}
C_5						
Unannealed	127	0.048	1.65×10^{-27}	246	0.248	3.39×10^{-24}
Annealed(573K)	118	0.038	7.94×10^{-28}	250	0.270	8.24×10^{-24}

Contd...

Contd.... Table 12.5

Sample	Peak a			Peak b		
	Tm (K)	E (eV)	Capture cross section (Cm^2)	Tm (K)	E (eV)	Capture cross section (Cm^2)
C_6						
Unannealed	142	0.085	3.02×10^{-26}	248	0.200	2.60×10^{-25}
Annealed(573K)	145	0.072	7.53×10^{-27}	232	0.171	1.13×10^{-25}
C_7						
Unannealed	148	0.075	8.48×10^{-27}	242	0.180	1.18×10^{-25}
Annealed(573K)	153	0.079	9.34×10^{-27}	235	0.183	1.92×10^{-25}
C_8						
Unannealed	143	0.065	4.29×10^{-27}	247	0.223	8.93×10^{-25}
Annealed(573K)	147	0.074	8.16×10^{-27}	245	0.195	2.30×10^{-25}
C_9						
Unannealed	135	0.058	3.22×10^{-27}	258	0.244	1.47×10^{-24}
Annealed(573K)	140	0.067	6.10×10^{-27}	252	0.214	4.42×10^{-25}

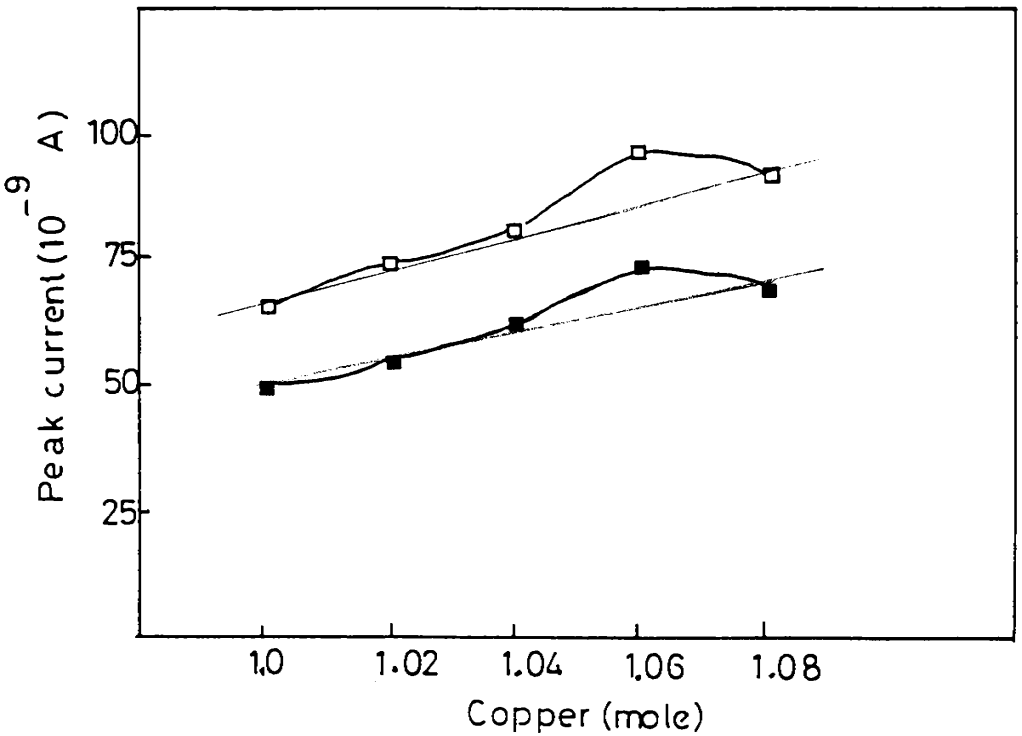

Fig 12.19 : Plot of peak height against number of moles of copper for the films annealed at 573 K for the peaks; (■) a and (□) b.

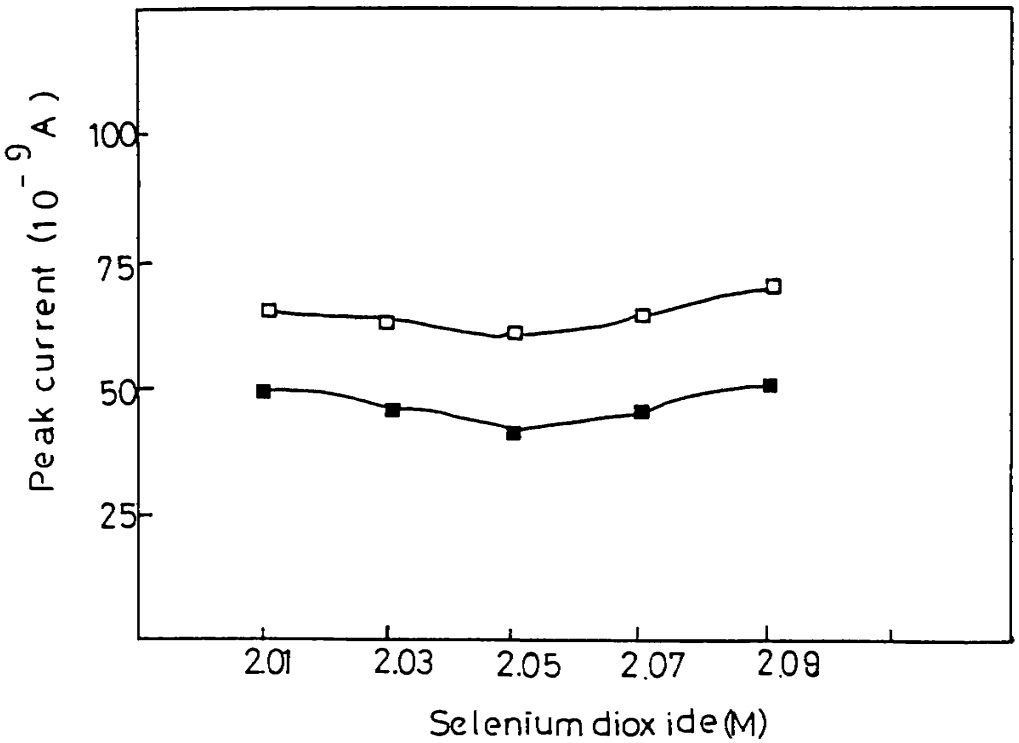

Fig 12.20 : Plot of peak height against concentration of selenium dioxide for the films annealed at 573 K for the peaks; (■) a and (□) b.

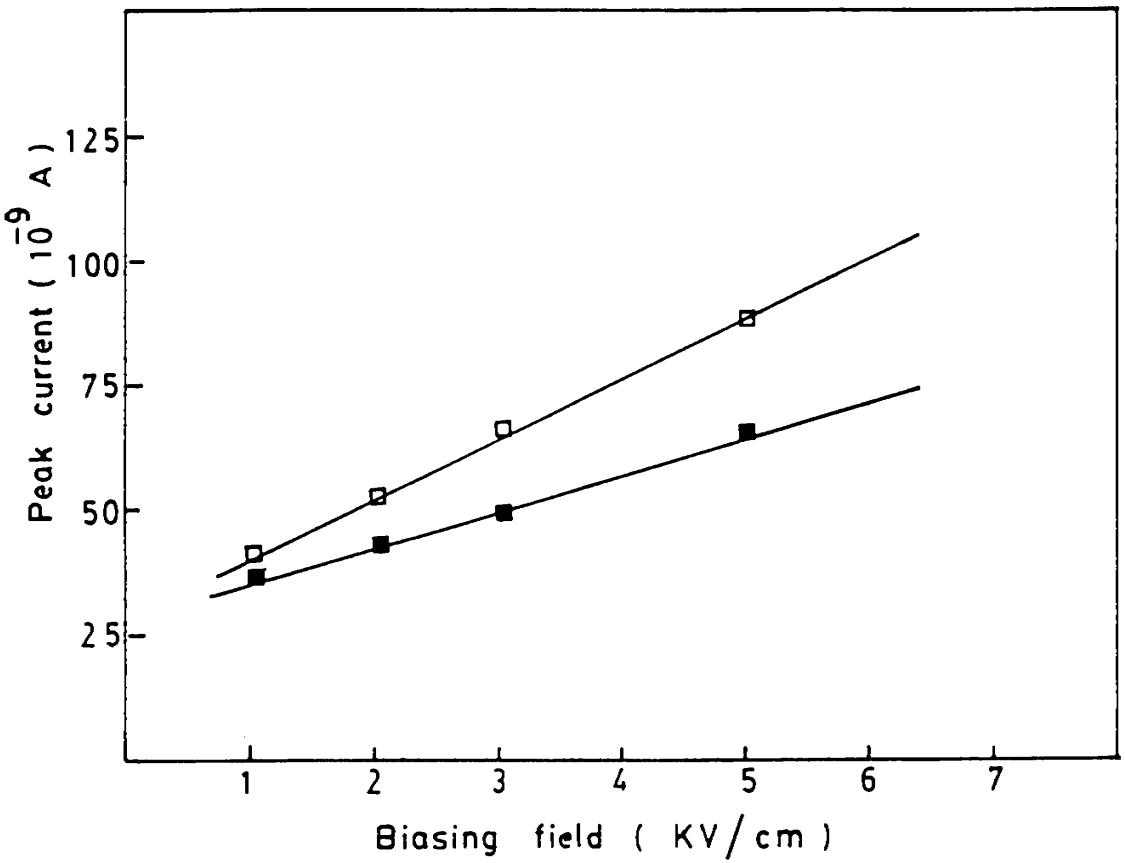

Fig 12.21 : Plot of peak height against biasing field for the film C_1 annealed at 573 K for the peaks; (■) á and (□) b.

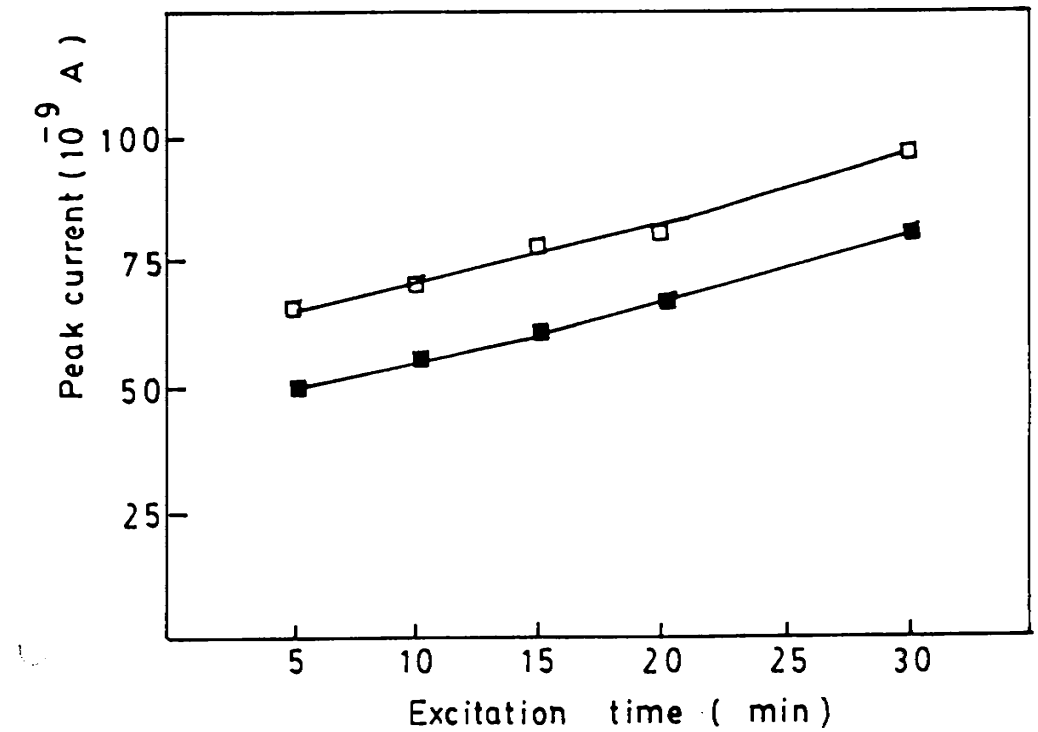

Fig 12.22 : Plot of peak height against excitation time for the film C_1 annealed at 573 K for the peaks; (■) a and (□) b.

12.5 REFERENCES

[1] S. Wagner, Inst. Phys. Conf. Ser. 35 (1977) 205.

[2] L.L. Kamzmerski, Inst. Phys. Conf. Ser. 35 (1977) 217.

[3] E. Bucher, Appl. Phys. 17 (1978) 1

[4] N. Romeo, Jpn. J. Appl. Phys. Suppl. 19 (1980) 25

[5] E.R.Don. R.R. Cooper and R. Hill, Proc. 6th EC Photovoltaic Solar Energy Conf. London, 1985, P. 768

[6] A. Knowles, H. Oumous, M.J. Carter and R. Hill, Conf. Record of the 20th IEEE Photovoltaic Specialist's Conf. USA, 1988.

[7] N.A.K. Abdul Hussein, A.N.Y.Samaan, R.D.Tomlinson, A.E.Hill and H. Neumann, Cryst. Res. Technol. 20 (1985) 509.

[8] S.V. Krishnaswamy, A.S. Manocha, and J.R.Szedon, J.Vac. Sci. Technol. 1 (1983) 510

[9] E. Elliot, R.D.Tomlinson, J.Parkes and M.J.Hampshine, Thin Solid Films 20 (1974) 525.

[10] L.L. Kazmerski, M.S. Ayyagari, F.R. White and G.A. Sanborn, J.Vac. Sci. Techmol. 13 (1976) 139

[11] J.Piekoszewski, J.J. Loferski, R. Beaulieu, J. Beall, R. Roeslev and J. Schewchun, Proc. 14th IEEE Photovoltaic specialist's Conf. San Diego, 1980

[12] S.P. Grindle, A.H. Clark, S. Rezaie-Serej, E. Falconer, J.Mc Neily and L.L. Kazmerski, J. Appl. Phys. 51 (1980) 5464.

[13] R.N. Bhattacharya, J. Electrochem. Soc. 130 (1983) 2040

[14] N. Khare, G. Razzini and L.P. Bicelli, Thin Solid Films 186 (1990) 113.

[15] K.R. Murali, Thin Solid Films 167 (1988) L19.

[16] T. Datta, R. Noufi and S.K. Deb, J. Appl. Phys. 59 (1986) 1548.

[17] A.K. Thomas, M.Phil Dessertation, (Cochin University of Science and Technology, 1988)

[18] JCPDS: International Centre for Diffraction Data, USA,1978

[19] W. Horig, H. Neumann, H. Sobotta, B. Schumann and G. Kuhn, Thin Solid films 48 (1978) 67

[20] Y. Kokubun and M. Wada, Jpn. J. Appl. Phys. 16 (1977) 879

[21] A.G. Valyomana and C. Purushothaman (Communicated)

[22] A.G. Valyomana and C. Purushothaman (Communicated)